Liquid crystal polymers for gas chromatography

Hickling, Simon James

Award date:
1999

Awarding institution:
University of Bath

LIQUID CRYSTAL POLYMERS FOR GAS CHROMATOGRAPHY

submitted by Simon James Hickling
for the degree of Ph.D.
from the University of Bath
1999

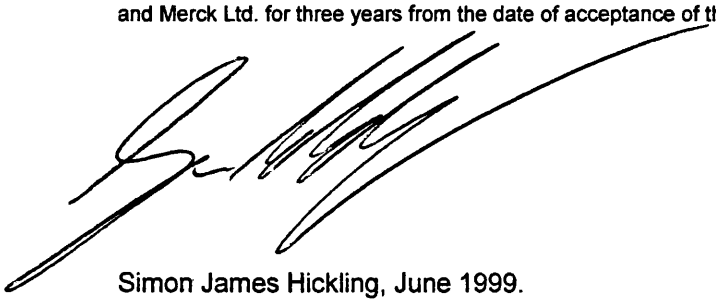

Simon James Hickling, June 1999.

ProQuest LLC
789 East Eisenhower Parkway
P.O. Box 1346
Ann Arbor, MI 48106-1346

ABSTRACT

This research was concerned with the development of novel liquid crystalline stationary phases for the gas chromatographic separation of closely related isomers, including enantiomeric compounds, over a wide range of operating temperatures.

The synthesis of liquid crystals and analogous liquid crystal polymers was undertaken, and their mesophase structures and transitions characterised using traditional methods. These compounds were then studied using Inverse Gas Chromatography (IGC) in order to determine the nature of the solute-solvent interactions between probe and stationary phase. The thermodynamic characteristics of such interactions were then related to the analytical performance observed to describe the mechanism by which liquid crystalline structures act as selective solvents. A knowledge of the relationship between mesogenic properties and molecular interactions then allowed the suggestion of stationary phases capable of efficient enantiomeric separations.

It was shown that the IGC method is applicable to the study of mesogenic materials, and that the mesophase structure of these materials imposes a strong entropic effect on solute-solvent interactions. It was determined that a well-ordered mesophase structure which retains this mesophase behaviour over a wide temperature range makes the most effective shape-selective solvent. Such properties are offered by side-chain liquid crystal polymers, in which the mesogen is appended to a polysiloxane backbone.

The analytical efficiencies noted with packed-column GC were too low to effect baseline separation, so future work in this area will need to utilise capillary column GC. Other future possibilities suggested include studies of the supercooled mesophase, polymer-liquid crystal blends, detailed diffusion studies using the IGC method, application of an electric field to induce order in the stationary phase, and application of new methods of liquid crystalline synthesis to fabricate materials with fixed mesogenic properties.

ACKNOWLEDGEMENTS

Firstly, I would like to thank Gareth Price for his support, experience and humour throughout my time at Bath.

Thanks go to George Gray and David Coates of Merck Ltd., Poole, who funded this research with an EPSRC 'CASE' award. Thanks also to Mark Verrell who supervised my synthesis of liquid crystalline materials in Merck's Poole laboratories.

The atmosphere in Bath University's polymer research laboratory has been very friendly and interesting, for which I thank the following: Peter West, Andy Clifton, Tom Hunter, Ian Shillcock, Emma Lenz, Steve Harrison, Simon Crook, Philip Drake, David Brown, Mike Lovell, Colin Moore, Neil Hunt and Roger Jardine.

Special thanks also go out to Mum and Dad, who's support and love throughout my life and education has been invaluable, and is much appreciated.

Finally, my love and thanks go to Sandy, who throughout the thesis-writing process has been there with love, support and coffee. Our adventures are only just beginning...

CONTENTS

Chapter One:

INTRODUCTION

Chemical analysis impacts our lives on a daily basis. The majority of products used in the modern world have been manufactured using some kind of chemical process, and in order for these products to be of the highest quality each stage of their manufacture must be carefully controlled - emphasising the need for their composition to be investigated. When the products concerned include foodstuffs and pharmaceuticals, which are taken into the body, the importance of analysis of the process and final product cannot be understated. In addition, the waste products of the modern age pose a growing threat, and chemical analysis must be employed to monitor the disposal of such waste and the mechanism by which it re-enters the environment. Chemical analysis covers many fields (including analysis of signals derived from the emission or adsorption of radiation, change in electrical parameters and the separation of analytes) and utilises many techniques, from high-tech mass spectrometry systems to simple titrimetric methods.

Of particular interest is the technique of *gas chromatography* (GC), where a volatile sample is vapourised and injected into the head of a chromatographic column, on which partitioning of the sample components between the mobile and stationary phases occurs. This leads to the separation, followed by the quantitative and qualitative analysis, of many samples of environmental and industrial importance. The technique is now ubiquitous in analytical chemistry laboratories around the world, and its use continues to expand to the analysis of ever more complex sample matrices. Traditional GC instrumentation may be linked to a selective detector, such as a mass spectrometer or infra-red spectrometer, allowing more in-depth characterisation of the sample components.

Many samples which require analysis are *chiral* in nature. That is, they lack symmetry and form mirror-image structures which have many identical chemical and physical properties, but may exhibit different chemical effects - particularly in biological systems. Their analysis is therefore of paramount importance, and dedicated methods must be applied for this to be undertaken due to the chemical similarity of the analytes. Such systems include essential oils, pheromones and environmental samples which are best analysed using GC as they are easily prepared from their sample matrix in a volatile form.

Gas chromatography has also been applied to the physiochemical study of the stationary phase, where a sample of known physiochemical properties can yield much information on an unknown stationary phase. This extension of traditional GC usage is termed *Inverse Gas Chromatography* (IGC), and has found wide application in the determination of physiochemical properties of polymeric stationary phases.

Liquid crystals were first discovered in 1888, though active research in the area was limited until the 1950's when some of their more unusual properties were discovered. Since then, the field of liquid crystal research has continued to grow, and these materials find application in a host of areas, having grown from their major application in monochrome display units to full-sized multicolour displays, non-linear optics, temperature sensors, lithographic applications and even cosmetics. Further fundamental research on liquid crystals will yield interesting results in the fields of biology, where liquid crystals are active in biological functions; physics, in the formulation of new products; mathematics, in the modelling of the liquid crystalline phase; and - of course - in chemistry, where new structures are devised and synthesised for both research and application purposes.

The fields of gas chromatography and liquid crystals primarily overlap where liquid crystalline stationary phases have been used to separate closely-related samples, although such techniques have so far met with limited success. Such separations are dependent upon the behaviour of the samples as solutions in a liquid crystalline medium, thus consideration of the solution behaviour of liquid crystals allows the mechanism by which separation occurs to be described. Whilst there has been much research on phase behaviour of liquid crystalline materials, less is known about their behaviour in solution; the theoretical models used being complicated by their anisotropic structure. However, Inverse Gas Chromatography may be applied to these materials as differences in solution behaviour from the pure liquid sample allow adequate description of the stationary phase's physiochemical properties.

This thesis examines the thermodynamic and analytical properties of a number of liquid crystalline stationary phases which may have potential for enantiomeric separations. Chapter 3 describes preliminary work carried out to utilise liquid crystals as stationary phases for Inverse Gas Chromatography, with Chapter 4 outlining the physiochemical behaviour of the stationary phases and Chapter 5 summarising their analytical performance. Chapter 6 looks at the diffusion of sample molecules within the stationary phases, as this also acts to affect analytical separations. Chapter 7 summaries and integrates the research described in the previous chapters, offers conclusions on this work, and suggests routes by which this research may proceed in the future. This research therefore opens up both an enhanced analytical technique with interesting theoretical and practical applications, and a potentially new market for liquid crystalline compounds.

1.1 LIQUID CRYSTALS

The solid crystalline state of matter consists of a regularly ordered lattice of molecules. The application of heat provides this lattice with vibrational energy, until at a certain temperature the molecules lose their regular order to become a liquid. The term *liquid crystal* is used to describe a collection of molecules in which a transitional state of matter - between the solid and liquid state - is observed under certain conditions. These states are known as *mesophases*, where order remains in some dimensions but is lost in others. The degree of ordering present is described by the type of mesophase observed.

1.1.1 HISTORY

Between 1850 and 1888, a variety of experiments were carried out on biological materials which noted that the outer covering of nerve fibres formed soft materials when left in water, and exhibited unusual effects under polarised light. Thus an intermediate phase between solid and liquid was discovered. Around this time, studies were also being carried out on cholesterol derivatives by Planer, Lobisch and Raymann, which showed the compounds to exhibit striking colours upon cooling. In separate studies whilst studying stearin, Heintz noticed a "second" melting point, when the material turned cloudy at 52°C, became completely opaque at 58°C, and finally cleared at 62.5°C. None of these phenomena could be explained at the time. During crystallisation studies Otto Lehmann, a German physicist, built a heating stage for his microscope to observe how materials crystallised on cooling. He added polarisers to this microscope, making an early prototype of the hot-stage microscope which would later become so valuable in liquid crystal research. He noted that some substances did not crystallise from a clear liquid, but gave an intermediate amorphous form which then went on to crystallise. At the time he thought that it was an extended solid-liquid phase transition, due to impurities.

Combined, these observations led to the discovery of liquid crystals in 1888, when Reinitzer, an Austrian botanist, noticed an intermediate phase between solid and liquid in cholesterol benzoate[1]. He postulated as to what was occurring between the first and second melting points, and laid the foundations for further work on liquid crystals. In following years, Lehmann and Reinitzer collaborated to study cholesterate benzoate, calling the intermediate phase "soft crystals". The effects noted on polarised light using Lehmann's hot stage microscope were of the type associated with solids, not liquids, so the combination of this behaviour and their flow properties led to the term "liquid crystals", which has been used since. This example of international multidisciplinary work has characterised liquid crystal research from the beginning.

Until World War 2, research into liquid crystals continued apace with over 80 doctoral theses being written on the subject, covering the structure of mesophases, synthesis of synthetic materials, the effects of surfaces on mesophase orientation, and materials exhibiting more than one mesophase. After this, interest in the field waned - perhaps because it was felt science now understood the liquid crystalline phase as a curious phenomena with little by way of practical application.

It was almost another twenty years, in 1958, before the Faraday Society held a conference on Liquid Crystals in response to the renewed interest by scientists concerned with further researching and utilising their unique properties. Following this meeting, much research was carried out on the structural properties of liquid crystals, notably by Wilhelm Maier and Alfred Saupe, which gave a theoretical basis for their use in technological applications; particularly considering the sensitivity of liquid crystals to small changes in temperature, electromagnetic fields, and mechanical stress. This led to the possibility of the liquid crystal display (LCD), which became viable when George Gray synthesised materials with improved stability and the ability to operate at room temperature, leading to LCDs becoming commonplace in the early 1980's. Research now is moving forward on the theory and application of liquid crystalline materials in full-colour LCDs, for non-linear optic applications, as temperature sensing films, as surfactants in oil recovery, in lithography, and as selective solvents.

1.1.2 STRUCTURE

Not all molecules form liquid crystalline phases. For ordered phases to be exhibited, molecules must be capable of arrangement into a variety of structures, and it is thought that indiscriminate synthesis of organic compounds would yield 1 in 200 to show properties of liquid crystalline materials[2].

Two types of liquid crystalline behaviour are known - lyotropic and thermotropic. The liquid crystalline structure of *lyotropic* systems is dependent on the concentration of the molecules in a particular solvent. Many lyotropic systems are amphiphillic, and the interactions between the polar head groups at certain concentrations gives rise to micelles and vesicles. Further increases in concentration allows a combination of these micelles or vesicles to form larger structures, such as the *hexagonal* phase (see Figure 1.1) and the *lamellar* phase, which are liquid crystalline structures in a dynamic relationship with amphiphilic molecules in the surrounding liquid. Temperature also acts to affect these lyotropic phases: At low temperatures, the phases do not form as there is no relative movement of the amphiphilic molecules, and at higher temperatures there is an area where the structures formed are not miscible with the liquid, giving

phase separation. The formation of lyotropic liquid crystals is therefore a fine balancing act of concentrations and temperatures. The most common lyotropic liquid crystalline materials are the soaps and phospholipids.

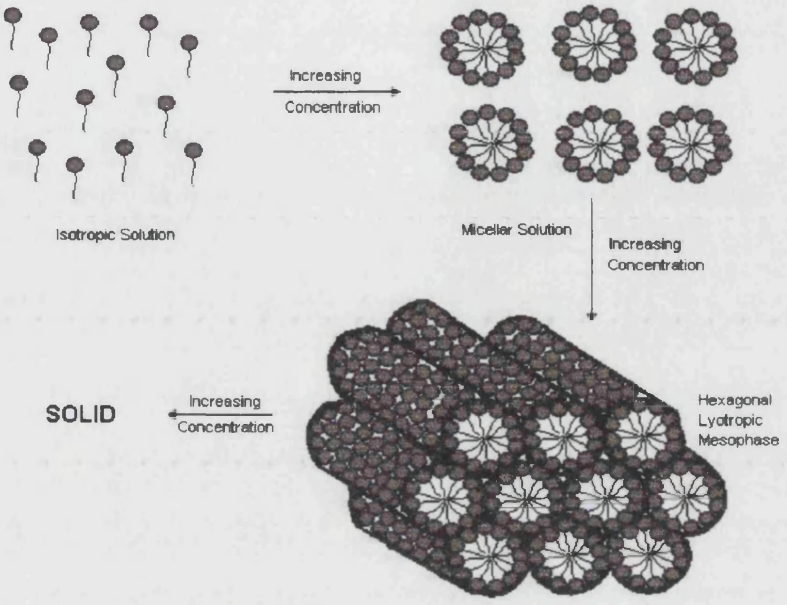

Figure 1.1: Hexagonal Lyotropic Phase Formation

In contrast, *thermotropic* liquid crystals exist in the pure component, and exhibit structural alterations as a function of temperature. Within this classification there are three more sub-classifications; discotic, phasmic and calamitic liquid crystals. *Discotic* liquid crystals are formed from structures with a flat disc-like structure and *phasmic* liquid crystals have a pyramid-like structure. Both may stack in a variety of ways to exhibit their mesophase structures.

The *calamitic* liquid crystals, with which this work is concerned, exhibit a common general shape - they are rod-like molecules with a rigid centre and flexible terminal groups which often exhibit a dipole moment, as represented in Figure 1.2. The rigid centre ensures the molecules are sufficiently linear to remain anisotropic when they rotate within their mesophases. Loss of this rigid centre leads to a loss of linearity reducing the interactions between neighbouring molecules, and hence loss of anisotropy. Hence, such elongated molecules have stronger attractive forces, and tend to exhibit fewer intermolecular collisions, giving rise to more stable aligned phases. At least one flexible terminal moiety is required to allow mesophase behaviour; should the molecule be too rigid, a crystalline phase will be exhibited up to a temperature where thermal motion will overcome the ability of the material to support a mesophase, and direct formation of an isotropic liquid will occur. The majority, but not all, liquid crystals conform to this structure.

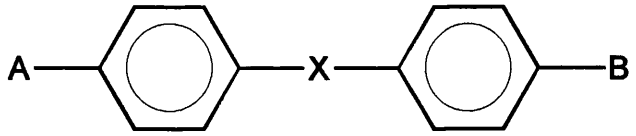

Figure 1.2: Typical Calamitic Liquid Crystal Molecular Structure

Where: A, B terminal units (e.g. CH_3-, C_nH_{2n+1}-, -CN, $-OCH_3$, etc.)
X central linkage (e.g. -N=N-, -C=C-, -COO-)

1.1.3 CLASSIFICATION

A variety of mesophase structures are shown by thermotropic liquid crystals, depending on the orientation of the molecular packing. On heating from the crystalline phase (where the structure exhibits rigid positional and orientational order) a compound may form an isotropic liquid, or pass through a semi-ordered mesophase. To investigate the structure of these mesophases, the most common method used is the hot-stage microscope which allows viewing of the liquid crystal between crossed-polarisers while adjusting the heating of the sample. The optical textures seen through the viewfinder allow classification of the mesophase, with such optical textures arising because of the birefringent properties of the mesophase. In an anisotropic macrostructure, differing refractive indices are shown dependent upon the incidence of light to the axes of the molecule; a phenomenon utilised in LCDs, where the presence of a dipole in the structure allows the application of an electromagnetic field to alter the anisotropy, switching between two distinct optical behaviours. Due to the fluidity of the mesophases, such switching occurs rapidly and sharply making LCDs compact, low-power devices.

On initial heating to the first mesophase transition temperature, a variety of *smectic* mesophases may be shown (for example S_A, S_B, S_C, S_E), where two-dimensional order in both the orientation and positioning of the molecules is exhibited. Although relatively free compared to the solid phase, the molecules arrange themselves into layers and adopt a preferred orientation, though as the molecules are not in a fixed position this preferred orientation is an average function. To determine this average, the order within the structure must be considered at a 'snapshot' in time, in which all component molecules form a three-dimensional angle, the *director*, from an arbitrary plane perpendicular to the long axis of the macromolecular structure. The average angle of the director is therefore a measure of the orientation within the structure with maximum orientational order giving an average angle of 0°, whilst no orientational order gives an average angle[3] of 57°. For studies involving the orientational order within liquid crystalline structures, it is more common to obtain the *order parameter*, S, of the liquid crystal (calculated by equation 1.1), which gives a value of 1 for full average

orientational order reducing to 0 for no average orientational order. Typically values between 0.3 and 0.9 are obtained from snapshots of smectic mesophases containing approximately 10^5 molecules[4].

$$S = \frac{\left(3\cos^2\theta - 1\right)}{2} \qquad [1.1]$$

A variety of smectic phases are observed, depending on the angle of tilt of the molecules within the layers from the director, and distinctive optical textures are given by the action of the liquid crystalline tilt on cross polarised light. This allow assignment of the mesophases formed.

By optical examination, the products synthesised for this research gave only S_A or S_C structures. The S_A phase involves two dimensional ordering of the molecules, where they are arranged into layers to which the director is perpendicular. The mesophase therefore has very little average tilt, allowing the structure to be represented as in Figure 1.3. The S_A phase is characterised optically by the observed focal conical fan texture, comprising a series of batonnets (as shown in Figure 1.4).

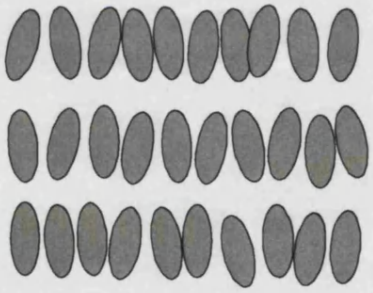

Figure 1.3: Molecular Ordering in the Smectic A Mesophase

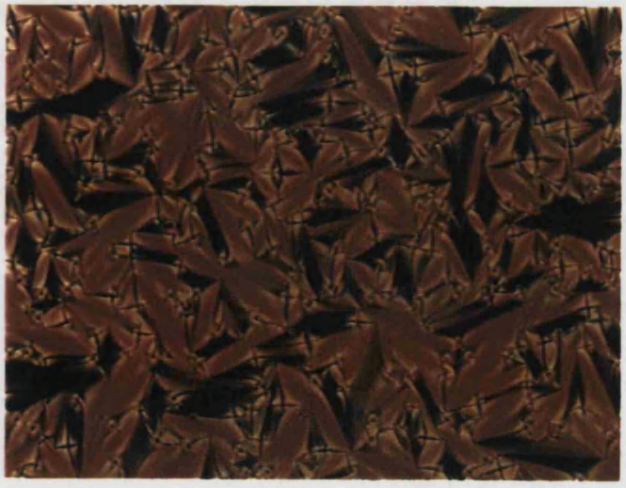

Figure 1.4: Focal Conical Fan Texture of LMM1 at 44°C (S_A Mesophase)

The S_C phase also involves two dimensional order, but the director of the molecules comprising the structure shows a tilt from the layered plane, as represented in Figure 1.5. Optically, the S_C phase mainly exhibits the schlieren texture, where black bands ("schlieren") occur throughout the sample's texture. These originate from point singularities which, in the case of S_C structures, have 4 bands ("bushes") radiating from them. Sanded textures are often observed, where the schlieren texture is small and blurred. Such textures are observed for the materials synthesised in this research, as shown in Figure 1.6.

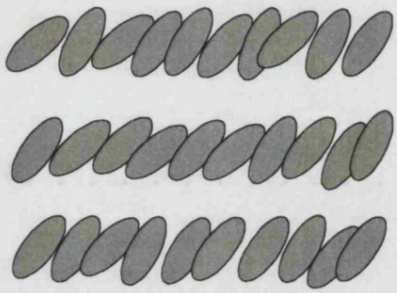

Figure 1.5: Molecular Ordering in the Smectic C Mesophase

Figure 1.6: Schlieren texture of LCP2 at 28°C (S_C Mesophase)

Other smectic mesophases exist, which generally exhibit a higher degree of order in each plane than the S_A and S_C mesophases[5]. This describes behaviour where the molecules are still free to diffuse through the plane, but tend to adopt preferred positioning more often on average. The smectic mesophase is named after the Greek for 'soap', as early research showed these materials to have mechanical properties similar to those observed for soap.

Further increases in temperature may reduce the order of the system further, to show one-dimensional order only. This is expressed by formation of a *nematic* mesophase (represented in Figure 1.7) where there is orientational order but no positional order. The molecules within such a structure show enhanced ability to move over those in a smectic mesophase, but are stabilised into an aligned phase by attractive forces between the elongated molecules and the fact that alignment reduced their tendency to bump in to one another. The nematic mesophase is named after the Greek for 'thread', as the optical textures observed in early research were reminiscent of threads.

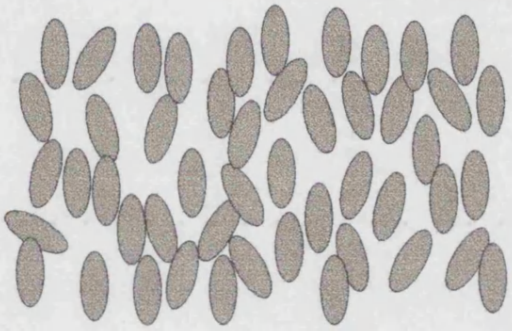

Figure 1.7: Molecular Ordering in the Nematic Mesophase

If a terminal chain incorporating a chiral moiety is present the structure of the nematic mesophase incorporates a helical twist, as the intermolecular forces favour alignment between molecules to be at a slight angle. This causes the director to rotate throughout a length of the structure, as represented in Figure 1.8. The distance in which the director makes one full rotation is known as the *pitch* of the liquid crystal (though it must be noted the twisted structure is repeated twice over the pitch, as the director is defined as pointing in either direction along a particular plane). The chiral nematic phase may also be referred to as the *cholesteric* phase, as this structure was first observed during studies of plant cholesterol derivatives, though this term is considered misleading as very few chiral nematic mesophases are derived from cholesterol. The effect of this helical twist on polarised light gives rise to some interesting optical textures, as shown in Figure 1.9.

Figure 1.8: Molecular Ordering in the Cholesteric Mesophase Over One Pitch Length

Yet further increases in temperature provide sufficient energy for the molecules to adopt random positioning, and behave as an isotropic liquid. The temperature at which this occurs is known as the *clearing point*, as an isotropic liquid has no effect on incident light, and the turbid liquid crystalline solution suddenly becomes clear. Between crossed-polarisers, this is signified by the disappearance of optical texture.

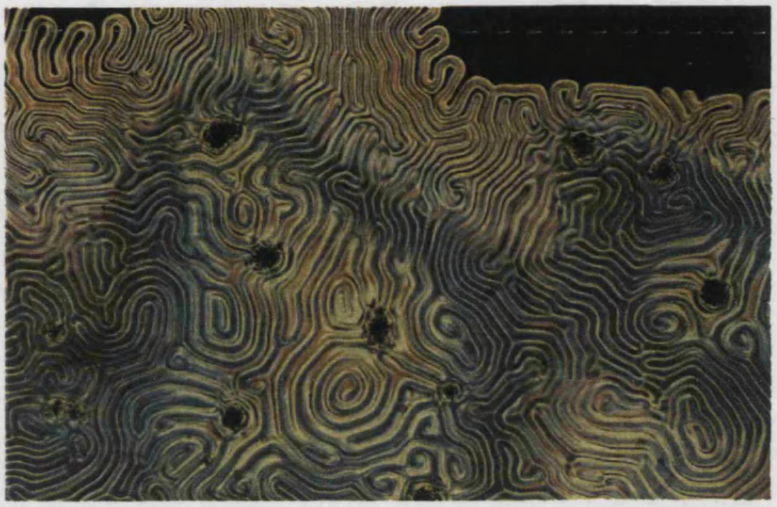

Figure 1.9: Optical Texture of a Chiral Nematic Mesophase[6]

Whilst liquid crystalline mesophases represent an intermediate stage between solids and liquids, experimentation has shown that their structure is actually closer to that of liquids than solids. This is explained by consideration of the enthalpy changes observed on the transition from crystalline → mesophase → isotropic liquid. The DSC thermogram shown in Figure 1.10 follows the crystalline → mesophase → isotropic liquid transitions for octyloxy cyanobiphenyl (8OCB) on both heating and cooling of the sample[7]. Here, the initial crystalline → mesophase transition shows a much greater enthalpy change than the mesophase → mesophase or mesophase → isotropic liquid transition (the former of which is almost invisible, stressing the importance of using DSC in conjunction with other identification techniques).

More energy is therefore required to disrupt the attractive forces holding together the solid phase in order to create a mesophase than is required to disrupt the mesophase to create an less ordered mesophase or an isotropic liquid. This gives rise to a liquid crystalline structure which may be considered as a liquid phase with a small amount of additional order. It is noted that on cooling the mesophase → crystalline transition occurs at a displaced temperature. This is due to supercooling occurring within the mesophase and the contribution of instrumental hysteresis due to the temperature scan rate.

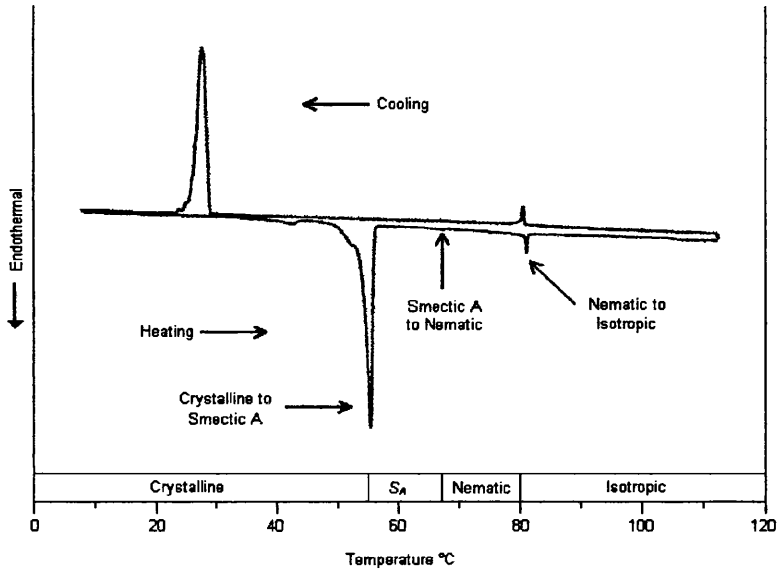

Figure 1.10: DSC Thermogram of a Typical Biphenyl Liquid Crystal

1.1.4 SYNTHESIS

Such molecules may be readily synthesised using standard organic methodologies, during which choice of the central linkage and terminal end groups may be used to engineer the molecules' mesophase behaviour[8]. Major effects on this are caused by the central linkage, whilst terminal chains allow further modification[9].

A breakthrough of particular importance in liquid crystal synthesis was the formation of the biphenyl linkage - direct linking of two aromatic rings - which was discovered by George Gray[10] at the University of Hull in 1973. This gave rise to the cyanobiphenyl family of liquid crystals which exhibit mesophase behaviour at room temperature, and allow the performance associated with liquid crystal displays which are now commonplace.

Liquid crystals may be constructed from smaller molecules using a series of reactions which are applicable to many liquid crystal syntheses. Usually, liquid crystal molecules are prepared in two distinct halves containing rigid ring structures, which are then linked by a rigid, planar central group. For this work, the most common reaction used was esterification, which leads to the formation of an ester linkage[11].

Predictions of mesophase behaviour cannot be made considering the molecular structure alone, though correlations have been attempted for low molecular mass liquid crystals, chiral liquid crystals[12-14] and polymer liquid crystals[15,16]. A more accurate way of controlling properties by molecular structure is by comparison with other liquid crystals in a homologous series. For example, work by Booth *et al*[17] considered the

positioning of fluro-substituents and their effect on mesophase transitions relative to the non-fluorinated parent molecule. These papers, and others[18,19], contain synthetic schemes for the preparation of LCs.

1.2 POLYMERS

Polymers are another development of the chemical industry that have become part of our everyday lives, with many consumer goods and materials being manufactured from polymers both cheaply and in large quantities. The majority of polymer products are carbon-based, with readily available starting materials being derived from the oil industry. Many studies have been carried out on the chemistry and material properties of polymers[20-22], and today's industry can produce products with a strength and durability which rivals and exceeds those of metallic and inorganic materials. Research in this area leads to continual improvements in the quality of available products, and crucially into reducing the cost and environmental impact of the polymer industry.

1.2.1 PROPERTIES OF POLYMERS

Polymers are macromolecules comprising repeating units of smaller "building-blocks" which are chemically linked in order to form a product with useful macroscopic properties. The basic units of the polymer are known as *monomers*, and they are linked by chemical reactions during *polymerisation.* The monomers used may be relatively simple molecules or may be far more complex, but ultimately the macromolecular properties of the polymer depend on the choice of monomer. In addition, the monomers must contain some species of reactive group in order to allow polymerisation. Some examples of monomers are shown in Figure 1.11.

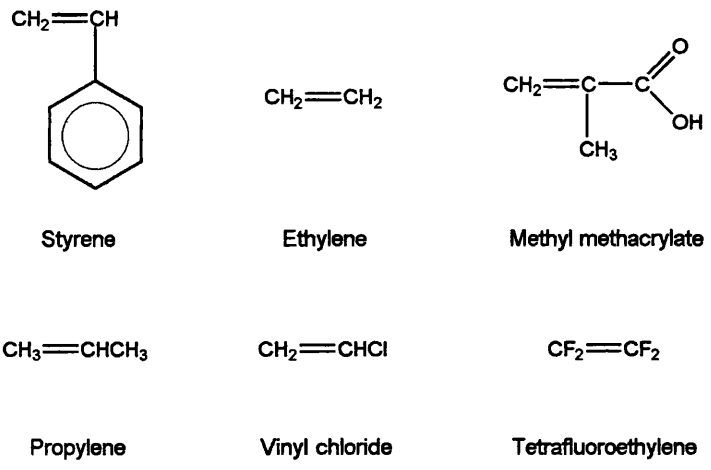

Figure 1.11: Examples of Monomeric Groups

By far the most important commercial polymers are the vinyl polymers, which find wide application from packaging film, through paints and adhesives, to hard-wearing plastics for construction.

The polymerisation reaction may either involve one type of monomer (to give a *homopolymer*), or a mixture of monomers (giving rise to a *co-polymer*, the properties of which are affected significantly by the type and proportion of the individual monomeric components). During mixing of monomer types three co-polymer sequences are possible, as shown in Figure 1.12.

Homopolymer:	X-X-X-X-X-X-X-X-X-X-X-X
Random co-polymer	X-X-Y-X-Y-Y-X-Y-X-X-Y-Y
Alternating co-polymer	X-Y-X-Y-X-Y-X-Y-X-Y-X-Y
Block co-polymer	X-X-X-X-X-X-Y-Y-Y-Y-Y-Y

Figure 1.12: Polymer Sequences

Reactions leading to polymerisation fall into two broad areas. In *addition polymerisation* reactions occur between unsaturated monomers, allowing the rapid formation of high mass polymers by addition of the monomer units to an active chain. This process goes through three stages - *initiation, propagation* and *termination* - and may be activated by free-radicals (as illustrated in Figure 1.13), anions, cations, or co-ordination complexes. During addition polymerisation the chain morphology, co-polymer type, and chain stereochemistry can all be controlled to some extent by choice of monomer and careful control of reaction conditions.

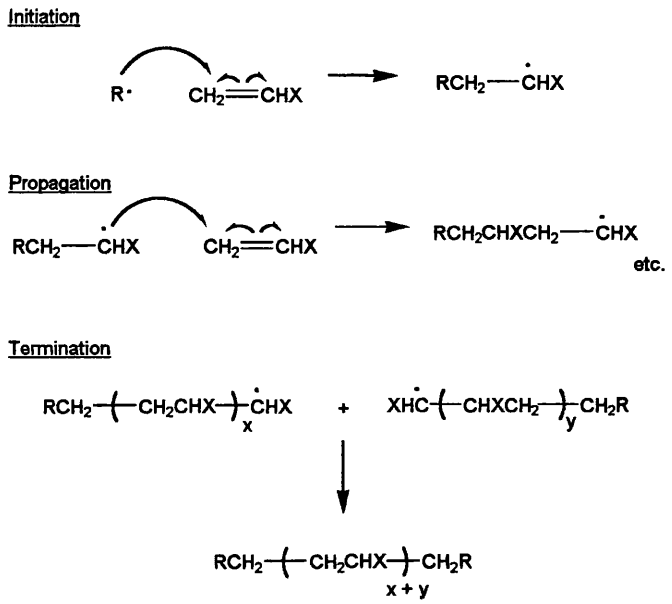

Figure 1.13: Example of Addition Polymerisation

With *step-growth* (or *condensation*) polymerisation, propagation of the chain is accompanied by the loss of a small molecule, such as H_2O or HCl. Figure 1.14 illustrates this, showing the polyesterification reaction leading to the production of "terylene", poly(ethylene terephthalate). The chains grow in a more ordered manner, with the reaction taking a greater time to reach a high molecular mass compared to addition polymerisation.

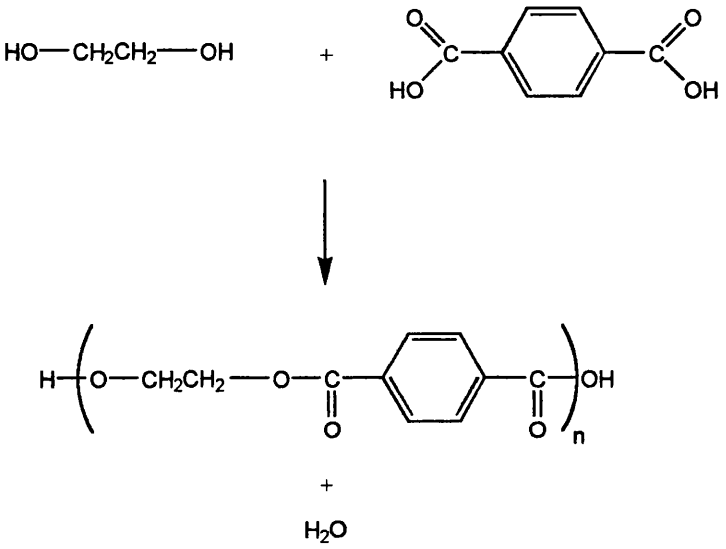

Figure 1.14: Example of Step-Growth Polymerisation[23]

Due to the way in which the polymerisation propagates and terminates, polymer chains of many lengths are formed, so the mass of the polymer is reflected by considering the *number-average molecular weight*, M_n, and the *weight average molecular weight*, M_w. The former is determined by summation of the *mole* fraction times molecular weight, whilst the latter is based on summation of the *weight* fraction times molecular weight. These may be determined using a variety of methods: M_n by *end-group analysis*, *membrane osmometry*, *vapour pressure osmometry* and *refractive index measurements*, and M_w by *light scattering* and *ultracentrifugation*. More commonly, *viscometry* is used to give both M_n and M_w (depending on the calibration sample), and *gel-permeation chromatography* is used as a powerful tool to give both M_n, M_w and the polydispersity of the sample (given as the *polydispersity index*, γ, which is determined by the ratio of M_w:M_n). The molecular weight and polydispersity of the polymer are of particular interest as they relate directly to the polymer's physical properties[24,25].

In addition, chains may adopt a variety of morphologies, as shown in Figure 1.15. The most common morphologies encountered are the *linear* polymers, where the chains have two ends; the *branched* polymers, where side-chains are present in addition to

the main chain; and the *cross-linked* polymers, where the chains are chemically bonded into networks.

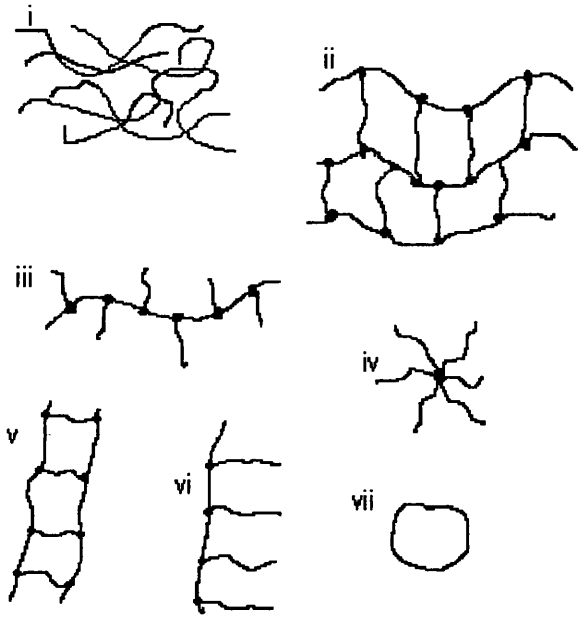

Figure 1.15: The Variety of Polymer Morphologies
(i. Linear; ii. Cross-linked; iii. Branched; iv. Star; v. Ladder; vi. Comb; vii. Cyclic)

In these morphologies long, random coils of the macromolecule align themselves to achieve the most favourable thermodynamic configuration. This leads to the formation of crystalline domains within the polymer's structure, though the time scales required for macromolecules to adopt these configurations usually preclude full crystallisation. Cooling a polymer below the *glass transition temperature*, Tg, prevents chain motion before the polymer has reached an internal equilibrium, and forms an amorphous glassy domain. An increase in temperature above Tg (which may cover a temperature range) is accompanied by a notable increase in free volume and the expression of properties more commonly associated with a "rubber" material.

Branched polymers exhibit many of the properties of the linear polymers, though the branching reduces the ability of the polymer to crystallise, and raises the melting temperature. Cross-linked polymers may be hard and rigid - forming insoluble, infusible thermosets in some instances - or may give rise to elastomers, rubbers etc.

1.2.2 LIQUID CRYSTAL POLYMERS

Liquid crystal polymers were first investigated in the 1970's, with the first side-chain liquid crystal polymer being synthesised by Finkelmann *et al*[26]. Liquid crystalline

polymers generally fall into two categories - the *main chain* liquid crystal polymers and *side chain* liquid crystal polymers.

Main chain liquid crystal polymers incorporate the mesogen along the polymer backbone (as represented in Figure 1.16), and allow orientation along the polymer's chains to give materials of exceptional strength. Examples of these are spiders silk, and Kevlar - frequently used in the manufacture of bullet-proof vests. The materials show phase structures obtained *via* steric hindrance and resonance, though due to the strength imparted to the macrostructure, liquid crystalline properties may not exhibited until temperatures well above those at which the polymer begins to decompose.

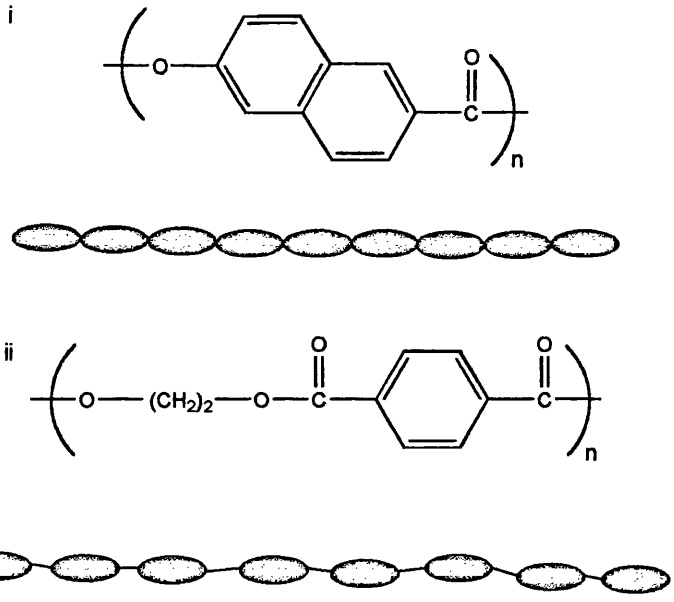

Figure 1.16: Structural Representations of Two Main Chain Liquid Crystal Polymers (i. poly(hydroxynapthoic acid) PHNA ii. poly(p-ethylene terephthalate) PET)

Side chain liquid crystal polymers are of more interest with reference to the more traditional applications of liquid crystals, as they incorporate a flexible spacer unit which allows retention of mesophase behaviour whilst gaining the advantages of stability and robustness associated with polymers. Their synthesis involves the mesogenic units being appended to the polymeric backbone *via* a flexible spacer chain, to give a structure such as that shown in Figure 1.17. The flexible spacer imparts a decoupling effect allowing orientation of the mesogenic groups, and is of crucial importance to the structure/property relationship; spacer chains containing different numbers of carbon atoms greatly affect the mesophase properties of the polymer[27]. Generally, the glass transition temperature decreases with increasing spacer length, with short spacers giving nematic phases, whilst longer spacers show smectic phases.

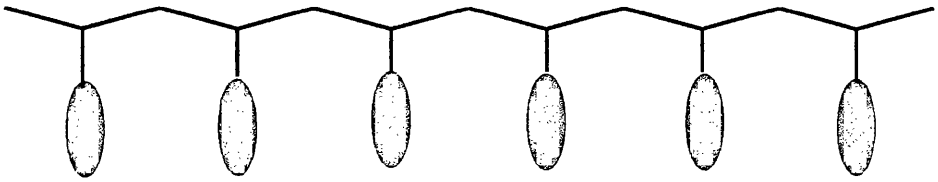

Figure 1.17: Mesogenic Unit Attached to Polymeric Backbone via a Flexible Spacer

Many different types of side chain liquid crystal polymer may be produced by variation of the polymeric backbone and mesogenic unit. Of most use are those with flexible backbones - this allows relatively free motion of the mesogenic units, so liquid crystal mesophase behaviour is exhibited, coupled with the benefits of a processable polymer. Synthesis of side chain liquid crystal polymers is relatively simple, and follows one of two common routes: The polymer can either be formed from a reactive liquid-crystalline intermediate which can be grafted onto a previously prepared reactive polymer in a modification reaction, or synthesised directly from a liquid-crystalline monomer.

For siloxane polymers, the former method is utilised, as backbones containing active groups are readily available commercially. From here, it is a straightforward matter of reacting a mesogen containing a reactive end group to give the desired product. The most common reaction involved here is the hydrosilyation reaction, where a mesogen containing a terminal alkene is attached *via* the polymer's reactive Si-H units using a platinum-containing catalyst, as shown in Figure 1.18. Descriptions of such syntheses - known as the hydrosilyation reaction - have been given by Gray *et al*[28], Gemmel *et al*[29], Ringsdorf[30] and Janini *et al*[31].

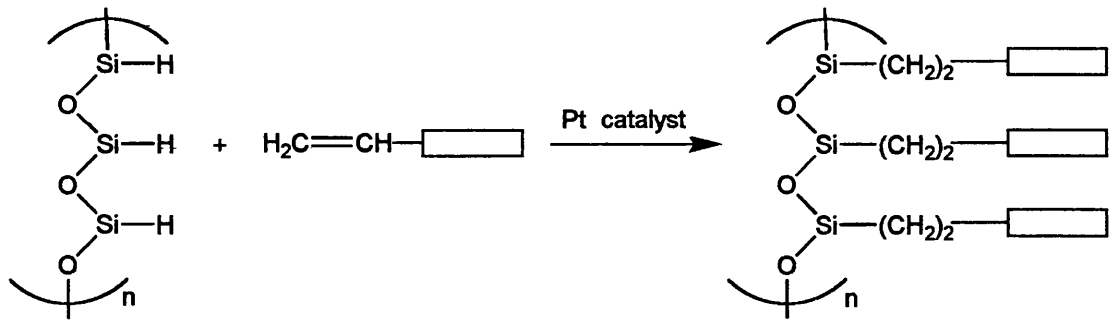

Figure 1.18: The Pt-Catalysed Hydrosilyation Reaction

The latter method allows direct polymerisation of a mesogen containing a reactive end-group. e.g. acrylate polymers may be formed from free radical polymerisation reactions of mesogens containing a vinyl group, as shown in Figure 1.19. This method

does have a major disadvantage - the production of co-polymers may be difficult if the monomers have very different reactivities.

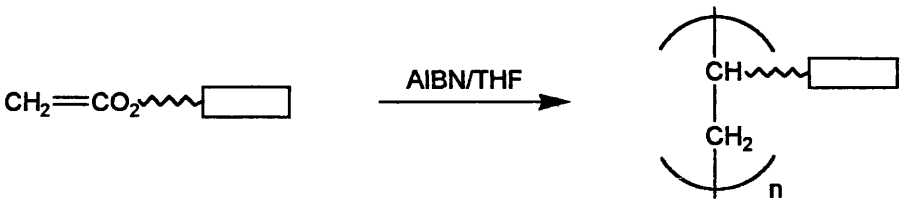

Figure 1.19: An Example of an Acrylate Polymerisation

Depending on the nature of the polymeric backbone, the properties of the polymer may be very different. The siloxane polymer backbone (-O-Si-O-) retains its flexibility even when at relatively high molecular mass and with large side-chains attached, making it ideal for liquid crystal applications. However, acrylate polymers are much less flexible, so can only be used for liquid crystal applications at lower molecular masses or higher temperatures. In general, there is only little change in the mesophase properties of these materials above the addition of tens of monomeric units[32], so most research has been carried out on materials which would be considered oligomeric in comparison to non-liquid crystalline polymers.

In both cases, the purity of the product is of great importance - for many applications a purity >99% is often required. Often, trace catalyst and unreacted starting material remain. It has been shown that the use of freshly prepared catalyst can help to alleviate this situation[33], giving a white polymer as opposed to the discoloured product obtained when stored catalyst is used.

Recent advances include the production of side chain liquid crystal polymers by cationic polymerisation[34]. This allows the production of living systems, which may then be stored and easily modified to give a whole variety of simply prepared liquid crystalline systems.

1.2.3 APPLICATIONS OF LIQUID CRYSTAL POLYMERS

Side chain liquid crystal polymers find applications in the fields of bandwidth filters, non-linear optics[35], doping in electro-optical displays[36] and information storage[37]. They have been used to dissolve metal cations to create "solid" polymer electrolytes[38], and to control the permeation of gasses through a membrane[39]. Finally, they show promise as stationary phases in gas chromatography systems[40]. Main chain liquid crystal polymers find application in high-strength fibres[41]. It is also possible to combine side chain and

main chain liquid crystal polymers to give a variety of unique high-tech materials[42] for which research is continually searching for applications.

1.3 GAS CHROMATOGRAPHY

The analysis of chemical compounds is an important aspect of science, but this can only be achieved if the analytical method allows selectivity between components, or if the analyte of interest has already been isolated. As most analytical methods do not offer such selectivity and analytes are often found within a complex matrix, the separation of analytes is often an essential first step in the analytical process. Such separations can be achieved using many techniques - but one technique offering separation, isolation, quantitation and identification of component analytes is chromatography.

Various chromatographic systems are available - but all share the common use of a stationary and a mobile phase. Components of a mixture are carried through the stationary phase by the flow of the mobile phase, with separations between components being based on differences in their migration rates through the system. The stationary phase may be solid or liquid, supported on solid or gel, and may be packed in a column, spread as a layer, or distributed as a film. The mobile phase may be a gas, liquid or supercritical fluid. The classification of the chromatographic system is dependent upon the types of stationary and mobile phase used.

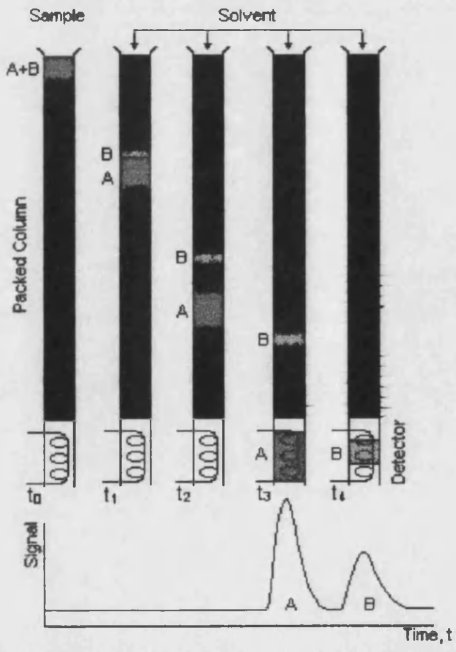

Figure 1.20: Partitioning of Analytes on a Stationary Phase

One of these systems - gas chromatography (GC) - is a separation technique based on the partitioning of an analyte between a gaseous mobile phase, and a liquid or solid stationary phase. When two analytes are injected simultaneously they have different affinities for the stationary phase, and as the carrier gas continues its journey along the column, further partitioning occurs with one of the analytes progressing down the column at a faster rate, as illustrated in Figure 1.20.

Eventually, the result is the separation of the analytes before elution from the column. This elution is then passed through a detector to give a *chromatogram*; a plot of signal against time, as shown in Figure 1.21.

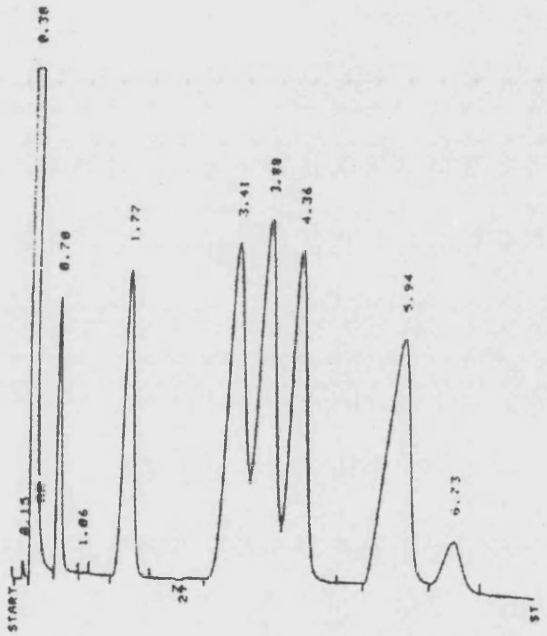

Figure 1.21: A Typical Chromatogram

Gas chromatography was pioneered by James and Martin[43] in 1952, for which they received the Nobel Prize for Chemistry, after modification of the liquid-liquid chromatographic technique first pioneered by Martin and Synge[44] in 1941.

1.3.1 ANALYTICAL GAS CHROMATOGRAPHY

The chromatograms obtained allow both the qualitative and quantitative analysis of injected analytes, making GC the method of choice for many analyses - and perhaps the most widely used analytical method.

Qualitative analysis is based on the retention times of the analyte components, which may be compared to those of known compounds under the same analysis conditions. The presence of unknown peaks indicates the presence of impurities (e.g. contaminants, starting products, side products, or degradation products), and hence this technique is applied in Quality Control, to follow reactions, and in stability and degradation testing - particularly within the pharmaceutical, agrochemical and petrochemical industries.

Quantitative analysis is based on the detector design giving a linear response over a wide range of concentrations so that the area underneath a peak on the chromatogram will be proportional to the amount of analyte present. Accurate work requires calibration by the use of internal or external standards of known composition and concentration. The peak areas for a range of these standards are obtained, and the data used to plot a calibration curve from which the analyte concentration may be determined.

In both cases, the retention times must be known, and they can only be accurately determined if the *dead volume* of the system is known. The dead volume is that volume through which the analyte passes without any interaction with the stationary phase, and is determined by the retention time shown by a non-interacting probe - such as methane. This should be minimised for maximum efficiency.

The type of separation achieved is dependent upon the stationary phase used. For routine analyses the following materials are often used: Squalane (a long chain alkane), polydimethylsiloxane (PDMS), polyethyleneglycol (PEG), polyisobutylene (PIB), and related co-polymers. The choice of stationary phase is largely determined by the volatility, polarity and chemical nature of the analytes involved[45].

More specialised - but increasingly necessary - applications such as the separation of closely related structural isomeric analytes, as well as optical isomers, requires stationary phases capable of separation based on minor differences in molecular shape; a task for which the above examples are not suited. Much work has been carried out on the cyclodextrin series of stationary phases[46-50], with liquid crystals also showing promise[51-53].

1.3.1a Packed Column Gas Chromatography

Two types of column are commonly used in GC work. The original technique - still used for routine analysis of easily resolved analytes - utilises a *packed column* in which the stationary phase is coated onto a solid support (usually diatomaceous earth) and

packed into a column 1-3 meters in length. Many analytes, however, require a greater deal of interaction with the column to effect a good separation. This increase in efficiency can be achieved using a *capillary column*, in which the stationary phase is coated directly onto the internal wall of a capillary tube 25-50 meters in length.

1.3.1b Capillary Column Gas Chromatography

Capillary columns may be produced from metal, glass or fused silica. Metal capillaries have uneven internal walls which cannot be further modified - leading to columns of poor efficiency when liquid crystals are used as the stationary phase. Glass or fused silica are therefore the materials of choice, however active sites (usually Si-OH) often remain on the glass surface causing peak distortions. Such columns must be deactivated before use.

Deactivation may be carried out by several methods, one of which is treatment with HCl followed by precipitation of barium carbonate crystals, making the surface more amenable to liquid crystal deposition[54]. Whilst essential for glass columns, fused silica columns do not require such vigorous preparation - some workers only passing nitrogen through them for several hours at 280°C before deposition of the liquid crystal[55]. A more modern approach is to react the column with "silylating" compounds such as dichloromethylsilane or hexamethyldisilazane to neutralise the polar groups[56]. Once the column has been prepared, one of three methods may be used to coat the column:

Using the *static coating* method, the column is filled with a solution of stationary phase, then sealed at one end. The column is then immersed in a water bath held at room temperature to allow gradual removal of the solvent over 40 hours[57]. This method would be suitable for the deposition of liquid crystals.

Dynamic coating[58] is the simplest but least effective method, where a solution of stationary phase is forced through the column, followed by carrier gas at a low flow rate to remove the solvent. An uneven coating is left, making this procedure unsuitable for the production of a high performance column[59].

"Superdynamic" coating, developed by Berezkin and Korolev[60], forces a solution of stationary phase through the column at high pressure, and subsequently removes the solvent at a much greater rate than in dynamic coating. An even coating is reported due to the high flow of carrier gas removing surplus stationary phase whilst simultaneously evaporating the solvent. With removal of the solvent, the stationary phase viscosity increases which may pose some practical difficulty in its transport down the column.

Whichever method is used in the column coating, one major problem is encountered - the effect of column surface on the orientation of the deposited liquid crystal layer. As the interaction of the liquid crystal stationary phase with the analyte depends on this orientation, the liquid crystal should remain as free as possible. It is also difficult to accurately determine the stationary phase contents of the column, giving rise in discrepancies of up to 20% in some Vg° measurements[61], where Vg° is "The volume of carrier gas per gram of stationary phase required under standard conditions to elute the sample" (as calculated in Section 1.4.3). However, with careful experimental technique, these limitations can be overcome[62].

1.3.2 MONITORING COLUMN PERFORMANCE

In order to assess the analytical suitability of a GC column, a number of values may be obtained directly from a chromatogram (as shown in Figure 1.22) in order to describe the separations obtained.

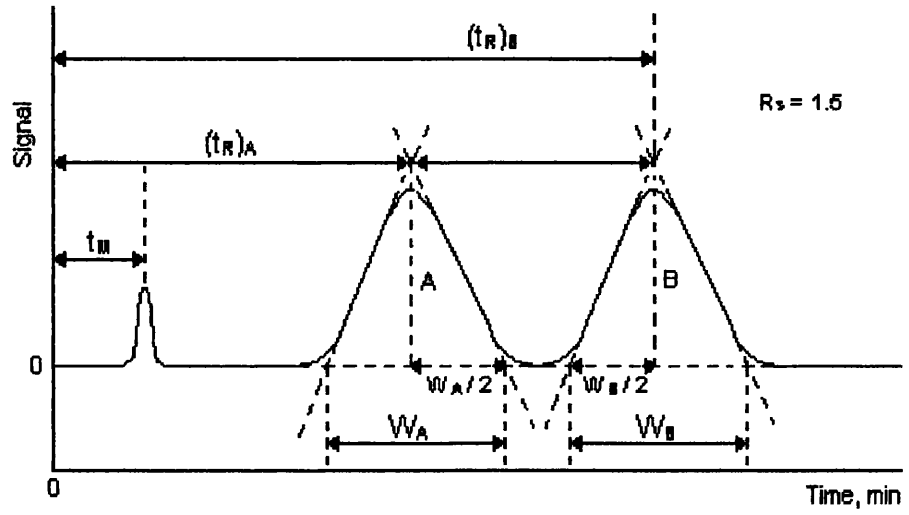

Figure 1.22: Chromatogram Showing Values Used to Calculate Analytical Results

These values allow the determination of the following parameters:

The *adjusted retention time* of the analyte, $t_{R'}$, is calculated simply by subtracting the retention time of a non-interacting marker (t_M) from that for the analyte (t_R), as show in equation [1.2]. This corrects for the dead volume; the residence time in which the analyte does not interact with the stationary phase.

$$t_R' = t_R - t_M \qquad [1.2]$$

From this, the *capacity factor*, k' or K', can be calculated. This is a constant for a particular analyte relating to its migration rate through the stationary phase. It is obtained using equation [1.3].

$$K \text{ or } K' = \frac{t_R'}{t_M} \qquad [1.3]$$

The *selectivity factor*, α, of the column is a measure of its ability to resolve two analytes A and B, and is given simply by the ratio of their retention times, calculated by equation [1.4].

$$\alpha = \frac{(t_R)_B}{(t_R)_A} \qquad [1.4]$$

A better expression of the column performance is the *resolution*, R_S, which gives information of the degree of separation or overlap between adjacent peaks in the chromatogram. This can be calculated using equation [1.5].

$$R_S = \frac{(t_R)_B - (t_R)_A}{0.5(W_A + W_B)} \qquad [1.5]$$

Where W represents the width of the peak at its base. The value of R_S can be related both to the separating power of the stationary phase and its efficiency at giving narrow peaks and minimising spreading. A system showing a resolution of 1.5 gives a complete separation of the analytes A and B. At a resolution of 1.0 there is a 4% overlap, and at a resolution of 0.75 separation is not satisfactory[63].

By analogy with distillation, the column efficiency can be measured by the *number of theoretical plates*, N. This is based on the consideration that the equilibrium of the analyte between the mobile and stationary phases occurs at a series of narrow plates along the length of the column. As the number of equilibrations increases, so the efficiency of the column increases. A high number of theoretical plates is desirable as this will yield more narrow peaks at the same retention time. The number of theoretical plates is obtained from equation [1.6].

$$N = 16\left(\frac{t_R}{W}\right)^2 \qquad [1.6]$$

Where again W is the basewidth of the peak. The number of theoretical plates can be related to column length, L, by defining the *height equivalent to a theoretical plate* (HETP).

$$HETP = \frac{L}{N} \qquad [1.7]$$

The HETP decreases as the column efficiency increases. Values of 2000 - 4000 plates m^{-1} are typical for packed columns[64], whilst efficiencies as high as 30000 plates m^{-1} can be achieved with capillary columns[65].

To increase the resolution for a particular stationary phase the column can be lengthened, which increases the number of theoretical plates. Once all the above properties of the column have been calculated, the *number of theoretical plates required for a desired resolution* may be calculated, since under any particular conditions k' and α remain constant if the column length and number of theoretical plates is increased.

$$N = 16 \cdot R_S^2 \cdot \left(\frac{\alpha}{\alpha - 1}\right)^2 \cdot \left(\frac{1 + K'_B}{K'_B}\right)^2 \qquad [1.8]$$

The corresponding *length of column* required to give the desired resolution using the same stationary phase can then be obtained.

$$L = HETP \cdot N \qquad [1.9]$$

Should the length required be practically unfeasible, a decrease in HETP may be achieved by the use of a more even packing material, a switch to capillary columns, or a decrease in mobile-phase flow rate.

Alternatively, an increase the resolution between two analytes may be effected by an increase in the value of α, and/or the value of k'. α cannot be altered significantly in GC using a particular column; it is normally improved by changing the polarity or composition of the stationary phase which can have drastic effects on the retention characteristics of particular analytes. k' can often be improved by increasing the temperature. However, if the selectivity factor is approaching unity this has little effect.

1.3.3 CHIRAL SEPARATIONS BY GAS CHROMATOGRAPHY

For a molecule to be chiral, it must lack symmetry so as to form a non-superimposable mirror image. A schematic chiral molecule is shown in Figure 1.23, along with its mirror image.

Figure 1.23: A Schematic Chiral Molecule

These two compounds are known as *enantiomers*, and whilst they share a majority of chemical and physical properties, they may exhibit vastly differing chemical effects - shown particularly in biological systems where stereoselectivity is the rule rather than the exception[66]. As, for example, pharmaceutical products become more complex, involving chiral functionalities to promote the desired biochemical reactions, the analytical and purification techniques available to the industry must also be capable of distinguishing between enantiomers for effective monitoring of the synthesis. If even trace amounts of the incorrect enantiomer find their way into the final product, the consequences could be disasterous.

This separation is currently a major problem, as the physical properties on which separations are based are so similar in enantiomeric systems. Some examples of current methods are discussed below.

1.3.3a Indirect Chiral Separations

A common method used to alter the properties of enantiomers to allow their separation to be achieved is to simply derivatise the enantiomers using a chiral reagent. The chemically distinct derivatives (which are now diastereoisomers) may then be separated, and the derivatisation reaction reversed leaving optically pure separated enantiomers.

Unfortunately, this method has two major drawbacks; Firstly, the chemical reagent used in the derivatisation reaction must itself be optically pure, else contamination of the product will result. Secondly, the enantiomers of interest must contain a functionality capable of reversible reaction with the chiral reagent which does not affect the optical activity of either component, and shows an acceptable yield. These factors limit the usefulness of indirect chiral separations somewhat.

1.3.3b Direct Chiral Separations

The limitations in time, expense and accuracy make indirect separations of enantiomers unfeasible for analytical services. A more favourable approach would be to effect direct separations.

As a general rule, enantiomers exhibit identical properties only in achiral conditions[67]. In a chiral medium the individual characteristics of each enantiomer emerge, thus a chiral reagent allows stereospecific interactions to occur. In gas chromatography, enantioselectivity will therefore arise out of differences in specific analyte/stationary phase interactions resulting from the use of a chiral stationary phase[68]. This leads to a difference in Gibbs free energy activity coefficients, and hence a difference in retention time.

For this stereochemical specificity, one commonly employed model[69] requires a "three point" attachment of the analyte molecule. i.e. three of the available groups attached to the chiral centre must interact with the stationary phase. This is represented in Figure 1.24, showing how one enantiomer will interact more favourably due to the positioning of its groups.

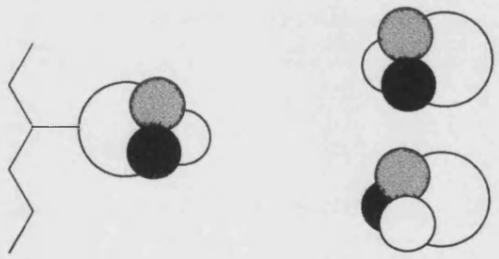

Figure 1.24: Diagram of the Three Point Model

Theoretically, the analytes are thought to form transitory associations with available sites on the stationary phase. These interactions are differentiated due to the steric factors involved with the chiral interactions imparting different energies of solution. Control of the interactions occurring is therefore dependent on the structure of the stationary phase used.

The first successful chiral stationary phases, utilising optically-active amino esters, were the *amide/peptide phases* introduced by Gil-Av[70]. They show good separations for α-amino acids, alcohols, and other chiral compounds exhibiting hydrogen bonding functionalities. However, such columns have an upper temperature limit of 100-140°C, above which there is a loss of selectivity and reduced column life - limiting their use for the analysis of complex pharmaceutical and environmental analytes.

Cyclodextrin phases are undoubtedly the most studied chiral stationary phases, with a number of papers published recently[71-76]. Most of this work has been carried out on the large β-cyclodextrins (example illustrated in Figure 1.25) containing various side-chains attached to their multiple-hydroxyl sites. It is thought that the enantiomeric separation depends on the formation of inclusion complexes between the chiral analytes and the cavity in the cyclodextrin ring. Selectivity may be controlled by the variation of the side-chain substituents, and the size of the ring. Such modifications have been utilised to give cyclodextrins the largest range of enantiomeric separations based on steric interactions. Unfortunately, cyclodextrins are thermally unstable, difficult to fabricate into GC columns (particularly capillary columns) and tend to be specific towards particular species of analyte.

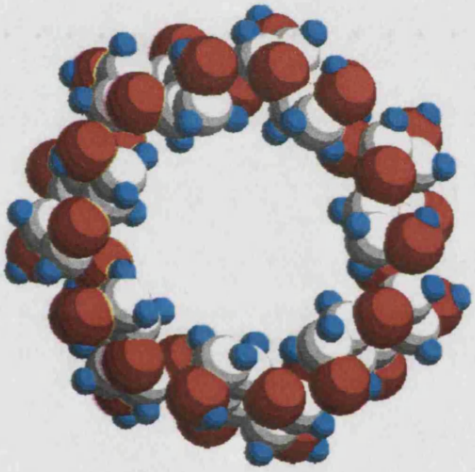

Figure 1.25: β-Cyclodextrin Structure

Polysiloxanes already find widespread use as stationary phases for gas chromatography. They can also be applied in chiral separations with both amides[78] and cyclodextrins being immobilised onto the polymer backbone to impart a greater thermal stability. Chiral groups may also be incorporated directly into the backbone, or crown ethers attached as side chains[79]. The study of *mixed phases*, e.g. side chain liquid crystalline crown ethers on a polysiloxane backbone[80] has also been carried out, but so far with little success.

In order to investigate the suitability of these chiral stationary phases for enantiomeric separation, lists of separation factors for various test mixtures are published[81-85] regularly. These allow development of methods and conditions for specific analyses, and comparative data for research into new stationary phases.

1.3.4 THE USE OF LIQUID CRYSTALS IN GAS CHROMATOGRAPHY

Of most importance to this research are the liquid crystal stationary phases. With some modification, it is thought these systems can overcome the limitations associated with the other chiral stationary phases discussed previously. Low molecular mass liquid crystals were first applied to chromatographic systems by Kelker when he separated o-,m- and p-xylene[86], and their use since has been regularly reviewed[87-89]. But why use liquid crystals as stationary phases?

Within most stationary phases separation occurs due to differences in the rate of partitioning, which is dependent upon the boiling points of the two analytes (assuming there are no specific interactions, such as with polar analytes). Such phases are therefore not suitable for the resolution of relatively non-polar analytes with very similar boiling points - which includes most isomers. Instead, these must be separated on the basis of their molecular structure.

Practical work by Chiavari[90] and Martire *et al*[91] has shown that analytes with a large length:width ratio and planar analytes show greater retention times on liquid crystal stationary phases than do more compact analytes. This is because separations on liquid crystal stationary phases depend on the molecular structure of the mesophase. Dissolution of an analyte into an ordered mesophase requires a greater energy than dissolution into an isotropic liquid due to the spatial limitations imposed by the ordered structure. Interactions therefore occur more favourably with analytes which can interact with the mesophases - i.e. long, planar analytes. It has also been demonstrated that separation increases with increasing mesophase order[92].

Work involving the switching of mesophases under the application of an electric field has been carried out[93]. Electric fields applied across a capillary column improved peak symmetry and increased the retention volume of analytes, suggesting an increase in order of the mesophase improving the partitioning process. This application has not yet been applied to enantiomeric separations, and may well be an interesting future study.

Both low molecular mass and polymeric liquid crystals have been used - the latter improving the temperature range over which the mesophases exist[94]. The most widely investigated polymeric liquid crystals are the polysiloxanes, which combine a wide mesophase range with thermal robustness. In addition, they are also accepted by customers as a wide range of other polysiloxane stationary phases have been used for some years[95-98]. Applications to which liquid crystal stationary phases have been applied include separations of isomers of benzene, alkanes, alkenes, heterocycles,

polyaromatic hydrocarbons, polychlorinated biphenyls, and benoxaprofen isomers, as reviewed by Witkiewicz *et al*[99-102].

1.4 INVERSE GAS CHROMATOGRAPHY

In addition to its analytical applications, Gas Chromatography can be applied to obtaining physiochemical data on the interactions between the analyte and stationary phase. This technique is termed Inverse Gas Chromatography (IGC)[103], as a substance of known physical properties is used to "probe" an unknown stationary phase; the opposite situation to analytical GC where a mixture of unknown analytes are separated on a stationary phase of known properties. IGC was first used to measure the partitioning of organic probes on inorganic and non-volatile organic stationary phases (such as chromatographic supports)[104]. Work still continues into these areas as the results allow the development of improved products for the analytical market, however the technique increasingly finds application particularly in the characterisation of polymers, copolymers and polymer blends[105], and less commonly in the analysis of biological polymers, carbon fibres and foodstuffs[106-109]. The many facets of polymer-probe interactions which may be investigated include transition temperatures, thermodynamics of interaction, interaction parameters, degree of crystallinity, surface properties and diffusion coefficients. Examples of some of these uses may be found in (1.4.7).

The instrumentation used is robust, and the method allows rapid accumulation of data, which is both accurate and precise, at low capital and running costs. IGC also overcomes problems associated with alternative techniques, which are hindered by the intractability of the polymeric sample. The technique is also applicable to molecules other than polymers, with an increasing number of studies being made of low molecular mass moleules[110] and liquid crystals[111].

1.4.1 BASIS OF INVERSE GAS CHROMATOGRAPHY

Historically, IGC was first proposed in 1967 by Kiselev[112], with development of the theory behind the method occurring from 1976 onwards by Smidsrod and Guillet[113]. Most early work on IGC was concerned with the development of methodology and in accounting for non-ideal vapour behaviour and the pressure dependence of the partition coefficient[114]. Early measurements of the activity coefficient were compared with static methods made by Ashworth and Everett[115] and McGlashen and Williamson[116], though such comparisons invited error by extrapolating static data to infinite dilution. Eventually, good agreement was found between static and IGC

results[117], though the use of polymeric stationary phases brought additional problems with some researchers (Summers *et al*[118], Hammers and deLigny[119]) obtaining agreement with bulk measurements for PDMS and PIB, whilst others (Lichtenthaler *et al*[120]) achieved consistently lower values. With improvements in GC systems, and agreed methods of implementing IGC methodology[121] these problems have largely been overcome, and recent studies have shown IGC and static data to be in agreement[122,123], allowing meaningful thermodynamic results to be obtained.

As IGC is primarily concerned with solution studies where the stationary phase is the major component and the probe is the minor component, usually found at an approximation of infinite dilution, the consideration of solution behaviour is necessary in this introduction, with the application of this theory to IGC being detailed in (1.4.3)

1.4.1a Solution Behaviour

Solutions comprise two or more components which, when added together, show miscibility and form a single phase. Such components may be miscible in all proportions (e.g. ethanol and water) or may be immiscible, forming two distinct portions (e.g. benzene and water) unless a large excess of one of the components is present. In order for mixing to occur, there must be an overall value for $\Delta G^{mix} < 0$. Under such solution conditions , it is often difficult to measure the thermodynamic properties which describe the whole system, so the partial molar quantities are described, which for free energy terms involves the *chemical potential* of the component in the mixture, μ_a.

In such systems, the solution behaviour is described in terms of its deviation from that of a pure solvent - eliminating the requirement to have detailed knowledge of both systems from which the final solution is comprised. To aid in the comparative description of such solution behaviour, the *ideal solution* may be defined. There are a variety of methods by which the ideal solution may be described, the most common of which is to state that the ideal solution obeys *Raoult's Law*, which is described by equation [1.10]. Here p_a and p°_a are the partial pressures of component a over the solution and pure liquid respectively, and x_a is the mole fraction of component a. In describing ideal mixing, the total vapour pressure and partial pressures for the components are proportional to the mole fractions of these components - as illustrated in Figure 1.26.

$$p_a = p^\circ_a \cdot x_a \qquad [1.10]$$

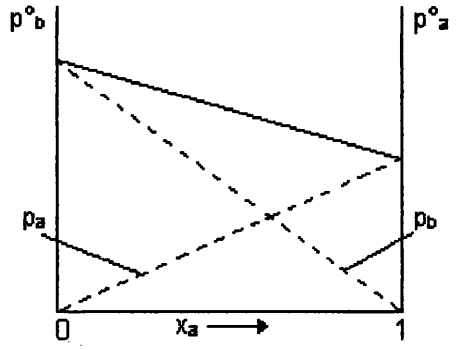

Figure 1.26: Illustration of Raoult's Law for an Ideal Mixture

Some mixtures in which the components have very similar chemical compositions (e.g. methanol and water) obey Raoult's Law well, and it follows that the chemical potential of a solvent in a solution are related by equation [1.11], in which μ_a^{ideal} is the chemical potential of the ideal mixture, μ°_a is the chemical potential of the pure liquid, and R is the gas constant.

$$\mu_a^{ideal} = \mu_a^\circ + R \cdot T \cdot \ln x_a \qquad [1.11]$$

On mixing, ideal solutions may show a change in entropy (due to size differences in component molecules), but no volume or enthalpy change may be shown ($\Delta V^{mix} = 0$ and $\Delta H^{mix} = 0$). This reflects the identical and random nature of all interactions, compared with interactions in the pure solutions, necessary to describe full miscibility. Thus, free energy of mixing an ideal mixture is solely due to changes in entropy, the expressions for which are shown in equations [1.12] and [1.13]. These expressions were developed by Stern[124], considering a lattice model of solution mixing.

$$\Delta S^{mix} = -R\left(x_a \cdot \ln x_a + x_b \cdot \ln x_b\right) \qquad [1.12]$$

$$\Delta G^{mix} = R \cdot T\left(x_a \cdot \ln x_a + x_b \cdot \ln x_b\right) \qquad [1.13]$$

Some binary mixtures approach this model and follow Raoult's Law within experimental uncertainty (e.g. mixtures of benzene and toluene[125]). However, the vast majority of *real* solutions show deviations from Raoult's Law, except where one component is present to great excess (i.e. $x_a \rightarrow 1$). Such real solutions may show negative or positive deviations, as illustrated in Figure 1.27.

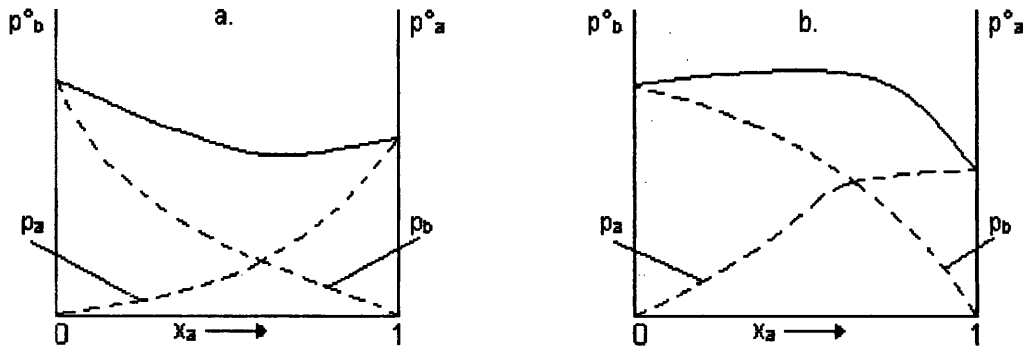

Figure 1.27: Deviations from Raoult's Law
(a - Negative Deviation, b - Positive Deviation)

Where the mixture of two components causes an increase in interaction between the components over that shown in the pure liquids (e.g. the mixing of chloroform and acetone leads to the formation of hydrogen bonding[126]), energy is released and the solution contracts. This is reflected in a negative ΔH^{mix} and a decrease in ΔS^{mix}. This increased association reduces the vapour pressure, and a *negative deviation* from Raoult's Law is shown (Figure 1.27a). Where mixture results in decreased interaction between the components (e.g. the mixing of tetrachloride and methanol acts to disrupt hydrogen bonding[127]), an input of energy is required to form the solution and the solution expands. This is reflected in a positive ΔH^{mix} and an increase in ΔS^{mix} . This reduced association increases the vapour pressure, and a *positive deviation* from Raoult's Law is shown (Figure 1.27b).

Where $x_a \rightarrow 0$ in a non-ideal mixture, Raoult's Law is also obeyed. At such compositions, the partial pressure of the minor component exhibits a linear dependence proportional to composition, though the constant of proportionality differs from the Raoult's Law value, as expressed in equation [1.14]. This equation describes *Henry's Law*, where p_a is the partial pressure of component a over the solution, K_a is the Henry's Law constant, and x_a is the mole fraction of component a. The chemical potential relationship is redefined to the standard state, as described by equation [1.15], where $\mu_a°$ describes a (hypothetical) situation where component a is at *infinite dilution*, where each solute molecule may be considered to be completely surrounded by solvent.

$$p_a = K_a \cdot x_a \qquad [1.14]$$

$$\mu_a^{ideal} = u_a^{\circ} + R \cdot T \ln x_a \qquad [1.15]$$

Deviations from Henry's Law occur when concentrations of solute are reached which allow interaction with other solvent molecules. When considering IGC there is a large excess of polymer (strictly speaking, the solvent), so injection of a small volume of probe (the solute) allows the resulting solution to be described in terms of Henry's Law. Therefore IGC measurements are taken at infinite dilution, allowing representative calculation of other thermodynamic parameters from IGC methodology. Henry's Law is commonly used to describe the solubility of gases in liquids, which allows for the mechanism of gas chromatographic separation to be explained.

The equation of chemical potential obtained for ideal solutions, equation [1.11], is not applicable when deviations from Raoult's Law are observed. Consequently, in order to apply this model to any given solution a variable must be introduced which describes the effective concentration of a component. Such a parameter is described by the *thermodynamic activity* of a component, a, expressed as in equation [1.16]. For ideal solutions $a_a \equiv x_a$, whilst in real solutions Raoult's Law may be re-defined as shown in equation [1.17]. Expressing the activity in terms of the mole fraction of component a gives rise to the *activity coefficient*, γ, which yields quantitative information on the deviation from ideal behaviour for a component in a binary mixture.

$$\mu_a^{ideal} = \mu_a^{\circ} + R \cdot T \ln a_a \qquad [1.16]$$

$$\left(\frac{p_a}{p^{\circ}_a}\right) = a_a = x_a \cdot \gamma_a \qquad [1.17]$$

Considering the negative and positive deviations from Raoult's Law discussed, it follows that a negative deviation where pressures are lower than the corresponding ideal values will show γ_a and γ_b to both be less than one. A positive deviation where pressures are higher than the corresponding ideal values will show γ_a and γ_b to both be greater than one.

Similarly, Henry's Law for ideal dilute solutions may be described in terms of activity, as shown in equations [1.18] and [1.19]

$$\mu_a^{ideal} = \mu_a^{\circ} + R \cdot T \ln a_a \qquad [1.18]$$

$$\left(\frac{p_a}{K_a}\right) = a_a = x_a \cdot \gamma_a \qquad [1.19]$$

The excess chemical potential shown in equation [1.20] is also a measure of deviation from ideal behaviour, and may be related to the activity coefficient considering the relationship in equation [1.21]. This is turn may be introduced to other thermodynamic relationships, for example equation [1.18], to give the resultant expression [1.22].

$$\mu^e = \mu - \mu^{ideal} \qquad [1.20]$$

$$\mu^e = R \cdot T \ln \gamma \qquad [1.21]$$

$$\mu - \mu^e = R \cdot T \ln(x \cdot \gamma) = \ln a \qquad [1.22]$$

As the chemical potential is a partial molar free energy term, equation [1.22] may be described in terms of the excess partial molar enthalpy and entropy of mixing for that particular solution, to give the relationship described by equation [1.23]. This is described, as applied to IGC, in (1.4.5b).

$$\ln \gamma = \left(\frac{\Delta H^e}{R \cdot T}\right) - \left(\frac{\Delta S^e}{R}\right) \qquad [1.23]$$

On introduction to the GC system a solute at infinite dilution will, within a well defined region, partition with the stationary phase. According to Henry's Law two distinct solutes at infinite dilution will exhibit two distinct solubilities in the solvent (stationary phase), and since they are injected at identical partial pressures they are solvated separately to equilibrate in the column. The more volatile component of an analysis mixture will exhibit less solubility than the less volatile component, and will show more 'spread' into the stationary phase. As the mobile phase acts to move the solute along the column, the more volatile component will move at a greater rate than the less volatile component, leading to separation on the column of the two analytes. This suggests GC has a mechanism analogous to that of fractional distillation, where the column may be theoretically divided into segments over which equilibration is successively established. This is the *plate theory* of chromatography, which is the basis for equation [1.6], used as a measure of column efficiency. In reality, this is a simplified theory as the GC system introduces complications in the form of equilibration of the solvent and solute not being instantaneous, diffusion causing peak spreading and the possibility of multiple pathways through the column. These factors are taken into account by the theory proposed by Van Deemter[128], considered in Chapter 6.

1.4.1b Polymer Solutions

The basic thermodynamic theory applicable to polymer solutions was addressed independently by Flory[129] and Huggins[130], who proposed a general solution model where size differences and interaction energies between the solvent and solute both contribute to cause deviations from the ideal solution model. Polymer solutions therefore show large deviations from Raoult's law. This theory, commonly termed *Flory-Huggins theory*, considers a lattice model, dividing the macromolecular chain into segments equal in size to the small molecular component. A consideration of the positioning of these segments on the lattice in order to allow adjacent segments in the chain to occupy adjacent lattice sites allows an expression for the molar enthalpy and entropy of mixing to be derived.

The enthalpy of mixing, ΔH^{mix}, is obtained considering the energy change, w, associated with a single polymer-solvent interaction, and multiplying this by the total number of these interactions. This results in equation [1.23], where Z represents the co-ordination of the polymer in the theoretical lattice, W is the sum of all w terms, n_1 is the number of moles of solvent, and ϕ_2 is the volume fraction of polymer. The parameter Z W may be described in terms of R T by use of the *interaction parameter*, χ, expressed in equation [1.24]. Substituting equation [1.23] into [1.24] leads to equation [1.25].

$$\Delta H^{mix} = Z \cdot W \cdot n_1 \cdot \phi_2 \qquad [1.23]$$

$$\chi = \frac{Z \cdot W}{R \cdot T} \qquad [1.24]$$

$$\Delta H^{mix} = R \cdot T \cdot \chi \cdot n_1 \cdot \phi_2 \qquad [1.25]$$

The entropy change occurring is dependent upon the number of configurations the macromolecular chain may adopt in both the dissolved and undissolved state. Statistical analysis for the mixing of molecules of identical size leads to equation [1.26], where n is the number of moles and x is the mole fraction for each component. However, polymeric solutions impose the restriction that macromolecular groups must be adjacent in the lattice structure. This leads to equation [1.27], which is identical to equation [1.26], though with volume fractions for solvent and polymer replacing molar fractions.

$$\Delta S^{mix} = -R \cdot \left(n_1 \cdot \ln x_1 + n_2 \cdot \ln x_2 \right) \qquad [1.26]$$

$$\Delta S^{mix} = -R \cdot \left(n_1 \cdot \ln \phi_1 + n_2 \cdot \ln \phi_2 \right) \qquad [1.27]$$

Equations [1.26] and [1.27] are often combined to give equation [1.28], an expression for the free energy of mixing between a polymer and solvent.

$$\Delta G^{mix} = R \cdot T \cdot \left(\chi \cdot n_1 \cdot \phi_2 + n_1 \cdot \ln \phi_1 + n_2 \cdot \ln \phi_2 \right) \qquad [1.28]$$

The interaction parameter, χ, shows low values for good solvents and higher values for poor solvents, with a value of χ = 0.5 indicating ideal behaviour. This can be observed in some polymer/solvent systems, should the solution be formed at a particular temperature. Such cases involve solvation with *theta solvents* at the *theta temperature* for that particular system. For example, polystyrene dissolved in cyclohexane shows theta conditions at 34°C, whilst PDMS dissolved in butan-2-one shows theta conditions at 20°C[131].

This theory is widely applied in the study of polymer solutions as it is relatively simple, has few adjustable parameters and explains the large deviations from ideality exhibited by polymer solutions. However, this method imposes some restrictions on the size of a lattice segment, and does not account for size differences of the components due to volume or temperature change on mixing. Such theories have been developed by Prigogine *et al*[132], who describe a *hard-core* equation of state; by Patterson *et al*[133] who utilised the cell model; and by Dee and Walsh[134], who consider a modified hexagonal lattice. Computer simulations based upon the Monte-Carlo model have greatly increased the speed in calculating these theories, and recent papers have contrasted theoretical models with simulation findings[135].

1.4.1c IGC at a Phase Change

Polymers and liquid crystalline materials exhibit phase changes at particular temperatures. For any particular solvent the partition coefficient will undoubtedly change at a phase change, due to the substantially differing physical properties causing differing mechanisms of solvation. As discussed in (1.4.5) the fundamental data obtained from IGC is *via* a plot of ln Vg° *vs* 1 / T, which exhibits changes in slope whenever phase changes occur. Such a retention diagram for a typical semi-crystalline polymer is shown in Figure 1.28. Within each phase there is a linear relationship, though on undergoing a phase transition a disruption of the gradient, followed by re-equilibration, occurs. Braun and Guillet were the first workers to utilise this method to measure glass transition temperatures and melting points of a variety of polymers[136].

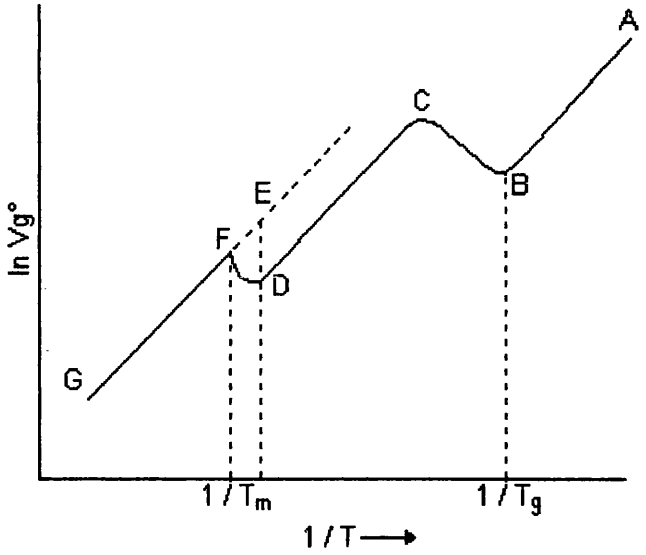

Figure 1.28: Retention Diagram for a Typical Semi-Crystalline Polymer

The section between A and B contains the polymer below its *glass transition temperature*, T_g. The polymer is glassy in this region, and retention of the probe occurs *via* condensation and adsorption of the probe onto the polymer surface as the probe is unable to diffuse into the bulk polymer to any great extent. At point B, T_g is reached and amorphous domains within the bulk polymeric structure may be penetrated by the probe, which exhibits a corresponding increase in Vg° and thus a deviation from the linear plot. Between B and C a non-equilibrium region exists where probe penetration depends on the both the rate of diffusion of probe through the polymer and the carrier gas flow-rate[137]. At point C probe diffusion reaches an equilibrium unaffected by the carrier gas, and plot linearity is again shown. For a semi-crystalline polymer, continued heating eventually leads to the melting of the crystalline regions, the onset of which (at point D) causes another non-equilibrium region where further probe penetration into a more amorphous structure occurs. At point F the *melting temperature*, T_m, is reached at which a wholly amorphous polymer structure exists. Probe penetration again reaches an equilibrium at this point, and the region between F and G only exhibits the isotropic liquid.

Stein *et al*[138] have used these relationships to determine the degree of polymer crystallinity below T_m, as described by equation [1.29]. This method relies on the assumption that the probe only penetrates amorphous polymer regions, with the crystalline regions not contributing to the retention of the probe. The retention time (and hence, retention volume) is therefore directly proportional to the amount of amorphous polymer present.

$$\%Crystallinity = 100 \cdot \left[1 - \left(\frac{Vg^{\circ}}{Vg^{\circ\prime}} \right) \right] \qquad [1.29]$$

This determination is carried out by the extrapolation of the linear segment G to F below T_m (illustrated here by point E) to obtain a hypothetical retention volume, Vg°', for a wholly amorphous polymer at any temperature. A comparison of this with the retention volume actually obtained at that temperature, Vg°, gives the percentage crystallinity. This method is of particular use as the properties of a 100% crystalline polymer do not have to be known, and therefore inaccuracies arising from surface energy effects of different sized crystal regions are overcome.

Whilst the use of IGC to determine phase transitions alone is time-consuming compared with more traditional methods (e.g. DSC), such studies serve as useful comparative tools whilst other data of interest is being collected. IGC experiments may therefore be designed to probe these regions, or to investigate the properties within the various phases without actually investigating the temperature ranges where phase transitions occur. This work has been extended to the measurement of phase transitions in liquid crystalline materials, as mentioned in (1.4.9), and is discussed in relation to this research in (3.2).

1.4.2 INSTRUMENTATION AND LIMITATIONS OF IGC METHODOLOGY

In order to use a gas chromatograph for the determination of physiochemical data, very little modification is required. A typical analytical GC is modified by addition of a manometer to measure the inlet pressure, as shown in (2.3.1).

There must be no dependence of Vg° on column loading, flow rate, or injection volume in order to obtain representative results. Various methods have been employed to overcome these effects; Optimum column loadings are employed for the particular stationary phase of interest, extrapolation of data to zero flow-rates is employed where diffusion through the stationary phase is slow compared to the flow-rate of the mobile phase, and the effect of injection volumes on retention are determined prior to the collection of experimental data.

Packed columns are usually used for IGC study since they are simple to prepare, and the loading of stationary phase may be easily determined. More recently, IGC studies using capillary columns have been carried out, though the columns must be carefully prepared so the amount of stationary phases is accurately known.

Various complications arise from the use of IGC methodology, with such effects having been widely studied by workers in IGC to minimise their impact on the results obtained. There is the possibility of dissolution of the carrier gas in the stationary phase complicating the equilibration model, however carrier gas solubilities have been found negligible[139], so the assumption that the carrier gas is not absorbed may be considered valid. Rather, the main instrumental problems encountered are due to the stationary phase support material in packed column IGC studies; The use of such a support material opens up the possibility of retention mechanisms taking effect between the probe molecules and support material at any support-stationary phase or support-mobile phase interface. In turn this may lead to irreproducible retention, peak tailing, and significant changes in retention behaviour with tiny changes in retention volume. Such effects were first observed by Martin[140] during studies of hydrocarbons on a polar stationary phase, with similar effects being observed for polar probes on hydrocarbon stationary phases. These results were confirmed by static measurements on support-stationary phase systems, as observed by Martire *et al*[141], leading Martin to propose a model where probe-stationary phase and probe-support material adsorption act independently and are additive[142]. The practical outcome of this research was the production of columns with sufficiently large amounts of stationary phase reducing the support material effects to negligible levels. For various polymer systems, column loadings of 5% - 7% w/w have been found effective[143], though this area attracts debate with some workers arguing the necessity for much higher loadings[144].

IGC instrumentation is also readily adaptable to automation, a step which has been investigated by Guillet *et al*[145]. Such automation by electronic and computer controlled instrumentation was found not only to reduce labour and increase throughput, but also to provide more reliable data - particularly concerning parameters where slope determination is required.

1.4.3 FUNDAMENTAL DATA

The fundamental data obtained by IGC is the specific retention volume, Vg°. The interaction between the probe and stationary phase is recorded experimentally as the retention time, t_R. This may be standardised to take into account the flow of carrier gas and the mass of stationary phase used to effect the separation by calculation of the specific retention volume, Vg°, using equation [1.30].

$$Vg^{\circ} = \frac{\left(t_R - t_M\right) \cdot F \cdot J}{W} \qquad [1.30]$$

Vg° is defined as "The volume of carrier gas per gram of stationary phase required under standard conditions to elute the probe molecules".

Where:

t_R	retention time of probe (min)
t_M	retention time of non-interacting marker (min)
F'	corrected flow rate ($cm^3\ min^{-1}$)
J	correction for gas compressibility
W	mass of stationary phase on the column (g)

The corrected flow rate is calculated from the measured flow rate, F, obtained using a soap-bubble flow-meter attached to the column outlet. This measured flow is then corrected to standard temperature and pressure, and for water vapour pressure above the bubble in the flow-meter, using equation [1.31]. The correction factor for gas compressibility is given by equation [1.32].

$$F' = F \cdot \left(\frac{273.15}{T}\right) \cdot \left(\frac{760}{p^\circ}\right) \cdot \left[1 - \left(\frac{p^w}{p^\circ}\right)\right] \qquad [1.31]$$

Where:

T	temperature of flow-meter (K)
p°	measured atmospheric pressure (mmHg)
p^w	water vapour pressure at T (mmHg)

$$J = \frac{3}{2} \cdot \frac{\left[\left(\frac{p^i}{p^\circ}\right)^2 - 1\right]}{\left[\left(\frac{p^i}{p^\circ}\right)^3 - 1\right]} \qquad [1.32]$$

Where:

P^i	pressure at the column inlet (mmHg)

The units of Vg° are $cm^3\ g^{-1}$. The values obtained may then be manipulated using well-known physiochemical relationships to give a range of thermodynamic and other parameters of interest. In order for the results to be reliable, Vg° must not show any dependence on column loading, flow rate, or injection volume. i.e. they must be equilibrium results which do not depend on kinetic factors. Vg° can show dependence on the loading of the stationary phase in the column, as discussed in (1.4.2). Too little coating, and the probe will interact with the support material or surface adsorb at the stationary phase / mobile phase interface. Too much coating, and prolonged use will cause aggregation of the particles on the column - causing practical problems such as

column blocking and pressure build-up. Shillcock[146] found a liquid crystal stationary phase loading of between 8 and 12% is suitable for IGC work on packed columns. Liquid crystalline stationary phases complicate the discussion in (1.4.2) further, as the deposition of liquid crystals on a support material may induce surface effects on the macrostructure compared with that same material in a bulk mesophase. These effects are considered further in (3.2). As the results are required at infinite dilution, the volume injected should also show no effect on the retention volume. To ensure this, a small volume of probe, usually 0.1 - 0.2 μl, is injected. This is also considered for the IGC system used in (3.2).

1.4.4 ACTIVITY COEFFICIENTS

As discussed in (1.4.2), an ideal solution model shows both the probe and stationary phase to be chemically similar, showing zero enthalpy of mixing, and any entropy of mixing due only to any increase in the number of arrangements the molecule can adopt. However, most systems are not ideal. The activity coefficient, γ^{∞}, is a measurement of the deviation of the solution from the ideal model and is therefore indicative of solvent / solute interactions. This theory, as applied to Inverse Gas Chromatography, was developed by Everett[147] who assumed the solute was at infinite dilution in both the mobile and stationary phases so as to give a true thermodynamic equilibrium constant, and therefore be applicable to normal thermodynamic relationships. Further modifications to this model to account for gas imperfections due to molecular forces have since been added[148], with the equation quoted most frequently to relate the specific retention volume to activity coefficients for use with IGC being given in equation [1.33].

$$\ln \gamma^{\infty} = \ln \frac{273.15 \cdot R}{Vg^{\circ} \cdot p_1^{\circ} \cdot M_2} - \frac{p \circ \left(B_{11} - V_1\right)}{R \cdot T} \qquad [1.33]$$

Where:

	γ^{∞}	molar activity coefficient of probe at infinite dilution
	p°	saturated vapour pressure of probe at T (mmHg)
	B_{11}	second virial coefficient of probe at T
	V_1	molar volume of probe at T (cm^3)
	M_2	molecular mass of stationary phase ($g\ mol^{-1}$)
	R	gas constant (8.314 $J\ mol^{-1}\ K^{-1}$)
	T	column temperature (K)

Polymeric stationary phases are often polydisperse, having a poorly defined molecular mass. This makes calculation of molar activity coefficients difficult for polymer

solutions, as equation [1.31] requires an accurate stationary phase mass to calculate the molar activity coefficient. Early work which ignored this resulted in activity coefficients which became increasing dependent on molecular mass as aliphatic chain length increased[149], in contrast to the observed physical properties. To overcome this Patterson *et al* proposed the weight fraction activity coefficient[150], Ω^{∞}, calculated by substituting the probe molecular mass (M_1) for the stationary phase molecular mass (M_2) in equation [1.33], to give equation [1.34]. The use of weight fraction activity coefficients is now standard in the study of polymers by IGC, with the values of γ^{∞} and Ω^{∞} being linked by equation [1.35] where the probe tends to infinite dilution[151].

$$\ln\Omega^{\infty} = \ln\frac{273.15 \cdot R}{Vg^{\circ} \cdot p_1^{\circ} \cdot M_1} - \frac{p \circ \left(B_{11} - V_1\right)}{R \cdot T} \qquad [1.34]$$

$$\ln\gamma^{\infty} = \ln\Omega^{\infty} + \ln\left(\frac{M_p}{M_s}\right) \qquad [1.35]$$

Where: M_p molecular mass of probe molecule (g mol^{-1})
M_s molecular mass of stationary phase (g mol^{-1})

Plots of ln Ω^{∞} *vs* 1 / T, discussed in (1.4.5), give identical gradients to those of ln γ^{∞} *vs* 1 / T, though the intercept must be adjusted by the above factor to allow calculation of excess entropies

1.4.5 ENTHALPIES AND ENTROPIES OF MIXING

The raw data obtained in the form Vg°, γ^{∞} and Ω^{∞} may now be manipulated to give physiochemical information on the stationary phase within the column. These terms (obtained at infinite dilution) are effectively free energy of solution parameters, their relationships being described by equations [1.36] and [1.37].

$$\Delta G_1^{s} = -RT\ln K^{\circ} \quad \text{(where } K^{\circ} = Vg^{\circ}\rho \text{ at temperature T)} \qquad [1.36]$$

$$\Delta G_1^{e} = -RT\ln\gamma \qquad [1.37]$$

Where: ΔG_1^{s} partial molar free energy of solution
K° partition coefficient at infinite dilution
ΔG_1^{e} excess partial molar free energy of solution
ρ density of solvent at temperature T

Such free energy terms may be divided into their enthalpic and entropic contributions, the values of which may be obtained from the appropriate plots of ln K° or ln γ^{∞} *vs* 1 / T.

1.4.5a Solution Properties

The specific retention volume is related to the partition coefficient, so practically Vg° is used in preference as it is readily calculated and does not require extra constants. Vg° and T are related by equation [1.38].

$$\ln Vg^{\circ} = -\left(\frac{\Delta H_1^{s}}{R \cdot T}\right) + \left(\frac{\Delta S_1^{s}}{R + \ln\left[273.15 \cdot R / M_2\right]}\right) \qquad [1.38]$$

Where: M_2 molecular mass of stationary phase (g mol^{-1})

Measurement of Vg° over a wide range of temperatures allows a plot of ln Vg° *vs* 1 / T to be made, giving a linear graph the gradient and intercept of which allow determination of the enthalpy and entropy of solution by application of equations [1.39] and [1.40].

$$\Delta H_1^{s} = -(gradient) \cdot R \qquad [1.39]$$

$$\Delta S_1^{s} = R \cdot \left[(intercept) - \ln\left(\frac{273.15 \cdot R}{M_2}\right)\right] \qquad [1.40]$$

These values give information on the overall solution process, showing the changes in enthalpy and entropy when one mole of gaseous probe molecules condense into solution and mix with the stationary phase. Thus they are a measure of the extent of interaction between stationary phase and probe. Such plots are only linear within a particular phase; different phases show different solution thermodynamics, as discussed in (1.4.1c).

1.4.5b Excess Properties

The relationship between ln γ^{∞} and 1 / T is given by equation [1.41].

$$\ln \gamma^{\infty} = \frac{\Delta H_1^{e}}{R \cdot T} - \frac{\Delta S_1^{e}}{R} \qquad [1.41]$$

Plotting ln γ^{∞} (or ln Ω^{∞}) *vs* 1 / T again gives a linear plot, the gradient and intercept of which may be used to obtain the excess enthalpy and entropy of solution using equations [1.42] and [1.43].

$$\Delta H_1^{\ e} = -(gradient) \cdot R \qquad [1.42]$$

$$\Delta S_1^{\ e} = -(intercept).R \qquad [1.43]$$

If weight fraction activity coefficients are used, the intercept value must be adjusted as described in (1.4.4). These values give information on the deviation of the solution mixture from the ideal, showing the excess enthalpies and entropies required above the ideal solution when one mole of probe gas condenses and mixes with the stationary phase. This allows more precise information to be gained as to the nature of the stationary phase / probe interaction. Again, plots are only linear within a given phase.

Whilst values for the solution properties of mixing will be obtained in cases where even an ideal mixture is approached, the existence of excess properties give quantitative information on the deviation of mixing from the ideal model. For mixtures which are very similar in their chemical composition, excess properties will therefore approach zero.

1.4.6 INTERACTION PARAMETERS

The Flory-Huggins interaction parameter, χ, discussed in (1.4.1b) may be determined at this point, and is of particular interest for polymeric stationary phases. Its calculation from IGC may be described by equation [1.44]. This equation requires the molar volumes of the probe and stationary phase at column temperature, which may be derived by knowledge of the density of the probe (ρ_1) and stationary phase (ρ_2) at each temperature using equation [1.45]. This data is not readily available for the liquid crystalline systems used, so χ values will not be calculated during this study.

$$\chi^{\infty} = \ln\Omega^{\infty} - 1 + \left(\frac{V_1^{\circ}}{V_2^{\circ}}\right) + \ln\left(\frac{M_1 \cdot V_2^{\circ}}{M_2 \cdot V_1^{\circ}}\right) \qquad [1.44]$$

$$\chi^{\infty} = \ln\Omega^{\infty} + \ln\left(\frac{\rho_1}{\rho_2}\right) - \left(1 - \left[\frac{V_1}{V_2}\right]\right) \qquad [1.45]$$

1.4.7 APPLICATIONS OF IGC

By far the most utilised application of IGC in recent years has been the study of interactions between probe molecules and polymeric stationary phases. Early studies were employed on stationary phases of use within chromatography, though later studies mainly concern the many polymeric materials with other industrial applications. Properties that may be studied include transition temperatures[152], degree of crystallinity[153], diffusion coefficients[154], and surface properties[155]. There has also been much work carried out on the thermodynamic properties of polymer blends[156] in a bid to understand and improve polymer-polymer miscibility.

Early studies were mainly centred on the comparison of IGC methodology with other techniques employed at the time to ensure accuracy and precision of the method. With particular importance to the extended application of IGC were the studies by Lichtenthaler *et al*, who compared the behaviour of PIB stationary phases in both packed and capillary columns[157]. The results obtained showed discrepancies between the columns, thought to occur due to slower diffusion of probes in the capillary column, which showed a thicker film due to their smaller surface area compared with the packed column. Lichtenthaler *et al* overcame these limitations by obtaining retention volumes over a range of flow-rates, and extrapolating to zero - a method which gives accurate results when the retention volume / flow-rate relationship is linear[158]. Thus, this method has become standard in the application of IGC to capillary chromatography.

Adsorption isotherms of cellulose acetate have been calculated using IGC by De Vries *et al*[159] by extracting the amount of gas adsorbed and partial pressure above the stationary phase surface from the area under the chromatogram, considering the run conditions. This methods has also been used to study polyamide and polystyrene systems by Sa and Serena[160], and Kontominas *et al*[161] respectively. Surface interactions have also been widely studied using IGC by Schreiber and co-workers, with their work covering styrene-butadiene rubbers below Tg[162], surface energy variations of polycarbonates[163-166], and more recently the surfaces of liquid crystals[167]. Surface analyses have also been carried out on pigments and wood pulp fibres by Hegedus[168], and Jacob and Berg[169] respectively.

Polymer solubility parameters, despite offering only a rough guide to polymer miscibility, are widely used industrially. Methods of obtaining these parameters using IGC have been developed by Guillet *et al*[170-173] by measuring the interaction parameter, χ^{∞}, for various probes with differing solubility parameters and resolving these using a variation on the Flory-Huggins interaction parameter and the Hildebrand-Scatchard

theory. Further work in this area has been carried out by Price[174], and the method has been extended to include other non-volatile stationary phases[175].

Pioneered at the University of Toronto in 1973 by Gray and Guillet[176], IGC was then used for determination of diffusion coefficients of antioxidants in polyethylene systems[177] in order to monitor the migration of stabilisers in a bulk polymer - work of interest to the packaging industry. Little work on diffusion was carried out by IGC following this initial research, with traditional methods, such as gravimetric vapour sorption/desorption, being used preferentially. However, as these methods rely on sorption and bulk equilibration they are error-prone when considering slow diffusion or when the solvent is present in small amounts. IGC studies restarted again during the late 1980's and early 1990's, when papers were written on diffusion of ε-caprolactam in nylon 6 to improve processing[178] and on cross-linked polymers[179], as use of solvents at infinite dilution gave meaningful, accurate results. Work was also carried out on the theoretical modelling of the diffusion process[180], and in evaluating the IGC method for measurement and prediction of diffusion coefficients[181].

Current work also extends into the analysis of binary polymer stationary phases, in which polymer-polymer interactions are studied. The polymer may comprise either or both parts of the binary mixture[182], or may be a co-polymer[183]. The majority of work in this area has involved probe behaviour, with other work concentrating on the prediction of retention behaviour. This latter application is being researched in order to develop standard polymers which may be mixed to give the separation behaviour desired by the chromatographer for a particular analytical methodology, and has been reviewed by Price[184]. This method has proven effective in studies by Purnell and Laub[185], where the retention described in an additive manner from the retention behaviour of the pure components - as expressed in Equations [1.46] and [1.47] - has lead to binary systems showing a reasonable approximation to the experimental results.

$$Vg^{\circ} = Vg_1^{\circ} \cdot w_1 + Vg_2^{\circ} \cdot w_2 \qquad [1.46]$$

$$K = K_1 \cdot \phi_1 + K_2 \cdot \phi_2 \qquad [1.47]$$

Another growing area for IGC is in the study of crystallisation kinetics of the stationary phase, determinations more commonly followed using optical methods[186] or DSC[187-189]. Initial studies were carried out by Stein *et al*[190] on polyethylene samples, though their work was not described in terms of any theoretical models. More recent work has been based on the crystallisation theories of Avrami[191], which have been used to describe crystallisation in main-chain liquid crystal polymers[192, 193] and low molecular mass liquid crystal materials[194].

1.4.8 STUDIES OF LIQUID CRYSTALS BY IGC

Whilst IGC research into liquid crystalline systems comprises only a small percentage of papers published, some studies have been carried out mainly in conjunction with analytical studies using liquid crystalline stationary phases.

Liquid crystals have also been mixed to obtain eutectic compositions in order to increase the temperature over which mesophases are formed. This often leads to a lower crystalline → mesophase transition temperature, which may be utilised for analytical purposes[195]. The mesophase range may also be extended by the use of polymeric liquid crystalline materials, and recently work has been carried out by Janini and Laub, whose MEPSIL (mesogenic polysiloxane) materials[196-200] have shown promise in the separation of PAHs. There have also been studies on LCPs with acrylate polymer backbones[201].

IGC also allows determination of the mesophase transition temperatures in mesogenic systems due to disruptions in the linear gradient on the retention diagrams, as well as the thermodynamic parameters in each mesophase. Such research has been carried out by Price and Shillcock[202,203], who measured the transitions in a range of low molecular mass and polymeric LCs and found these to be comparable to transitions measured by more traditional methods. This work built upon the research of Guillet *et al* into phase transitions of non-mesogenic polymers, discussed in (1.4.2c).

Diffusion measurements in polymers by IGC, as discussed in (1.4.8), have received scant attention, with even fewer research groups studying diffusion in liquid crystalline materials by IGC. Medina is the exception, having examined diffusion in smectic, nematic and isotropic phases of cholesteryl myristate[204] and 4,4'-bis(heptyloxy)azoxybenzene[205]. This area leaves much scope for research, particularly in adding to the understanding of the behaviour of liquid crystals as stationary phases and in the permeation of gasses[206].

1.5 THESIS CONTENTS

The purpose of this thesis is to outline the programme of research into the applications of liquid crystals and liquid crystalline polymers to gas chromatography - describing the results both in terms of the observed analytical properties of the liquid crystal stationary phases, and of their solution properties. The diffusion of analytes through the liquid crystals, and use of the results obtained will be considered, and suggestions of suitable

systems for further study will be made. The work will therefore move the study of liquid crystalline stationary phases a step further than has been previously considered.

1.5.1 AIMS AND OBJECTIVES

The aims and objectives of this work were:

- To describe the preparation of IGC instrumentation and methodology to elucidate meaningful results with respect to liquid crystalline systems. This covers such areas as probe selection, physical effects, determination of transition temperatures, and comparison of IGC studies on known systems to previous literature studies.

- To extend the use of IGC to the study of a variety of low molecular mass and polymeric liquid crystalline systems, developing a theory of how solution properties of liquid crystals and liquid crystal polymers are affected by the presence and state of mesogenic moieties, using PDMS as a reference polymer.

- To examine the analytical performance of these mesogenic systems by GC, and describe the observed results in terms of the thermodynamic interactions between the samples and stationary phase. Samples used include aliphatic, aromatic and isomeric structures.

- To investigate the diffusion properties of analytes in liquid crystalline stationary phases, in order to enhance the description of their separation.

- To discuss and conclude the mechanisms involved, and thus suggest probable mesogenic structures which may exhibit enhanced selective properties when used as an analytical stationary phase for GC.

Chapter Two:

EXPERIMENTAL METHOD

The major experimental techniques involved in this project were the synthesis of the liquid crystals and their application as GC stationary phases. For the initial phases of the work, liquid crystals were supplied by Merck, with further work requiring the synthesis of novel liquid crystalline materials.

2.1 LIQUID CRYSTALS

During the initial stage of studies, Merck synthesised and provided four low-molecular mass liquid crystals in order to give an idea of the factors of importance in the separation process. The fluro-substituted samples were BDH509 (chiral) and BDH770 (racemic), while the samples containing two chiral centres were BDH849 (chiral) and BDH1029 (racemic). The structures and properties of these are given in Figure 2.1. Transition temperatures are those quoted by Merck, with no dependency noted on their optical purity.

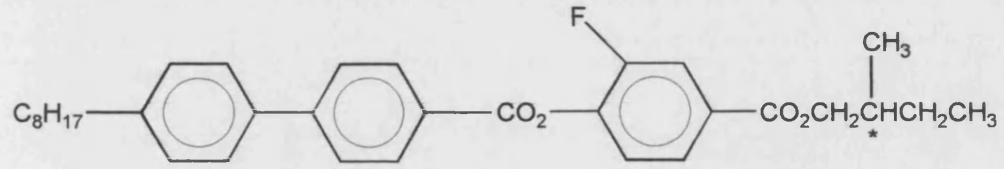

BDH509 - chiral **BDH770** - racemic

K → 57°C → S_C → 111°C → N → 151°C → I

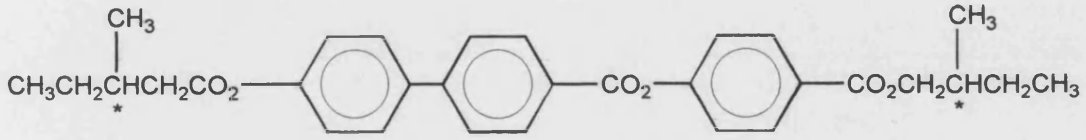

BDH849 - chiral **BDH1029** - racemic

K → 103°C → S_C → 118°C → I

Figure 2.1: Supplied Liquid Crystalline Structures for Initial Research

This initial stage of research led to some ideas as to the liquid crystalline properties required to further this study (discussed in Section 5.2). To commence work on polymeric systems a sample of LCP1 was provided for study by Merck. This polysiloxane containing a 2-ringed mesogenic side chain exhibits the structure and measured properties shown in Figure 2.2.

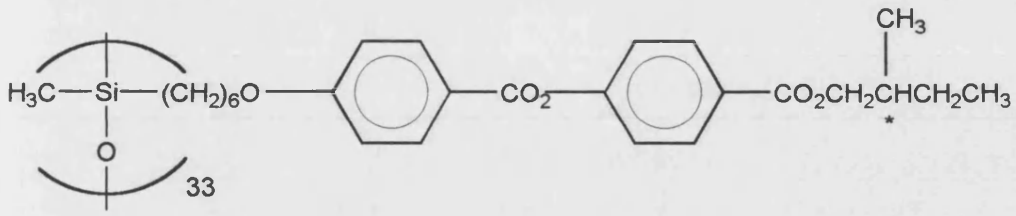

LCP1

M_w; 26560 M_n; 15170 M_w/M_n; 1.75

Transitions: Tg; -19.4°C $S_C \rightarrow$ 62.6°C $\rightarrow$ I

Figure 2.2: The Structure of LCP1

In order for comparative studies to be carried out, the synthesis of a series of molecules with structures similar to LCP1 which exhibit mesophase behaviour was carried out, as described in *Appendix One*. Analogous low molecular mass structures containing 2 aromatic rings were also synthesised, as were 3-ringed structures. All liquid crystal structures synthesised and used in this research are shown in Figure 2.3, and all materials were synthesised to be optically pure.

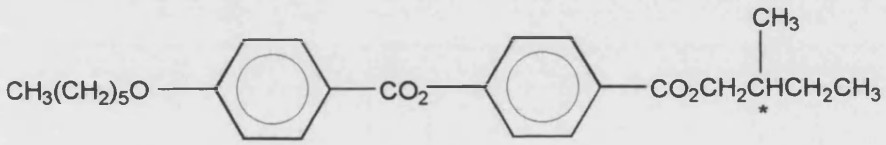

LMM1

Transitions: K $\rightarrow$ 39°C $\rightarrow$ $S_C \rightarrow$ 52°C $\rightarrow$ I

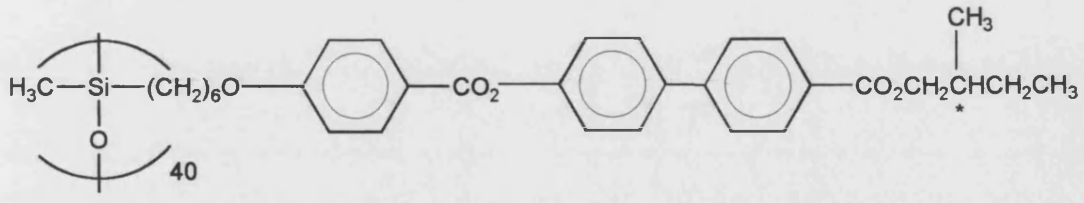

LCP2

M_w; 33200 M_n; 14100 M_w/M_n; 2.34

Transitions: Tg; 22°C $S_C \rightarrow$ 226°C $\rightarrow$ $S_A \rightarrow$ 238°C $\rightarrow$ I

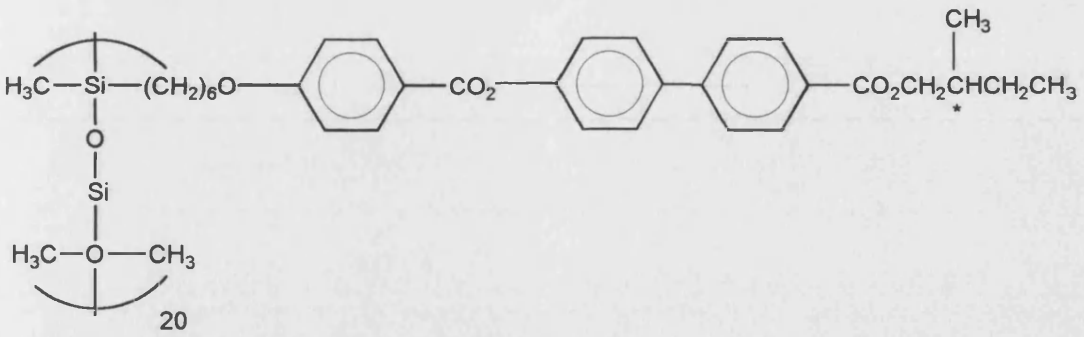

LCP3

M_w; 23300 M_n; 12500 M_w/M_n; 1.85

Tg; 4°C $S_C \rightarrow 191°C \rightarrow I$

Figure 2.3: Liquid Crystalline Structures Utilised in this Research

2.1.1 MATERIALS

Reagents used were of standard reagent grade, obtained from Aldrich, BDH or Fisons. Toluene for the hydrosilyation reaction was dried over molecular sieve before use. The hydrosiloxane polymer (40 active units) and co-polymer (20 active units) were obtained from Dow Corning, with low molecular mass impurities having been removed previously by distillation. Other intermediates used had previously been synthesised and characterised in the liquid crystal research department at Merck.

2.1.2 INSTRUMENTAL METHODS

During the syntheses carried out, various instrumental methods were used to determine the extent of reaction and purity of products obtained.

High performance liquid chromatography (HPLC) is a liquid-liquid chromatographic technique where a sample is carried through a column by a liquid mobile phase, and partitioned with a liquid stationary phase to effect a separation. It is commonly applied as an analytical technique, and in this case was used to follow the extent of reaction for non-polymeric syntheses. A Hewlett-Packard HP1050 instrument was used under the following conditions: Column temperature, 40°C; mobile phase MeCN:H_20 (80:20 ratio) initially, ramped to MeCN after 10 minutes; Flow rate, 2 cm^3min^{-1}. Detector wavelength, 254 nm.

Gel permeation chromatography (GPC) is a variation of liquid chromatography, where the mobile phase carries the sample through a porous stationary phase. Molecules are then separated according to size - smaller molecules are retained within the pores, and

therefore elute at longer retention times than larger molecules, which pass through the column relatively unhindered. The technique is primarily used in polymer analysis to determine the molecular weight, polydispersity and purity of a polymeric analyte. A Gilson 303 GPC instrument was used, attached to a Keithley 175 multimeter. The column used was a 10 cm PLgel 5 μm mixed C column, calibrated with respect to polystyrene standards. The mobile phase was THF at a flow rate of 1.5 cm^3min^{-1}, with each sample having a small volume of toluene added as an internal standard. Molecular weights were calculated using a spreadsheet macro developed at Merck, which utilises the Mark-Houwink relationship to compensate for the differences between the polysiloxane sample and polystyrene standards.

In this research, *infra-red spectroscopy* was used to follow the progress of the hydrosilyation reaction[207]. The Si-H bond of the unreacted polymer gives a distinct peak at 2160 cm^{-1}, so from comparison with the peak area for the initial reaction mixture the remaining amount of unreacted polymer may be estimated. When the Si-H bond was no longer visible, it was assumed that full substitution had occurred. The instrument used was a Perkin Elmer 883 IR spectrophotometer.

Differential scanning calorimetry (DSC) delivers heat to the sample and an inert reference to maintain them at the same temperature. When a phase transition occurs there is a difference in the amount of heat provided to the two cells, which is measured to give a thermogram (plot of heat flow *vs* temperature). The transition temperatures may then be assigned, and the enthalpy of transition measured as this is proportional to the peak area. A Perkin Elmer DSC7 instrument was used, incorporating an intercooler and associated software.

The *hot stage microscope* is an essential tool in the classification of liquid crystalline mesophases. It is essentially an optical microscope modified to place the sample between two crossed polarisers on a 'hot stage' to allow adjustment of the sample temperature. Plane polarised light enters the sample, and interacts with the anisotropic liquid crystalline macrostructure, where it is rotated according to the mesophase. The rotated light then passes through the other polariser and is viewed by eye. The action of the liquid crystal on the polarised light gives distinctive patterns depending upon the mesophase the sample is in, as discussed in Section 1.1.4. The temperature of the hot stage can be adjusted to allow the transitions to be viewed, and therefore to assign mesophases at various temperatures. The instrument used in this research was a Olympus CH2 polarising microscope incorporating a Mettler FPS hot stage. Optical textures were determined by eye, and then captured using a JVC TK 1085E video camera and a Sony UP-3000P video printer.

Nuclear magnetic resonance was employed to ensure the required liquid crystalline structures were successfully synthesised. The instrument used was the Jeol GX270/EX400 NMR.

Mass spectrometry (MS) is one of the most versatile analytical tools, giving both qualitative and quantitative information on the atomic and molecular composition of analytes. The sample is introduced to the instrument where it is volatalised and fragmented, and the fragments passed into a mass analyser. This separates the fragments according to their mass / charge ratio, and upon detection allows a mass spectrum to be constructed (plot of signal intensity *vs* mass / charge ratio). This can then be interpreted to give the molecular masses of the sample and its associated fragments. The instrument used in these studies was the JEM100-CX.

2.2 ROUTES TO COMPOUNDS EXHIBITING LIQUID CRYSTALLINE BEHAVIOUR

Here follow the basic schemes used for the synthesis and characterisation. *Appendix One* contains details of the methodology used to synthesise the materials used in this research.

2.2.1 ESTERIFICATION

The esterification reaction, shown in Figure 2.4, is a convenient way of linking two groups to form a large molecule capable of liquid crystalline behaviour, and with the correct selection of R and R' groups acts to form a liquid crystalline molecule. The reaction is simple, relatively safe, and produces a very good yield of the final product.

Figure 2.4: The Esterification Reaction

The general procedure for the esterification reaction is as follows: The carboxylic acid was dissolved in dichloromethane (DCM) in a round-bottomed flask, and placed under nitrogen. Trifluroacetic acid (TFAA) (molar excess) was dissolved in DCM, and added dropwise to the reaction mixture with constant stirring. The reaction mixture was then left for an hour, stirring constantly. A stoichiometric amount of alcohol was dissolved in

DCM, and added dropwise to the reaction mixture over a period of 2 hours. The reaction mixture was then left stirring overnight under nitrogen.

Water was added to the reaction mixture, and left stirring for an hour to wash the organic phase. The organic phase was then separated and washed with a further 2 x 100 cm^3 portions of water. The organic phase was dried using sodium sulphate, and analysed by HPLC. If starting products or impurities were detected, they were removed using a silica column - a step which was repeated as necessary until the product was HPLC pure. Finally, the solvent was removed by rotary evaporation to leave a solid product, which was dried in a vacuum oven at 40°C overnight.

2.2.2 RADICAL POLYMERISATION

Monomer, azo-isobutylnitrile (AIBN) initiator, and tetrahydrofuran (THF) were combined in a round-bottomed flask. The reaction mixture was degassed by the application of a vacuum followed by the slow input of nitrogen. This step was repeated 3 or 4 times, and a positive pressure of nitrogen left above the mixture. The reaction mixture was then heated to 60°C, and left to react overnight.

The extent of polymerisation and purity of the product was determined by GPC. Initially, the reaction mixture was poured into excess cold IMS where the polymer precipitated out, was filtered off, washed in cold IMS, and analysed by GPC. If over 1% impurity remained, the polymer was taken up in 20 cm^3 DCM and re-precipitated from 150 cm^3 cold IMS.

2.2.3 THE HYDROSILYATION REACTION

As discussed in Section 1.2.2, the synthesis of a side chain liquid crystal polymer with a siloxane backbone is carried out by the modification of a pre-formed reactive polymer backbone using the hydrosilyation reaction. The general procedure followed for the hydrosilyation reaction follows.

The polymethylhydrosiloxane was dissolved in dried toluene in a round-bottomed flask. The alkene was then added, and the reaction mixture stirred. As the reaction is oxygen sensitive, the reaction mixture was degassed by application of a vacuum followed by the slow input of nitrogen. This step was repeated 3 or 4 times, and a positive pressure of nitrogen left above the mixture. The catalyst was then added, and the reaction mixture brought to reflux with constant stirring, and left to reflux overnight.

At regular intervals the reaction mixture was cooled, a small sample taken, and the extent of reaction determined by IR and GPC. If reaction required more time, the reflux was resumed (after degassing), and more catalyst added if necessary. Approximate reaction time was 72 hours.

When the reaction had reached completion the polymer was purified. Toluene was removed using a rotary evaporator until 20 cm^3 remained. This was then poured into cold IMS, where the monomer dissolved into solution, and the polymer precipitated out as a white powder. The polymer was removed by filtration, rinsed in cold IMS, and analysed by GPC. If over 1% of alkene remained, the polymer was taken up in 20cm^3 DCM and re-precipitated from 150 cm^3 cold IMS. Approximately 4 reprecipitation steps were required to give a pure polymer.

2.3 GAS CHROMATOGRAPHY

Two gas chromatographs were utilised throughout this work - the majority of measurements being carried out using a packed column system, with additional analytical measurements being made using the more efficient capillary column.

2.3.1 PACKED COLUMN GAS CHROMATOGRAPHY

The instrument utilised extensively for this work was the Pye Unicam 204, adapted to enable inverse gas chromatography by attachment of a mercury manometer (accurate to ±1 mm Hg) to the column head. The signal recorded by a flame ionisation detector (FID) was recorded using a HP3394 integrator. The packed column resided within the GC oven, the temperature of which was constantly monitored to ±0.1 K using a digitron thermocouple which had been calibrated against a Tinsley Type 5840 platinum resistance thermocouple between 293K and 353K in an isothermal water-bath. A schematic diagram of the instrumentation is given in Figure 2.5.

Once the apparatus had been assembled, nitrogen carrier gas was passed through the system at flow rates between 14 - 32 cm^3min^{-1}, with any leaks being detected and eliminated prior to injection of the probes. Results were obtained over a range of increasing temperatures to avoid supercooling effects, with at least 15 minutes being left for the column to equilibrate at each oven temperature before injection of the probes.

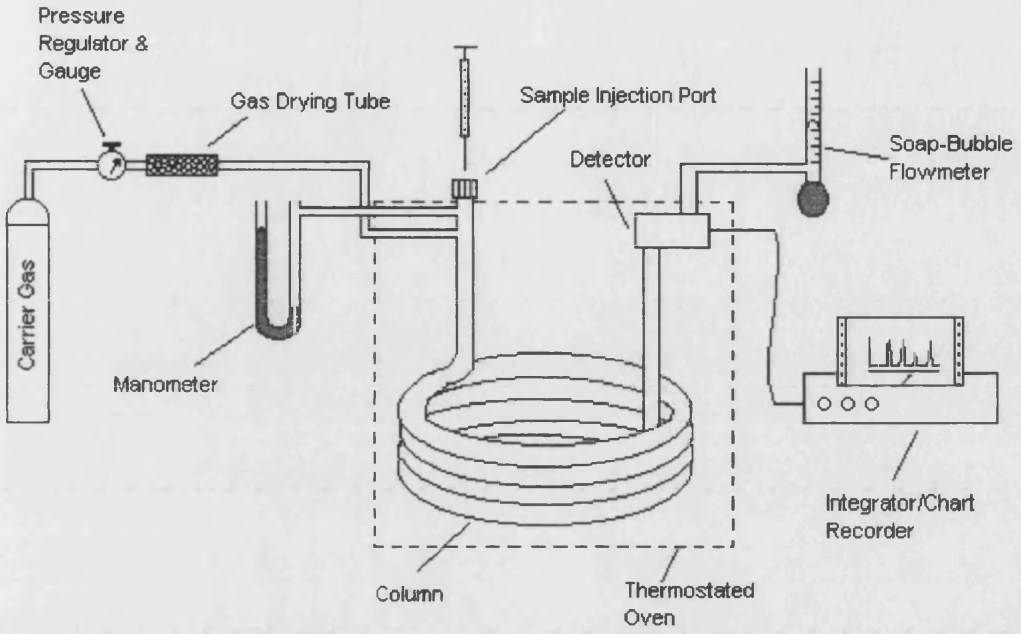

Figure 2.5: The Gas Chromatography System

Packed columns were prepared using PDMS, BDH 509, BDH 770, BDH 849, BDH1029, LMM1, LCP1, LCP2 and LCP3. Approximately 10% stationary phase loadings were required. In order to achieve this, approximately 1 g of material was taken up in approximately 40 cm^3 of chloroform - just enough to cover the 10 g of Chromosorb W used as the support material. This support had previously be subjected to soxhlet extraction with chloroform for 24 hours to ensure removal of soluble impurities which might interfere with chromatographic separations.

The support was added to the stationary phase solution, mixed well, and the solvent slowly removed using a rotary evaporator - which also acted as a continuous agitant to ensure thorough coating of the packing material. The resultant material was then dried in a vacuum oven at approximately 30°C overnight, until two consecutive weighings showed no further loss of solvent. Copper columns were then prepared by cutting copper tubing with an internal diameter of 6.5 mm to approximately 144 cm in length, and thoroughly washing with hexane, acetone and ethanol to remove any grease and impurities remaining from their production. They were then dried and coiled, one end of the column being plugged with silyanised glass wool, covered with a gauze and attached to a vacuum pump. The packing material was inserted at the other end *via* a funnel. Upon insertion of the packing material the length of the copper tubing was agitated to ensure even packing. After packing the vessel containing packing material was re-weighed, and the difference in weight before and after taken as the amount of packing material in the column. From this, the proportion of stationary phase on the column could be calculated.

Finally, the open end of the column was plugged with glass wool, and screw attachments added. Before use the columns were conditioned overnight in the GC system by passing nitrogen through them at a temperature 10°C above the phase transition giving an isotropic liquid - too low and conditioning would not be effective; too high and the stationary phase would bleed from the column. The columns were then ready for IGC and analytical studies to be undertaken.

Table 2.1 summarises the preparation stage for the liquid crystalline phases used, and shows the mass of stationary phase present on the column, for use in calculation of physiochemical parameters.

Stationary phase material	Mass material used / g	Mass support material used/ g	% Loading	Mass stationary phase used / g	Mass material on column / g
PDMS	1.125	10.084	10.04	8.365	0.840
BDH509	0.972	9.432	9.34	9.879	0.923
BDH770	0.966	10.136	8.70	7.005	0.610
BDH849	0.974	9.872	8.98	8.373	0.752
BDH1029	1.011	10.158	9.05	8.479	0.768
LMM1	1.021	10.414	8.93	10.809	0.965
LCP1	1.042	9.568	9.82	8.626	0.847
LCP2	1.221	11.220	9.82	9.927	0.975
LCP3	1.143	11.270	9.21	8.370	0.773

Table 2.1: Mass of Materials Used in Packed Column Preparation

2.3.2 CAPILLARY GAS CHROMATOGRAPHY

Initially, the untreated fused silica columns (15 m x 0.25 mm, supplied by Supelco) were deactivated by sucking a 10% solution of dichloromethylsilane in dichloromethane through the column. This was repeated twice, followed by drying of the tube at room temperature overnight. The extent of deactivation was monitored on the capillary gas chromatograph (Analytical Instruments GC93) using a test mixture of butane and methanol at 50°C. With these analytes, untreated columns retain methanol with respect to butane, and show extensive peak tailing for methanol. Deactivation allows co-elution, and improves peak symmetry.

Using the static coating method, the concentration of solution required to give a particular film thickness can be calculated from equation [2.1][208].

$$V_L = 2 \cdot d_f \cdot \frac{100}{r} \qquad [2.1]$$

Where: V_L concentration of stationary phase in solution (%w/v)
d_f film thickness required (μm)
r internal radius of capillary (μm)

For general purpose separations on a column of 0.25 mm i.d. (i.e. r = 125 μm) a film thickness of 0.25 μm is commonly employed[209]. Therefore, a 0.4% w/v solution (i.e. 4 mg cm^{-3}) of liquid crystalline material in dichloromethane is required. This solution was prepared and sucked through the capillary column under vacuum using the same apparatus as used in the deactivation stage. The columns were then conditioned overnight at 10°C above the clearing point of the liquid crystalline material, and used to measure the analytical properties of the column.

There are three main problems with ensuring the capillaries had been coated properly. Firstly, it is necessary to determine the *mass* of liquid crystalline material deposited - a very small change in a large overall mass. Gray and Guillet[210] measured the length of a plug of solution entering and leaving the capillary column to calculate the amount of solution deposited on the column walls, and hence give the column loading. Alternatively, the use of a very accurate balance capable of detecting small changes in mass before and after coating would give the mass deposited. In this case it is crucial that the solvent has been completely removed from the column. The second problem is the confirmation of *film thickness* and uniformity throughout the column. This was carried out by examination of a cross-section of the coated column using a scanning electron microscope. Cross-sections taken at various intervals along the length of the column confirmed uniformity. However, this method is destructive, and was only carried out after the column had been utilised. Finally, as the separation on the liquid crystalline phase is highly dependent on the mesophase structure, any *disruption* of this structure by surface interaction with the wall of the column - a common phenomenon in liquid crystal studies[211] - would affect the performance. Studies have found that this is not a measurable problem provided the liquid crystalline film thickness is greater than approximately 0.1 μm[212].

2.3.3 PROBE SELECTION

A varied choice of probes was made to reflect the linear alkanes (Figure 2.6) and simple aromatic probes (Figure 2.7) traditionally used in IGC[213], along with probes exhibiting slight structural differences, and isomers (Figure 2.8).

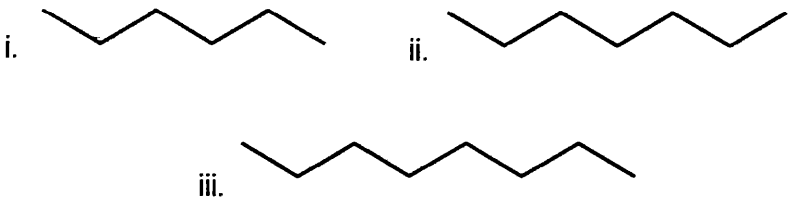

Figure 2.6: Aliphatic Probes
(i, hexane; ii, heptane; iii. octane)

The choice of isomeric probes (diastereoisomers and enantiomers) and branched probes was largely governed by ease of availability and proven use in literature studies[214-219], though studies were conducted on a range of possible structural types to select those with optimum performance on the GC system. Chiral alcohols (the most commonly available enantiomers) and the cyclic ketones were found to be unsuitable, showing severe, unacceptable peak tailing and multiple integrations. However ketones, esters, and haloalkanes all gave reasonable retention times and peak shape, which lead to the choice of methyl-2-chloropropionate as the chiral probe used.

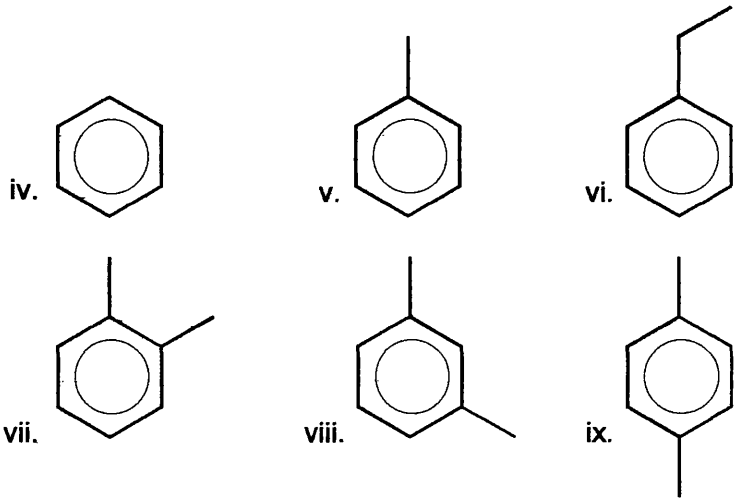

Figure 2.7: Aromatic Probes
(iv. benzene; v. Toluene; vi. Ethylbenzene; vii. o-xylene; viii. m-xylene; ix. p-xylene)

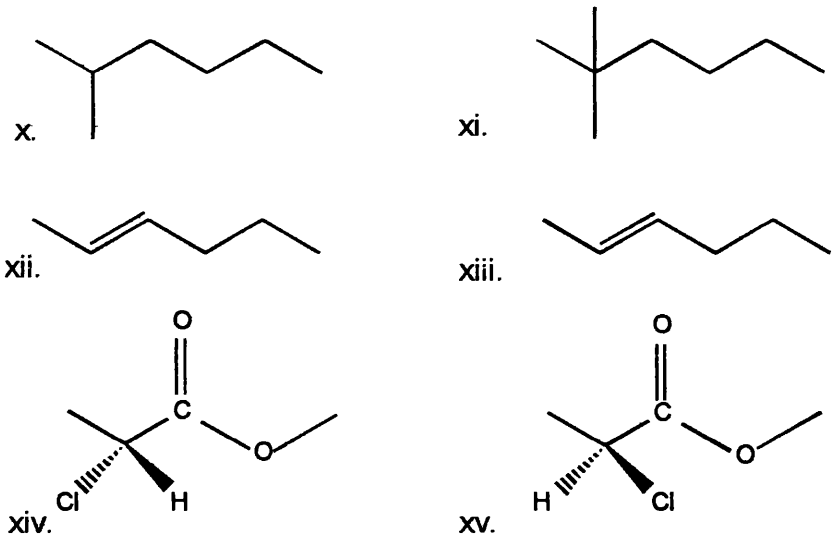

Figure 2.8: Isomeric Probes

(x. 2-methylhexane; xi. 2,2-dimethylhexane; xii. cis-hex-2-ene; xiii. Trans-hex-2-ene; xiv. R(+)-2-methylchloropropionate; xv. S(-)-2-methylchloropropionate)

Chapter Three:

PRELIMINARY IGC WORK

In order to undertake a study of liquid crystals and liquid crystal polymers by Inverse Gas Chromatography, it is necessary to ensure that the systems and methods used enable representative physiochemical results to be obtained. In the case of the method and systems studied, the final results obtained depend upon:

- Choice of probe (as discussed in 2.3.3)
- Loading of material on the stationary phase
- Injection volume of probe
- Effect of supercooling
- Transition temperatures

This chapter therefore considers each of these parameters in turn, and describes the practical methodology adopted to ensure accuracy and precision in the final results.

In addition, the physiochemical and analytical performance observed for PDMS using IGC methodology is described here. PDMS is a commonly-employed GC stationary phase, and the basis for the liquid crystalline polymers studied. Results obtained from PDMS therefore act as a reference for discussion throughout the remainder of the thesis.

3.1 OBTAINING MEANINGFUL RESULTS *via* IGC METHODOLOGY

The methodology employed for IGC studies is simple and the data obtained gives rise to a very wide range of physiochemical measurements. There are, however, some practical considerations to be made to ensure the results obtained are accurate and precise. Two of these factors which play particular roles in the research undertaken here are the effect of stationary phase loading, and the volume of probe injected into the system.

3.1.1 EFFECT OF STATIONARY PHASE LOADING

Obtaining the minimum stationary phase loading on the support material to produce meaningful results is a prerequisite in the development of any chromatographic system, as the materials used are often expensive or available only in small quantities. However, too little coating and the effects observed will be due to interaction between the probe and the support material - giving inaccurate results. Various methods may be employed to overcome these effects, such as treatment of the support material by silanes[220], but the problem may be solved more simply considering the loading of stationary phase on the support material. It has been determined[221] that a stationary

phase loading of 4% w/w gives retention that is affected by probe interaction with the support material. Increasing the loading to between 8-10% w/w shows satisfactory performance for IGC. Further increases to 14% w/w show satisfactory performance in the short term, but after periods of continual use partial blocking of the column can occur - leading to high back-pressures. Unpacking of such supports also shows the material to no longer be free-flowing, but to have formed agglomerations of particles.

The considerations described on column loading were based on the need to obtain full coverage of the support material to avoid unwanted interactions. It is also important in studies of liquid crystalline materials to ensure that the integrity of the mesophase structure remains when the material is coated onto a stationary support. There is a strong possibility of disruption to this structure occurring as it is a well known phenomenon that the deposition of liquid crystals on a thin film acts to align the molecules with the surface. Indeed, this is the basis for certain liquid crystal display devices[222]. It has been shown by Rayss *et al*[223] that modification of the liquid crystal properties by the support surface takes place to a distance of approximately 2 nm from that surface. In further work on the effects of such alignment, Marciniak and Witkiewicz[224] showed that above 5% w/w loading of a liquid crystalline stationary phase on the support material the liquid crystal transition temperatures are identical (within experimental uncertainty) to those determined by other means. Thus, whilst there is still further work to be undertaken to fully understand the effect of a support material on liquid crystal alignment, the use of a high loading minimises such effects.

In this research the use of stationary phase loadings of approximately 10% w/w on a Chromosorb W support material minimises the effects of both probe interaction with the support material, and effects on the liquid crystal alignment from the support material.

3.1.2 EFFECT OF INJECTION VOLUME

On a packed column in which all support material has been effectively coated with stationary phase, the retention volume of the probe is related to its distribution between the gas phase and the liquid phase. If the volume of probe injected is of *finite dilution* (i.e. of relatively large volume) then after initial mixing of the probe with stationary phase, further portions of the probe interact with the probe molecules already present - leading to probe/probe interactions and a Langmuir-type isotherm, rather than probe/stationary phase interactions. This in turn leads to peak tailing (particularly for polar probes), irreproducibility of retention, and inaccurate physiochemical results. Whilst finite dilution IGC is not the method by which work in this thesis was undertaken, it does find use with many researchers in the description of adsorption isotherms for a variety of materials[225-227].

Practical methods of overcoming such effects have been considered by Card *et al*[228], who in studies with a PIB stationary phase proposed a correction factor to overcome inconsistencies in both injection volume and stationary phase loading by the extrapolation of results to infinite dilution. This work demonstrated that on a column with sufficient loading and small enough injection volume, the results obtained were identical to those calculated after extrapolation, and could therefore be considered "true" results.

In order to ensure all probes used in this research gave infinite dilution physiochemical parameters, repeated injections were made onto a column containing BDH509, with variation in the injection volume. Across the volume range 0.01 μl - 5.0 μl, the probe retention volume varied within experimental uncertainties associated with the methodology, giving peaks approximately gaussian in shape and of reproducible retention. Thus a 0.1 μl injection volume was decided upon for all measurements carried out in this study, as this balances an infinite dilution for accurate determination of results with a volume which may be reproduced experimentally.

3.1.3 SUPERCOOLING EFFECTS

Supercooling is a well-known phenomenon in liquid crystalline materials. The mesophase changes occurring on heating a thermotropic liquid crystalline material have been described. However, on cooling the identical material the mesophase may be retained below the transition temperature noted on heating. Whilst supercooling in the inter-mesophase transitions has been found to be relatively insignificant, large hystereses have been noted around the mesophase → crystalline transition, and it is widely considered that the existence of the supercooled region is due to kinetic factors on re-alignment of the mesophase to that of a crystalline structure[229]. This supercooled mesophase has been applied to analytical gas chromatography[230] as the kinetics of crystallisation for liquid crystalline materials impart a stability on the phase of a few days. It was originally thought that the supercooled mesophase exhibited identical properties to its original higher temperature mesophase, but studies have shown that this is not the case - with aromatic probes showing marked changes in retention behaviour in such phases[231].

With respect to this study all work was carried out in the mesophases exhibited on heating the thermotropic materials, as the supercooled mesophase has not to date been fully characterised. This was achieved by, after initial conditioning of the column above the clearing temperature of the stationary phase material, allowing the column to cool for a few days. On use in IGC methodology, the column was then allowed to

equilibrate in the GC oven before probe injection, and only heating of the oven was used to achieve the temperatures at which data was collected.

3.2 DETERMINATION OF TRANSITION TEMPERATURES USING INVERSE GAS CHROMATOGRAPHY

The dynamic technique of differential scanning calorimetry (DSC) is the method of choice in many determinations of transition temperatures within polymeric systems. For the study of liquid crystalline materials, classification of the mesophase and supplementary information on the transition temperatures are obtained utilising the hot stage microscope, as discussed in (1.1.3). Both of these methods have been used to assign the transition temperatures of the materials used in this research. However, in addition to the determination of physiochemical properties, Inverse Gas Chromatography may also be used as a static method to assign the transition temperatures of polymers, as described in (1.4.2c).

Little work has been carried out in this area using liquid crystalline stationary phases. Work by Romansky and Guillet on main chain liquid crystal polymers[232] suggested the IGC technique did not elucidate transitions in LCPs as effectively as in non-mesogenic polymer systems. However in work on side-chain LCPs, Price and Shillcock[233] showed that mesophase transitions may be determined by IGC to an accuracy and precision comparable with DSC.

This section of the chapter presents results obtained for a low molecular mass liquid crystal and a liquid crystal polymer (BDH509 and LCP1, respectively) by DSC, hot stage microscopy and IGC. The relative merits of the various methods are then discussed. The performance of IGC around mesophase transitions allows suggestion of the most suitable practical methodology to be adopted for extension of the research programme. The discussion of IGC methodology is illustrated by consideration of Vg° and Ω^{∞} values, but is limited to the role these play in determination of mesophase transition. Descriptions of solution properties in terms of these parameters will be made in (3.3.1) and Chapter 4.

3.2.1 TRANSITION TEMPERATURES FOR BDH509

The mesophase transition temperatures for BDH509 were obtained by DSC, hot stage microscopy, and inverse gas chromatography to allow a comparison of these methods.

3.2.1a Differential Scanning Calorimetry

For meaningful results to be obtained from DSC, it is necessary to consider both a pure sample of material and a sample coated onto a chromatographic support. The latter sample mimics the behaviour expected by the material in the gas chromatography column, and reveals the effects (if any) of coating the material onto a stationary phase support. As described in (3.1.1), some workers have investigated the differences in mesophase transition temperatures of a supported liquid crystalline material. With a sufficient material loading on the support, effects on the chromatographic performance of the column can be minimised. Any differences in the mesophase transition temperatures would also suggest an effect on the mesophase ordering, and thus results obtained by IGC would be examining a system with potentially differing properties to those of the bulk material.

The differential scanning calorimeter was set at a heating rate of 5°C min^{-1}, with a sample size of approximately 5 mg for the bulk BDH509, and 12 mg for the BDH509 coated support material. These parameters were assigned as they gave results which could be both obtained in a reasonable level of time, and with reasonable precision and accuracy. The thermograms obtained for these samples are shown in Figure 3.1 and Figure 3.2 respectively. The uncertainties from the instrumental method at this heating rate are ± 0.5°C.

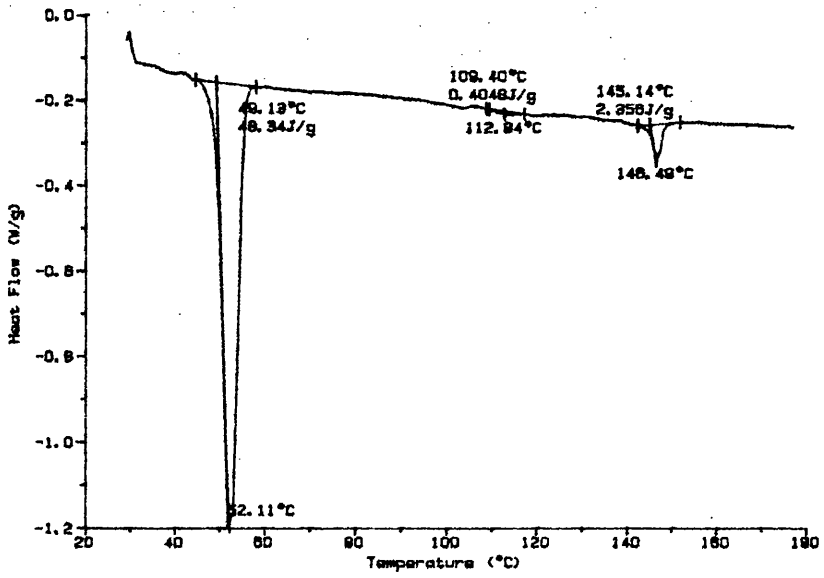

Figure 3.1: DSC Thermogram for Bulk BDH509

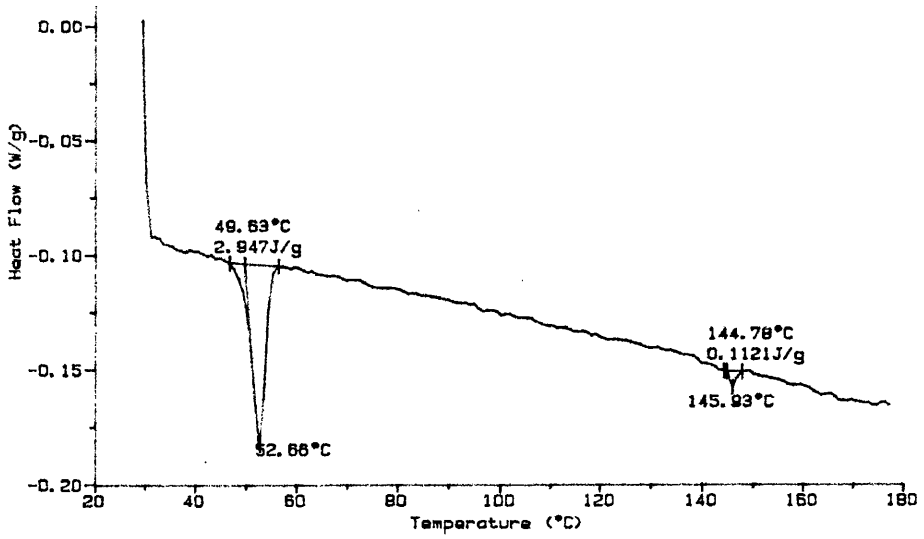

Figure 3.2: DSC Thermogram for BDH509 Coated on Chromosorb W

The transition temperatures of the transitions are summarised in Table 3.1. From these observations, it was confirmed that the description of mesophase structures given in (1.1.3) is indeed an accurate model of the mesophase transitions in BDH509. The largest energy change was exhibited by the transition from the crystalline phase to the first mesophase, as a large molecular realignment is involved in the reduction of order in the structure. In the pure liquid crystal the energy change associated with the $S_C \rightarrow N$ transition is very small, due to the change in structure being only a subtle realignment. However, the liquid crystal coated onto the support material showed no evidence of this mesophase transition. From the results obtained by HSM and IGC (3.2.1b and 3.2.1c) it is confirmed that this transition indeed occurs, so it can be assumed that the lack of a visible transition is not due to the mesophase behaviour changing when the material is coated on the column. Rather, the already small energy change at this transition is diluted below the sensitivity of the calorimeter by the support material.

BDH509	Bulk material	Coated support
$K \rightarrow S_C$ (°C)	52.1 ± 0.5	52.7 ± 0.5
$S_C \rightarrow N$ (°C)	112.8 ± 0.5	not shown
$N \rightarrow I$ (°C)	146.5 ± 0.5	145.9 ± 0.5

Table 3.1: Summary of Transition Temperatures for BDH509 from DSC

Whilst there are differences in the transition temperatures obtained between the two samples, they are within the experimental uncertainties of the instrumentation. Thus, it may be safely assumed from DSC studies that the liquid crystalline material coated onto support material exhibits very similar (if not identical) thermotropic behaviour.

3.2.1b Hot Stage Microscopy

At room temperature, viewing a sample of BDH509 through cross polarisers clearly showed the presence of large crystalline structures throughout the structure, with no defined texture being exhibited. This is consistent with the crystalline phase of the material. On increasing the temperature, an abrupt change in the optical structure of the material was observed at a temperature of 57°C, with the crystalline structure changing over a very narrow temperature range to exhibit the "schlieren texture". This indicates the formation of the S_C mesophase.

This texture remained visible with further increases in temperature until 111°C was reached. At this point there was another rapid transition to a blurred grainy texture denoting the formation of a nematic mesophase in which the structure shows enough order to deviate the course of plane polarised light, but does not posses enough order to give distinct optical textures. Further increases in temperature eventually lead to the view in the microscope going black where all ordered structure is lost. The clearing point for BDH509 occurs at 151°C, and is again accompanied by a very small temperature range of transition.

The transition temperatures as assigned for BDH509 from hot stage microscopy have therefore been experimentally determined as: $K \rightarrow 57° \rightarrow S_C \rightarrow 111°C \rightarrow N \rightarrow 151°C$. However, whilst the hot stage microscope is of invaluable use in characterisation of the mesophase structure, the information presented on the transition temperatures must be treated with more caution. As described, the phase transitions occurred virtually instantaneously to the naked eye allowing the assignment of transition temperatures between characterised phases. However, the accuracy and precision of these temperatures are not certain due to factors such as the rate of heating and environment of the sample: The instrumentation does not account for detailed temperature measurements at low heating rates, and the input of heat to the sample will show some losses due to the bulk nature of the sample, the glass surround of the sample mounting, and the open nature of the hot stage microscope instrumentation. Thus the results obtained may be used for characterisation purposes, with allied assignments from other techniques, such as DSC, providing more detailed information on the phase transition temperatures. In addition, such measurements may only be made on the bulk material, making comparison with IGC methods which contain supported material invalid.

3.2.1c Inverse Gas Chromatography

The choice of probe, as defended in (2.3.3), is also of importance in the determination of mesophase transitions by IGC. It has been reported previously[234] that polar probes

(such as chloroform) which act as good solvents for liquid crystalline materials may interfere with the transitions by dissolving in the phase.

Thus, the aliphatic and aromatic probes utilised in this study should have minimal impact on the mesophase transitions observed. As discussed in (1.4.1c), deviations from linearity in plots of ln Vg° *vs* 1/T obtained during IGC studies denote phase transitions in materials. For the column containing BDH509 retention volume plots and activity coefficient plots were obtained for hexane and benzene, as shown in Figure 3.3 and Figure 3.4. Rather than the large change in retention volume noted in the idealised retention plot for a semi-crystalline polymer (Figure 1.28) at a phase transition, the liquid crystalline material shows more subtle effects.

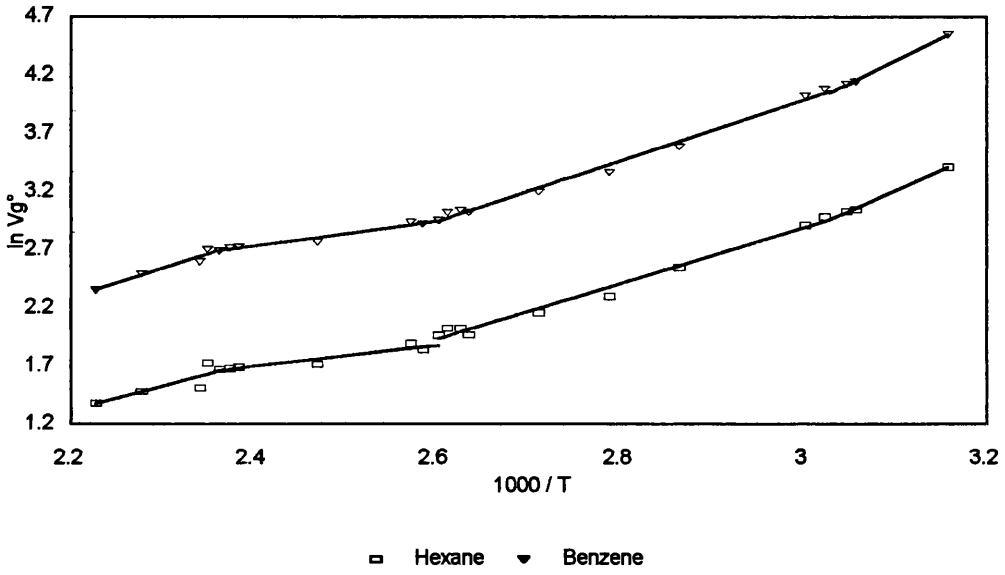

Figure 3.3: ln Vg° vs 1/T for Hexane and Benzene in BDH509

Around a transition, there is a distinct change in the gradient observed on the retention diagram. Such transitions may be described as *first-order* or *second-order*, as classified by Ehrenfest[235]. A first-order phase transition is shown where the first derivative of chemical potential across a phase transition is discontinuous, leading to enthalpy and entropy changes. A second-order transition is given where the first derivative of the chemical potential shows a continuous change over the phase transition (and is therefore not accompanied by any enthalpy or entropy change), but the second derivative is discontinuous. The DSC thermogram for BDH509 clearly shows an endothermic peak at the phase transitions, allowing these transitions to be described as first order. However, the subtle changes in retention volume noted on the transitions would indicate that the mesophase transitions approach second order. This is countered by evidence from the DSC thermogram which shows endothermic peaks

to accompany all phase transitions in the material, thus rendering them first-order. It is thought[236] that the "weakly first-order" transitions noted on the retention diagrams are due to the minimal change in bulk structure at a mesophase transition. No fully second order mesophase transitions in liquid crystalline systems have thus far been reported.

The transition temperatures obtained from the retention plot are summarised in Table 3.2. The temperatures are assigned at the point of the retention maximum around a transition. At this point it is assumed that the phase transition has fully occurred and the interaction between probe and stationary phase has reached equilibrium.

BDH509 (IGC)	K → Sc	Sc → N	N → I
Hexane (ln Vg°)	57 ± 2.3	109.5 ± 1.9	147.9 ± 1.7
Benzene (ln Vg°)	57 ± 2.3	109.5 ± 1.9	152.4 ± 2.4
Hexane (ln Ω^{∞})	57 ± 2.3	109.5 ± 1.9	147.9 ± 1.7
Benzene (ln Ω^{∞})	57 ± 2.3	109.5 ± 1.9	152.4 ± 2.4

Table 3.2: Summary of Transition Temperatures for BDH509 from IGC

Similarly, the plots obtained from ln Ω^{∞} *vs* 1/T also show distinct breaks in gradient at a phase transition. The values of Ω^{∞} obtained for this plot are derived from Vg°, however consideration of the activity coefficient plots often shows greater deviation than Vg° alone, making the determination of transition temperatures from these plots more precise.

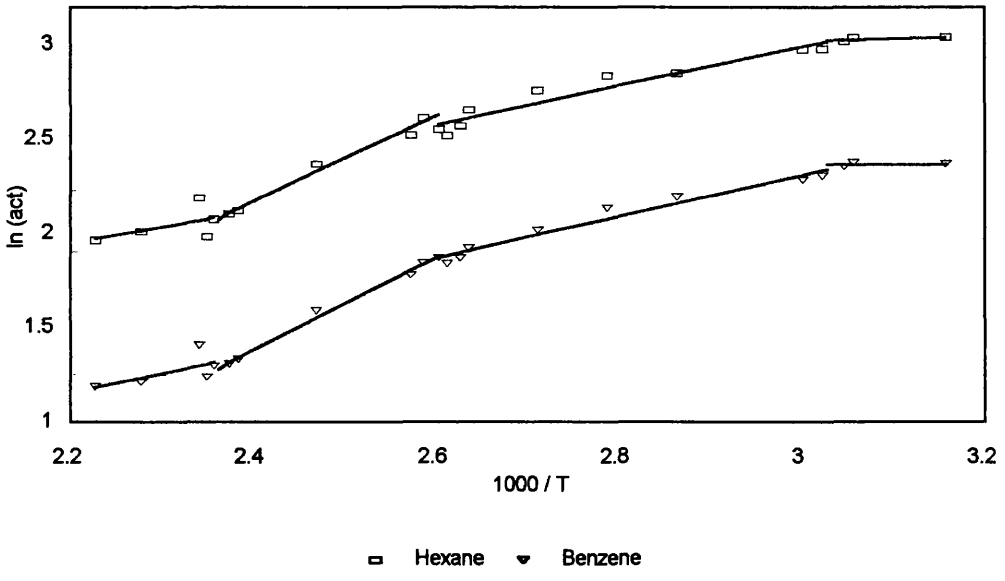

Figure 3.4: ln Ω^{∞} vs 1/T for hexane and benzene in BDH509

The transition temperatures as obtained from the plot of ln Ω^{∞} *vs* 1/T were identical to those obtained from the plot of ln Vg° *vs* 1/T within experimental uncertainty. This is due primarily to the nature of the experimental uncertainty: As the transition assigned is at the maxima of the plot around that transition (for ln Vg°), then the exact point of deviation can only be assigned relative to the temperatures at which results are collected. Thus, the experimental uncertainties quoted here are dependent on the experimental conditions adopted, and whilst a greater deviation in gradient is shown in plots of ln Ω^{∞} compared to plots of ln Vg° the experimental uncertainty remains identical. To improve the precision of the method it therefore follows that the experimental conditions be adjusted to allow smaller temperature steps around a transition.

It is noted that the transition temperature for the N $\rightarrow$ I transition observed by the aliphatic probe is different from that observed for the aromatic probe. This may be explained by considering that the differing probe structures undergo differing interactions with the stationary phase; liquid crystals are better solvents for aromatic materials, and from the results it appears benzene shows tendency to remain in solution with the stationary phase at the clearing point, whilst hexane is not solvated to the same degree and elutes more readily.

3.2.1d Summary of BDH509 Mesophase Transition Temperatures

The results obtained for BDH509 by the three methods considered are summarised in Table 3.3. As previously stated, the transition temperatures obtained from hot stage microscopy do correlate generally with those obtained by DSC and IGC. However, due to the uncertainties associated with the method the results were used to assign the mesophases rather than be indicative of the mesophase transition temperatures.

	K $\rightarrow$ S_C (°C)	$S_C \rightarrow N^*$ (°C)	$N^* \rightarrow I$ (°C)
DSC			
Pure material	52.1 ± 0.5	112.8 ± 0.5	146.5 ± 0.5
Coated Chromosorb	52.7 ± 0.5	not shown	145.9 ± 0.5
HSM			
Pure material	57	111	151
IGC			
Hexane	57 ± 2.3	109.5 ± 1.9	147.9 ± 1.7
Benzene	57 ± 2.3	109.5 ± 1.9	152.4 ± 2.4

Table 3.3 - Transition Temperatures for BDH509

Comparison of the transition temperatures obtained by DSC and IGC does reveal some differences. The results obtained by DSC shows the K $\rightarrow$ S_C transition to occur at a slightly depressed temperature, compared with the results obtained from IGC. It appears this is due to the determination of the transition temperature from the thermogram being made before the transition has fully occurred and the trace has returned to the baseline. As mentioned, no $S_C \rightarrow$ N transition is visible on the coated chromosorb due to the dilution of sample, though the other results show that within experimental error the coating of a liquid crystalline sample onto a support does not affect its mesophase behaviour at approximately 10% w/w loading. The methods give good agreement on the clearing temperature, within experimental uncertainty, except for the temperature observed using an aromatic probe in IGC studies, due to that probe's affinity for the stationary phase. This reiterates the work of Llorente[237] mentioned previously, where a relatively good solvent for the stationary phase acts to affect the observed transition temperatures of that phase. However, in the circumstances noted here this observation does not indicate finite solution of the probe; rather, the aromatic probe at infinite dilution has a greater affinity for the mesophase structure than the aliphatic probe, giving rise to differences in observation between the systems.

These results emphasise that accurate determination of liquid crystal mesophase transition temperatures require a comparison of results obtained from different methods: Methods used without cross-referencing may give a misleading picture. IGC under the correct experimental conditions can match the accuracy and precision of the DSC method. However, IGC alone is not an efficient method for the measurement of transition temperatures, but when also used to determined physiochemical parameters it is an extremely versatile tool.

3.2.2 TRANSITION TEMPERATURES FOR LCP1

In order to ensure this method is also applicable to liquid crystalline polymers, identical measurements were carried out on LCP1. DSC analysis and HSM classification showed the glass transition temperature to be -7°C, with the polymer existing in the S_C mesophase until a clearing point of 67.0 $\pm$ 0.5°C was reached. The IGC retention diagrams obtained from ln Vg° and ln Ω^{∞} across the mesophase temperature range for LCP1 using hexane and benzene are shown in Figure 3.5 and Figure 3.6 respectively, with the transition temperatures observed by all methods being summarised in Table 3.4. The glass transition temperature was not obtained as it was not possible to carry out measurements at sub-ambient temperatures with the IGC instrumentation used.

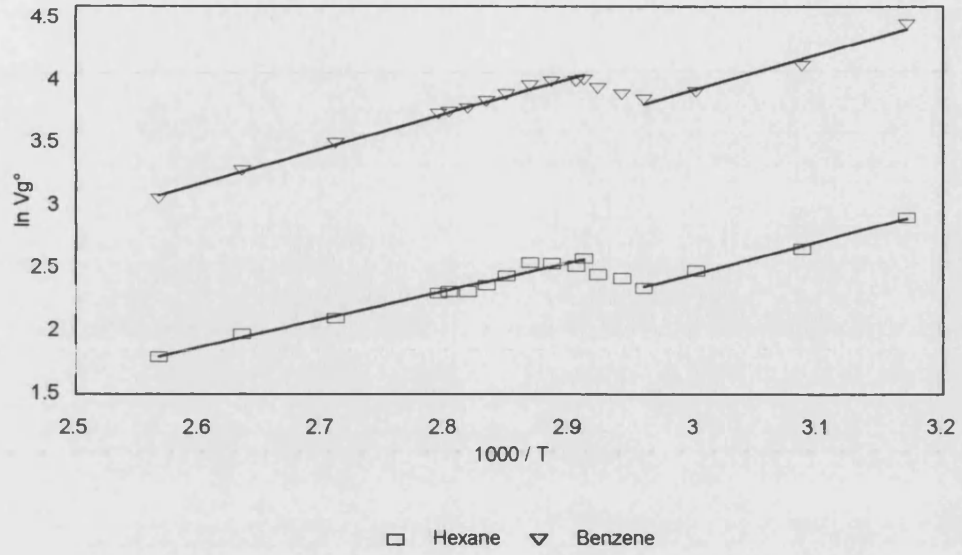

Figure 3.5: ln Vg° vs 1/T for Hexane and Benzene in LCP1

The temperature range over which the transition occurs in the polymeric liquid crystalline material is much greater than that noted for the low molecular mass material. The retention volume of both aliphatic and aromatic probes begins to show deviation from 64.8°C, finally re-equilibrating to give a linear gradient at 70.3°C. This shows a situation similar in nature to the semi-crystalline polymer discussed in (1.4.1c) where a premelting transition is noted before re-equilibration is achieved.

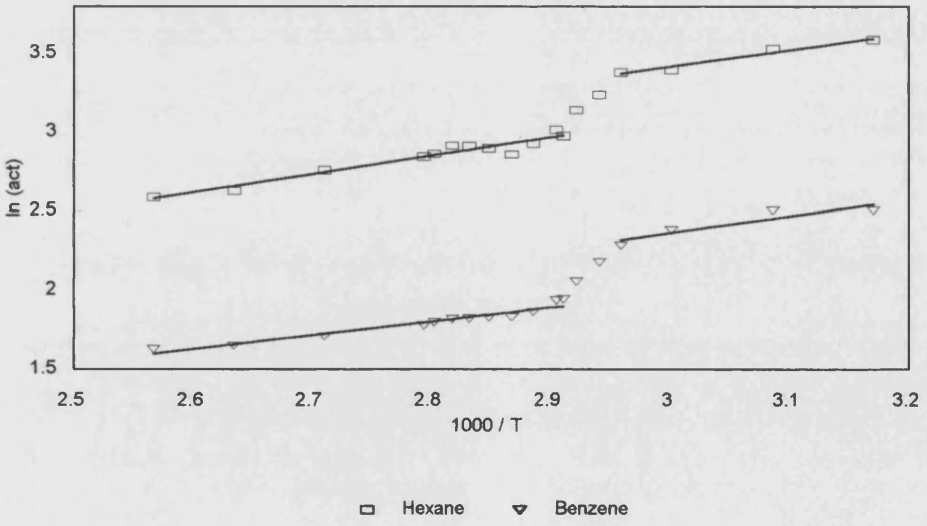

Figure 3.6: ln Ω^{∞} vs 1/T for Hexane and Benzene in LCP1

The transition is clearly first order, and indicates that the probe molecules are able to penetrate into the isotropic region of the LCP with a far greater ease than they

penetrate into the S_C mesophase. This phenomenon is far more pronounced in the polymeric material, suggesting the siloxane backbone plays an increased role in solvation. This will be investigated more fully in Chapter 4. Within experimental uncertainty, no difference is shown in the retention behaviour of the aliphatic and aromatic probes with this material indicating the nature of the probe does not have such a pronounced effect on mixing with the stationary phase where contributions to mixing are derived from both a polymeric backbone and mesogenic side chain.

The results obtained from DSC may therefore be compared with the mid-point of the phase change, rather than the point at which the isotropic liquid is the sole phase observed. This work on a liquid crystalline polymer therefore allows identical conclusions to be drawn as from the work on the low molecular mass material. Namely, the determination of transition temperatures is best carried out using a combination of methods, but IGC does offer a similar level of accuracy and precision compared with DSC when the results obtained are carefully considered, and has the advantage of allowing the simultaneous measurement of other physiochemical parameters.

LCP1	$S_C \rightarrow I$ (°C)
DSC	
Pure material	67.0 ± 0.5
Coated Chromosorb	67.0 ± 0.5
HSM	
Pure material	63
IGC	
Hexane	70.3 ± 0.7
Benzene	70.3 ± 0.7

Table 3.4: Transition Temperatures for LCP1

Practically, the results obtained for the remainder of this research were determined by selecting operational temperatures which avoided the mesophase transition temperature regions. This allowed determination of physiochemical and analytical parameters in confidence that the results were unaffected by any anomalous behaviour observed around a mesophase transition.

3.3 IGC RESULTS FOR PDMS

PDMS, the structure of which is shown in Figure 3.7, was selected as a reference material as it is widely used as an efficient commercial stationary phase for many separations, yet no work to the author's knowledge describes PDMS as having selectivity towards enantiomeric analytes. PDMS is also the basis for the polymeric liquid crystalline stationary phases studied in this work, and therefore provides a standard by which to evaluate the liquid crystalline materials from both a thermodynamic and analytical perspective. PDMS has also been the subject of many physiochemical studies, so may be used for confirmation of the experimental apparatus and method used for IGC in this study.

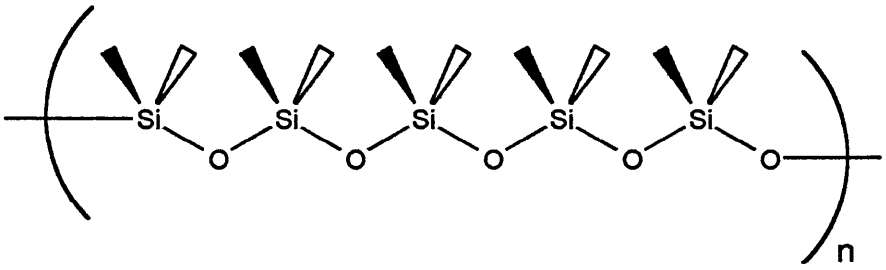

Figure 3.7: Structure of PDMS

The work covered in (3.3) will therefore investigate the suitability of the IGC methodology by comparison with results obtained by other workers, and extend the discussion so far to investigate the solution behaviour of probes with PDMS and consider the analytical performance for the chosen probes. This work will provide the basis of discussion for the experimental results obtained for the materials studied in Chapters 4 and 5.

3.3.1 PHYSIOCHEMICAL RESULTS

The physiochemical results obtained for PDMS by IGC are obtained from plots of ln Vg° *vs* 1/T and ln Ω^{∞} *vs* 1/T, as shown in Figure 3.8 to Figure 3.13. The enthalpies and entropies of solution calculated from these graphs are then presented in Table 3.5. The reader is here referred to (1.4.3) to review equations used in these calculations.

3.3.1a Experimental Uncertainties

Experimental uncertainty in Vg° was calculated by consideration of the individual terms in equation [1.30]:

- The flow rate used was of reasonable magnitude (< 40 cm^3min^{-1}) allowing measurement to 1% uncertainty when considering the ± 0.1 cm^3 uncertainty in volume measurement at each end of the burette, and the ± 0.2 s uncertainty in time measurement at each end of the burette.

- Replicate retention times were measured to ± 0.01 min, which allows uncertainty to be determined dependent upon the relative values of t_M and t_R. e.g. where (t_R - t_M) = 10 min, an uncertainty of 0.1% is shown and where (t_R - t_M) = 1 min, an uncertainty of 1.4% is shown. Overall approximation allows a 1% uncertainty to be assigned to measurements made in this work.

- The mass of material in the column is measured ±0.002 g in 10 g, and mass of polymer on the packing material measured to ±0.0002 g in 1 g. This leads to an uncertainty in the mass of polymer on the column of approximately 1%.

Approximation by adding these uncertainties show experimental uncertainties in the determination of Vg° to be ± 2.5%, the value quoted throughout this work. It is noted that as Vg° values increase, the associated uncertainties decrease due to the magnitude of the retention time parameter, and it is reasonable to suggest uncertainties in Vg° of between 1% and 5% depending on the magnitude of the result.

A similar analysis of γ^∞ (as obtained *via* equation [1.33]) was made to obtain the associated experimental uncertainty. The exponential term consists of literature data, with any uncertainty being small and unaffected by experimental considerations. Uncertainty would also be present in the measurement of P_1° and M_2, as discussed for Vg° measurements, so Vg° is the dominant term and values of γ^∞ will therefore show an uncertainty of ± 2.5%.

In the consideration of the solution properties of mixing calculated using the IGC methodology, inherent uncertainties associated with the method may be carried through to physiochemical calculations. Uncertainty limits quoted throughout this work represent the σ values of the slope (for ΔH^s and ΔH^e) and the intercept (for ΔS^s and ΔS^e) as obtained from least-squares regression on the retention diagrams. This method considers the experimental uncertainty incurred, whilst minimising the errors inherent in the experimental method (such as the flow-rate and mass of polymer on the stationary phase), and has been utilised by various workers in the field[238-240].

3.3.1b Comparison With Literature Values

Before consideration of the physiochemical parameters obtained from this IGC study of PDMS, the basic data of the method - the specific retention volume - was compared with data obtained by other workers[241-245]. The results, extrapolated to 60°C and presented in Table 3.5, show good agreement for all probes considered.

Probe	Vg° (Literature) $cm^3 g^{-1}$	Vg° (Experimental) $cm^3 g^{-1}$
Hexane	59.9 - 61.3	60.6 ± 1.5
Heptane	137.0 - 144.3	138.6 ± 3.5
Octane	310.6 - 332.1	315.5 ± 7.9
Benzene	91.6 - 105.5	96.0 ± 2.4
Toluene	212.8	224.3 ± 5.6
Ethylbenzene	446.1	471.7 ± 11.8

Table 3.5: Comparison of Vg° Values for PDMS at 60°C

These comparisons inspire confidence in the methodology adopted, and allow the results obtained throughout this research to be described in terms of, and compared with, those of other workers in the field of IGC.

3.3.1c Retention Volume

The retention volumes obtained for the aliphatic, aromatic and isomeric probes give indications as to the extent of interaction between probe and stationary phase. All retention plots are typical of those for a polymer above its glass transition point, with a linear decrease in Vg° exhibited for all probes as temperature increases. This indicates the change in penetration of the probe into the stationary phase structure is dependent solely upon the thermal and diffusive properties of the probe. There is the strong possibility that the increased mobility of the stationary phase as temperature increases also affects interaction with the probe, though the polymer does not undergo any major structural change with increases in temperature.

Linear variation in Vg° at a given temperature is noted for the *aliphatic probes*, increasing with an increase in the number of carbon atoms or degree of branching present in the aliphatic chain. For example, at 60°C the ln Vg° values obtained for hexane, heptane and octane are 4.10, 4.93 and 5.75 respectively - showing a correlation of 99.99%. Such linearity of these results allows the retention behaviour of other probes in a homologous series to be accurately predicted.

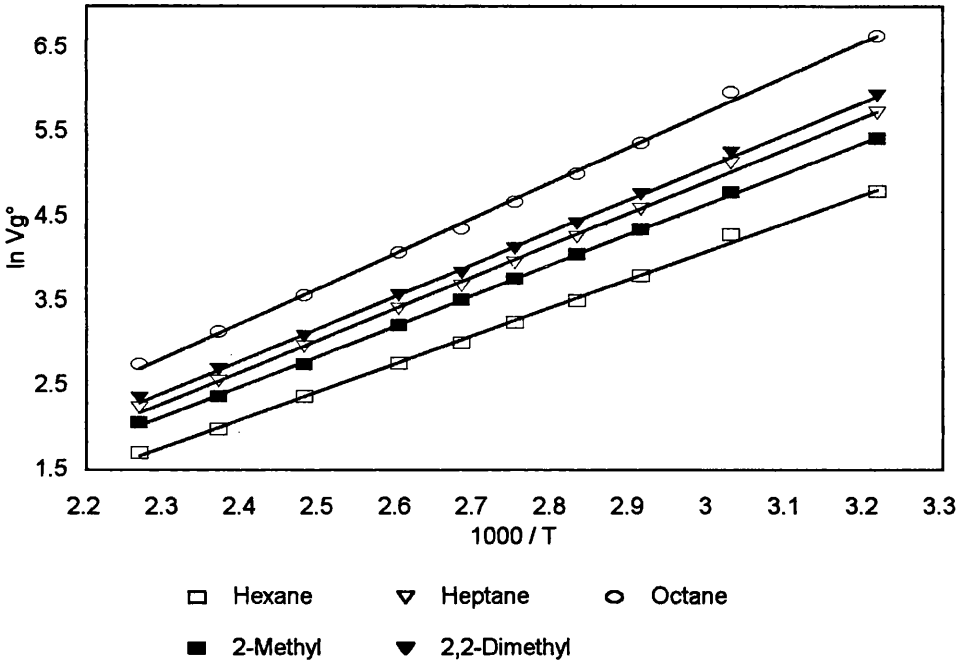

Figure 3.8: ln Vg° vs 1/T for Aliphatic Probes in PDMS

The *aromatic probes* show higher Vg° values than the aliphatic probes, with Vg° through the series increasing with additional aliphatic side-chains and branching. The xylene isomers show very similar retention behaviour. This increased retention may be considered, on the surface, to be a consequence of increased interaction between probe and stationary phase. However, for Vg° measurements the Henry's Law model of gas chromatography, described in (1.4.1a), shows that these effects are due to the aliphatic probes being more volatile and therefore being re-equilibrated more rapidly on the column, and thus eluting more rapidly than the less volatile aromatic probes. Little information of substance on the exact nature of the probe/stationary phase interaction may be elucidated from a retention plot alone.

The *isomeric probes* exhibited retention volumes intermediate between the aliphatic and aromatic probes. Again, no inference as to the nature of the probe/stationary phase interaction may be made at this point. It is noted that whilst slight differences in retention behaviour between the cis- and trans- isomers are shown, the retention of the enantiomers is identical within experimental uncertainty.

This underlines the Henry's Law model of chromatography, as the geometrical isomers have differing physical properties while the enantiomers do not.

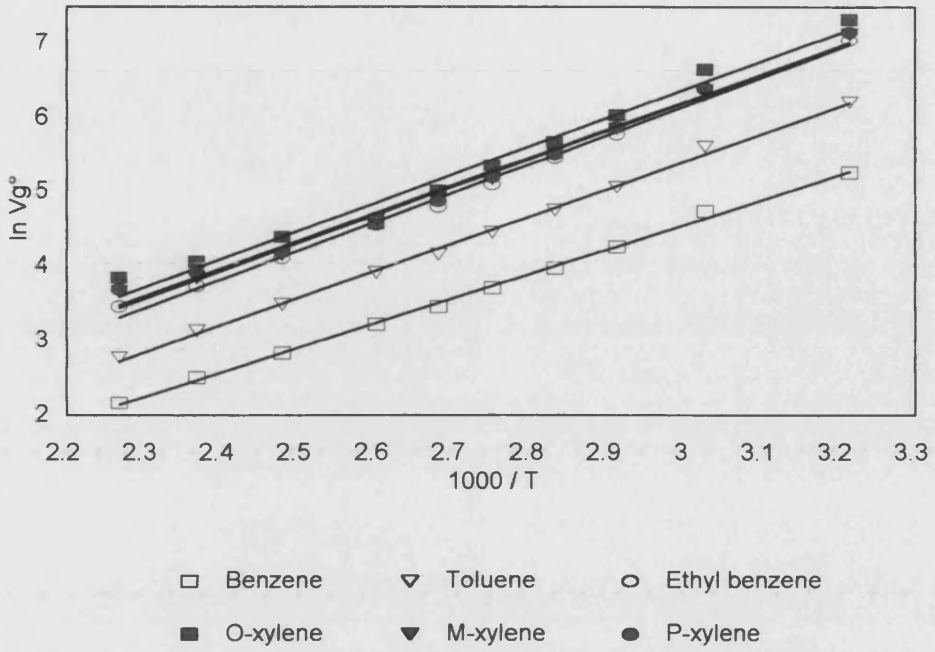

Figure 3.9: ln Vg° vs 1/T for Aromatic Probes in PDMS

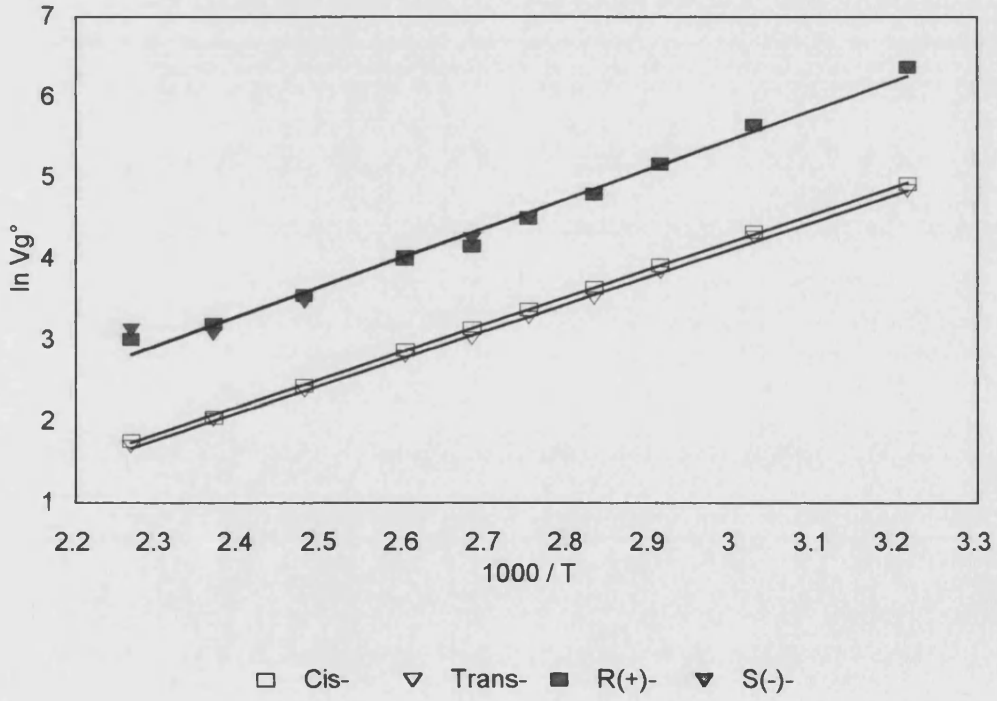

Figure 3.10: ln Vg° vs 1/T for Isomeric Probes in PDMS

The values obtained for Vg° and saturated vapour pressure of the probes were then used to calculate the weight-fraction activity coefficients for the probe/PDMS interactions, allowing further description of these interactions to be made.

3.3.1d Activity Coefficients

The weight-fraction activity coefficients, Ω^{∞}, were calculated for PDMS using equation [1.34], as meaningful determination of mole-fraction activity coefficient, γ^{∞}, is made difficult by the polydispersity of the polymeric stationary phase (see 1.4.4). The current discussion will therefore be made in terms of Ω^{∞}, with a full comparison of γ^{∞} and Ω^{∞} values in an identical system being presented in (4.1.2). The activity coefficients obtained are shown in Figure 3.11 (for aliphatic probes), Figure 3.12 (for aromatic probes) and Figure 3.13 (for isomeric probes). Values for Ω^{∞} have also been quoted in the literature, and the comparison made in Table 3.6 with the work of Lichtenthaler *et al*[246] at 70°C shows the results for aliphatic probes to be in good agreement, whilst those obtained for aromatic probes are slightly lower. These differences may be due to the method of calculation, in which the B_{11} values used in correction factors were calculated by different methods (shown to cause experimental uncertainty by Roth and Novak[247]) or by difference in molecular mass of the stationary phase affecting interaction with the aromatic probes. The molecular weight of the PDMS used was not obtained during this work, so will not be commented upon.

Probe	Ω^{∞} (Literature)	Ω^{∞} (Experimental)
Hexane	5.94	5.91 ± 0.15
Heptane	5.96	5.89 ± 0.15
Octane	6.05	5.92 ± 0.15
2-Methylhexane	5.84	5.89 ± 0.15
Benzene	5.97	5.53 ± 0.14
Toluene	6.05	5.89 ± 0.15
Ethylbenzene	6.19	5.80 ± 0.15
o-xylene	6.58	6.14 ± 0.15
m-xylene	6.46	6.10 ± 0.15
p-xylene	6.22	5.81 ± 0.15

Table 3.6: Comparison of Ω^{∞} Values for PDMS at 70°C

The trend noted initially, in contrast to the trend in retention volumes, is that there is very little variation in Ω^{∞} across the temperature range studied. This in part may be attributed to the macromolecular structure of PDMS remaining of consistent morphology throughout the temperature range examined, but points even more clearly

at the interactions between probes and PDMS being mainly dependent upon energetic rather than interactive factors. This is clarified further by consideration of the excess solution properties (3.3.1d).

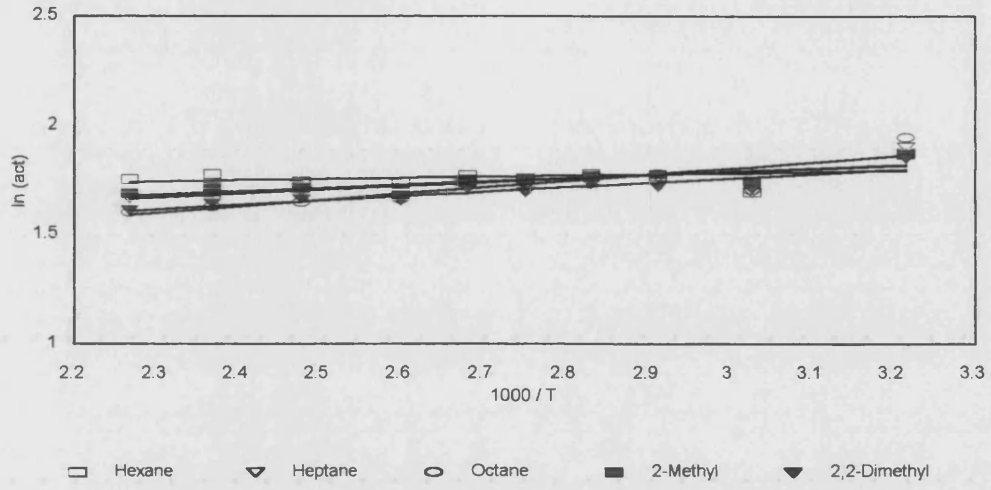

Figure 3.11: ln Ω^{∞} vs 1/T for Aliphatic Probes in PDMS

As the length of the *aliphatic probe* chain increases, an increased dependence on temperature is noted; hexane shows very little temperature dependence, with heptane being effected slightly, and octane showing greater effects. Similarly, branching increases the temperature dependence, with 2-methylhexane showing slight effects and 2,2-dimethylhexane showing greater dependence. In terms of molecular interactions, the overall description indicates that at lower temperatures the interaction of linear and branched-chain aliphatic probes show more unfavourable mixing as the number of carbon atoms and branches increases, but as the stationary phase becomes more thermally mobile the interactions become more favourable.

At temperatures of approximately 90°C, the *aromatic probes* exhibit similar values of Ω^{∞} to both the aliphatic probes and each other. However, as the temperature is varied the values of Ω^{∞} show a much greater dependence than observed for the aliphatic probes, with Ω^{∞} decreasing as T increases. As the aliphatic portion of the probe increases, a greater variance with T is noted in the order: benzene < toluene < ethyl benzene < xylenes. All xylenes present very similar Ω^{∞} values and temperature dependence. This infers at lower temperatures the more rigid structures of the aromatic probes have more difficulty in interacting with the PDMS macrostructure, but as PDMS becomes more thermally mobile, a greater degree of interaction occurs showing more marked differences compared with the aliphatic probes. Interactions of aromatic probes become more favourable at higher temperatures as their aliphatic portions increase in length and number.

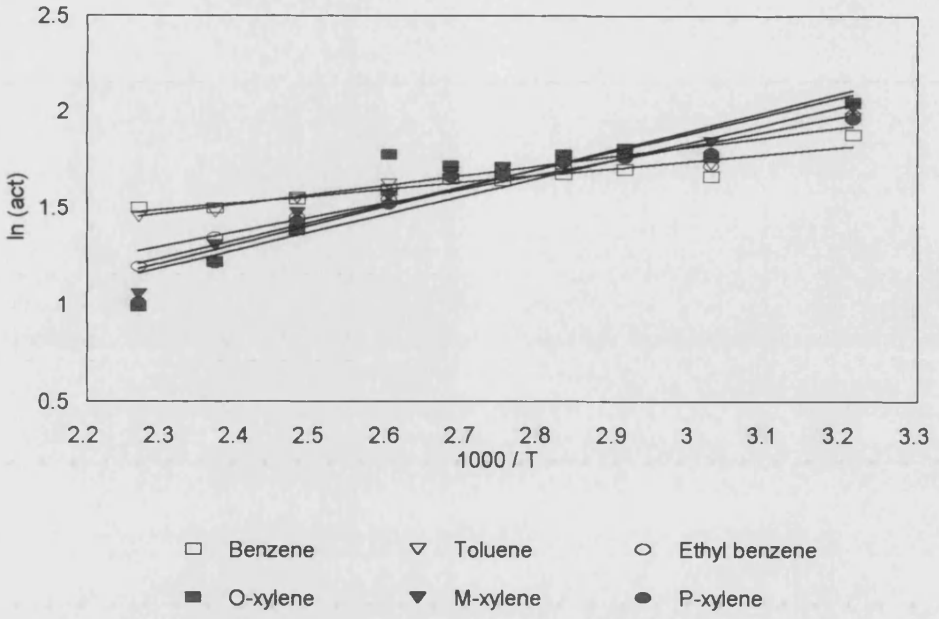

Figure 3.12: ln Ω^{∞} vs 1/T for Aromatic Probes in PDMS

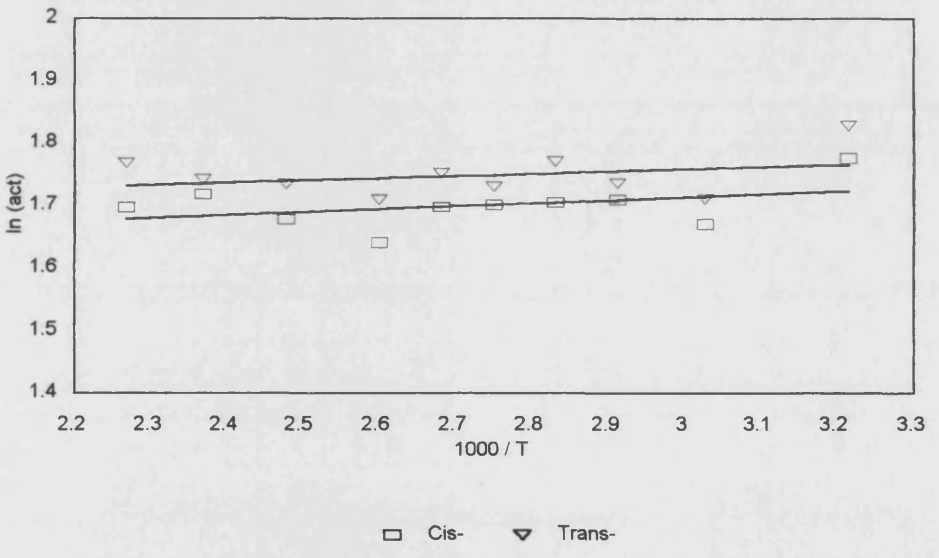

Figure 3.13: ln Ω^{∞} vs 1/T for Isomeric Probes in PDMS

At a reference temperature of 90°C the *isomeric probes* show values of Ω^{∞} raised slightly over those for both the aliphatic and aromatic probes, suggesting that the restricted mobility and interactions due to the C=C bond interfere with the solution process. The cis-isomer shows a lower activity coefficient than the trans-isomer, suggesting the effect of the conformation on molecular shape effects the interaction with the stationary phase quite significantly. As temperature increases Ω^{∞} values

remain virtually constant, showing this interaction to have little dependence on interactive factors.

It may be inferred from activity coefficient measurements alone that changes in temperature over the range studies show little effect on the probe/PDMS mixture. Where effects are exhibited, mixture becomes more favourable with an increase in temperature; perhaps due to the thermally mobile chains allowing heightened interaction with probes which previously showed more unfavourable interactions.

3.3.1e Solution and Excess Enthalpies and Entropies

The enthalpic and entropic contributions to probe/stationary phase mixing, calculated from Vg° measurements and Ω^{∞} values as described in (1.4.5a) and (1.4.5b), are presented in Table 3.7.

Probe	Enthalpic kJ mol^{-1}			Entropic J mol^{-1} K^{-1}		
	ΔH^s	ΔH^e	ΔH^{vap}	ΔS^s	ΔS^e	ΔS^{vap}
Hexane	-27.64 (0.05)	0.47 (0.05)	-28.11 (0.10)	-34.68 (0.04)	1.33 (0..04)	-36.01 (0.08)
Heptane	-31.25 (0.06)	1.39 (0.05)	-32.64 (0.11)	-38.63 (0.05)	2.77 (0.05)	-41.40 (0.10)
Octane	-34.67 (0.06)	2.43 (0.06)	-37.10 (0.12)	-42.04 (0.06)	4.68 (0.05)	-46.72 (0.11)
2-Me	-29.94 (0.02)	1.25 (0.03)	-31.19 (0.05)	-36.90 (0.02)	2.37 (0.03)	-39.27 (0.05)
2,2-DiMe	-31.81 (0.04)	1.67 (0.03)	-33.47 (0.07)	-38.88 (0.04)	2.80 (0.03)	-41.68 (0.07)
Benzene	-27.48 (0.05)	2.96 (0.05)	-30.44 (0.11)	-30.36 (0.04)	9.63 (0.04)	-39.99 (0.08)
Toluene	-30.50 (0.06)	4.11 (0.05)	-34.60 (0.11)	-32.36 (0.06)	11.39 (0.04)	-43.75 (0.10)
Ethylbenzene	-32.22 (0.10)	6.15 (0.07)	-38.37 (0.17)	-31.35 (0.09)	16.31 (0.06)	-47.66 (0.15)
o-Xylene	-31.64 (0.19)	8.08 (0.16)	-39.72 (0.35)	-27.71 (0.17)	21.45 (0.14)	-49.15 (0.31)
m-Xylene	-31.33 (0.13)	7.63 (0.09)	-38.97 (0.22)	-28.27 (0.11)	20.20 (0.08)	-48.48 (0.19)
p-Xylene	-31.01 (0.14)	7.67 (0.10)	-38.69 (0.24)	-27.23 (0.12)	20.72 (0.09)	-47.95 (0.21)
Cis-	-28.16 (0.02)	0.40 (0.04)	-28.56 (0.06)	-35.25 (0.02)	1.89 (0.03)	-37.14 (0.05)
Trans-	-27.82 (0.03)	0.30 (0.04)	-28.12 (0.07)	-35.02 (0.03)	1.21 (0.04)	-36.23 (0.07)
R(+)	-30.26 (0.12)	n/a	n/a	-31.06 (0.11)	n/a	n/a
S(-)	-30.23 (0.15)	n/a	n/a	-30.94 (0.04)	n/a	n/a

Table 3.7: Physiochemical Results for PDMS Above Tg

For practical purposes the partial molar enthalpies and entropies of solution, ΔH^s and ΔS^s respectively, are measured considering a reference state of an infinitely dilute solution and are therefore applicable to all probes from an identical reference state. Conversely, the partial molar excess parameters, ΔH^e and ΔS^e, are calculated relative to the pure probe solvent (as introduced in equation [1.34] when considering the

saturated vapour pressure and molecular mass of the probe). Thus, the excess results for each probe may be used to describe solution behaviour for individual probes between phases, but will not necessarily give correlation of solution behaviour between probes as the reference state is different in each case.

The solution and excess enthalpies and entropies obtained from such calculations may be basically considered by application of the Chow and Martire model[248], which classifies the interaction type in terms of the activity coefficient and solution properties, and therefore helps separate the individual contributions to the overall thermodynamic solution behaviour. Considering this model, large negative ΔH^s values equate to a strong interactions and restriction of probe movement when transferred from the gas phase into an infinitely dilute solution. The presence of excess enthalpic contributions indicate deviations from the ideal mixing described by solution processes, and suggest alternative interactions occur from those shown in the bulk probe solvent. Similarly, large negative ΔS^s values are indicative of significant restrictions in probe movement on transferring from the gas phase into an infinitely dilute solution, and are thus indicative of a strong interaction between the probe and stationary phase. Excess contributions describe a deviation from the ideal model in terms of the probe-probe interaction, and their presence therefore indicates the role of molecular shape in interactions with the stationary phase.

Considering *solution properties*, values for ΔH^s become more negative with an increase in aliphatic chain length and branching, following a linear relationship for a homologous series. As substitution is added to an aromatic core, there is also a slight decrease in ΔH^s values. Similar values are noted for all three xylenes, suggesting little difference in their solution behaviour on mixing. Values for the geometrical isomers showed slight differences, but the enantiomers were identical to within experimental uncertainty. Values for ΔS^s show similar trends, with a linear decrease in ΔS^s as increase in aliphatic chain length and branching increases, again showing linear dependence in a homologous series and showing the behaviour described previously where probes with more "freedom" (i.e. longer chains) undergo more restriction under infinite dilution conditions. There is little effect shown on ΔS^s throughout the aromatic probe series considered, and the values shown for the geometric and positional isomers were identical to within experimental uncertainty.

The *excess properties* observed were all generally of low magnitude. ΔH^e values showed very little significance throughout the aliphatic probes and geometrical isomers, and only started to show an increase as substitution to the aromatic core increased. The most significant values were obtained for the xylenes; m- and p-xylene showing identical results to within experimental uncertainty, and o-xylene giving a greater

excess contribution. Similarly, ΔS^e values showed little significance through the aliphatic probes and geometric isomers, only coming into play for the aromatic systems. As substitution to the aromatic core increased, so did the value of ΔS^e. These values reached their maximum for the xylenes, with o-xylene showing a slightly elevated value over m- and p-xylene. This suggests deviations from ideality in solution formation and contributions from shape interactions of the substituted aromatics and xylenes. This fits with the model suggested by the activity coefficient trends, where interaction only becomes more favourable as the temperature increases and the polymeric structure "opens up" to penetration by molecular probes of differing chemical composition. This may be compared with the situation facing aliphatic probes, where the initial interaction with PDMS is energetically more favoured due to the presence of many methyl side-groups on the polymer surface, and structural interactions are therefore less likely to affect solution behaviour.

Whilst excess properties are low for all probes studied, this does not suggest mixing is approaching an ideal model. Rather, interactive forces are playing a minor role in the overall solution process, with the dominating driving force in solution formation being due to favourable energetic solution formation. This description of the mixing of probes with a PDMS stationary phase therefore gives good comparative potential for the description of interactions occurring between probe molecules and mesogenic stationary phases, both low molecular mass and polymeric.

3.3.2 ANALYTICAL RESULTS

Analytically, PDMS is used routinely for the separation of many analytes of interest. The success of the material may be attributed to the unique properties of PDMS, namely low glass transition temperature and high chain mobility imparting low viscosity which, combined with excellent thermal stability, makes PDMS easily processable as well as an effective stationary phase. To consider the analytical performance of PDMS on the analytes described herewith, the reader is referred to the introductory chapter (1.3.2) to review the equations used to calculate analytical parameters from gas chromatography. Of the possible parameters which may be used to describe the analytical performance of the column, those presented here in Table 3.8 to Table 3.11 refer to the *selectivity* and *resolution* observed between two analytes. These two parameters are crucial in describing the analytical performance of the column, with the selectivity measuring the ability of the column to separate the analytes, and the resolution being describing their experimentally observed separation and overlap. In addition, it is possible to calculate the length of column required in order to effect a resolution of 1.5, equating to full separation of the analytes with no overlap in retention. This is calculated from equation [1.9], and presented here for illustrative purposes.

All analytical results were obtained from triplicate injections of the analytes, the retention times of which agreed to within 1%, Experimental uncertainties due to systematic factors were experienced to the same degree by all analytes, and so those quoted are due strictly to the uncertainty in retention times being carried through the calculation of analytical parameters outlined in (1.3.1).

Analytical parameters were calculated between each pair of probe molecules injected for IGC studies, but for brevity and the presentation of meaningful results this work will consider the analyte pairs hexane/heptane, m-/p-xylene, cis-/trans-2-hexene and R(+)/S(-)-2-Methylchloropropionate. The rationale behind consideration of these pairs is to use the C_6/C_7 pair, known to separate on a variety of GC stationary phases by virtue of differences in the physical and chemical properties, to reference and describe the separations of the other isomeric pairs. It is the aim of this research to utilise the IGC method to describe solution processes with LC stationary phases to describe systems which separate isomers which are traditionally difficult to separate. Just as PDMS is the reference material for IGC studies of liquid crystalline systems, it is also the chosen reference for the analytical results presented in Chapter 5.

To consider the effects of temperature on the analytical performance, the resolution may be plotted against temperature as in Figure 3.14 to give a profile. Such a plot clearly shows a good resolution for hexane and heptane well into higher operational temperatures. This is accompanied by good selectivity values across the temperature range. A general phenomena of GC analysis is observed here, with increasing temperature reducing the equilibration time during which analytes interact with the stationary phase; again in accordance with the Henry's Law model of gas chromatography. This reduces the relative elution times of the analytes, and decreases the resolution between them.

Temperature (°C)	α	R_S	N for Rs=1.5 (m)
40	2.54 (0.03)	6.70 (0.13)	50
55	2.34 (0.02)	5.90 (0.12)	65
70	2.20 (0.02)	3.13 (0.06)	85
80	2.11 (0.02)	2.20 (0.04)	105
90	2.03 (0.02)	1.64 (0.03)	130
100	1.97 (0.02)	1.42 (0.03)	165
110	1.90 (0.02)	1.36 (0.03)	210
130	1.81 (0.02)	0.79 (0.02)	335
150	1.76 (0.02)	0.82 (0.02)	530
170	1.69 (0.02)	0.38 (0.01)	805

Table 3.8: Analytical Results for Hexane/Heptane in PDMS

Temperature (°C)	α	R_S	N for Rs=1.5 (m)
40	1.02 (0.01)	0.29 (0.01)	5700
55	1.02 (0.01)	0.17 (0.01)	3600
70	1.01 (0.01)	0.09 (0.01)	260000
80	1.00 (0.01)	-0.03 (0.01)	2342000
90	1.01 (0.01)	0.11 (0.01)	94000
100	1.00 (0.01)	-0.02 (0.01)	1315000
110	1.02 (0.01)	0.05 (0.01)	44000
130	1.02 (0.01)	0.03 (0.01)	44000
150	1.08 (0.01)	0.06 (0.01)	45000
170	0.86 (0.01)	-0.12 (0.01)	1000

Table 3.9: Analytical Results for m- /p-Xylene in PDMS

Temperature (°C)	α	R_S	N for Rs=1.5 (m)
40	1.09 (0.01)	0.60 (0.01)	3200
55	1.07 (0.01)	0.42 (0.01)	5100
70	1.08 (0.01)	0.30 (0.01)	5200
80	1.06 (0.01)	0.28 (0.01)	5500
90	1.08 (0.01)	0.24 (0.01)	6000
100	1.08 (0.01)	0.20 (0.01)	7500
110	1.09 (0.01)	0.17 (0.01)	8000
130	1.07 (0.01)	0.10 (0.01)	20000
150	1.03 (0.01)	0.03 (0.01)	∞
170	1.07 (0.01)	0.07 (0.01)	39000

Table 3.10: Analytical Results for cis-/trans-2-Hexene in PDMS

Temperature (°C)	α	R_S	N for Rs=1.5 (m)
40	1.00 (0.01)	0.02 (0.01)	1484000
55	1.01 (0.01)	0.06 (0.01)	94000
70	0.99 (0.01)	-0.07 (0.01)	112000
80	1.01 (0.01)	0.05 (0.01)	398000
90	0.99 (0.01)	-0.06 (0.01)	179000
100	0.99 (0.01)	-0.05 (0.01)	200000
110	0.97 (0.01)	-0.06 (0.01)	22000
130	1.08 (0.01)	0.09 (0.01)	6000
150	1.12 (0.01)	0.14 (0.01)	3000
170	0.89 (0.01)	-0.07 (0.01)	3000

Table 3.11: Analytical Results for R(+)/S(-)-2-Methylchloropropionate in PDMS

Whereas the expected separation was shown for the aliphatic pair of analytes, the picture is not so clear when considering the isomeric pairs. From the physiochemical data collected on these analytes, some resolution would be expected between the m-/p- and cis-/trans- isomers due to differences noted, though there was no indication that the enantiomers would exhibit any selectivity. These predictions were borne out by the analytical results obtained, where some selectivity was shown between cis-/trans-2-hexene and m-/p-xylene at lower temperatures, although not of any significant magnitude. The fabrication of PDMS columns with sufficient efficiency to fully separate these analytes would present great physical difficulties. No discrimination was shown at all for the enantiomeric pair at any temperature; the expected analytical behaviour of PDMS was therefore observed.

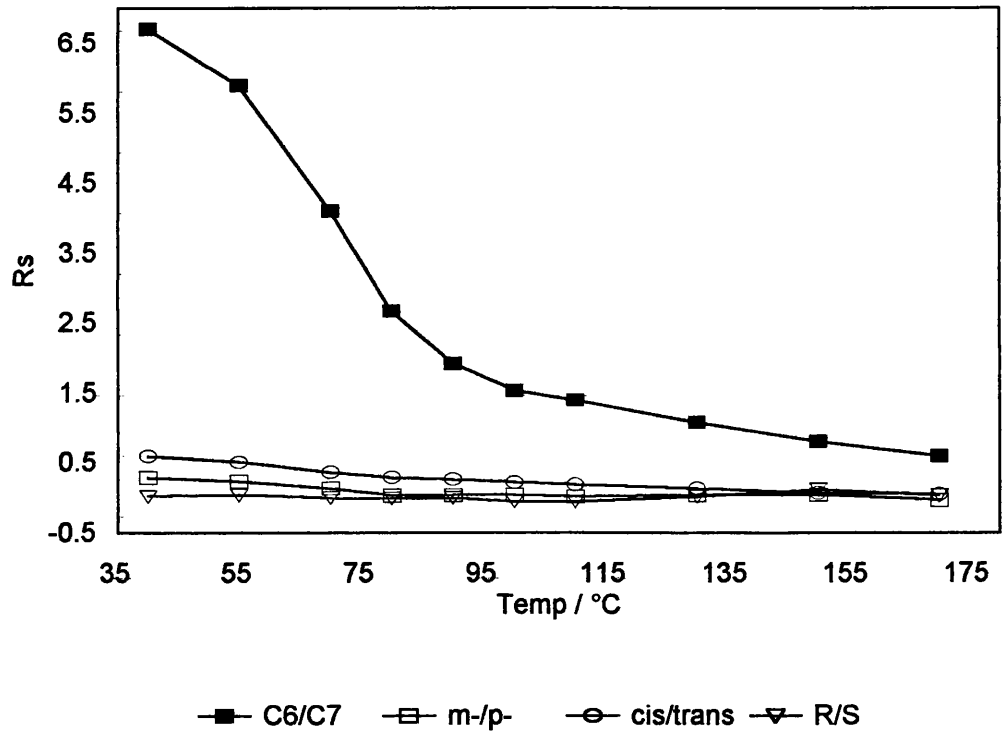

Figure 3.14: Resolution vs Temperature for PDMS

3.4 PRELIMINARY CONCLUSIONS

Making reference to (1.5.1), the objective of describing the preparation of IGC instrumentation and methodology to elucidate meaningful results with respect to liquid crystalline systems has been achieved. Summarising the research described in this chapter it has been shown that:

- Probes were selected which were readily available, proven in previous IGC studies, of known physiochemical behaviour, and involved minimal interference with the stationary phase materials studied.

- Loading of liquid crystalline materials onto the stationary phase of approximately 10% w/w enabled results to be obtained in confidence that the interactions are due primarily to probe/stationary phase interactions, minimising probe/support material interactions and effects on orientation within the mesophase due to interaction with the support material.

- Probe injection volumes of 0.1μl were used in all work, as these approximated to infinite dilution on the stationary phase considered, and were of sufficient volume to allow reliable reproduction.

- In order to overcome the effects of liquid crystalline supercooling on the stationary phase, the GC columns containing the mesogenic materials were allowed to equilibrate at room temperature for at least 24 hours after initial conditioning. Experimental work was then carried out using only increases in GC oven temperature, with an equilibration time of at least 30 minutes before data collection commenced.

- Transition temperatures obtained for low molecular mass and polymeric liquid crystalline materials by DSC and IGC were found to be comparable within experimental uncertainty. Methodology adopted for the rest of this research utilised temperatures away from the mesophase transition temperatures to avoid observed transitional effects.

- Initial work on the IGC system using a PDMS stationary phase gave results comparative to those elucidated by previous researchers in this field. This gave confidence that the methodology describes meaningful physiochemical and analytical results using liquid crystalline materials, within experimental uncertainty, and provides a comparative reference for the remainder of the work presented in this thesis.

Chapter 4 will now describe the solution behaviour observed between probe and stationary phase, using low molecular mass and polymeric liquid crystalline systems as stationary phases for IGC

Chapter Four:

PHYSIOCHEMICAL RESULTS

FOR LIQUID CRYSTALLINE SYSTEMS

This chapter presents the physiochemical results obtained using IGC with liquid crystalline stationary phases, allowing a description of the solution properties of probes with liquid crystalline materials to be made. An analysis of the results is presented prior to consideration of the analytical properties of the liquid crystalline stationary phases in Chapter 5.

All results were obtained using the GC columns described in (2.3.1). GC oven temperatures were selected to enable experimental results to be obtained in each of the mesophases exhibited by the stationary phase. At each temperature a suitable flow rate was selected to both enable efficient retention times and peak integrity to be maintained, and to establish a reasonable pressure difference between the column inlet and outlet. All calculations were carried out as outlined in (1.4.3).

The results are presented in roughly chronological order, starting with the materials supplied by Merck UK Ltd., moving to the low molecular mass system and concluding with the polymeric liquid crystals. Retention diagrams and activity-coefficient plots include values calculated in the crystalline phase. The reader is reminded that all interactions of the probe with the crystalline phase are attributable to *surface effects only* (such as adsorption), and are included to act as a reference to solution properties. The retention behaviour for each 'family' of probes in system is described, followed by trends in activity coefficients and enthalpic and entropic properties of solution. The comparisons begin with PDMS, and proceed to build on the preceding liquid crystalline systems studied in order to describe the differences in solution properties of interactions between probes and the various types of stationary phase.

Throughout this chapter, the term "favourable mixing" is used to describe thermodynamic parameters which match ideal conditions most closely. This is a comparative term, and does not in itself suggest ideality. For enthalpic and entropic terms, "favourable" indicates a contribution which acts to enhance the solution formation relative to the other systems considered.

4.1 COMPARISON OF MOLE FRACTION AND WEIGHT FRACTION ACTIVITY COEFFICIENTS

The liquid crystal BDH509 was studied initially in order to ensure the system, which had been proven for PDMS, was also suitable for the study of liquid crystalline materials. The structure of BDH509 is shown in Figure 4.1, with discussion of the structure and properties being found in (2.1) and (3.3.1).

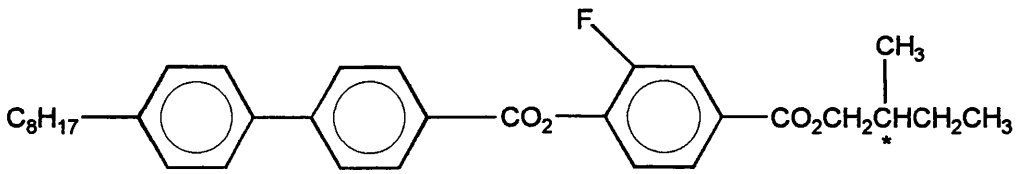

BDH509 - chiral **BDH770** - racemic

Figure 4.1: Structure of BDH509 and BDH770

4.1.1 RETENTION BEHAVIOUR

The retention diagrams obtained, shown in Figure 4.2 to Figure 4.4, illustrate the expected behaviour for a liquid crystalline system; on a phase transition a distinct change in the temperature dependence of Vg° within a particular phase is noted. For all probes, the same trends are noted as with PDMS in (3.4.1b). The *aliphatic* probes show the trend $Vg°_{C6} < Vg°_{2\text{-methylhexane}} < Vg°_{C7} < Vg°_{2,2\text{-dimethylhexane}} < Vg°_{C8}$. An identical trend is noted in all phases, and an increase in the number of carbon atoms and extent of branching is accompanied by a linear increase in Vg°.

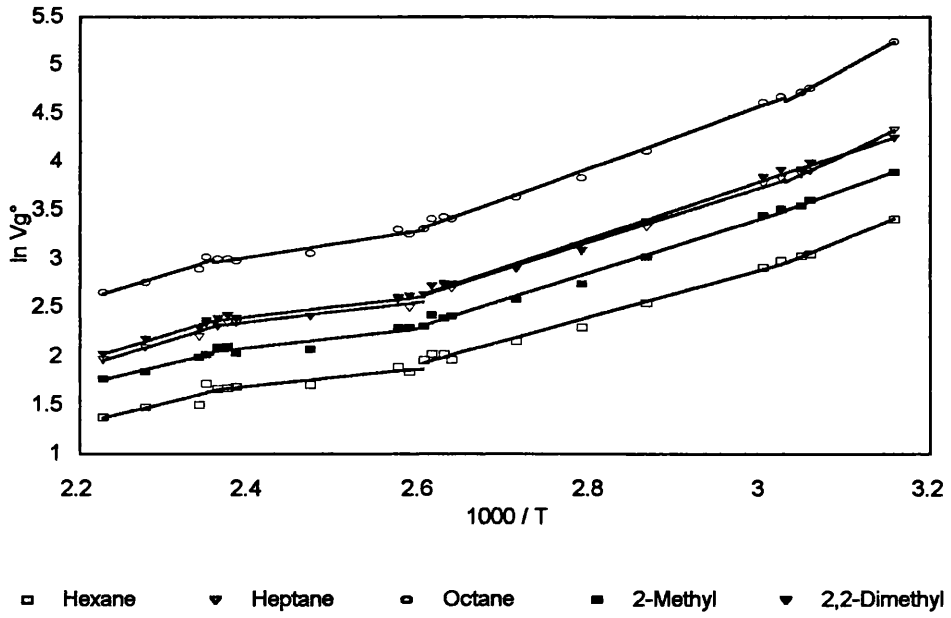

Figure 4.2: ln Vg° vs 1/T for Aliphatic Probes in BDH509

The *aromatic* probes have a greater retention volume than the aliphatic probe with a corresponding number of carbon atoms, and the trend in $Vg°_{benzene} < Vg°_{toluene} < Vg°_{ethylbenzene}$ shows a linear correlation. Compared with PDMS, the xylenes show differing retention properties, exhibiting an increased Vg° above that shown by ethylbenzene.

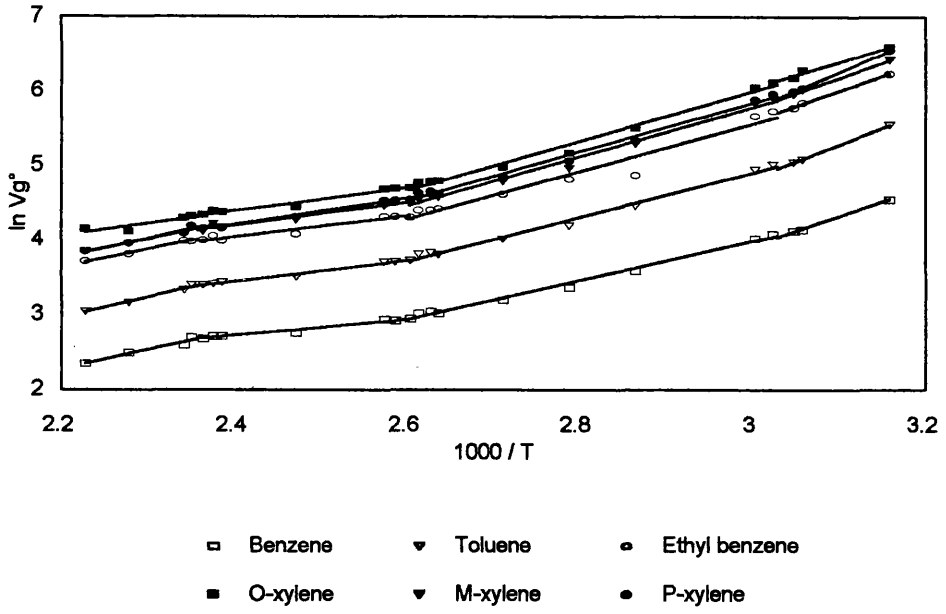

Figure 4.3: ln Vg° vs 1/T for Aromatic Probes in BDH509

While o-xylene shows greater retention than either m- or p-xylene, the latter probes now show differences in retention which were not apparent in PDMS, particularly within the S_C mesophase. This does not allow for a full description of the interaction between the probes and stationary phase, but indicates a greater degree of selectivity for the xylenes in the liquid crystalline stationary phase.

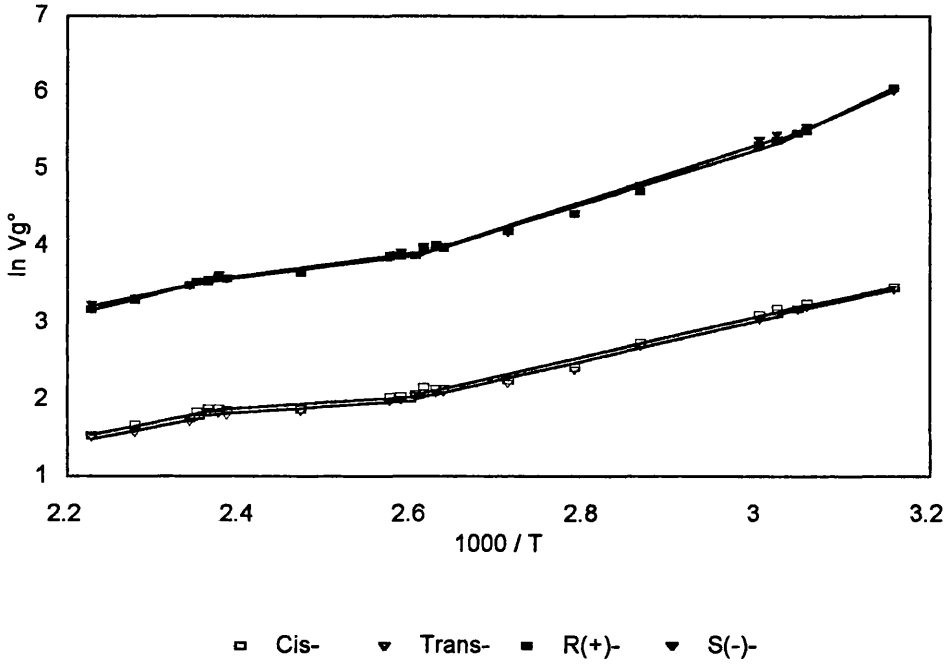

Figure 4.4: ln Vg° vs 1/T for Isomeric Probes in BDH509

Considering the *isomeric* probes, the geometrical isomers show similar Vg° values and trends with BDH509 as they did with PDMS at all temperatures, and exhibit small differences in retention. The enantiomers show increased retention in BDH509 over that shown in PDMS, but there is very little discrimination apparent except for some small difference in Vg° (above that accounted for by experimental uncertainty) in the S_C mesophase.

For all probes the liquid crystalline transitions are accompanied by a small increase in Vg° (after compensation for temperature change) and a change in linear dependence on temperature. However, all such changes are of a smaller magnitude and over a smaller range than would be shown for transitions in non-mesogenic material, so aside from determination of mesophase transition temperatures (see 3.3.1c) little information on the relative adsorption and absorption of the probes with the stationary phase can be obtained from the retention diagrams.

4.1.2 ACTIVITY COEFFICIENTS

As described in (1.4.4) the weight fraction activity coefficient, Ω^∞, may be obtained for polymeric materials, whilst the mole fraction activity coefficient, γ^∞, may be calculated for low molecular mass materials. Polymeric systems studied later in this chapter (4.4) are described in terms of Ω^∞, so a comparison is made here between Ω^∞ and γ^∞ values obtained for BDH509 in order to allow meaningful conclusions to be drawn. Mathematically, the difference between γ^∞ and Ω^∞ is described by a constant change in intercept for any given probe, which may act to reverse trends noted for γ^∞ from those described by Ω^∞, and *vice versa*. The plots of ln γ^∞ and ln Ω^∞ *vs* 1/T are shown in Figure 4.5 to Figure 4.10. Note that activity coefficients may not strictly be calculated in the crystalline phase, as such interactions are due solely to surface adsorption.

A consideration of activity coefficients for the aliphatic probes immediately illustrates the considerable differences between γ^∞ and Ω^∞. Prior to consideration of the trends within individual series of probes, the comparative values of γ^∞ and Ω^∞ are presented in Table 4.1. A molar activity coefficient of 1 indicates the formation of an ideal solution, with $\gamma^\infty>1$ indicating a positive deviation from Raoult's law and $\gamma^\infty<1$ showing a negative deviation from Raoult's law, as discussed in (1.4.1a). The correlation between γ^∞ and Ω^∞ for all low molecular mass stationary phases used in this study are identical to those presented in the table, therefore descriptions of the ideality of solution behaviour may be made considering these values as reference points.

PROBE	Ω^{∞} when $\gamma^{\infty} = 1$	ln Ω^{∞} when ln $\gamma^{\infty} = 0$
hexane	5.18	1.65
heptane	4.45	1.49
octane	3.91	1.36
2-me	4.45	1.49
2,2-dime	3.91	1.36
benzene	5.50	1.71
toluene	4.85	1.58
ethylbenzene	4.21	1.44
o-xylene	4.21	1.44
m-xylene	4.21	1.44
p-xylene	4.21	1.44
cis-	5.31	1.67
trans-	5.31	1.67

Table 4.1: Comparison of γ^{∞} and Ω^{∞} at Ideal Mixing

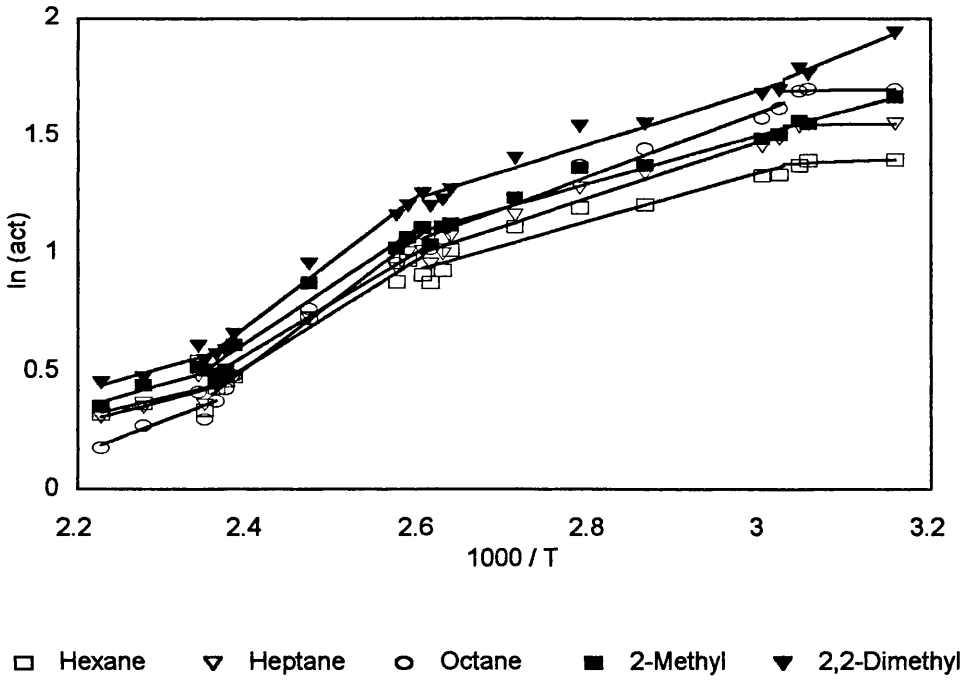

Figure 4.5: ln γ^{∞} vs 1/T for Aliphatic Probes in BDH509

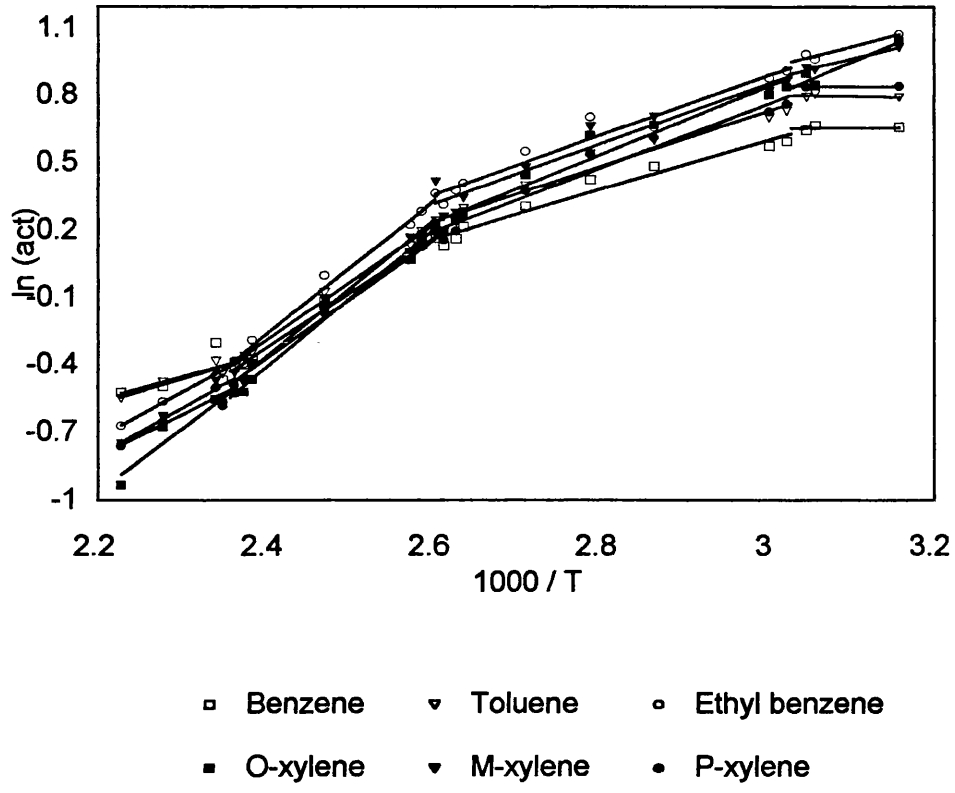

Figure 4.6: ln γ^{∞} vs 1/T for Aromatic Probes in BDH509

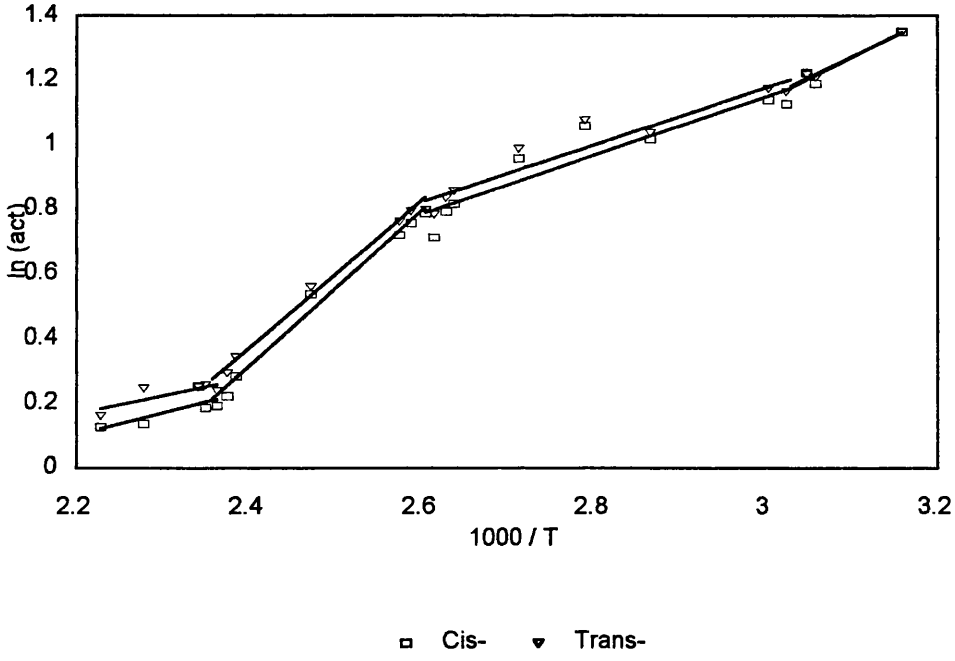

Figure 4.7: ln γ^{∞} vs 1/T for Isomeric Probes in BDH509

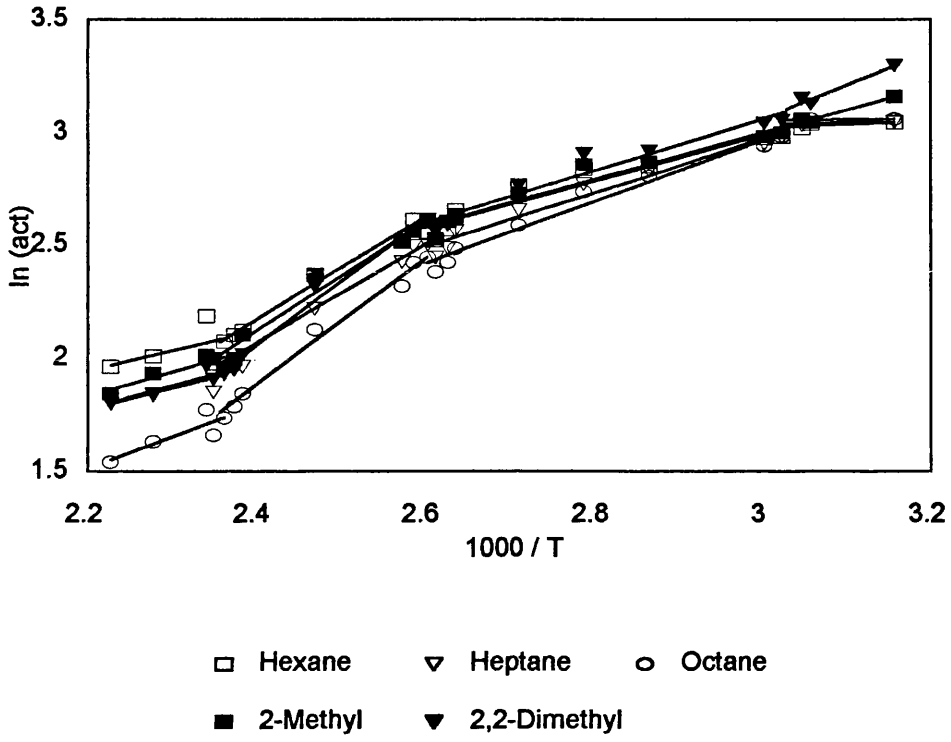

Figure 4.8: ln Ω° vs 1/T for Aliphatic Probes in BDH509

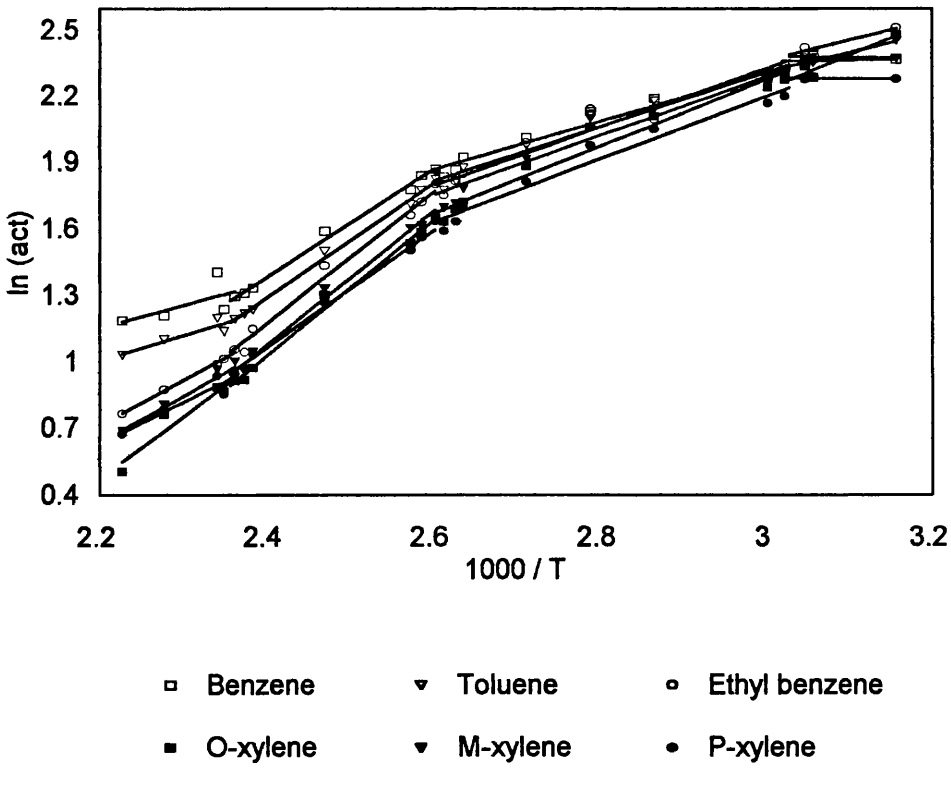

Figure 4.9: ln Ω° vs 1/T for Aromatic Probes in BDH509

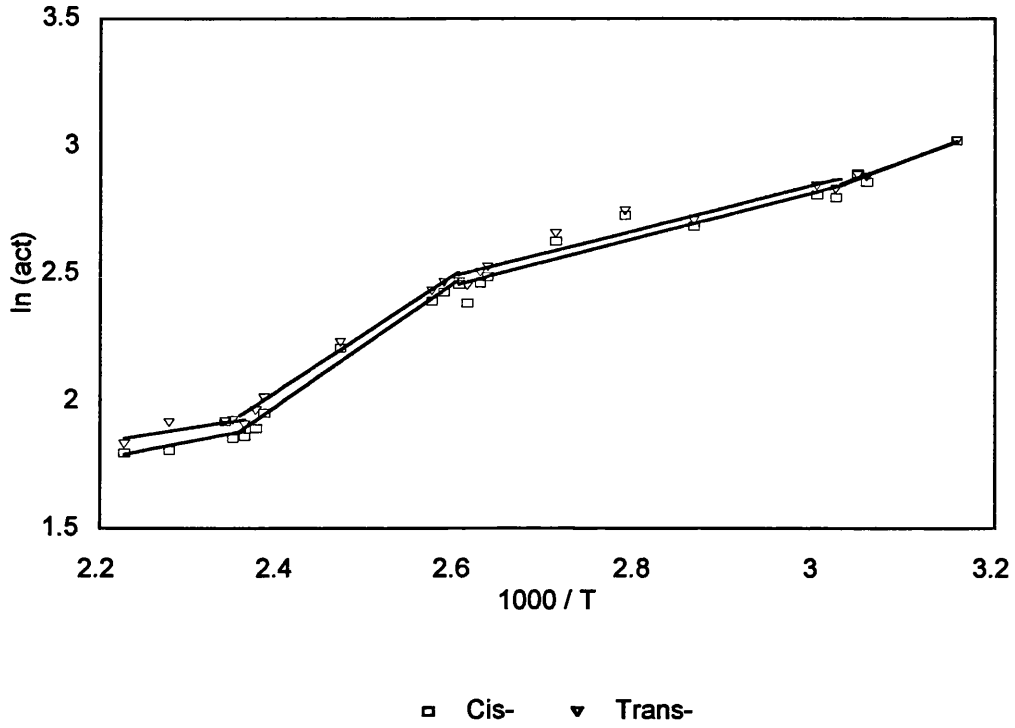

Figure 4.10: ln Ω^{∞} vs 1/T for Isomeric Probes in BDH509

A consideration of γ^{∞} and Ω^{∞} show different trends to be observed as a consequence of the adjustment to the weight fraction activity coefficient. Whilst these trends do not in themselves mean different results are being obtained by the two methods, they emphasise the importance of carefully considering the consequences in using Ω^{∞} values to describe the solution behaviour in terms of deviations from Raoult's law.

In all phases, the *aliphatic* probes show the trend $\gamma^{\infty}_{C6} > \gamma^{\infty}_{C7} > \gamma^{\infty}_{C8}$ with the branched probes showing the trend $\gamma^{\infty}_{2,2\text{-dimethylhexane}} > \gamma^{\infty}_{2\text{-methylhexane}} > \gamma^{\infty}_{C6}$. The branched alkanes show larger activities than the n-alkanes. At a change in a mesophase with increasing temperature there is a decrease in activities for all probes, showing the deviation from ideality to be reduced. The temperature dependence of γ^{∞} within a phase varies, with the greatest effect being exhibited in the nematic mesophase. These observations suggest that for all aliphatic probes, solution formation improves as the mesophase becomes less ordered. In addition, an increase in chain length increases compatibility with the mesophase, but branching acts to prevent solution. In molecular terms this may be explained considering the structure of the mesophase; the short chains have no particular affinity for any portion of the stationary phase, and the addition of branching acts to hinder interaction further, whilst an increase in chain length allows enhanced interaction with the aliphatic terminal group (on a "like dissolves like" basis).

Drawing comparisons with PDMS, γ^{∞} for all probes on mixing with BDH509 show a substantial temperature dependence not noted previously. At lower temperatures, γ^{∞} values for all probes are of a far greater magnitude than at the equivalent temperature in PDMS, showing a greater non-ideality behaviour in mixing with the liquid crystalline stationary phase. Furthermore, there are more notable differences in γ^{∞} values between individual probes and families of probes. With respect to the aliphatic probes this indicates unfavourable solution formation, particularly in more ordered mesophase structures. The trend $\gamma^{\infty}_{C6} < \gamma^{\infty}_{2\text{-methylhexane}} < \gamma^{\infty}_{2,2\text{-dimethylhexane}}$ is noted on further consideration of the branched probes. This may be explained considering the thermal energy available to branched probes: Considering the mesophase and a rigid probe as two rigid systems, an input of thermal energy causes the systems to rotate relative to one another, reducing the strength of their interaction. If one system (the probe) were totally flexible its thermal energy would be utilised to adopt different conformations, allowing a flexible probe to increase interaction with the stationary phase over that shown by a rigid probe.

Slightly different trends are observed when considering weight fraction activity coefficients; the general order $\Omega^{\infty}_{C6} > \Omega^{\infty}_{C7} > \Omega^{\infty}_{C8}$ is again exhibited, but the branched chains show the reversed trend $\Omega^{\infty}_{C6} > \Omega^{\infty}_{2\text{-methylhexane}} > \Omega^{\infty}_{2,2\text{-dimethylhexane}}$. This again emphasises the need to carefully consider weight fraction activity coefficient data.

For all *aromatic probes* the activity coefficients are substantially lower than for the aliphatic probes, showing more favourable solution formation. As temperature increases through the nematic to the isotropic phase, all aromatic probes show ideal mixing (where $\gamma^{\infty}=1$) and proceed to show negative deviations from Raoult's law. This indicates a significant difference from the behaviour exhibited with PDMS, showing the liquid crystal to be a more favourable solvent for aromatic probes. The probes show the trend $\gamma^{\infty}_{ethylbenzene} > \gamma^{\infty}_{toluene} > \gamma^{\infty}_{benzene}$ throughout the mesophases, but this trend reverses in the isotropic phase. No trend is discernible for the xylenes, though in the S_C mesophase $\gamma^{\infty}_{xylenes} > \gamma^{\infty}_{benzene}$, a trend which is reversed in the nematic and isotropic phases, which show $\gamma^{\infty}_{benzene} > \gamma^{\infty}_{xylenes}$. These trends indicate that in the more ordered mesophases, the interaction between probe and stationary phase is hindered by the presence of substitution, the "like dissolves like" generalisation is not applicable, and therefore the mesophase structure must be having some effect on the solution process. In the S_C mesophase and isotropic liquid, favourable solvation occurs with increases in aliphatic chain length and substitution resulting in enhanced solvation, and disruption of the phase structure by the probe. This suggests the mixing in the less ordered structures is reliant solely interactions between the probe and stationary phase, with minimal hindrance from the mesophase structure and liquid crystal-liquid crystal

interactions. A comparison of Ω^{∞} shows a reversal in the noted trends, with $\gamma^{\infty}_{ethylbenzene} < \gamma^{\infty}_{toluene} < \gamma^{\infty}_{benzene}$ and $\gamma^{\infty}_{benzene} < \gamma^{\infty}_{xylenes}$ with the nematic and isotropic phases.

The magnitude of γ^{∞} values shown by the *isomeric probes* is greater than those shown by the aromatic probes, and similar to those shown by the aliphatic probes - except in the S_C mesophase where $\gamma^{\infty}_{isomer} < \gamma^{\infty}_{aliphatic}$. This is an indication that the C=C bond is acting to improve the interactions with a more ordered mesophase structure, but as this order is lost no advantage is conferred to the alkene isomers over the aliphatic probes. Due to the presence of the C=C bond, the alkenes may be considered to be both more rigid and more polarisable than a comparable alkane. The corresponding increase in rigidity leads to weaker solute-solvent interactions, whilst the increase in polarisability gives rise to stronger interactions. The trends in activity coefficients for the alkenes, with the S_C mesophase therefore indicate polarisability to predominate in the solute-solvent interactions, whilst the nematic and isotropic phases show $\gamma^{\infty}_{aliphatic} < \gamma^{\infty}_{alkene}$ where rigidity predominates. Similar results have been shown in previous work by Oweimreen[249], who noted that as the C=C bond moves towards the centre of an alkene rigidity is increased and γ^{∞} decreases. In a particular phase the cis- and trans- isomers have different γ^{∞} values, with $\gamma^{\infty}_{cis} < \gamma^{\infty}_{trans}$ in all phases, indicating an enhanced interaction for cis-2-hexene.

Overall, it is shown from the activity coefficient values that substantial deviations from ideality exist for the aliphatic and isomeric probes in all phases, and that the aromatic probes form favourable solutions - particularly in the less ordered nematic mesophase and isotropic liquid. The discussion will now consider the solution and excess properties of these mixtures in order to explain the mechanism by which these activity coefficient observations arise.

4.1.3 SOLUTION AND EXCESS PROPERTIES

From the plots of ln Vg°, ln γ^{∞} and ln Ω^{∞} *vs* 1/T, the solution and excess properties for probe/stationary phase mixing were calculated. These results are shown in Table 4.1 to Table 4.4, and their interpretation allows an explanation of the activity coefficient trends noted in (4.1.2). The tabulated values in parentheses are the experimental uncertainties calculated from the standard deviation of regression.

From these results, it is shown that the excess enthalpies and entropies for all probes in the S_C, N and isotropic phases are positive. Combined with the activity coefficient data presented in (4.1.2) it may be stated than the probes used show non-ideal solution

Probe	Enthalpic kJ mol^{-1}			Entropic J mol^{-1} K^{-1}		
	ΔH^s	ΔH^e	ΔH^{vap}	ΔS^s	ΔS^e	ΔS^{vap}
Hexane	-29.21 (0.17)	1.23 (0.17)	-30.44 (0.34)	-49.69 (0.01)	-6.68 (0.01)	-43.01 (0.02)
Heptane	-34.64 (0.10)	0.60 (0.10)	-35.24 (0.20)	-59.21 (0.01)	-9.98 (0.01)	-49.22 (0.02)
Octane	-39.66 (0.08)	0.39 (0.08)	-40.04 (0.16)	-67.44 (0.01)	-11.84 (0.01)	-55.60 (0.02)
2-Me	-25.28 (0.19)	8.29 (0.20)	-33.57 (0.39)	-33.26 (0.02)	13.41 (0.02)	-46.67 (0.02)
2,2-DiMe	-23.38 (0.32)	12.50 (0.32)	-35.87 (0.64)	-24.31 (0.03)	24.43 (0.03)	-48.75 (0.06)
Benzene	-32.26 (0.18)	0.40 (0.17)	-32.66 (0.35)	-49.88 (0.02)	-3.21 (0.02)	-46.67 (0.04)
Toluene	-37.47 (0.12)	-0.58 (0.11)	-36.89 (0.33)	-58.03 (0.01)	-7.40 (0.01)	-59.63 (0.01)
Ethylbenzene	-33.11 (0.24)	7.88 (0.25)	-40.99 (0.49)	-38.56 (0.02)	16.98 (0.02)	-55.54 (0.04)
O-Xylene	-29.15 (0.54)	13.10 (0.54)	-42.25 (1.08)	-23.05 (0.05)	33.73 (0.05)	-56.79 (0.10)
M-Xylene	-33.99 (0.14)	7.47 (0.14)	-41.46 (0.28)	-39.80 (0.01)	16.18 (0.01)	-55.98 (0.02)
P-Xylene	-41.34 (0.11)	-0.19 (0.11)	-41.15 (0.22)	-61.95 (0.01)	-6.57 (0.01)	-55.39 (0.02)
Cis-	-19.36 (0.38)	11.19 (0.38)	-30.55 (0.76)	-18.14 (0.03)	25.17 (0.03)	-43.31 (0.06)
Trans-	-19.77 (0.17)	10.67 (0.17)	-30.44 (0.34)	-19.69 (0.02)	23.53 (0.02)	-43.22 (0.02)
R(+)	-44.72 (0.19)	n/a	n/a	-76.66 (0.01)	n/a	n/a
S(-)	-40.54 (0.23)	n/a	n/a	-63.74 (0.02)	n/a	n/a

Table 4.1: Physiochemical Results for BDH509 in the Crystalline Phase

Probe	Enthalpic kJ mol^{-1}			Entropic J mol^{-1} K^{-1}		
	ΔH^s	ΔH^e	ΔH^{vap}	ΔS^s	ΔS^e	ΔS^{vap}
Hexane	-20.07 (0.11)	8.58 (0.11)	-28.66 (0.22)	-22.01 (0.05)	15.64 (0.05)	-37.65 (0.10)
Heptane	-23.33 (0.10)	9.99 (0.08)	-33.31 (0.18)	-24.73 (0.05)	18.73 (0.04)	-43.47 (0.09)
Octane	-26.50 (0.10)	11.33 (0.08)	-37.83 (0.18)	-27.25 (0.05)	21.73 (0.04)	-48.98 (0.09)
2-Me	-23.08 (0.10)	8.63 (0.09)	-31.71 (0.19)	-26.66 (0.05)	14.44 (0.04)	-41.10 (0.09)
2,2-DiMe	-24.56 (0.11)	9.60 (0.10)	-34.16 (0.22)	-27.89 (0.05)	15.76 (0.05)	-43.65 (0.10)
Benzene	-21.89 (0.09)	9.13 (0.08)	-31.01 (0.17)	-18.32 (0.04)	23.43 (0.04)	-41.75 (0.09)
Toluene	-24.88 (0.10)	10.31 (0.09)	-35.19 (0.19)	-19.65 (0.05)	25.88 (0.04)	-45.53 (0.09)
Ethylbenzene	-26.56 (0.25)	11.10 (0.11)	-37.66 (0.36)	-19.27 (0.12)	26.93 (0.05)	-46.21 (0.17)
O-Xylene	-27.65 (0.13)	12.66 (0.12)	-40.31 (0.25)	-18.96 (0.06)	32.04 (0.06)	-50.99 (0.12)
M-Xylene	-27.46 (0.13)	11.17 (0.15)	-38.63 (0.28)	-20.14 (0.06)	27.44 (0.07)	-47.58 (0.13)
P-Xylene	-27.42 (0.11)	11.84 (0.10)	-39.26 (0.21)	-19.50 (0.05)	30.21 (0.05)	-49.71 (0.10)
Cis-	-21.54 (0.14)	7.53 (0.13)	-29.06 (0.27)	-24.77 (0.06)	14.08 (0.05)	-38.85 (0.11)
Trans-	-21.42 (0.12)	7.35 (0.10)	-28.77 (0.22)	-24.91 (0.05)	13.32 (0.05)	-38.23 (0.10)
R(+)	-29.08 (0.14)	n/a	n/a	-29.35 (0.06)	n/a	n/a
S(-)	-30.36 (0.16)	n/a	n/a	-32.66 (0.05)	n/a	n/a

Table 4.2: Physiochemical Results for BDH509 in the Smectic C Mesophase

Probe	Enthalpic kJ mol^{-1}			Entropic J mol^{-1} K^{-1}		
	ΔH^s	ΔH^e	ΔH^{vap}	ΔS^s	ΔS^e	ΔS^{vap}
Hexane	-7.36 (0.14)	18.86 (0.17)	-26.22 (0.32)	10.62 (0.43)	41.96 (0.04)	-31.33 (0.47)
Heptane	-8.31 (0.17)	18.11 (0.28)	-26.41 (0.45)	13.81 (0.04)	39.75 (0.06)	-25.93 (0.10)
Octane	-11.21 (0.19)	23.11 (0.21)	-34.32 (0.40)	12.38 (0.22)	52.20 (0.04)	-39.83 (0.26)
2-Me	-8.18 (0.26)	20.10 (0.29)	-28.28 (0.54)	11.92 (0.27)	44.10 (0.06)	-32.17 (0.33)
2,2-DiMe	-8.38 (0.18)	23.15 (0.22)	-31.53 (0.40)	14.08 (0.01)	50.86 (0.04)	-36.78 (0.05)
Benzene	-8.73 (0.11)	20.20 (0.14)	-28.92 (0.25)	15.94 (0.21)	52.22 (0.03)	-36.28 (0.24)
Toluene	-11.61 (0.10)	21.36 (0.11)	-32.98 (0.21)	14.98 (0.10)	54.74 (0.02)	-39.75 (0.12)
Ethylbenzene	-11.78 (0.19)	24.66 (0.24)	-36.44 (0.43)	19.55 (0.64)	62.44 (0.05)	-42.90 (0.69)
O-Xylene	-12.57 (0.17)	25.40 (0.21)	-37.97 (0.38)	20.58 (0.77)	65.44 (0.04)	-44.85 (0.81)
M-Xylene	-12.72 (0.17)	25.10 (0.19)	-37.82 (0.36)	18.60 (0.53)	64.30 (0.04)	-45.70 (0.57)
P-Xylene	-14.77 (0.10)	21.91 (0.11)	-36.68 (0.21)	13.76 (0.05)	56.74 (0.02)	-42.98 (0.07)
Cis-	-6.19 (0.16)	20.10 (0.18)	-26.29 (0.34)	15.02 (0.10)	46.67 (0.04)	-31.64 (0.14)
Trans-	-6.58 (0.13)	19.04 (0.10)	-25.62 (0.23)	13.61 (0.07)	43.65 (0.02)	-30.04 (0.09)
R(+)	-11.95 (0.13)	n/a	n/a	15.38 (0.14)	n/a	n/a
S(-)	-12.72 (0.16)	n/a	n/a	13.65 (0.43)	n/a	n/a

Table 4.3: Physiochemical Results for BDH509 in the Nematic Mesophase

Probe	Enthalpic kJ mol^{-1}			Entropic J mol^{-1} K^{-1}		
	ΔH^s	ΔH^e	ΔH^{vap}	ΔS^s	ΔS^e	ΔS^{vap}
Hexane	-17.56 (0.99)	7.11 (0.77)	-24.67 (1.76)	-13.54 (0.10)	14.17 (0.09)	-27.70 (0.19)
Heptane	-22.06 (0.56)	7.76 (0.47)	-29.82 (1.03)	-18.68 (0.06)	15.78 (0.05)	-34.46 (0.11)
Octane	-22.24 (0.54)	11.47 (0.46)	-33.72 (1.00)	-13.41 (0.05)	25.04 (0.05)	-38.45 (0.10)
2-Me	-17.15 (0.17)	8.78 (0.29)	-25.93 (0.46)	-9.39 (0.02)	17.56 (0.03)	-26.95 (0.05)
2,2-DiMe	-21.62 (0.29)	8.41 (0.29)	-30.03 (0.58)	-17.14 (0.03)	16.11 (0.03)	-33.25 (0.06)
Benzene	-20.93 (0.43)	8.41 (0.66)	-29.34 (1.09)	-12.86 (0.04)	24.12 (0.08)	-36.97 (0.12)
Toluene	-23.00 (0.26)	9.36 (0.25)	-32.36 (0.51)	-11.80 (0.03)	26.37 (0.02)	-38.17 (0.05)
Ethylbenzene	-19.37 (0.17)	16.90 (0.08)	-36.27 (0.25)	1.89 (0.02)	44.25 (0.10)	-42.35 (0.12)
O-Xylene	-12.98 (0.64)	23.38 (0.46)	-36.37 (1.10)	19.46 (0.06)	60.51 (0.05)	-41.05 (0.11)
M-Xylene	-20.37 (0.37)	17.47 (0.37)	-37.84 (0.74)	0.72 (0.04)	46.14 (0.04)	-45.42 (0.08)
P-Xylene	-21.44 (0.38)	15.53 (0.35)	-36.98 (0.73)	-1.66 (0.04)	41.92 (0.04)	-43.57 (0.08)
Cis-	-18.51 (0.40)	5.54 (0.32)	-24.05 (0.72)	-14.20 (0.04)	12.37 (0.04)	-26.56 (0.08)
Trans-	-17.41 (0.34)	4.48 (0.23)	-21.89 (0.57)	-12.21 (0.03)	9.48 (0.03)	-21.69 (0.06)
R(+)	-23.67 (0.16)	n/a	n/a	-12.18 (0.02)	n/a	n/a
S(-)	-20.36 (0.24)	n/a	n/a	-4.42 (0.10)	n/a	n/a

Table 4.4: Physiochemical Results for BDH509 in the Isotropic Phase

formation with all phases of the liquid crystalline material. The general trends within the phase for the solvents used may be described as:

$$\gamma^{\infty}_{\text{isotropic}} < \gamma^{\infty}_{\text{nematic}} < \gamma^{\infty}_{\text{smectic C}} \quad [1]$$

$$\Delta H^{s}_{\text{nematic}} > \Delta H^{s}_{\text{isotropic}} > \Delta H^{s}_{\text{smectic C}} \quad [2]$$

$$\Delta H^{e}_{\text{nematic}} > \Delta H^{e}_{\text{isotropic}} > \Delta H^{e}_{\text{smectic C}} \quad [3]$$

$$\Delta S^{s}_{\text{nematic}} > \Delta S^{s}_{\text{isotropic}} > \Delta S^{s}_{\text{smectic C}} \quad [4]$$

$$\Delta S^{e}_{\text{nematic}} > \Delta S^{e}_{\text{isotropic}} > \Delta S^{e}_{\text{smectic C}} \quad [5]$$

The activity data presented in trend [1] shows that the most favourable mixtures in terms of activity coefficients are formed with the isotropic phase, followed by the nematic phase and finally the smectic C phase. Thus a decrease in phase structural order increases the ideality of mixing. However, information is not given here on the mechanisms by which these mixtures are formed, so the trends in solution and excess enthalpies and entropies of mixing must be considered.

Trend [2] considers the enthalpies of solution. Values of ΔH^{s} were most negative for all probes with the S_C mesophase, indicating the most favourable solvent-solute interactions occurred with this phase. Within the isomeric phase, values of ΔH^{s} for the aliphatic probes were of a similar magnitude to those shown by the S_C mesophase, whilst the aromatic probes show less negative ΔH^{s} values than the S_C mesophase, indicating that interactions between the aromatic probes and S_C mesophase are comparatively more favourable than such interactions with the isotropic phase. The N mesophase shows significantly less negative ΔH^{s} values for all probes, indicating a weaker solvent-solute interaction.

Trends in the excess enthalpies of solution, ΔH^{e}, are shown in [3]. The N mesophase exhibits the largest excess for all probes, followed by the isotropic phase and the S_C mesophase. Whilst ΔH^{e} values in the isotropic phase for the aliphatic probes are lower than the nematic, those for the aromatic probes are of a similar magnitude. The S_C mesophase shows reduced values for both families of probes. The high excess enthalpies in the N mesophase indicate unfavourable enthalpies of mixing for all probes, whilst the aliphatic probes mix more easily in the isotropic phase (when the aromatic probes do not), and both sets of probes show more favourable enthalpies on mixing with the S_C mesophase. Thus, the solution behaviour in the S_C mesophase is indicative of enthalpically-driven mixing. It would be expected that the more ordered S_C mesophase would require higher excess enthalpies to disrupt the layer-structure in order to form solutions. That this is not the case suggests the formation of solutions occurs locally within the macrostructure; with aliphatic probes interacting between the

smectic layers with the flexible end-groups of the liquid crystalline material, and aromatic probes interacting with the aromatic core of the smectic layers. Unfavourable interactions are therefore minimised, and both sets of probes show reasonable enthalpic properties for solution formation.

Thus, consideration of the enthalpies of mixing suggests the most favourable mixtures are formed with the S_C mesophase, followed by the isotropic phase, and that the N mesophase is least favourable. These trends contradict the results summarised in trend [1] for activity coefficients, so other factors must be taken into consideration when determining the mechanism by which probe/liquid crystal mixtures are formed.

Considering the entropy of solution, ΔS^s, trend [4] is observed. The S_C mesophase has the most negative ΔS^s, which along with the highly negative ΔH^s values for this mesophase indicate the formation of strong solvent-solute interactions. Such interactions act to restrict the translational freedom of the solvent in the mixture, and decrease the entropy contribution to the mixture - as shown by solutions with the S_C mesophase having the least positive ΔS^e values. The isotropic phase would be expected to allow more entropic freedom than the mesophases, though the values obtained show less favourable entropy than the nematic mesophase. This behaviour has been previously encountered by Ghodbone *et al*[250], and is explained by the lack of long-range orientational order between solvent molecules in the isotropic phase allowing greater rotational and conformational freedom to the solute, thus decreasing entropy on mixing. Within the isotropic phase, the aliphatic probes show strongly negative ΔS^s values, whilst the aromatic probes show less negative values, and in the case of ethylbenzene and the xylenes, positive values for ΔS^s are shown. This indicates unfavourable entropy for mixing of aliphatic probes with the stationary phase, but positive entropy for the aromatic probes - especially substituted aromatics. The nematic mesophase shows positive values for ΔS^s, so despite mixtures in this mesophase being the least favoured considering their enthalpic properties, their strong entropic contributions act to overcome this. The excess entropies of solution, ΔS^e, shown in trend [5] confirm the discussion on ΔS^s values. The most positive values for all probes are shown by the nematic mesophase, followed by the isotropic mesophase, with the S_C mesophase showing the least positive ΔS^e values for all probes.

The *aliphatic probes* may be considered in terms of their chain length. As the number of carbon atoms (and therefore chain length) increases, the polarisability of the probe also increases. This in turn leads to stronger interactions between solute and solvent, which is reflected by a decrease in ΔH^s. Indeed, this is the trend observed in the results for aliphatic probes with BDH509. These interactions are enthalpy-dominated.

Conversely, as chain length increases restrictions in solvation may occur where the available conformations of the probe result in less favourable entropy on mixing, and hence show more negative ΔS^s values. The values obtained indicate that enthalpy dominates in the S_C mesophase, entropy plays a predominant role in N, and enthalpy is favourable in the isotropic liquid. These observations are borne out in the activity coefficients where $\gamma^\infty_{isotropic} < \gamma^\infty_{nematic} < \gamma^\infty_{smectic\ C}$ and $\gamma^\infty_{C8} < \gamma^\infty_{C7} < \gamma^\infty_{C6}$. Branching may be considered in similar terms. As branching increases, the probe becomes more rigid and the molecular shape becomes more "globular" and therefore able to adopt fewer conformations. By consideration of the interaction *vs* restriction model for branched probes, identical trends to those shown by the *n*-alkanes are shown, as expected. In the S_C mesophase, the greater restriction is evidenced in increasingly negative ΔS^s values, however branched probes exhibit more positive ΔS^s values in the nematic mesophase, and no trend is discernible in the isotropic phase. This indicates some entropic restriction mechanism is applied in the mesophases, but not in the isotropic phase, and confirm the activity trend noted in (4.1.2).

The *aromatic probes* all contain a rigid core, with toluene and the xylenes having substitution and ethylbenzene being the only probe to contain a rigid core and flexible chain. By consideration of the structures it would be expected that the interaction between the aromatic core of these probes and the rigid core of the liquid crystal would lead to enhanced solvency. This indeed appears to be the case, with benzene showing a more negative ΔH^s value than hexane (which is also a 6-carbon molecule). Also in comparison with the aliphatic probes, benzene has less a negative ΔH^s value than hexane or heptane, which may be explained by the ability of the aliphatic probes to adopt other conformations to maximise interaction. As substitution to the aromatic core increases, the value of ΔH^s becomes more negative and ΔH^e increases, reflecting the need for extra energy to be put into the system to solvate aromatic probes. ΔH^e is more positive for all aromatic probes than any of the aliphatic probes. In the S_C mesophase, all ΔS^s values for the aromatic probes are similar, and are lower than those noted for aliphatic probes - indicating there is less restriction on solvation on the aromatic probes (possibly due to the major aromatic component in the liquid crystalline molecular structure) and that entropic contributions to aromatic solution formation are similar for all probes considered. As substitution increases, a small increase in ΔS^e is noted indicating that some small differences due to solvent shape are present. This behaviour is to be expected considering the model whereby the aromatic probes interact with the aromatic layer in the S_C mesophase structure. In the nematic mesophase, the aromatic probes show significantly positive ΔS^s values and more positive ΔS^e values compared with aliphatic probes, emphasising that the strong entropic factors shown in this phase are enhanced further for aromatic probes. This is

a direct consequence of the mesogenic structure exhibited in the nematic phase, else similar entropic contributions would occur in the S_C mesophase and isotropic phase. Finally, the isotropic phase shows more favourable entropy than the S_C mesophase, resulting from less negative ΔS^s values (and some small positive ΔS^s values for aromatic probes) and sizeable contributions from ΔS^e. Thus, enthalpic contributions dominate mixtures of aromatic probes with S_C, entropic contributions play a very strong part in the solvation with the nematic phase, and both enthalpic and entropic contributions contribute in the isotropic phase.

The *isomeric probes* show almost identical values of ΔH^s and ΔH^e for the cis- and trans-isomers in all phases, whilst in the S_C mesophase ΔS^s and ΔS^e are almost identical, $\Delta S^s_{trans} < \Delta S^s_{cis}$ in the nematic mesophase, and $\Delta S^s_{cis} < \Delta S^s_{trans}$ in the isotropic phase. The closeness of these values and lack of discernible trend makes the role of enthalpic and entropic contributions difficult to distinguish for such probes. It has been postulated previously that trans-isomers, being more rod-like, align more easily than cis-isomers, which themselves may expose their C=C bond more favourably for interaction with the rigid liquid crystal core.

The solution formation in the various mesophases is therefore governed by the interplay of enthalpic and entropic contributions, with the isotropic phase exhibiting the lowest γ^∞ values due to the more favourable entropy over that observed with the nematic phase, and the more favourable entropy over that observed with the smectic phase. The smaller value of γ^∞ obtained for the nematic phase is due to the highly favourable entropy overcoming the unfavourable enthalpy to form mixtures. This is also indicative of the role the mesophase structure plays in the formation of mixtures between solutes and liquid crystalline solvents. Whilst the formation of mixtures with strong solute-solvent interactions in the S_C mesophase are favourable due to enthalpic considerations, the entropic contributions are unfavourable leading to deviations from the ideal mixture. Again, this is indicative of the role the ordered mesophase structure plays in the formation of probe/stationary phase mixtures.

4.1.3 PRELIMINARY SUMMARY

From the study of BDH509, it may be summarised that:

- When analysing IGC results, weight fraction activity coefficients must be carefully considered by reference to of molar activity coefficients in order to correctly describe the solution behaviour observed, and to elucidate meaningful trends from the data.

- Substantial deviations from ideality are shown for aliphatic and isomeric probes in all phases, though aromatic probes form favourable solutions with the nematic mesophase and the isotropic phase. These observations are reflected in the activity coefficient trend, $\gamma^{\infty}_{isotropic} < \gamma^{\infty}_{nematic} < \gamma^{\infty}_{smectic\ C}$.

- The smectic C mesophase shows strongly favourable enthalpy and unfavourable entropy of mixing; the nematic mesophase shows strongly favourable entropy and unfavourable enthalpy of mixing; and the isotropic phase shows favourable entropy and enthalpy of mixing.

- The factors affecting the mesophase enthalpic and entropic contributions (either favourable or unfavourable) to mixing are a direct consequence of the ordered mesophase structure.

4.2 COMPARISON OF RACEMIC AND CHIRAL MATERIALS

The consideration of solution properties of probes with BDH509 was made in (4.1). This section aims to apply these general observations to describe the solution behaviour observed for series of probes in comparable liquid crystalline materials. Initially, interactions with BDH509 are compared to interactions with BDH770 - where the two materials are of identical chemical structure, but BDH509 is enantiomerically pure whereas BDH770 comprises a racemic mixture of enantiomers. This is followed by a comparison of the enantiomerically pure BDH849 and the racemic mixture of BDH1029, allowing differences in the solution behaviour due to the structural differences imparted on the mesophase by chirality to be explored. The retention plots, activity coefficients and tables of physiochemical results obtained experimentally are contained in Appendix 2, sections (A2.1), (A2.2) and (A2.3). These results will be referred to in the text as necessary.

4.2.1 PHYSIOCHEMICAL STUDIES OF BDH770

The results for BDH770 are summarised in Appendix 2, section (A2.1). Plots of ln Vg°, ln γ^{∞}, and ln Ω^{∞} *vs* 1/T are shown in Figure A2.1 to Figure A2.9, and physiochemical results derived from these are contained in Table A2.1 to Table A2.4.

In terms of retention, Vg° values in all phases are of a similar magnitude to those shown with BDH509, and identical trends are observed. Considering the activity coefficients, higher values are shown in the smectic C mesophase compared with

BDH509, indicating further deviation from the ideal, and there is much less pronounced temperature dependence in the nematic mesophase. All activity coefficients show a positive deviation from Raoult's law, except for aromatic probes with the nematic mesophase (at higher temperatures) and with the isotropic phase. This trend, and the activity coefficient trends within probe series, are identical to those shown with BDH509. At a brief glance these observations may well be due to the lack of chirality in BDH770 forming a mesophase structure which differs to that formed with BDH509, which in turn shows different solute-solvent interactions with the probe molecules. When considering the solution properties calculated from these plots, the following trends are noted:

$$\gamma^{\infty}_{\text{isotropic}} < \gamma^{\infty}_{\text{nematic}} < \gamma^{\infty}_{\text{smectic C}} \quad [1]$$

$$\Delta H^{s}_{\text{nematic}} > \Delta H^{s}_{\text{isotropic}} > \Delta H^{s}_{\text{smectic C}} \quad [2]$$

$$\Delta H^{e}_{\text{nematic}} > \Delta H^{e}_{\text{smectic C}} > \Delta H^{e}_{\text{isotropic}} \quad [3]$$

$$\Delta S^{e}_{\text{nematic}} > \Delta S^{e}_{\text{isotropic}} > \Delta S^{e}_{\text{smectic C}} \quad [4]$$

$$\Delta S^{e}_{\text{nematic}} > \Delta S^{e}_{\text{smectic C}} > \Delta S^{e}_{\text{isotropic}} \quad \text{For aliphatic probes} \quad [5]$$

$$\Delta S^{e}_{\text{nematic}} > \Delta S^{e}_{\text{isotropic}} > \Delta S^{e}_{\text{smectic C}} \quad \text{For aromatic probes} \quad [6]$$

The solution properties in BDH770 show identical trends to those noted for BDH509, but there are differences in the trends for excess properties, with ΔH^{e} for all probes and ΔS^{e} for aliphatic probes (but not aromatic probes) showing more positive values with the S_C mesophase than with the isotropic liquid. This may be a consequence of the mixture of racemic mesogens affecting the mesophase structure; in the S_C mesophase of BDH509 the layers show some degree of tilt relative to one another, this tilt rotating from one layer to the next in a similar way to the cholesteric mesophase described in (1.1.3). When a mixture of two enantiomers is used, such a tilt will either be disrupted or a separate S_C mesophase will form involving an opposite twisting angle, which alters the mesophase structure from that shown by the chirally pure structure. Interactions with such structures have the possibility of proceeding *via* a different mechanism, and it is shown here that aliphatic and aromatic probes do indeed exhibit different solution behaviours in this environment. It is interesting to note that ΔH^{vap} and ΔS^{vap} values in the S_C mesophase of BDH509 and BDH770 are virtually identical, suggesting the differences in enthalpic and entropic contributions are due solely to the adopted structure of the mesophase. This phenomenon is particularly notable when considering the entropic contributions, indicating the chirality of the mesophase plays an important role in the nature of the solute-solvent interaction.

In comparison with BDH509, the *aliphatic probes* in the S_C mesophase show less negative ΔH^{s} values, slightly more positive ΔH^{e} values, less negative ΔS^{s} values and

slightly more positive ΔS^e values. Trends within each parameter remain identical to those observed with BDH509. This indicates more favourable enthalpic contributions to the solute-solvent interaction, combined with less favourable entropic contributions, which would be expected considering the mesophase structure disruption described above. In the nematic mesophase, enthalpic contributions are more favourable compared with BDH509, though the entropic contributions are less favourable. The change in trends is opposite to those shown with the S_C mesophase, but implies a disruption to the nematic mesophase structure in the racemic mixture of mesogens, confirmed by the ΔH^{vap} and ΔS^{vap} values again being virtually identical. Combined, these results suggest the S_C and N mesophase structures, whilst remaining distinct, become more similar when composed of racemic mesogens. The isotropic phase shows virtually identical enthalpic contributions with both BDH509 and BDH770, and only slight differences in entropic contributions with no discernible trend - which may well be accounted for considering the presence of the two chiral mesogens in the isotropic liquid. This suggests the solute-solvent interactions in the isotropic phase of BDH509 and BDH770 operate *via* almost identical mechanisms.

The *aromatic probes* are affected slightly differently, with their solution behaviour in BDH509 and BDH770 being virtually identical in the S_C mesophase. In the nematic mesophase the interactions of these probes are slightly more favourable enthalpically compared with BDH509 and slightly less favourable entropically, though these trends are not evident to the same extent as those noted with the aliphatic probes. Mixtures with the isotropic phase show very similar enthalpic and entropic contributions, suggesting similar interactions for benzene, toluene and ethylbenzene. However, the xylenes show differing properties; the trends are identical (with m-xylene forming the most favourable solute-solvent interactions) though the enthalpic contributions are less favourable and the entropic contributions more favourable. Overall, ΔH^{vap} and ΔS^{vap} values are very similar with all mesophases.

The *isomeric probes* show a combination of effects noted by the aliphatic and aromatic probes; slightly stronger interactions in the S_C mesophase, weaker interactions with the N mesophase (with loss of favourable entropy) and similar interactions with the isotropic phase. Interactions with the trans- isomer are slightly more favourable than with the cis- isomer are shown overall in the nematic and isotropic phases of BDH770, but no difference is evident in the S_C mesophase.

From the IGC results obtained for BDH509 it appears the mesogen containing one enantiomeric conformation forms distinct, well-formed chiral smectic and chiral nematic mesophases the structural properties of which are disrupted on heating to the isotropic liquid. BDH770, comprising a racemic mixture of the enantiomeric mesogens, shows

identical overall physiochemical properties of vaporisation to BDH509 in all phases, these properties being imparted by differing solution and excess contributions in the mesophases. The chiral S_C mesophase in which the alignment of the mesogen's rigid core remain intact whilst the flexible end-groups adopt an alternate confirmation disrupting the overall mesogenic structure. The racemic mixture of mesogens also gives rise to a disrupted chiral nematic mesophase, with a small disruption in the mesophase order of the rigid core, and a larger effect on the flexible end-groups. Overall, the two mesophases - whilst remaining distinct - show less difference in their solvent-solute interactions and thus less difference in their mesophase structure. The isotropic phase for each liquid crystal shows identical solution properties, confirming that the trends noted in the mesophase are due to mesogen structural effects.

4.2.2 PHYSIOCHEMICAL STUDIES OF BDH849

The structure of BDH849 and BDH1029 is shown in Figure 4.11, with the results for BDH849 being summarised in Appendix 2, section (A2.2). Plots of ln Vg°, ln γ^{∞}, and ln Ω^{∞} *vs* 1/T are shown in Figure A2.10 to Figure A2.18, and physiochemical results derived from these are contained in Table A2.5 and Table A2.6. The use of the term 'previous systems' refers to BDH509 and BDH770.

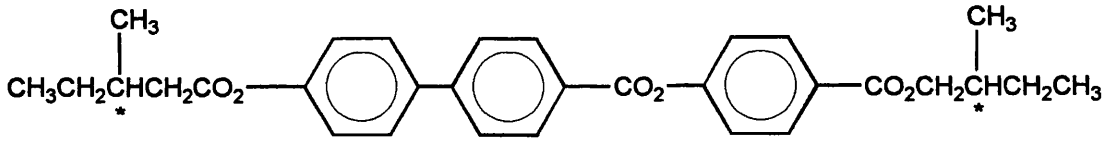

BDH849 - chiral **BDH1029** - racemic

Figure 4.11: Structure of BDH849 and BDH1029

In terms of retention, Vg° values for the aliphatic probes are notably higher at a given temperature in all phases than those shown in BDH509, with aromatic and aliphatic probes giving retention of a similar magnitude. All trends in Vg° remain identical to those noted in BDH509 and BDH770. In the crystalline phase, the retention volume does not conform to a linear relationship with 1/T, suggesting the K → N mesophase transition takes place over an extremely large temperature range. However, this trend is not confirmed by DSC analysis of the material, which shows complete transition over approximately 6°C. Considering the activity coefficients, identical trends within mesophases and families of probes are shown in BDH849 as were evident in BDH509 and BDH770. For both aliphatic and aromatic probes the temperature dependence of γ^{∞} is much lower than in the previous systems, and on the N → I phase transition there is a very small increase in the favourability of interaction suggesting the structural difference between the mesophase and isotropic liquid is very small. All aliphatic

probes show $\gamma^{\infty} > 1$ and all aromatic probes show $\gamma^{\infty} < 1$ indicating favourable solution formation and negative deviations from Raoult's law. The cis/trans isomers show a notable difference to the previous systems; where a positive deviation from Raoult's law was shown there is now a strong negative deviation where $\gamma^{\infty} \approx 0.17$. At a brief glance these observations suggest interactions with more polarisable probes occur to a greater extent than with the previous systems, possibly due to the removal of the laterally-substituted fluorine allowing probes to adopt a conformation favourable for interaction with the rigid mesophase core. The presence of two chiral flexible end-groups may also aid this process by weakening the liquid crystal-liquid crystal interactions and thus opening the structure to more thorough penetration by the probe molecules. The mechanism by which the system is disrupted is described further by consideration of the solution properties obtained. A consideration of these properties showed the following trends:

$$\gamma^{\infty}_{\text{isotropic}} < \gamma^{\infty}_{\text{nematic}} \quad [1]$$

$$\Delta H^{s}_{\text{nematic}} > \Delta H^{s}_{\text{isotropic}} \quad [2]$$

$$\Delta H^{e}_{\text{nematic}} > \Delta H^{e}_{\text{isotropic}} \quad [3]$$

$$\Delta S^{s}_{\text{nematic}} > \Delta S^{s}_{\text{isotropic}} \quad [4]$$

$$\Delta S^{e}_{\text{nematic}} > \Delta S^{e}_{\text{isotropic}} \quad [5]$$

For all probes the above trends show that the formation of mixtures with the mesophase has moderately favourable enthalpy, enhanced by very favourable entropy effects. The isotropic phase shows favourable enthalpy driving mixing, with favourable entropy contributing for the substituted aromatic probes and the cis/trans isomers.

The *aliphatic probes* show more favourable enthalpies of solution in the mesophase compared with the previous systems. The inference here is interactions between the probes and two branched end-groups are more favourable than the interactions between one branched and one flexible end-group. All aliphatic probes show similar enthalpic values, indicating the more favourable interaction is less selective in this system, perhaps because the number of conformations the end-groups can adopt has been reduced - showing an opposite situation from that described in (4.2.1). As this would act to weaken the interactions, there must be another mechanism improving the mixing which may be due to the distancing effect of two branched end-groups allowing more effective penetration of the probe and thus actually increasing the solute-solvent interaction. The entropic contributions to mixing are favourable for all probes, becoming more favourable as chain length and branching increases. The values of ΔS^{s} and ΔS^{e} are smaller than those shown for the previous systems, showing the molecular conformation of the system does not impart such a great effect on the solute-solvent interactions, strengthening the argument describing weaker liquid crystal-liquid

crystal interactions. In the isotropic phase, the enthalpic contributions become more favourable and entropic contributions less favourable, leading to the conclusion that on the disruption of the mesophase the probes are free to interact with the end-groups without hindrance from the end-group/end-group interactions.

The *aromatic probes* show more favourable enthalpies than the aliphatic probes in the mesophase, and similar enthalpies to the aliphatic probes in the isotropic phase, indicating that solute-solvent interactions between these probes and the rigid core of the mesogen are equally possible in the mesophase or isotropic liquid. Entropy gives generally favourable contributions to mixing, particularly through the series benzene > toluene > ethylbenzene, but no discernible trends are shown for the xylenes. It appears that there is little to differentiate between the mesophase and isotropic phase where aromatic probe-solvent interactions occur, which differs greatly from the previous systems where very notable differences in interaction were shown on the N $\rightarrow$ I transition.

The *isomeric probes* show great disruption to the mesophase and isotropic structure, with both the cis- and trans- isomer showing favourable enthalpy and entropy in both phases. The probes themselves are relatively small compared to the mesogenic structure of the liquid crystal but their observed behaviour may be explained by considering strong interactions occur between the C=C bond and the rigid core of the mesogen, whilst the flexible aliphatic portion of the probe interacts with and disrupts the end-group/end-group interactions. In the mesophase the cis- isomer shows more favourable enthalpy and less favourable entropy of solution, the trend reversing in the isotropic phase. However, these combined factors result in very little difference between their activity coefficients, suggesting this system will not effect their successful separation.

These results therefore suggest BDH849 adopts a 'loose' mesophase structure, in which the end-groups compete with each other to disrupt, rather than enhance, the mesogen alignment. This allows deeper probing of the structure by small molecules and results in enhanced solute-solvent interactions for both aliphatic and aromatic probes. This model also explains the relatively small loss of order on the N $\rightarrow$ I transition, and the consequently minimal effects this has on interaction with the probes. In comparison with the previous systems, this structure imparts fewer physiochemical differences (particularly entropic) on the probes. Whilst this leads to more favourable solution formation, it does not enhance the properties desired to separate analytes of similar chemical structure but differing molecular conformation.

4.2.3 PHYSIOCHEMICAL STUDIES OF BDH1029

The results for BDH1029 are summarised in Appendix 2, section (A2.3). Plots of ln Vg°, ln γ^{∞}, and ln Ω^{∞} *vs* 1/T are shown in Figure A2.19 to Figure A2.27, and physiochemical results derived from these are contained in Table A2.7 to Table A2.9.

Comparing retention in BDH1029 with BDH849, Vg° values for the aliphatic probes are reduced, with aromatic and aliphatic probes giving retention of a similar magnitude in the mesophase, but the stronger temperature dependence of Vg° leads to smaller retention volumes in the isotropic phase. All trends in Vg° for probes remain identical to those noted in BDH849 and the previous systems. The crystalline phase does show a linear relationship between ln Vg° and 1/T. The activity coefficient trends within mesophases and families of probes are reversed when compared to BDH849 and the previous systems, with the smaller unbranched and unsubstituted probes having lower γ^{∞} values. The temperature dependence of γ^{∞} is again very low, and on the N $\rightarrow$ I phase transition there is a very small decrease in γ^{∞}. All aliphatic and aromatic probes show $\gamma^{\infty} > 1$, with the exception of benzene with which $\gamma^{\infty} \approx 1$. The cis/trans isomers show a positive deviation from Raoult's law with this system. These observations suggest interactions overall are less favourable with BDH1029 than they were with BDH509, with the presence of branching and substitution on the probe hindering solute-solvent interactions; the opposite case to all materials studied so far. This indicates a stronger liquid crystal-liquid crystal structure which is "loose" enough to allow penetration of small probes, but "tight" enough to preclude larger probe molecules. The mechanism by which the system is disrupted is described further by consideration of the solution properties obtained. A consideration of these properties showed the following trends:

$$\gamma^{\infty}_{\text{isotropic}} < \gamma^{\infty}_{\text{nematic}} \quad [1]$$

$$\Delta H^{s}_{\text{nematic}} > \Delta H^{s}_{\text{isotropic}} \quad [2]$$

$$\Delta H^{e}_{\text{nematic}} > \Delta H^{e}_{\text{isotropic}} \quad [3]$$

$$\Delta S^{s}_{\text{nematic}} > \Delta S^{s}_{\text{isotropic}} \quad [4]$$

$$\Delta S^{e}_{\text{nematic}} > \Delta S^{e}_{\text{isotropic}} \quad [5]$$

For all probes the above trends are identical to those shown with BDH849, though an analysis of the contributing terms shows the formation of mixtures with both the mesophase and isotropic phase to be driven by favourable enthalpy. Entropy effects are unfavourable in both phases.

In comparison with BDH849, the *aliphatic probes* all show more favourable enthalpy and less favourable entropy of interaction. Clearer trends are shown compared with

probe mixing with BDH849, with favourable entropy and less favourable entropy being shown with an increase in chain length and substitution. The isotropic mesophase shows similar enthalpies to the mesophase, accompanied by more negative ΔS^s values and relatively small excess properties. Thus, on mixing with the isotropic phase small deviations from ideality are observed. The *aromatic probes* show the same trends; all probes showing favourable enthalpy and unfavourable entropy in the mesophase (large, negative ΔH^s; small, positive ΔH^e; large negative ΔS^s; moderately positive ΔS^e), with a transition to the isotropic phase showing more negative ΔH^s, more negative ΔS^s and much smaller excess properties. Branching and substitution of the aromatic core increases enthalpic and decreases entropic favourability. The *isomeric probes* show weaker interactions in the mesophase (although their entropy is more favoured), though their behaviour is very similar to the aliphatic probes in the isotropic phase. There are differences noted between the isomers, with the trans- isomer showing more favourable enthalpy and less favourable entropy in each phase.

These trends show marked differences from BDH849, and can only be due to the structure and interactions available to the probe molecules. As suggested previously, a more ordered mesophase structure *may* be formed precluding larger probes from interacting, explaining the reversal in trend compared with BDH849. However, this is accompanied by a loss in entropic favourability for all probes, which suggests the mesophase structure is further disrupted when a chirally pure mesogen is used. A more probable explanation suggests that the structure adopted may well be stronger with the rigid mesogen core being shielded from penetration by aliphatic and larger probes by the relatively rigid branched chain end-groups, leading to less favourable entropic effects and higher activity coefficients. This explanation appears particularly relevant to the cis-/trans- isomers which no longer cause the disruption to the structure shown previously. It follows from this that direct comparisons between the previous systems (BDH509 and BDH770) and these systems (BDH849 and BDH1029) are difficult as the structural composition of the mesophases arise in very different environments. Methods of extending this study of mesophase structure are considered in Chapter 7. As the mechanisms by which mesophase formation occurs appear different in these materials due to their end-groups, the contribution the laterally-substituted fluorine makes is considered further in the comparison with LMM1 in (4.3).

4.2.4 PRELIMINARY SUMMARY

It has been shown in (4.1.3) that the mesophase structure directly affects the nature of the solute-solvent interaction for the probes used in this study. Extending this theory to comparative study with chiral/racemic mesogens leads to the following conclusions:

- IGC methodology may be extended to probe the structure of the liquid crystalline mesophase, particularly when studying comparative systems such as those comprising of a chirally pure and racemic mixture of mesogens.

- Structurally the mesogen structure with a rigid core, a flexible end-group and a chiral branched end-group showed more marked effects due to its mesophase structure. This suggests it is more able to form strongly ordered structures which in turn affects solute-solvent interactions. Two competing chiral branched end-groups result in disruption of mesophase formation and damping of observed physiochemical affects.

- Overall solution properties remain identical in a given phase of both the chirally pure and racemic mixture of mesogens, whilst mechanisms of interaction as indicated by enthalpic and entropic contributions differ. These results show the mesophases formed by the racemic mixture lose order compared with the chirally pure mesogen, and while they remain distinct their solution properties become more alike.

- The above effects lead to the conclusion that in order to enhance the differences due to shape selectivity, a chiral material is required to impart maximum variation in physiochemical effects on interacting with probe molecules.

4.3 LOW MOLECULAR MASS MATERIAL

After analysis of the results for the chiral/racemic systems described previously in this chapter, the synthesis of a material which contained an aromatic centre, a flexible end-group and a chiral end-group was undertaken, along with the syntheses of analogous polymeric materials. These syntheses were described in Chapter 2, and the results obtained considering these material are presented during the remainder of Chapter 4.

The structure of the low molecular mass material, LMM1, is shown in Figure 4.12, with physiochemical results for this system being summarised in Appendix 2, section (A2.4). Plots of ln Vg°, ln γ^{∞}, and ln Ω^{∞} *vs* 1/T are shown in Figure A2.28 to Figure A2.36, and physiochemical results derived from these are contained in Table A2.10 to Table A2.12.

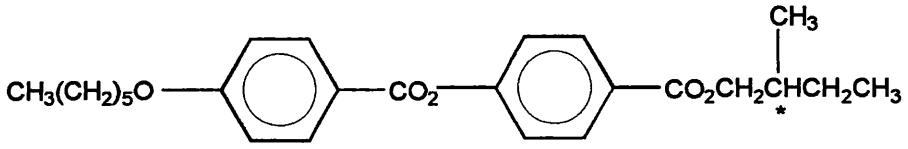

LMM1

Figure 4.12: Structure of LMM1

In comparison with BDH509, the retention volumes of probes in LMM1 show very different trends; at equivalent temperatures Vg° values for all probes are significantly greater, and trends in the probe families are identical. After the K → S_C transition there is a decrease in Vg°, and after the S_C → I transition there is a significant increase in Vg° suggesting the probes are more able to undergo solute-solvent interactions (maybe because they are more able to penetrate the solvent structure) and are thus retained more effectively. Throughout the S_C mesophase Vg° exhibits significant temperature dependence, the effect of which is reduced in the isotropic phase. Considering activity coefficients, the aromatic probes show significantly lower γ^{∞} values than the aliphatic probes, indicating they undergo much more favourable interactions. All probes in the mesophase and aliphatic probes in the isotropic phase show $\gamma^{\infty} > 1$, with aromatic probes in the isotropic phase showing $\gamma^{\infty} < 1$ revealing negative deviation from Raoult's law where as the aromatic molecules act to disrupt the mesogen-mesogen interactions. These trends suggest the presence of strong liquid crystal-liquid crystal interactions in the S_C mesophase with undergo considerable interruptions at the clearing point to give a solution which is a favourable solvent for aromatic probes. In considering the solution properties obtained from these plots, the following trends are shown:

$$\gamma^{\infty}_{\text{isotropic}} < \gamma^{\infty}_{\text{smectic C}} \quad [1]$$

$$\Delta H^{s}_{\text{smectic C}} > \Delta H^{s}_{\text{isotropic}} \quad [2]$$

$$\Delta H^{e}_{\text{smectic C}} > \Delta H^{e}_{\text{isotropic}} \quad [3]$$

$$\Delta S^{s}_{\text{smectic C}} > \Delta S^{s}_{\text{isotropic}} \quad [4]$$

$$\Delta S^{e}_{\text{smectic C}} > \Delta S^{e}_{\text{isotropic}} \quad [5]$$

Enthalpically, the trends favour formation of mixtures in the isotropic phase, whilst entropic trends favour the mesophase. The less favourable enthalpy in the S_C mesophase may well be due to the twisted conformation adopted being less available to the probe molecules for interaction; the same phenomena which allows stronger entropic interactions to arise from the positional and orientational order not present in the isotropic phase. These trends are different to those observed with BDH509, where the isotropic phase was more favourable enthalpically and less favourable entropically than the S_C mesophase structure. Such differences appear to be due to the stronger interactions within the mesophase structure reducing the tendency of "like dissolves

like" solution formation with the aliphatic and aromatic layers. In this model, the S_C mesophase structure of LMM1 shows more similarity to the nematic mesophase structure of BDH509.

The *aliphatic probes* show less favourable enthalpies in S_C than in I, with ΔH^s becoming more favourable on increasing aliphatic chain length, but remaining constant with increased branching. ΔH^e remains constant on increasing chain length, and increases with increasing branching. Entropically, both ΔS^s and ΔS^e become more unfavourable with increasing chain length, and more favourable with increased branching - illustrating the ability of the chains to alter their conformation allowing more favourable interactions with the aliphatic end-group of the mesogen, whilst being subject to increased restriction by the mesophase structure. Branching appears not to affect the ability of the chain to interact *via* dispersion forces, but aids the probe in overcoming entropic restrictions. Higher γ^∞ values are shown with increasing branching, with hexane undergoing the most favourable interaction. The interplay between enthalpic and entropic effects therefore govern the formation of aliphatic-S_C solutions. In the isotropic phase ΔH^s and ΔH^e become more favourable for all probes and the disruption of the mesophase shows branching is no longer a hindrance to more favourable interactions. Entropically, the trends noted in S_C remain unchanged, but values for all probes are unfavourable indicating the mesophase structure no longer plays a role in solution formation, and enthalpic effects dominate.

In the S_C mesophase *aromatic probes* show increased enthalpic favourability on increasing substitution, possibly reflecting the ability of the aliphatic portion of the probe to disrupt the mesophase structure enough to allow primary interactions between the aromatic probe and rigid aromatic mesogen core. Entropically, aliphatic substitution decreases the favourablilty of interaction, though the xylenes do show favourable entropy in comparison with toluene and ethylbenzene in the order o > m > p. This suggests the length:breadth ratio of the probes play a role in their interaction. As $\gamma^\infty_{benzene} < \gamma^\infty_{ethylbenzene}$, it is indicated that entropic factors are more predominant in the solute-solvent interactions of aromatic probes with the S_C mesophase. In the isotropic phase more favourable enthalpies are shown for all probes, improving further with substitution and branching. Entropically, all probes are unfavoured, with branching and substitution being further detrimental. The trend in activity coefficients still shows $\gamma^\infty_{benzene} < \gamma^\infty_{ethylbenzene}$, which may be explained by considering that ethylbenzene shows $\gamma^\infty \approx 1$, so lower activities result in negative deviations from Raoult's law and are therefore indicative more unfavourable interactions. Enthalpic effects therefore dominate in the isotropic phase.

The cis/trans *isomeric probes* show γ^{∞} intermediate between the aliphatic and aromatic probes, indicating solute-solvent interactions occur involving both the C=C bond and the aliphatic chain. In the S_C mesophase their solution formation is enthalpically less favoured than the aromatic probes and entropically more favoured than the aliphatic probes. The cis- isomer exhibited lower activity and more favourable entropy than the trans- isomer, suggesting the cis-conformation to interact more readily with the twisted structure of the chiral mesophase whilst the conformation of the trans- isomer prevented this from occurring. Contributions from both enthalpic and entropic factors therefore drive the solution formation. In the isotropic phase enthalpic factors are more favourable and entropic factors less favourable for both probes, with the reduced γ^{∞} values showing enthalpy to predominate. Small differences in entropy for the cis-isomer cause more favourable mixing - illustrating that the rod-like nature of the molecules and chirality of the end-group may also pose an asymmetric environment on the probe molecules when no mesophase is exhibited.

Overall, these results paint a more complicated picture of the mesophase structure exhibited by LMM1 than that shown by BDH509. The S_C mesophase in this system evidently comprises strong mesophase-mesophase interactions as indicated by the change in properties on the loss of mesophase structure. However, the structure formed is not so distinct as to allow favourable solution formation between the probes and the aliphatic and aromatic layered structure - suggesting there is actually a less rigid order in this system. The properties shown by this S_C mesophase show good enthalpic contributions to solution formation and moderately favourable entropies (particularly for aromatic probes) suggesting that the properties of LMM1 for use as a potential stationary phase are more favourable than the nematic mesophase of BDH509. Whilst the nematic structure showed very strong entropic selectivity, the solutions formed were very poorly favoured enthalpically leading to shorter retention volumes, and hence analytically less ability to separate. The validity of these conclusions will be discussed in Chapter 5.

4.3.1 PRELIMINARY SUMMARY

The results for five low molecular mass liquid crystalline materials have now been presented, allowing some inferences to be made as to how solute-solvent interactions in these systems occur:

- It has been demonstrated that entropic effects drive solution formation in some mesophases, particularly the nematic mesophase. However, the relatively minor differences between mesophase structures, as evidenced by their low enthalpies of transition, show the solution behaviour within a phase to be governed primarily by the difference in probe-mesophase interactions, rather than by mesophase-mesophase interactions alone. These probe-mesophase interactions may well be a direct consequence of the changes in mesogen-mesogen interactions.

- Comparing mesophases, the nematic mesophase appears to offer the greatest differences in solution properties based upon probe-mesophase interactions. However, the nature of these interactions depends on the molecular composition of the mesophase, as evidenced by the S_C mesophase of BDH509 acting as a favourable solvent for probes within its layer structure, and the S_C mesophase for LMM1 showing favourable entropic differences between different aromatic probes. The factors governing the relative amounts of order in mesophases will be considered further in Chapter 7 when suggesting a liquid crystalline material with the "ideal" properties to effect enantiomeric separations. This phenomenon is due to the mesophase structure rather than temperature effects, as the observations were made over similar temperature ranges for these materials.

- To have the necessary order and mesogen-mesogen interaction properties to show physiochemical differences in solution formation, an enantiomerically pure mesogen is required. Racemic mixtures of mesogens act to disrupt the liquid crystalline mesophase structure reducing the observed effect of these unique properties on solute-solvent interaction.

The discussion will now consider the effect of liquid crystal polymers on solution behaviour, in order to determine whether the predominant contributions are due to the backbone or appended mesogens.

4.4 LIQUID CRYSTAL POLYMER STATIONARY PHASES

The liquid crystal polymers examined by IGC in this study are analogous in structure to LMM1, allowing direct structure-property relationships to be drawn. The structures of the materials used are shown in (2.1), and comprise a 2-ringed structure, a 3-ringed structure and a co-polymer.

4.4.1 PHYSIOCHEMICAL STUDIES OF LCP1

The structure of LCP1 is shown in Figure 4.13, with physiochemical results for this system being summarised in Appendix 2, section (A2.5). Plots of ln Vg° and ln Ω^{∞} *vs* 1/T are shown in Figure A2.37 to Figure A2.42, and physiochemical results derived from these are contained in Table A2.13 and Table A2.14.

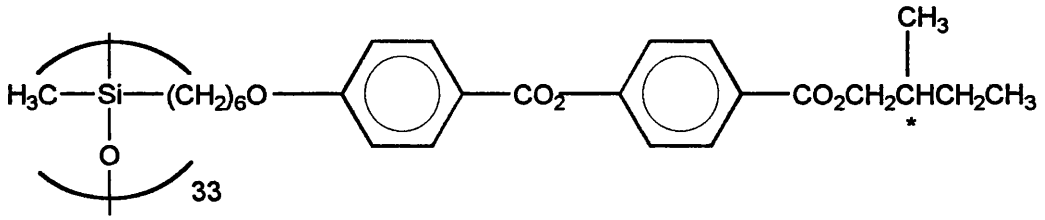

LCP1

Figure 4.13: Structure of LCP1

The trends in retention volume are identical in LCP1 and LMM1, though at a given temperature Vg° is reduced, with the differences in Vg° for a series of probes also reduced. These differences were of a similar magnitude for aliphatic and aromatic probes indicating the decrease in interaction with the polymer affected all probe types. As with LMM1, similar temperature dependencies within the phases are shown. On the $S_C \rightarrow I$ transition there is a distinct increase in Vg°, indicating improved interaction or penetration of the probe with the isotropic liquid. Considering activity coefficients, aromatic probes showed significantly lower values of Ω^{∞} than the aliphatic probes, showing almost ideal mixing in the isotropic phase (on comparing Ω^{∞} with γ^{∞}). All Ω^{∞} values are higher than those observed with LMM1, the magnitude of this difference being similar for aliphatic and aromatic probes. This appears to account for the observed differences in retention volumes. These trends suggest the mesophase structure exhibited in the S_C mesophase has some effect on the interactions shown by the probes. On formation of an isotropic liquid, the behaviour becomes more similar to the PDMS environment for aromatic probes, though the higher Ω^{∞} values for aliphatic probes suggest the appended mesogens interrupt the aliphatic-polymer backbone interaction. In considering the solution properties obtained from these plots, the following trends are shown:

$$\Omega^{\infty}_{PDMS} < \Omega^{\infty}_{isotropic} < \Omega^{\infty}_{nematic} \quad [1]$$

$$\Delta H^{s}_{smectic\ C} > \Delta H^{s}_{isotropic} > \Delta H^{s}_{PDMS} \quad [2]$$

$$\Delta H^{e}_{smectic\ C} \cong \Delta H^{e}_{isotropic} > \Delta H^{s}_{PDMS} \quad [3]$$

$$\Delta S^{s}_{isotropic} > \Delta S^{s}_{smectic\ C} > \Delta S^{s}_{PDMS} \quad \text{For aliphatic probes} \quad [4]$$

$$\Delta S^{s}_{isotropic} > \Delta S^{s}_{PDMS} > \Delta S^{s}_{smectic\ C} \quad \text{For aromatic probes} \quad [5]$$

$$\Delta S^{e}_{isotropic} > \Delta S^{e}_{smectic\ C} > \Delta S^{e}_{PDMS} \quad [6]$$

These trends show identical enthalpic trends to LMM1, where solvation with the isotropic phase is favoured compared with the mesophase, and PDMS is yet more favourable. Considering entropic contributions, solution formation with the isotropic mesophase is also more favoured, reversing the trend shown with LMM1. This indicates the polymer mesophase forms solute-solvent interactions *via* a mechanism similar to that shown by BDH509. As the polymeric mesophase consists of the same mesogens as LMM1, the inference is that interactions with the ordered layered structure occur between aromatic probes and the rigid mesogenic core, while aliphatic probes interact with a combination of the polymer backbone and the chiral end-groups. Trends [4] and [5] elucidate this interaction further, suggesting PDMS is entropically least favourable for aliphatic probes whilst the polymer mesophase is least favourable for aromatic probes. It is interesting to note that the excess entropies for all probes are of a large magnitude in both the mesophase and isotropic phase, indicating an increased restriction on all probes by the molecular structure due to the appending of the mesogenic unit onto the polymeric backbone.

The *aliphatic probes* show similar enthalpic and entropic trends to LMM1. The isotropic phase shows more favourable enthalpy of mixing for all probes, and a decrease in ΔH^S with increased branching over that shown in the S_C mesophase. In the S_C mesophase the entropy of mixing becomes more unfavourable with increasing chain length and more favourable with increased branching, and ΔS^e increased with both chain length branching. This again indicates increased restriction of the longer chains by the mesophase structure over and above the restrictions imposed by the siloxane backbone, and the effect of branching in overcoming these entropic restrictions. In the isotropic phase the similar hindrance observed for all probes would be caused by the restrictive nature of the polymeric backbone not allowing the mesogens to express the same degree of freedom as with low molecular mass materials. This restrictive nature also appears to give rise to a "stronger" mesophase, where the lack of dynamic movement in the mesophase structure causes a smaller perturbation with the probe, acting to concentrate the probe in the layered mesophase structure. This model is strengthened by comparison of results for LMM1 and PDMS, and appears to suggest that the behaviour of the liquid crystalline polymer adopts aspects of both these materials as well as giving rise to unique effects. In particular, entropic contributions arise from the mesogenic structure, whilst the enhanced retention and enthalpic contributions arise from the polymeric backbone.

The *aromatic probes* show similar behaviour modification. In the S_C mesophase, identical trends to those observed in LMM1 are shown, though the enthalpy contributions are more favourable, and entropy more unfavourable. As Ω^∞ is less

favourable for aromatic probes with LCP1, the predominance of entropic contributions to solute-solvent interactions with these mesophases is suggested. On clearing, the isotropic phase shows slightly less unfavourable enthalpy and more favourable entropy with less negative ΔS^s values and slightly more positive ΔS^e values than shown with the S_C mesophase. Of most interest is the behaviour of the xylenes in the mesophase. In LMM1, o-xylene showed the most distinct physiochemical differences with the S_C mesophase, while m-xylene and p-xylene showed almost identical characteristics. In the S_C mesophase of LCP1, all three xylenes show different properties according to the trends:

$$\Delta H^s_{m\text{-xylene}} > \Delta H^s_{p\text{-xylene}} > \Delta H^s_{o\text{-xylene}} \quad \& \quad \Delta H^e_{m\text{-xylene}} > \Delta H^e_{p\text{-xylene}} > \Delta H^s_{o\text{-xylene}} \qquad [7]$$

$$\Delta S^s_{m\text{-xylene}} > \Delta S^s_{p\text{-xylene}} > \Delta S^s_{o\text{-xylene}} \quad \& \quad \Delta S^e_{m\text{-xylene}} > \Delta S^e_{p\text{-xylene}} > \Delta S^e_{o\text{-xylene}} \qquad [8]$$

$$\Omega^\infty_{p\text{-xylene}} < \Omega^\infty_{o\text{-xylene}} < \Omega^\infty_{m\text{-xylene}} \qquad [9]$$

Trend [7] indicates o-xylene to have the most favourable enthalpy contributions, whilst m-xylene has the least favourable enthalpy. Conversely, trend [8] shows o-xylene to be least favoured entropically and show the least excess effects, whilst m-xylene shows the most favourable entropy and the greatest excess effects. Tying these observed effects in with trend [9] shows no direct correlation between enthalpy and entropy effects on the activity coefficient, indicating a more complex involvement of enthalpy and entropy effects on the solute-solvent interactions between the xylenes and LCP1. Considering the shape and polarisability of the xylenes should allow further explanation of the effects observed. The length:breadth ratio of the xylenes shows p-xylene > m-xylene > o-xylene, whilst the polarisability follows the trend o-xylene > m-xylene > p-xylene. By consideration of trend [9] it appears high length:breadth ratio and low polarisability acts to give the most favourable mixture; a trend that has been observed by other workers[251-253], and appears to over-ride the enthalpic and entropic contributions when comparing p-xylene and o-xylene with this system. Whereas with PDMS the similarity between the physiochemical interactions of the xylene isomers indicated that shape did not play any role in their retention, the behaviour with LCP1 indicates the mesogen structure does play a major role in the system's solution behaviour. This observation is further strengthened considering the behaviour of xylenes in the isotropic phase, where their activity coefficients reflect the enthalpic trend where o < p < m.

A distinct difference between the behaviours of aliphatic and aromatic probes were noted in the S_C mesophase of LMM1, which was no longer present in the polymeric material - both families of probes showing similar entropic effects in LCP1. This indicates the importance of the siloxane backbone adding to the restrictive nature of

the solvent in this material, whilst the other results so far discussed show the mesogen to also have significant influence on the solute-solvent interaction.

The *isomeric probes* form less favourable solutions considering energy effects, with similar entropy to the branched alkanes. The cis- isomer is more entropically favoured than the trans- isomer, indicating increased restriction by the mesophase, but activity coefficients are virtually identical suggesting energy considerations are predominant. In comparison, the isotropic phase shows $\gamma^{\infty}_{cis} < \gamma^{\infty}_{trans}$ which is reflected in the more favourable ΔS^{s} for the cis-isomer. However, the excess properties for both isomers are very similar, suggesting the entropic effects are due to the interaction of the probes with individual mesogens rather than with any ordered structure.

From the results observed with a liquid crystal polymer, it is therefore apparent that intermediate effects between the siloxane backbone and LMM1-like mesogens are occurring. Shape selectivity by the mesophase is shown to a greater extent than LMM1 due to the nature of the appended mesophases. This results in smaller differences in interaction between aliphatic and aromatic probes in a homologous series, but greater differences where probe shape plays an important role. These effects are reduced in the isotropic phase, though interactions with the mesogens due to their restricted movement still occur. In the mesophase it would appear this polymeric liquid crystal exhibits the necessary attributes for the stationary phase aimed for in this study; thermal stability, good retention, and selectivity of probes due to molecular shape.

4.4.2 PHYSIOCHEMICAL STUDIES OF LCP2

The structure of LCP2 is shown in Figure 4.14, with physiochemical results for this system being summarised in Appendix 2, section (A2.6). Plots of ln Vg° and ln Ω^{∞} *vs* 1/T are shown in Figure A2.43 to Figure A2.48, and physiochemical results derived from these are contained in Table A2.15 and Table A2.16.

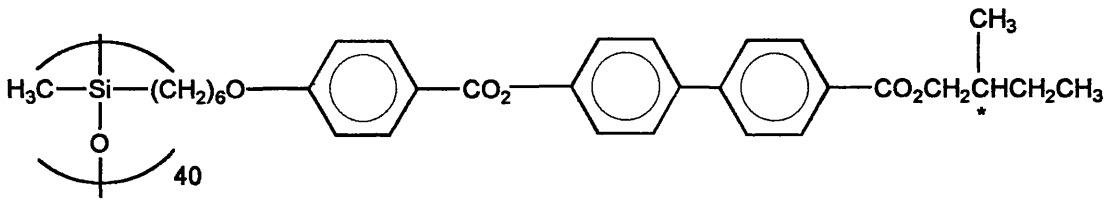

LCP2

Figure 4.14: Structure of LCP2

LCP2 has a structure analogous to LCP1, with the addition of a third aromatic ring *via* a biphenyl linkage. This acts to increase the mesophase range of the material further. Results were obtained in the S_C mesophase up to 226°C. Results in the S_A mesophase (226°C - 228°C) contained showed no linearity, averaging 20% correlation, which introduced substantial uncertainties into the results obtained. No results for this mesophase are therefore contained herein. Similarly, whilst results were obtained in the isotropic phase, the short retention times observed introduced substantial uncertainties to further calculations, with values accurate to only ± 15%. These results should therefore be analysed with care, so the discussion of mixing with the isotropic phase will be confined to trends only. In considering the solution properties obtained from these plots, the following trends are shown:

$$\Omega^{\infty}_{PDMS} < \Omega^{\infty}_{isotropic} < \Omega^{\infty}_{nematic} \quad [1]$$

$$\Delta H^{s}_{isotropic} > \Delta H^{s}_{smectic\ C} > \Delta H^{s}_{PDMS} \quad [2]$$

$$\Delta H^{e}_{smectic\ C} \cong \Delta H^{e}_{isotropic} > \Delta H^{s}_{PDMS} \quad [3]$$

$$\Delta S^{s}_{isotropic} > \Delta S^{s}_{PDMS} > \Delta S^{s}_{smectic\ C} \quad [4]$$

$$\Delta S^{e}_{isotropic} > \Delta S^{e}_{smectic\ C} > \Delta S^{e}_{PDMS} \quad [5]$$

These trends are identical to those noted with LCP1, except for the more favourable enthalpic contributions in the S_C mesophase. Retention volumes obtained at a given temperature for all probes were smaller than those observed for LCP1. This reduced interaction was reflected in the activity coefficients. The trends observed were identical to those shown with LCP1, but at a given temperature $\Omega^{\infty}_{LCP2} > \Omega^{\infty}_{LCP1}$. The difference in magnitude was similar for both aliphatic and aromatic probes, suggesting the change in interaction is due somehow to the presence of the additional aromatic ring.

The *aliphatic probes* show similar ΔH^{s} values, with ΔH^{e} values increasing with additional carbon atoms and branching. Entropically mixing is favoured, with chain lengthening and branching acting to improve mixing, and greater excess properties suggest the mesophase plays a key role in this. The *aromatic probes* also exhibit these trends, though entropically they are even more favoured, perhaps due to the additional aromatic ring in the mesogenic core enabling easier interaction with similar probe structures. The *isomeric probes* show no discernible differences in physiochemical properties, which is reflected in their retention volumes and activity coefficients.

Overall, these results indicate poor interactions in terms of enthalpy and activity coefficients between the probes and LCP2, and whilst the interactions are entropically favoured, the high thermal energy available to the probe at the operational temperatures lead to short retention times and high activity coefficients. The large excess entropies show the importance of the mesophase structure in the interactions,

however it appears this structure is quite impenetrable to the probes, reducing the efficiency of the stationary phase. This may be due to the strength of interaction between the mesogens, but considering the small enthalpy change accompanying the mesophase → isotropic transition the properties shown potentially arise due to the proximity of the mesogens on the polymer backbone actively precluding the formation of a highly organised mesophase. This structure would bear similarities to the "loose" mesophase structure described in (4.2.3) for BDH849, and its formation in LCP2 is confirmed by similar trends in the entropic results observed for these systems.

4.4.3 PHYSIOCHEMICAL STUDIES OF LCP3

The structure of LCP3 is shown in Figure 4.15, with physiochemical results for this system being summarised in Appendix 2, section (A2.7). Plots of ln Vg° and ln Ω^{∞} *vs* 1/T are shown in Figure A2.49 to Figure A2.54, and physiochemical results derived from these are contained in Table A2.17 and Table A2.18.

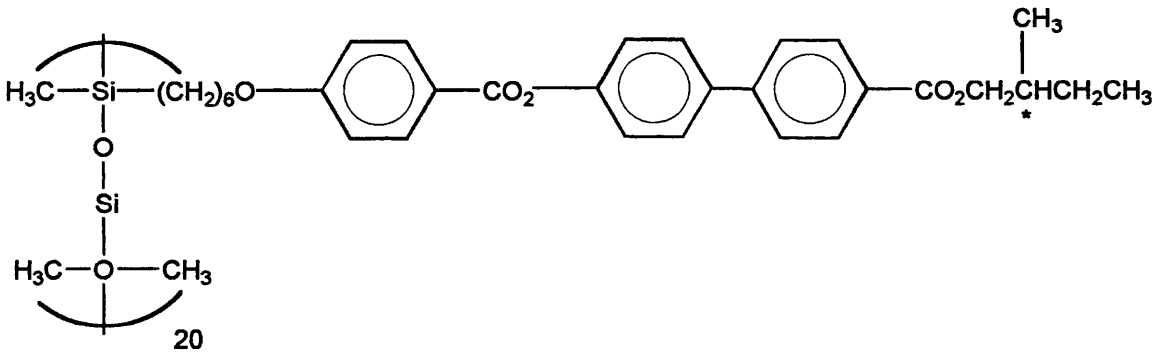

LCP3

Figure 4.15: Structure of LCP3

LCP3 contains the same mesogen appended to LCP2, but spaced on the siloxane backbone with methyl groups in order to impart higher backbone flexibility and therefore allow free expression of the inherent mesogenic properties. In considering the solution properties obtained from these plots, the following trends are shown:

$$\Omega^{\infty}_{PDMS} < \Omega^{\infty}_{isotropic} < \Omega^{\infty}_{nematic} \quad [1]$$

$$\Delta H^{s}_{isotropic} > \Delta H^{s}_{smectic\ C} > \Delta H^{s}_{PDMS} \quad [2]$$

$$\Delta H^{e}_{smectic\ C} \cong \Delta H^{e}_{isotropic} > \Delta H^{s}_{PDMS} \quad [3]$$

$$\Delta S^{s}_{isotropic} > \Delta S^{s}_{PDMS} > \Delta S^{s}_{smectic\ C} \quad [4]$$

$$\Delta S^{e}_{isotropic} > \Delta S^{e}_{smectic\ C} > \Delta S^{e}_{PDMS} \quad [5]$$

The retention volumes observed for LCP3 are much reduced compared with LCP1. In fact, at higher temperatures the possibility of differentiation between probes is minimal

due to the closeness in retention. Little is therefore indicated about the retention behaviour of the mesophase, except to say poor interactions are occurring between the probes and stationary phase. The activity coefficients show similar values to LCP2 for all probes, indicating that within the phase the favourability of the interactions is similar, though less likely. This leads to the suggestion the higher operational temperature imparts enough energy to the probes to prevent full equilibration. From these results the above trends are obtained, which show great similarity to those noted for LCP1 suggesting the mesophase has a more ordered structure than LCP2 which is more amenable to interaction with the probes. The improved enthalpic and entropic contributions to LCP3 over those observed for LCP2 further confirm this.

The *aliphatic probes* show decreasing ΔH^s on increasing chain length, and increasing ΔH^e on increasing chain length and branching, indicating that enthalpic considerations are of more importance in LCP3 than in LCP1. Entropically, interactions are generally less favourable than LCP2, but the magnitude of all ΔS^s values are similar, suggesting the probes are more able to penetrate the mesophase layering to form interactions. The *aromatic probes* show very similar enthalpic and entropic properties to those shown with LCP2 again indicating the more favourable penetration to the mesogenic core. No great differences are noted for the xylenes. The *isotropic probes* again show very similar properties - with more favourable entropy indicating the structure proposed. There is very little to differentiate the two isomers.

Overall, these results indicate relatively poor interactions between the probes and LCP3, and in comparison with LCP2 enthalpy is more favourable and enthalpy less so. Again, the retention volumes are a consequence of the high thermal energy available to the probe at such temperatures. The large excess entropies again show the importance of the mesophase structure in the interactions, though it appears this structure is more penetrable by the probes than LCP2, increasing the efficiency of the stationary phase. This can only be to the spacing between the mesogens allowing the freedom to form a more organised mesophase structure, which is confirmed considering the mesophase $\rightarrow$ isotropic transition enthalpy obtained experimentally by DSC; 4.90 J g^{-1} (LCP2) compared with 7.25 J g^{-1} (LCP3). The magnitude of these transition enthalpies do not indicate the mesophase structure in LCP3 is highly organised with reference to a crystalline state (the K $\rightarrow$ S_C transition in LMM1 shows ΔH^t = 40.15 J g^{-1}), but that improved mesogenic properties over LCP2 are observed.

4.4.4 PRELIMINARY SUMMARY

The results for the three polymeric systems studies allow some generalisations to be made about how solute-solvent interactions in these systems occur:

- In order to form effective mesophases, the appendages must have minimal restriction from the polymeric backbone which may act to restrict effective mesophase formation.

- In comparison with PDMS, the mesogenic appendages exert considerable influence on both the structure of the material and its interactions with probe molecules.

- Comparison with low molecular mass materials shows the mesophases formed are less ordered in structure, and the backbone restrictions that give rise to this phenomenon also influence the solute-solvent interaction. These contributions from both mesogenic and non-mesogenic portions of the material also give rise to properties unique to the polymeric systems.

- Whilst the ability to differentiate between probes in a homologous series is reduced, these materials shows far more selectivity due to shape (in this study, the xylenes are the prime example). Combined with the enhanced thermal properties of the systems, the potential application in GC analysis would appear more favourable for polymeric liquid crystalline systems.

4.5 GENERAL CONCLUSIONS

With reference to (1.5.1), the study of liquid crystalline systems has been carried out, and methods by which solute-solvent interactions occur have been suggested. The aim of this work is to characterise and develop novel stationary phases. The separation in such systems is due to differences in interaction between probes and the stationary phase, so a detailed understanding of these interactions is required to enable to design of new phases. Summarising the research described in this chapter, it has been shown that:

- The factors affecting the mesophase enthalpic and entropic contributions (either favourable or unfavourable) to mixing are a direct consequence of the ordered mesophase structure.

- To have the necessary order and mesogen-mesogen interaction properties to show physiochemical differences in solution formation, an enantiomerically pure mesogen is required. Racemic mixtures of mesogens act to disrupt the liquid crystalline mesophase structure reducing the observed effect of these unique properties on solute-solvent interaction.

- Comparing mesophases, the nematic mesophase appears to offer the greatest differences in solution properties, though the nature of these interactions depends on the molecular composition of the mesophase. The factors governing the relative amounts of order in mesophases will be considered further in Chapter 7 when suggesting a liquid crystalline material with the "ideal" properties to effect enantiomeric separations.

- Comparison with low molecular mass materials shows the solute-solvent interactions to be governed by the mesophase, with contributions from the backbone. The isotropic phase also shows greater involvement of the mesogens, due to their inability to form a freely dissociated solution. This gives rise to properties unique to the polymeric systems, these materials showing far more selectivity due to shape, making their use as stationary phases appear more favourable.

Chapter 5 will now consider the analytical performance observed using these materials as stationary phases, and describe the performance in terms of the interactions and solution properties presented in this chapter.

Chapter Five:

ANALYTICAL RESULTS

FOR LIQUID CRYSTALLINE SYSTEMS

This chapter contains the analytical results obtained for all the liquid crystalline stationary phases studied, in order to allow comparisons to be drawn between different stereochemical structures, different chiral moieties, and fundamentally different basic liquid crystalline structures.

The results listed in Appendix 3 comprise the selectivity, α, resolution, R_S, and number of theoretical plates required to effect a resolution of 1.5, which represents baseline separation of the analytes. The methods by which these parameters are calculated are described in (1.3.1), to which the reader is here referred. The results are calculated using a constant order of elution, so any reversal of elution order results in values of $\alpha < 1$ and negative R_S values. All results were obtained using the GC system described in (2.3.1), avoiding supercooling regions of the mesophases. Although the analytical use of supercooled mesophases has been considered previously[254,255], their ability to revert to the lower-temperature phase over a period of hours to days impairs their use for non-specialist applications.

For each of the columns studied, analytes belonging to a homologous series were adequately separated, as expected, and the results obtained for hexane and heptane are quoted to give an indication of this separation. The main concern of this chapter is therefore the analytical performance of the columns in separating the closely-related isomers:

m-xylene & p-xylene
cis-2-hexene & trans-2-hexene
R(+)-2-methylchloropropionate & S(-)-2-methylchloropropionate

These pairs were selected as they give an indication of the efficiency of the stationary phase to separate positional isomers, geometric isomers and enantiomers. In the case of the closely-related xylenes, there is also much literature available for comparison using both liquid crystalline[256-260] and non-mesogenic[261-264] stationary phases. For all analytes, comparisons were drawn with PDMS (3.4.2), with the other stationary phases, and with the solution properties of the analytes with the stationary phase (Chapter 4).

5.1 COMPARISON OF RACEMIC AND CHIRAL MATERIALS

It was demonstrated in (4.2) that the solute-solvent interactions between probes and chiral stationary phases were notably different than those between probes and racemic stationary phases. The effect of mesogen chirality on probes from a homologous series and isomeric probes suggested this interaction was in some way connected with

the molecular shape of the mesophase. The results herein consider the analytical performance of racemic and chiral stationary phases in order to ascertain whether the advantages to solution behaviour conferred to the chiral systems are reflected in analytical performance. Comparisons of results with PDMS and between the systems BDH509 & BDH770 and BDH849 & BDH1029 are made.

5.1.1 BDH509 AND BDH770

As described in (2.1) these materials have identical chemical structures, with BDH509 being enantiomerically pure whilst BDH770 contains a racemic mixture of mesogens. The analytical results obtained for these materials are summarised in Appendix 3, section (A3.1) and (A3.2), Table A3.1 to Table A3.8. To visualise these results, plots of R_S *vs* T are shown in Figure 5.1 (for BDH509) and Figure 5.2 (for BDH770).

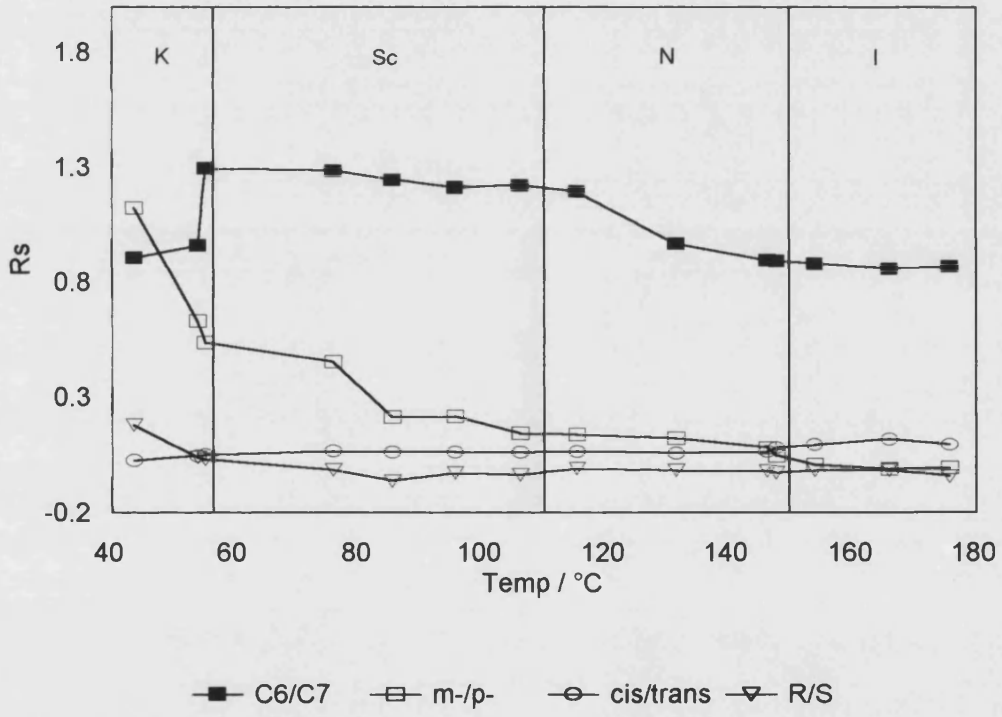

Figure 5.1: Resolution vs Temperature for BDH509

The results obtained for BDH509 and BDH770 show that in comparison with PDMS, the resolution obtained between hexane and heptane at all temperatures (despite being more favourable than the closely-related analytes) has decreased significantly. It is also apparent from the results for both mesophases that as temperature increases, the resolution obtained for the majority of analytes decreases - a trend also noted with PDMS. This suggests the thermal energy available to the probes as temperature

increases is a primary consideration in the solute-solvent interaction. However, this is an oversimplification of the results and does not account for the trends and differences between the liquid crystalline mesophases.

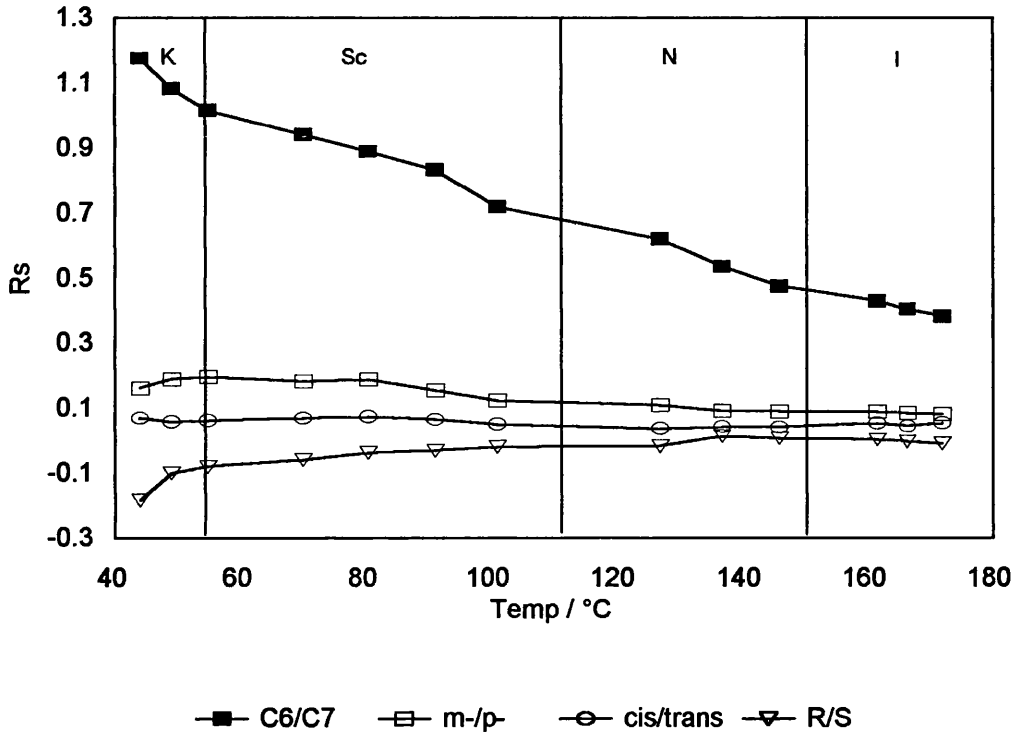

Figure 5.2: Resolution vs Temperature for BDH770

Considering the *alkanes*, baseline resolution was effected at all temperatures using PDMS as the stationary phase, despite the reduction in efficiency mentioned previously. The liquid crystalline stationary phases did not give rise to baseline separation at any temperature, and whilst a decrease in resolution occurred with increasing temperature, the decrease was far smaller than that shown by PDMS over the temperature range. This difference in retention behaviour is a consequence of the interaction between the analyte and stationary phase rather than the fabrication of the column, as the columns containing mesogenic stationary phases were prepared in an identical manner and with similar loading to that containing PDMS. From a comparison of retention volumes of PDMS (Figure 3.8) and BDH509 (Figure 4.1) at identical temperatures, it is obvious that more interaction occurs between analytes with PDMS than with the mesogenic stationary phase, leading to a decrease in efficiency for the mesogenic materials.

The racemic stationary phase showed a linear dependence of resolution on temperature, whilst the chiral material showed linear dependence within a particular mesophase; a phase transition affecting the gradient of this dependence. This

indicates the mesophase structure plays a role in the separation of the analytes for the chiral material, whereas no such effect was noted for the racemic stationary phase. Within a mesophase the temperature dependence was still evident, but to a much lesser extent than in PDMS, suggesting retention due to the interaction with the mesogenic structure over-rides the enhanced energy available to the analyte. Further weight to this theory was given by extrapolation of resolution in a mesophase to the lower temperature phase: Both the nematic and smectic C phases at a lower temperature show improved selectivity over the phase present at that lower temperature. Extrapolation of the isotropic phase lead to lower resolution. Of particular interest for the chiral material is the crystalline phase, which indicates far lower resolution than the mesophases. This is a direct consequence of the mechanism of interaction between analyte and crystalline phase - where rather than solvate into the structure, analyte molecules condense onto the surface. This mechanism must also be effective for the racemic stationary phase, but as a corresponding increase in resolution doe not accompany the transition temperature, a less ordered crystalline structure is indicated.

In comparison with the trends described in Chapter 4, the analytical separation of the *alkanes* in PDMS can be attributed to the far more favourable interactions (i.e. lower γ^{∞}) the effect of which for such analytes leads to improved mixing and retention in the stationary phase. In the mesophases of BDH509 and BDH770, the trends noted tie in with the observed solution behaviour when considering the enthalpic and entropic contributions to mixing. The chiral mesophase shows a greater entropic contribution to mixing due to its macrostructure, which is reflected in the observed analytical behaviour. Conversely, the racemic mixture shows a predominance of enthalpic effects, leading to little change between analytical results in each phase. Where these effects converge in the isotropic phase, similar trends were noted. However, even in this region there was greater resolution with the chiral material, confirming that interactions between analytes and the individual mesogens may act to give slightly different environments for solvation.

The *xylenes* show a small measure of resolution with PDMS until a temperature of 85°C, where they elute at the same retention time. On analysis with BDH509, the xylenes showed good resolution in the crystalline phase, though this decreased extremely rapidly with an increase in temperature. Resolution in the S_C mesophase was also more favourable than PDMS at low temperatures, but again temperature dependence was noted. In the nematic mesophase slight resolution was obtained, with $R_S \approx 0$ at the clearing point and thereafter. Extrapolation to lower temperatures suggests the Smectic C mesophase makes the best stationary phase for these analytes. Trends in BDH770 were different; resolution across the crystalline and

smectic mesophases remained similar, though of a very small magnitude, decreasing to $R_S \approx 0.1$ in the nematic and isotropic phases. Within experimental uncertainty it may be stated that no selectivity due to mesophase structure is noted with the racemic mesogen. The trend suggested by the α values for BDH770 suggests greater selectivity, especially in the cholesteric mesophase, and a relatively small number of theoretical plates required to effect a good separation. However, the poor resolution shown may therefore be attributed to overlap of peaks due to high peak widths on this column.

Considering the solution properties for the *xylenes*, the trend is again for the highly favourable interaction (low γ^{∞}) with PDMS to form better mixtures. However, little differentiation between the analytes is shown due to their similar properties. With the chiral stationary phase, the solution behaviour with the S_C mesophase indicates favourable energetic mixing, as reflected in the temperature dependence of resolution in the mesophase. However, this does not explain the large differences in R_S between the chiral and racemic materials; from their energetic properties alone identical separation would be expected. The difference can therefore only be explained considering the more ordered layered structure of the mesophase in the chiral material allowing expression of the entropic differences to lead to a more efficient interaction between the analytes and mesogenic core. In the nematic mesophase, the resolution is higher for the chiral material than the racemic material, which may be fully attributable to the more favourable entropy observed. Extrapolation of resolution in the nematic mesophase to S_C mesophase temperatures shows a lower level of resolution, but greater temperature stability. The isotropic phase shows similar resolution of the analytes in both materials, but their solution behaviour - whilst being overall identical - comprises different enthalpic and entropic contributions. This suggests interaction with a mesophase is necessary to express differences in the enthalpic and entropic behaviour of an analyte.

The *alkenes* showed very little tendency to separate. Whilst $R_S \approx 0.2$ was shown at 45°C with PDMS, there was no observable separation of these analytes at higher temperatures. Similarly, values of α and low values of R_S were shown with BDH509 regardless of mesophase. If anything, closer examination of the results shows a slight increase in values of R_S as the isotropic phase is formed. No resolution of the alkenes occurred with BDH770 column for these analytes, regardless of temperature or mesophase, though again a slight trend to increase occurred in the isotropic phase.

The solution behaviour of the *alkenes*, better retention was again shown with PDMS, again as a consequence of more favourable mixing. There were some slight differences shown for the solution behaviour of the cis- and trans- isomers with the

chiral and racemic stationary phases, though these differences did not translate to analytical separations. It appears that the differences shown in the isotropic phases are a combination of the ability of the analyte to interact with the non-ordered structure and arise due to the conformation of the cis- analyte allowing more favourable interaction between π-electrons in the C=C bond and the mesogenic core. Such interactions are not dependent on mesophase structure, and are thus apparent for both the chiral and racemic material.

Finally, the *enantiomers* also show very little tendency to separate. With PDMS, $R_S \approx 0$ across all temperatures. With BDH509 slight separation is exhibited at low temperatures in the crystalline phase, but as temperature increases and the mesophase behaviour changes there is no evidence of separation. Elution order even switches on numerous occasions, α values approach unity, and very high numbers of theoretical plates are required for effective separations. Any suggestion of resolution would appear to be due to experimental uncertainty. Similarly, no resolution is noted for the enantiomers with BDH770, and there is a tendency for the elution order to switch between mesophases.

The determination of solution behaviour for the enantiomers lead to determinations of ΔH^s and ΔS^e, which show greater differences in the racemic stationary phase than the chiral stationary phase. However, these differences do not translate to analytical separations and it therefore no inference can be made as to the factors affecting separation of these enantiomers.

5.1.2 BDH849 AND BDH1029

As described in (2.1) these materials again have identical chemical structures, with BDH849 being enantiomerically pure whilst BDH1029 contains a racemic mixture of mesogens. The analytical results obtained for these materials are summarised in Appendix 3, section (A3.3) and (A3.4), Table A3.9 to Table A3.16. To visualise these results, plots of R_S *vs* T are shown in Figure 5.3 (for BDH849) and Figure 5.4 (for BDH1029).

The results obtained for BDH849 and BDH1029 again show that in comparison with PDMS, the resolution obtained between hexane and heptane at all temperatures has decreased significantly. This resolution is also lower (on average) than the previous liquid crystalline systems. Unlike PDMS and the previous LC systems, very little temperature dependence for resolution is apparent. This suggests the thermal energy available to the probes as temperature increases is no longer a primary consideration in differences between solute-solvent interactions. However, as very little resolution is

shown for the systems this trend may describe the same input of thermal energy affecting the probe pairs in identical ways.

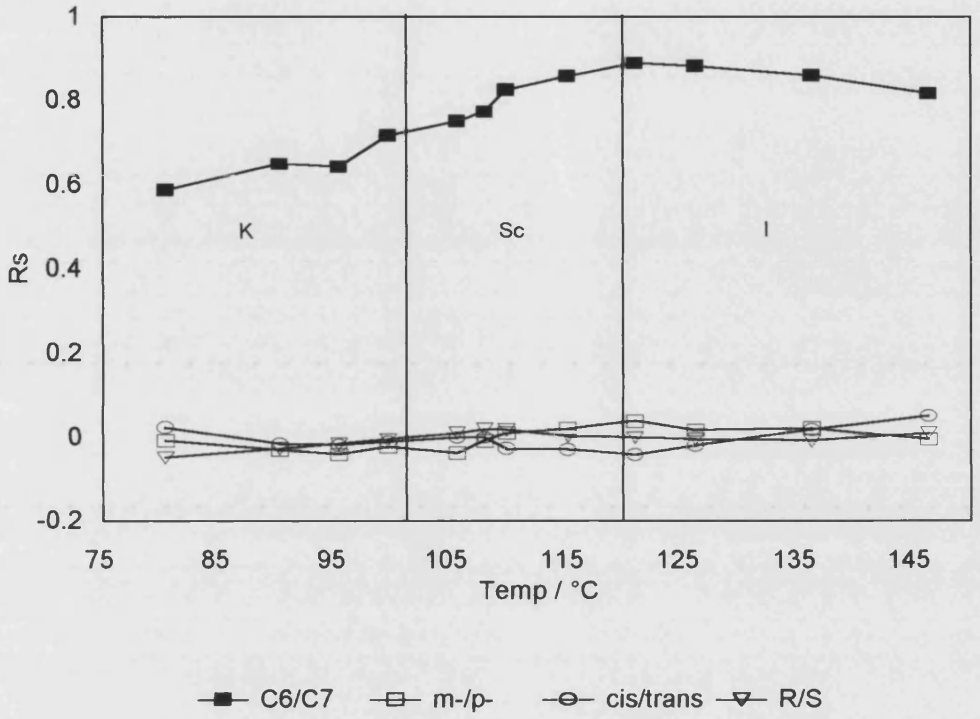

Figure 5.3: Resolution vs Temperature for BDH849

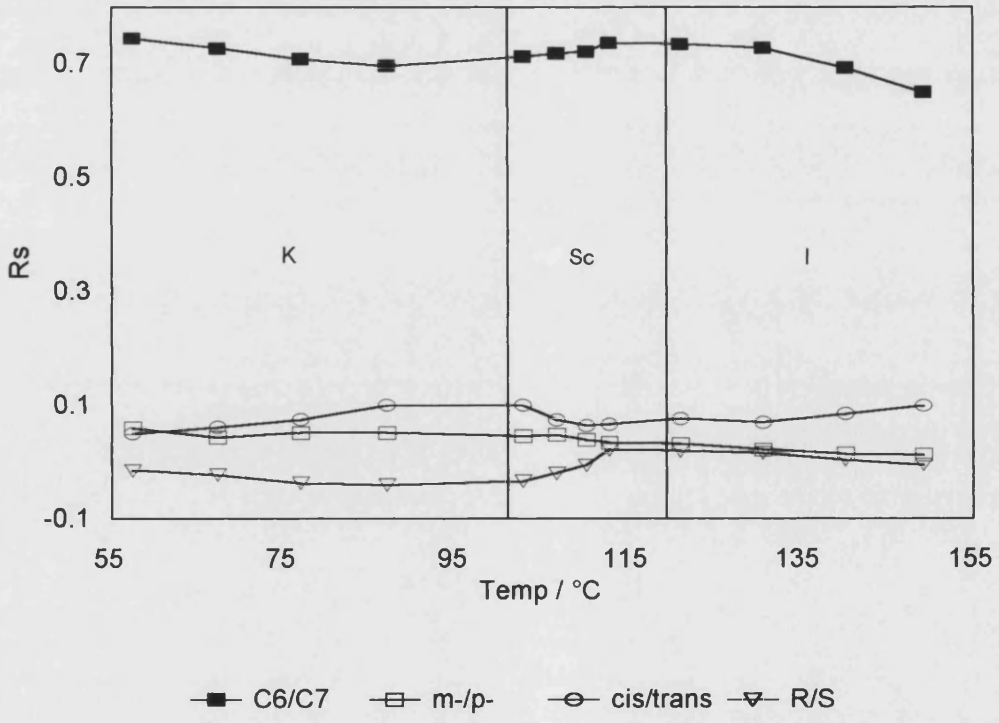

Figure 5.4: Resolution vs Temperature for BDH1029

For the *alkanes* with both materials good α values are shown at all temperatures, and low numbers of theoretical plates are required to effect good resolution, particularly in the mesophases. The chiral mesophase shows an increase in resolution through the crystalline and mesophase structures, decreasing slightly in the isotropic liquid. The racemic mesophase shows a more even resolution, with a slight increase in the mesophase and slight decreases in the crystalline and isotropic phases. Despite the favourable entropy shown by the mesophase for all probes, it appears there are no differences in retention which may be attributed to the mesophase structure in either the chiral or racemic mesophases. This may be a consequence of the chiral branch end-groups at either end of the mesogen forming a less ordered mesophase structure which is less amenable to differential retention of these analytes. The alkane analytes exhibit the expected behaviour considering the solution model of the mesophase proposed in (4.2.3), in which solute-solvent interactions are strengthened due to the increased ability of the analyte to penetrate the mesophase structure, but selectivity is reduced due to the reduced order inherent in the structure.

The *xylenes* show discrimination with regard to o-xylene which exhibits a higher retention time and reasonable resolution from m-xylene and p-xylene across all temperatures and stationary phases studied. However, m-xylene and p-xylene exhibit similar elution times, leading to small α values and resolutions - with correspondingly large numbers of theoretical plates required to effect a separation. No trend is noticed with regard to resolution as temperature increases or mesophase transitions occur, showing none of the stationary phases used have a particular affinity for separating these analytes. This confirms the lack of trends noted for the solution behaviour of the xylenes with these materials.

The *alkenes* show better retention with PDMS than with the mesogenic materials considered here. Elution from both of these stationary phases shows very close retention times at all temperatures, translating to α values approaching unity and very small values for resolution. Close examination of the R_S values obtained shows the elution of the probes is so close they occasionally elute in reverse order. This suggests the elution is subject to experimental uncertainty, and thus no effective separation occurs. The same can be said for the *enantiomers*, which show no effective resolution. Considering the solution behaviour for both of these sets of probes more separation would have been expected.

Thus, BDH849 and BDH1029 do not make good selective solvents for any of the isomeric pairs considered. As (5.1.1) showed the chiral material BDH509 to have greater selectivity than the racemic BDH770, the inability of BDH849 and BDH1029 to

separate such analytes is due to more fundamental interactions between the solute and solvent. By reference to the IGC data in (4.2.4) it would appear that this inability to differentiate similar analytes is due to the less ordered mesophase structure imparting less restriction on interactions between analyte and stationary phase.

5.1.3 PRELIMINARY SUMMARY

Just as (4.2.5) stated solution behaviour was directly affected by the mesophase structure, the results obtained here also show analytical behaviour to be similarly affected. Considering the analytical results obtained with chiral and racemic stationary phases, the following conclusions are made:

- The mesophase must be sufficiently ordered to allow any expression of solution differences to affect the analytical behaviour observed.

- In such ordered systems, entropic effects dominate solute-solvent interactions in chiral mesophases whilst enthalpic effects dominate in racemic mesophases. Chiral stationary phases are therefore essential in achieving shape-selective separations using GC methodology.

- The most efficient mesophase for separation depends on the nature of the probe to be separated. In general the more ordered in the system, the more resolution shown, though the crystalline systems which reliant on surface absorption only prove unreliable as stationary phases. This generalisation fails to account for kinetic effects on the analyte due to temperature, and systems should be selected according to the analytes to be separated.

- Deviations from ideality help separation, but do not improve retention time. Column fabrication therefore depends on the balance between good mixing (leading to high retention times) and deviations from ideality from entropic contributions in well-ordered mesophases allowing shape-based selectivity.

5.2 COMPARISON WITH LMM1

In the IGC characterisation of LMM1 described in (4.3) it was demonstrated that the mesophase showed good enthalpic and entropic properties of solution, and therefore than LMM1 has the potential to make an efficient GC stationary phase for the analytes of interest.

The structure and synthesis of LMM1 are described in (2.1), and the analytical results obtained for this materials are summarised in (A3.5), Table A3.17 to Table A3.20. To illustrate these results, a plot of R_S *vs* T is shown in Figure 5.5.

Analytically, good resolution is shown for the *alkanes* throughout the temperature range over which mesophase behaviour is exhibited. Values of α are also very favourable, showing a slight decrease over the temperature range studied, and the numbers of theoretical plates required for a resolution of 1.5 are easily achieved in packed column GC for this stationary phase. The values of R_S at lower temperatures are lower than the corresponding values for PDMS, but the resolution of the alkanes remains constant as temperature increases suggesting enhanced kinetic energy affects both analytes to the same extent. The solution behaviour in (4.3) showed more favourable entropy with the S_C mesophase and more favourable enthalpy with the isotropic liquid, suggesting the interplay of enthalpic and entropic effects results in analytical properties which overcome the mesogenic effects felt by the aliphatic analytes.

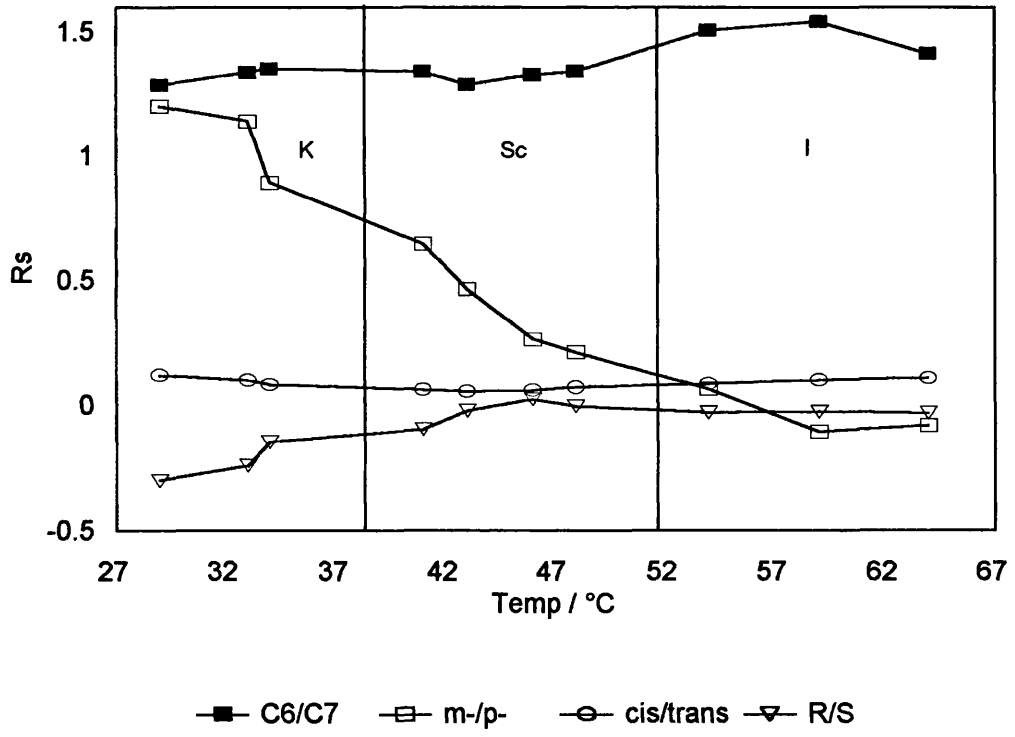

Figure 5.5: Resolution vs Temperature for LMM1

For the *xylenes*, o-xylene shows a higher elution time than m-xylene and p-xylene, which show similar elution times. Phase transitions show a marked effect on the separation of the xylenes, with good resolution in the crystalline phase decreasing with

increasing temperature through the S_C phase, leading to the order of elution reversing and very poor resolution in the isotropic phase. Extrapolation to lower temperatures again suggests the S_C mesophase to be the most efficient stationary phase for these analytes. This pattern is reflected in the α values and number of theoretical plates required to give a resolution of 1.5, and suggests the degree of order displayed by the liquid crystalline stationary phase has a marked effect on the separation of these xylenes. In the crystalline mesophase the marked decrease in resolution with temperature is attributable to surface adsorption being easily disrupted with an input of kinetic energy to the analytes. Considering the solution behaviour of these probes, m-xylene was shown to have more favourable entropy than p-xylene in the S_C mesophase, which indicates the trend observed is due to entropic effects between the probe and the mesophase structure. In the isotropic phase, where enthalpic effects dominate solution behaviour, there is little to differentiate the xylenes physiochemically, therefore little separation is observed.

The *alkenes* again show very little tendency to separate, with small R_S values being shown with the crystalline phase, decreasing to no separation in the mesophase, and increasing again slightly in the isotropic mesophase. This suggests the liquid crystalline structure shows no affinity for these alkenes, and illustrates the separation in the two non-mesophases occurs *via* differing mechanisms; by surface adsorption in the crystalline mesophase, and by direct interaction with the individual mesogens in the isotropic liquid. The indications from solution parameters that the cis-isomer would interact more favourably in the mesophase have not been shown experimentally, suggesting that for these analytes other effects are predominant. However, in the isotropic mesophase it was suggested that the mesogens present an asymmetric environment for the analytes by giving a lower γ^{∞} for the cis-isomer. This is confirmed as some resolution is shown with cis-2-hexene having the greater retention time.

In contrast to all the liquid crystalline mesophases studied so far, the *enantiomers* do show a tendency to separate on this column. The values of R_S are very small, but even accounting for experimental uncertainty there is a clear trend for the S(-) isomer to elute prior to the R(+) isomer in the crystalline phase. Throughout the S_C mesophase separation continues, with R_S decreasing as temperature increases, until the clearing point when no discernible separation is observed. Extrapolation to lower temperatures shows the mesophase to be most favourable phase for the separation of enantiomers in this stationary phase. The solution behaviour shows the S(-) enantiomer to have slightly less favourable enthalpy than the R(+) isomer, and whilst both show favourable entropy, the entropy effect for S(-) is greater resulting in more favourable interaction and a longer retention time. Thus, the mesophase structure is responsible for the separation of these enantiomers.

The behaviour observed by this chiral low molecular mass liquid crystalline stationary phase shows values and trends similar to BDH509 reiterating the observations made in (5.1.3), with improved separation for the enantiomers. However, it must be noted that the temperature of operation for a column containing this mesophase preclude its wide use as an analytical stationary phase, and so other materials which show similar mesophase structure and behaviour are desirable. Such materials are the 2 and 3 ringed liquid crystal polymers based on LMM1, the analytical properties of which are described in (5.3) and (5.4).

5.2.1 PRELIMINARY SUMMARY

In considering the analytical results for the five liquid crystalline systems studied, the following conclusions may be drawn as to their analytical performance and correlation of this performance with the IGC results described in Chapter 4.

- Generally, the separation observed is a consequence of differences in solution properties giving preferential retention to one of the analytes. These differences may be due to the mesophase structure of the stationary phase, or to other factors in the crystalline and isotropic phases. Kinetic factors due to the thermal energy of the probes also play a significant role in the analytical performance observed.

- There is a distinct difference in analytical performance between chiral and racemic mesophases, with entropic effects dominating interactions with the former and enthalpic effects dominating interactions with the latter. Chiral stationary phases are therefore essential in achieving shape-selective separations.

- The chiral mesophase must be part of an ordered system, with hindrances to this order (such at lateral groups and lack of a flexible end-group) reducing the ability of the stationary phase to separate enantiomers.

- The most effective phases for a particular system is dependent upon the individual system, but considering the results obtained so far the following trends are noted. i.e. closely related compounds require ordered mesophase structures for separation.

  Xylenes are separated most effectively in the S_C mesophase.
  Alkenes are separated most effectively in the isotropic phase.
  Enantiomers are separated most effectively in the S_C mesophase.

5.3 LIQUID CRYSTAL POLYMER STATIONARY PHASES

The results obtained so far indicate that the S_C mesophase is most desirable for the separation of a variety of isomeric pairs. However, the practical application of the materials considered so far is limited, so it is necessary to identify materials which exhibit the same mesophase structures yet express these at higher temperatures. Such materials are the liquid crystal polymers which offer the thermal stability and durability of siloxane polymers whilst allowing the expression of mesophase behaviour. The synthesis and properties of the liquid crystal polymer materials used in this study are described in (2.1). These materials are similar in structure to LMM1 allowing direct comparisons between results obtained for each system to be compared.

The physiochemical studies of these materials described in (4.4) illustrated the influence of the mesogenic units on the properties of these materials, and suggest the role played by the siloxane backbone may also aid the chromatographic properties of stationary phases using these materials.

5.3.1 ANALYTICAL PERFORMANCE: LCP1

The structure and synthesis of LCP1 are described in (2.1), and the analytical results obtained for this material are summarised in (A3.6), Table A3.21 to Table A3.24. To visualise these results, a plot of R_S *vs* T is shown in Figure 5.6.

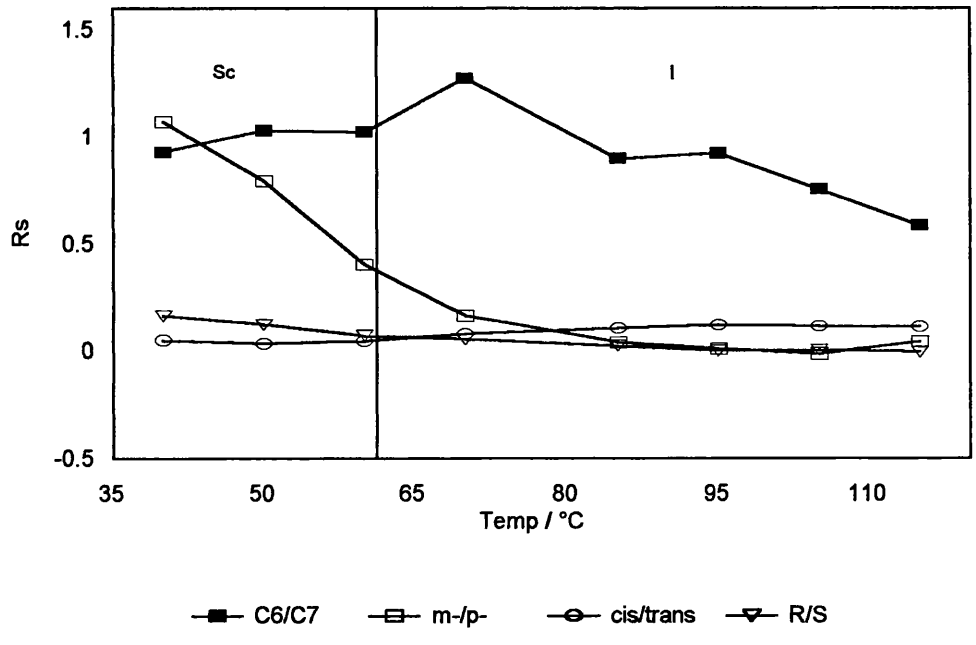

Figure 5.6: Resolution vs Temperature for LCP1

In LCP1, the resolution obtained for the *alkane* analytes is satisfactory at all temperatures. R_S is significantly reduced from that observed using PDMS as a stationary phase, though a feasible number of theoretical plates are available to separate these analytes on this stationary phase. Unlike LMM1, alkane resolution and α values decrease with an increase in temperature, suggesting the thermal energy available to them acts to reduce their relative affinity for the stationary phase and enthalpic effects predominate. The solution properties showed higher activities and lower retention volumes in LCP1, which explains the slightly lower resolution for these analytes. In the S_C mesophase enthalpy of interaction is more favourable for hexane than heptane, and entropy is less favourable, so whilst energetic factors predominate in the solute-solvent interactions they are moderated by the mesophase structure. In isotropic liquid the more rapid decrease in resolution may be attributable to energetic considerations dominating entropic factors.

The *xylenes* show similar resolution to that exhibited in LMM1, with good resolution in the crystalline phase decreasing as temperature increases through the S_C phase, leading to very poor resolution in the isotropic phase. This is a direct consequence of the solution differences between the analytes as shown in Table A2.13, where p-xylene has more favourable enthalpy and m-xylene has more favourable entropy. The higher retention volume for m-xylene shows that shape-selective entropy plays a major role in the separation of xylenes in this mesophase. In the isotropic mesophase such selectivity is lost, and almost identical solution properties are shown for the two isomers, again reinforcing the importance solute interaction with the mesophase.

The *alkene* isomers also show similar resolution to that exhibited in LMM1, with negligible resolution in the mesophase improving slightly in the isotropic region, with the value of R_S increasing significantly compared with R_S prior to the transition. The α values exhibited as temperature increases improve, though the efficiency of the column is still unsatisfactory. This is again a reversal of the expected trend, with a more disordered system giving rise to improved separation, and again indicates direct interaction with the individual mesogens in the isotropic liquid occurs. The solution properties of the alkenes were very similar enthalpically and exhibited only slight entropic differences in the S_C mesophase, and similar trends are shown in the isotropic liquid, making it difficult to draw a direct comparison between solution properties and retention in this case. It would therefore appear that the enhanced separation noted in the isotropic phase would have an element of selectivity due to asymmetric interactions, but a greater contribution due to the physiochemical differences (such as partial pressure) of the analytes in their solute-solvent interactions.

The *enantiomers* exhibit also show a tendency to separate on this column. As with LMM1, the values of R_S are very small but there is clear resolution of the enantiomers throughout the S_C mesophase, with R_S decreasing as temperature increases until the clearing point when no discernible separation is observed. Enthalpically, solution formation of the R(+) isomer is more favourable, though entropically the S(-) isomer is favoured. The elution of S(-) prior to R(+) shows energy considerations to predominate in this system, though these must undoubtedly arise from the mesophase structure as the isotropic liquid shows identical solution properties and no resolution. The order of elution is reversed from that shown by LMM1 which suggests that the mesophase formed will be ordered in a slightly different manner as a consequence of the mesogen appendages.

The behaviour observed with this polymeric liquid crystalline stationary phase shows values and trends virtually identical to LMM1, though extending these properties to a higher temperature. Again, the temperatures of operation for a column containing this mesophase still preclude wide use as an analytical stationary phase, and so 3-ringed liquid crystal polymers based on this structure, which exhibit mesophase behaviour to higher temperatures, were also studied.

5.3.2 ANALYTICAL PERFORMANCE: LCP2 AND LCP3

The structure and synthesis of LCP2 and LCP3 are described in (2.1), and the analytical results obtained for these materials are summarised in (A3.7) and (A3.8), Table A3.25 to Table A3.32. To visualise these results, plots of R_S *vs* T is shown in Figure 5.7 and Figure 5.8.

The temperatures at which the majority of results are obtained are much higher than for the previous columns studied, as the polymeric liquid crystalline stationary phase remains in the Smectic C mesophase to 226°C and 191°C for LCP2 and LCP3 respectively. Consequently, the observed resolution is reduced at higher temperatures due to the enhanced energy of the probe molecules at these elevated temperatures preventing interaction of the probe with the stationary phase for the time scales required to effect a good separation[265].

As mentioned in (4.4.2), the results obtained in the S_A mesophase and isotropic liquid contained substantial uncertainties, and are therefore not considered. This allows the results obtained here to be compared with the S_C mesophases of the other materials studied.

The *alkanes* are resolved to a lower extent with LCP2 and LCP3 than with either the PDMS stationary phase or LCP1. With LCP2, R_S values for hexane and heptane show some separation, and are subject to decrease with no mesophase distinction as the temperate increases. Resolution with LCP3 shows much lower temperature dependence in the mesophase than was noted for LCP2, with a large drop in resolution at the clearing point. LCP3 exhibits mesophase behaviour over a wide range of temperatures, and it is possible to measure the separation of these analytes at high temperatures in the ordered structure. This behaviour is not shown by LCP2.

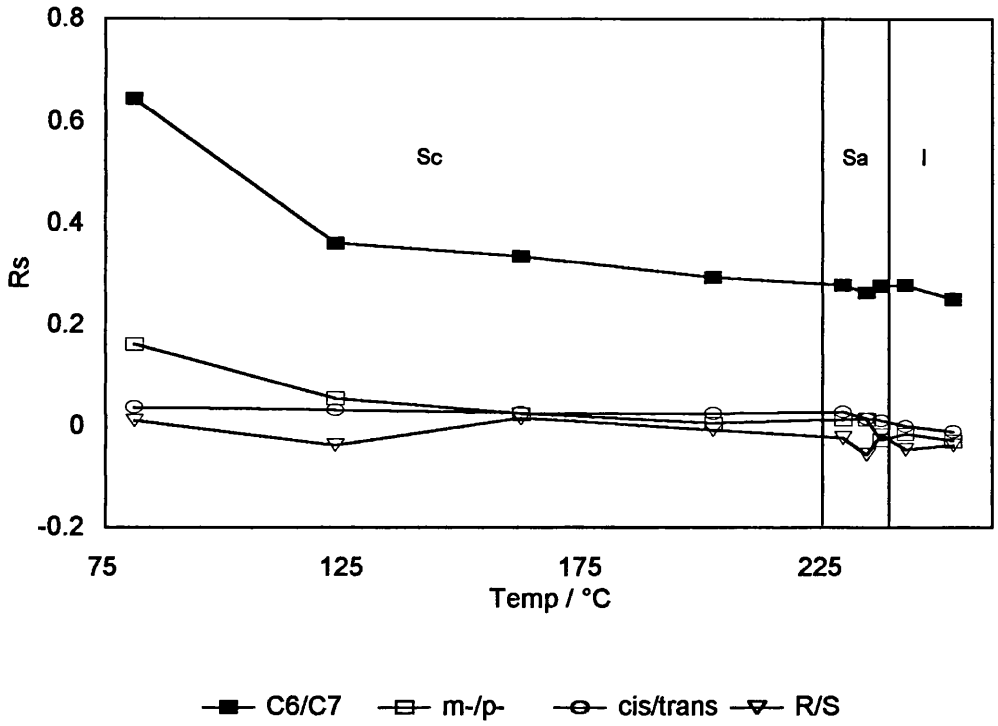

Figure 5.7: Resolution vs Temperature for LCP2

The *xylenes* also show distinct trends in LCP2 and LCP3. As noted for BDH509 and LMM1, the m- and p-xylenes show some resolution at the lower temperatures, though this resolution is suppressed compared with previous systems. This resolution decreases as the amount of order in the system decreases, until the clearing point where elution order is reversed and negligible resolution shown. Within the systems, LCP2 shows poor resolution at all temperatures within the mesophase, whilst LCP3 shows very good resolution at low temperatures in the S_C mesophase which rapidly decreases as temperature increases. These results suggest strong interactions with LCP the mesophase which were overcome by enthalpic factors as temperature increased. With both mesophases the m-xylene shows similar enthalpies of interaction and slightly improved entropic contribution. From these trends alone, similar resolution would be expected in both mesophases if their structures were identical. The enhanced

separation shown by LCP3 therefore suggests a more ordered structure than LCP2, and confirms the observations described in (4.4.3).

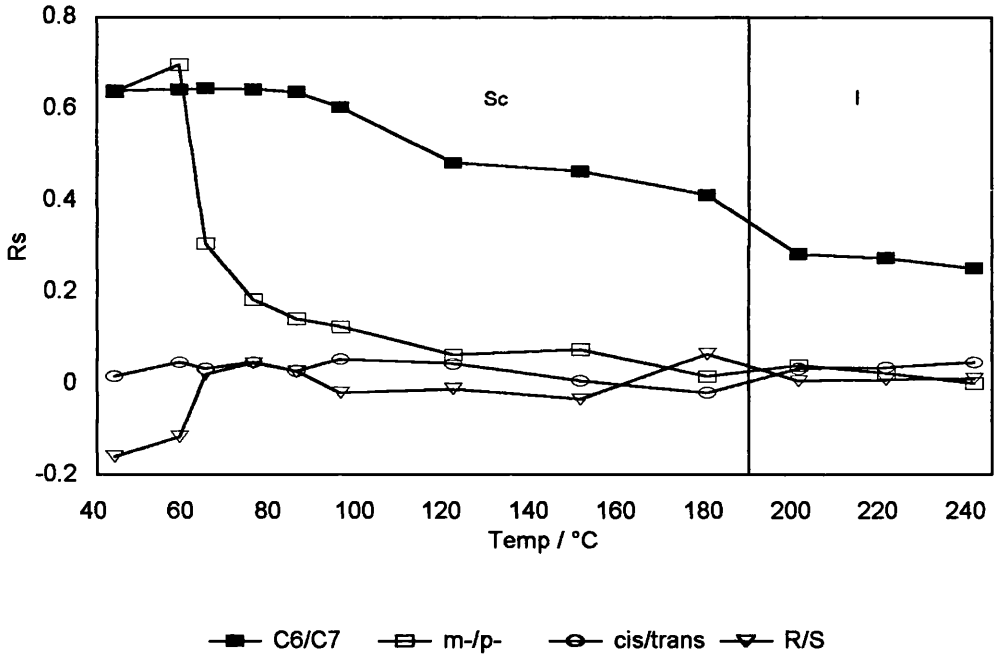

Figure 5.8: Resolution vs Temperature for LCP3

No discernible resolution is exhibited for either the *alkenes* with LCP2 or LCP3 in the mesophase structure, though the isotropic phase of LCP3 shows improved separation. This echoes the findings for the other liquid crystalline systems studied, with no selection due to mesophase structure, but improved interaction with the isotropic liquid. This is reflected in the solution properties, where the mesophases show identical solution properties for each isomer and the isotropic phase of LCP3 shows enhanced entropic and reduced enthalpic contributions for cis-2-hexene, indicating the importance of the asymmetric environment on these analytes in the isotropic phase.

The *enantiomers* exhibit variable results with LCP2, with α values approaching unity, reversals of elution order, and negligible R_S values. This is reflected in the almost identical solution properties for these analytes in the mesophase. LCP3 shows an improved performance in the mesophase, with the trend exhibited by LMM1 repeated; The values of R_S are very small, showing a clear trend for the S(-) isomer to elute prior to the R(+) isomer. Separation continues, with R_S decreasing as temperature increases, until the clearing point when no discernible separation is observed. Although no extrapolation to a lower temperature phase is possible, the similarities with LMM1 show this mesophase to also be favourable for the separation of enantiomers. The solution behaviour of these analytes with LCP3 shows identical enthalpies for both enantiomers, with the R(+) enantiomer showing more favourable entropy. This entropy

effect therefore allows differentiation and results in a longer retention time for the R(+) enantiomer. In the isotropic phase differences in solution behaviour are still exhibited, but at the temperatures of operation allow no analytical separation. This indicates an asymmetric environment is imposed on the enantiomers even in the isotropic mesophase, due to the mesogenic units being appended to the siloxane backbone, and therefore having less opportunity to form a true isotropic liquid.

5.3.3 PRELIMINARY SUMMARY

By comparison with low molecular mass and other polymer liquid crystalline materials, the following conclusions may be drawn about the performance of liquid crystal polymers as stationary phases for GC:

- The analytical performance of polymer liquid crystal polymers is dominated by the affect of mesogenic order on the system. If this order is hindered then shape-selective contributions to solvation (and hence separation) will be reduced.

- These systems do show greater potential as GC stationary phases than low molecular mass systems, though separation efficiencies are still very low and analytes must be selected so as to reduce the reductive effects of higher kinetic energy on the separations.

5.4 GENERAL CONCLUSIONS

Considering the aims and objectives outlined in (1.5.1), the analytical performance of the stationary phase has been described in terms of the solute-solvent behaviour observed with the analytes studied. Summarising the research described in this chapter, it has been shown that:

- In ordered, chiral mesophase systems entropic effects dominate the solute-solvent interactions with a variety of analytes, leading to enhanced ability to separate isomers.

- Whilst entropic effects dominate, significant contributions are also noted from enthalpic effects of mixing, and from kinetic effects due to the analyte's own thermal energy.

- The use of polymeric liquid crystalline stationary phase materials is highly desirable, as enhanced shape-selective properties due to mesogenic order are exhibited alongside the thermal stability and durability associated with polymers.

- The resolutions obtained for all analytes with liquid crystalline probes are very low in comparison to commercially available stationary phases, and efforts must be made to increase the efficiency of the separation in order to maximise the shape-selectivity inherent in the mesophases.

These observations will be further considered in Chapter 7, where the development of an "ideal" stationary phase will be discussed. However, it is interesting to note that the efficiencies for such separations using packed column GC are so low. In an attempt to increase these efficiencies work was carried out on fabricating and utilising a capillary column, as described in (5.5).

5.5 CAPILLARY COLUMN GC

Analysis of the results obtained using packed column chromatography showed that some separation of isomeric probes is in evidence in the LC mesophases - but the efficiencies noted were too small for these stationary phases to find commercial application. In order to assemble a system which offers suitable efficiency it was necessary to utilise the liquid crystalline stationary phases with capillary column GC - which has been shown to exhibit up to 4000 plates m^{-1} for liquid crystalline systems[266], compared with only the 100 to 200 plates m^{-1} noted here for packed column systems. To physically assemble this system, the preparation of untreated fused silica columns was carried out before they were coated with the desired LC systems.

5.3.1 THE CAPILLARY GC SYSTEM

Having set up the instrument as described in (2.3.2) its suitability was confirmed by observation of a satisfactory separation between members of a series (e.g. benzene, toluene and ethyl benzene) using a commercially available siloxane capillary column (5% phenylmethylsiloxane, 50 m x 0.2 mm i.d., supplied by Hewlett Packard). Columns were then prepared in the laboratory in confidence that the instrument was performing to a satisfactory standard.

5.3.2 COLUMN COATING

Liquid crystalline stationary phases are not readily available coated onto capillary columns, which necessitates this procedure to be carried out in the laboratory. Columns were coated using both the static and dynamic coating methods, which are described widely in the literature[267]. Untreated fused silica columns (10 m x 2.5 mm i.d.) were obtained from Supelco, and deactivated prior to coating by passing nitrogen gas through them overnight at 280°C[268] Dichloromethylsiloxane (DCMS) was then injected to neutralise any active Si-OH sites present[269] - the deactivation being monitored by observing injections of a test mixture of butane and methanol at 50°C. Under this procedure untreated columns retain methanol with respect to butane, and show extensive peak tailing for methanol. Deactivation allowed co-elution, and improved peak symmetry, and the columns were then ready for coating with liquid crystalline materials.

5.3.2a Static Coating

As described in (2.3.2), a 4 mg cm^{-3} solution of BDH849 was prepared and forced through the column by a constant nitrogen pressure. Once the column had been filled, one end was sealed. A variety of methods were used to effect this sealing, including flame annealing and plugging the end of the column with epoxy resin, candle wax and paraffin wax. However, after a large number of attempts with varying conditions the most suitable method was found to be plugging the end with sealing wax, which was heated and drawn into the end of the column under vacuum until approximately 2 cm was full before being left to cool and form a gas-tight seal. Practically, the stationary phase material was drawn through the column, followed by a 2 cm plug of hexane to prevent dissolution of the sealing was by the stationary phase[270], followed by the sealing wax. One the seal had cooled, the column was immersed in a water bath at 40°C and a vacuum applied to the open end. After overnight evacuation the solvent had been removed, but instead of an evenly coated column, "clumps" of white liquid crystalline material were clearly visible. The stationary phase had not coated the column, but agglomerated with like molecules - perhaps due to incompatibility with the fused silica inner-surface of the column. Repeated attempts replicated this result, so the dynamic coating method was attempted.

5.3.2b Dynamic Coating

In order to coat a capillary column using the dynamic coating method, the speed of flow of the solution through the tube was controlled to establish a linear relationship with the pressure applied. 3 cm^3 of a 10% w/v solution of BDH849 in chloroform was prepared

and passed through the column, with nitrogen gas left to flow overnight to evaporate any residual solvent. Following this, the column was placed in the GC oven where nitrogen gas was passed through at a pressure of 10 p.s.i. whilst a temperature program was underway. The column was heated 100°C from room temperature at a rate of 0.5°C min^{-1}, and held at this temperature overnight. Again, "clumps" of liquid crystal were repeatedly found in the tubing - proving this method to also be ineffective for low molecular mass liquid crystalline materials.

In attempts to improve the coating alternative solvent systems were used. Firstly toluene was investigated, as this is less volatile than chloroform and therefore less like to boil in the column and "bump" to perturb the surface. It is also a better solvent for the liquid crystalline structure, which may act to prevent the material from agglomerating. Repeating the above procedure, clumping again occurred. Finally, the use of dichloromethane as the solvent was attempted. This is an opposite approach to the use of toluene - with the more volatile solvent which has a boiling point of 40°C perhaps being removed more easily by the flow of nitrogen at the drying stage rather than in the oven - where agglomeration was noticed previously. Unfortunately clumping again occurred, so it was decided to take an alternative approach.

It has been shown that capillary columns can be readily coated by "straightforward" polymers as a capillary column was successfully coated with PDMS. Such polymeric materials are also capable of forming a solution with liquid crystalline mesogens, so it should therefore be possible to coat a capillary column with either a blend of PDMS and a liquid crystalline material, or by a mesogen-containing siloxane to give a satisfactory coating whilst retaining the necessary mesogenic behaviour to impart shape-selectivity[271]. Initially attempts were made to coat the column using LCP1 with dicholormethane, chloroform and toluene as solvents. As with the low molecular mass liquid crystals, clumps of stationary phase formed in the columns. The resulting columns were therefore not suitable for chromatography. It was decided not to proceed with the coating of LC/PDMS blends, as even if these were to coat successfully in the column, the thermodynamic data obtained so far would not be applicable to the blend.

The coating of capillary columns was therefore an unsuccessful exercise in relation to the overall thesis. However, perfecting column coating for liquid crystalline materials is important in terms of future development in the analytical use of liquid crystals for gas chromatography, and is considered further in (7.3), along with other means of improving analytical performance using these stationary phases.

Chapter Six:

DIFFUSION STUDIES

Knowledge of the diffusion of molecules in polymeric phases is of wide importance in a variety of industries. For example, the food industry requires information on the migration of substances to food from its surrounding packaging; and the chemical industry requires such information in considering storage, piping and packaging of substances. Diffusion is also major factor in the performance of Gas Chromatographic systems; separation depends on the interactions between analyte and stationary phase, which is itself dependent on the distribution of the analyte between the vapour and liquid phases - as described by the thermodynamic parameters, and the diffusion of the analyte whilst in the stationary phase. A better understanding of the chromatographic performance can therefore be obtained from the characterisation of the diffusion process.

Peak broadening is also due to both the diffusion of the probe into the stationary phase and the diffusion of the probe into the carrier gas, thus information on diffusion may be elucidated from data obtained on a Gas Chromatographic system. The use of GC to study diffusion in polymers was pioneered by Gray and Guillet in 1972[272], who investigated peak shape in IGC to consider the validity of physiochemical results obtained by this method. Since then, GC has been applied to the determination of diffusion coefficients by various workers, including Braun *et al*[273], who considered antioxidants in polyethylene; Hattam and Munk[274], who undertook theoretical modelling of the diffusion process using computer simulations; Bonifaci and Ravanetti[275], who examined ε-caprolactam in nylon 6 with reference to polymer processing; Surana *et al*[276], who predicted diffusion coefficients near the glass transition temperature of poly(vinyl acetate) by extrapolation of high temperature IGC measurements; and Jackson and Huglin[277], who measured diffusion in amine and anhydride cured cross-linked polymers. However, the use of IGC to measure diffusion coefficients in liquid crystalline systems is in its infancy, with the only published work being by Medina, who has studied diffusion in the mesophases of cholesteryl myristate[278] and 4,4'-bis(heptyloxy)azoxybenzene[279]. The results presented in this thesis are the first known examples to this author involving liquid crystalline polymers.

This research initially measured diffusion coefficients in PDMS to confirm the methodology, before extending the study to a low molecular mass liquid crystalline material (LMM1) and a polymeric liquid crystalline material (LCP1).

6.1 MEASUREMENT OF DIFFUSION BY GC

The study of diffusion describes the method by which the peak shape is influenced by the finite time required for the probe and stationary phase to reach equilibrium. In turn,

this peak shape exerts an influence on the retention data obtained from inverse gas chromatography, and therefore has a relationship with the thermodynamic and kinetic properties of the polymer-probe interaction.

In an ideal situation, the input of an infinitely sharp probe into a GC system should result in an infinitely sharp peak being eluted and detected after a retention time dependent only on the interaction between the probe and stationary phase. Practically though, the injection of probe is not infinitely sharp, and the detected peak is broadened by a variety of factors, of which there are three classes:

The *instrumental factors* include sample injection technique, column and detector dead volume, and time delays between peak detection and recording. These may be minimised by optimal design of the chromatographic system, but cannot be wholly eliminated. Secondly, and more fundamentally, the *thermodynamics* of the interaction between the probe and stationary phase affect peak shape. Should equilibrium between probe and stationary phase be reached instantaneously, the peak shape will remain gaussian if the concentration of probe in the mobile phase is linearly related to the concentration in the stationary phase. These effects are noted at infinite dilution, though deviations from the linear relationship described lead to dramatic changes in peak shape. Thirdly, *kinetic factors* play a role in shaping the peak, resulting from the finite time equilibrium is reached at each stage along the column. Collectively these factors were described by Van Deemter[280], as shown in equation [6.1].

$$H = A + \frac{B}{u} + C\bar{u} \qquad [6.1]$$

Where:

	H	height equivalent to a theoretical plate
	u	linear velocity of carrier gas
	A,B,C	constants (independent of flow rate)

The *theoretical plate* describes the theory of GC where a column is viewed as a series of discrete bands at which equilibration of the probe between the stationary and mobile phases occurs. As the efficiency of the column increases, the number of equilibrations also increases leading to an increase number of theoretical plates, and therefore a smaller *height equivalent to a theoretical plate.* At high linear velocities of the carrier gas, B/u $\rightarrow$ 0, leaving H = A + C u. Therefore, a plot of H *vs* u (the "Van Deemter" plot) gives the graph illustrated in Figure 6.1, the linear portion of which yields a gradient equivalent to C. The C term contains the diffusion coefficient, as described by equation [6.2].

$$C = \left(\frac{8}{\pi^2}\right) \cdot \left(\frac{{d_f}^2}{D_1}\right) \cdot \left(\frac{K}{\left[1+K^2\right]}\right) \qquad [6.2]$$

Where:

	d_f	film thickness of stationary phase
	D_1	diffusion coefficient of probe in stationary phase
	K	partition coefficient of probe retention

The partition coefficient, K, is a quantitative description of the equilibrium between probe and stationary phase. K is calculated in terms of the relative concentration in the stationary and mobile phases using equation [6.3].

$$K = \frac{[stationary]}{[mobile]} \qquad [6.3]$$

Deviations from linearity may occur, though the vast majority of GC methodology (particularly where conditions of infinite dilution are adhered to) allows assumption of linearity with little introduction of error. Under such conditions, the partition coefficient may be described by the capacity factor given in equation [1.3].

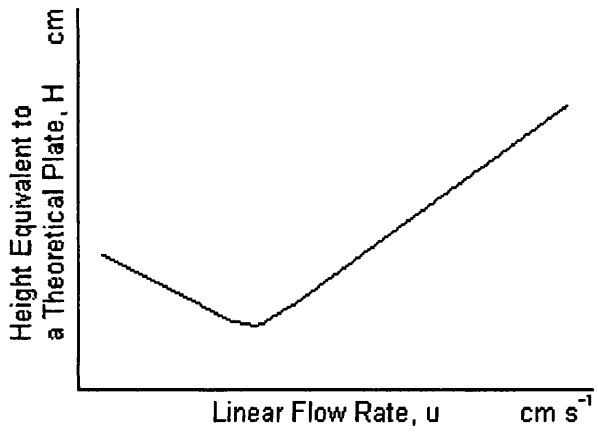

Figure 6.1: A Typical Van Deemter Plot

This model of the Van Deemter equation does not consider broadening effects due to non-instantaneous equilibration of vapour across the column by molecular mass transfer. The assumptions used to derive the C term are also unrealistic for practical packed-column GC, as the geometry of the column packing is far more complex. In

order to overcome these problems, Giddings[281] derived a nonequilibrium model which considered various dispersion factors. For a uniform film thickness, Giddings' equation is identical to the Van Deemter C term, with 2/3 being substituted for $8/\pi^2$. However, the values given by this approximation are adequate for consideration of the kinetic factors affecting chromatographic peak shape, particularly where comparisons within systems are being made.

Experimentally, the data used was that collected by IGC methodology for the probes hexane, heptane and octane at a variety of temperatures suitable to allow diffusion in various mesophases to be calculated. The measurement of diffusion in PDMS was considered first, followed by that for LMM1 and then LCP1. Injections of 0.1 μl of probe were used, approximating experimentally to infinite dilution as shown in (3.2.2). The values of H were calculated according to equation [6.4] using the chromatograms obtained experimentally.

$$H = \left(\frac{L}{5.54}\right) \cdot \left(\frac{W_{0.5}}{t_R}\right)^2 \qquad [6.4]$$

The linear flow rate, u, was calculated using equation [6.4] from measurements taken using a soap bubble flow meter.

$$\bar{u} = \left(\frac{JF'}{\bar{a}}\right) \cdot \left(\frac{T_{col}}{T}\right) \qquad [6.5]$$

Where:

	J	correction for gas compressibility, equation [1.32]
	F'	corrected flow rate ($cm^3\ min^{-1}$), equation [1.31]
	a	volume of gas phase per unit length of column, equation [6.6]
	T_{col}	temperature of column (K)
	T	temperature of flow meter (K)

In order to determine u, the volume of gas phase per unit length of the column was required. This was calculated according to equation [6.6], which when substituted into equation [6.5] gave equation [6.7].

$$\bar{a} = \left(\frac{t_M \cdot F'}{L}\right) \qquad [6.6]$$

$$\bar{u} = \left(\frac{J \cdot L}{t_M}\right) \cdot \left(\frac{T_{col}}{T}\right) \qquad [6.7]$$

Where: t_M retention of non-retained marker (min)
L length of column (cm)

After plots of H *vs* u had been constructed, the C term of the Van Deemter equation was obtained by linear regression and substituted into equation [6.2]. The partition coefficient, K, was obtained according to equation [1.3], and the film thickness, d_f, estimated according to equation [6.8]. Thus, D_1 could be obtained.

$$d_f = \left(\frac{\omega}{\rho}\right) \cdot \left(\frac{3 \cdot V}{r}\right) \qquad [6.8]$$

Where: ω weight of stationary phase material
ρ density of stationary phase
V volume occupied by stationary phase
r average radius of support material particles

It is in the calculation of the film thickness that the greatest experimental uncertainties are introduced to the calculation, though comparisons within a given column show greatly reduced uncertainties as d_f values are identical for the purposes of the calculation. For this work the value of ρ is unavailable, as mentioned in (1.4.6), so an average film thickness of 2.0×10^{-4} cm is assumed. This value is comparable with film thickness values determined by other workers[282,283], and whilst accurate values for D_1 in these systems will not be obtained, the results do allow for comparison of diffusion in PDMS, a low molecular mass liquid crystal and a polymeric liquid crystal. Such comparisons are valid due to the similarity in column preparation; the support material, mass of support and stationary phase loading are all of similar magnitude - leading to very similar values of d_f for the columns used.

After derivation of D_1 for the probe at a variety of temperatures, a plot of ln D_1 *vs* 1/T (the "Arrhenius" plot) may be made, the gradient of which yields the activation energy for diffusion according to equation [6.9]. Due to the uncertainty of the results obtained in this study the activation energy for diffusion is not calculated.

$$D = D^{-\left(\frac{E}{R \cdot T}\right)} \qquad [6.9]$$

6.2 DIFFUSION IN PDMS

The PDMS column was chosen as a reference material. The Van Deemter plots were obtained from retention at high linear velocities in order to cover the linear area of the plots. These are shown for hexane, heptane and octane in Appendix 4; Figure A4.1 to Figure A4.4. From these plots, the C constant was calculated, leading to elucidation of D_1 as shown in Table 6.1.

Probe	D_1 ($cm^2 s^{-1}$) x 10^8
Hexane	
60°C	230
71°C	94
81°C	190
91°C	77
Heptane	
60°C	170
71°C	57
81°C	300
91°C	110
Octane	
60°C	93
71°C	34
81°C	270
91°C	88

Table 6.1: Diffusion Coefficients for Probes in PDMS

The values of D_1 obtained depend upon a number of factors: the viscosity and density of the stationary phase, the path through which the molecules diffuse; the size and shape of the probe molecule; and the interaction between probe and stationary phase. As the latter has been considered in Chapter 4, values for D_1 allow commentary on the former factors to be made.

The values obtained for D_1 in PDMS show no distinct pattern with an increase in temperature. However, the overall trend observed is that these probes in PDMS have a relatively high magnitude of diffusion, suggesting that their passage through the stationary phase is relatively free in comparison with systems showing low values of D_1.

6.3 DIFFUSION IN LMM1

The Van Deemter plots for hexane, heptane and octane in LMM1 are shown in Appendix 4; Figure 4.5 and Figure 4.6 (for the S_C mesophase) and Appendix 4; Figure 4.7 to Figure 4.9 (for the isotropic phase). From these plots, the C constant is calculated, leading to elucidation of D_1 as shown in Table 6.2.

Probe	D_1 (cm^2 s^{-1}) x 10^8
Hexane	
46°C	6.2
49°C	9.3
56°C	9.57
61°C	4.80
66°C	3.70
Heptane	
46°C	3.1
49°C	6.4
56°C	14.5
61°C	8.2
66°C	6.5
Octane	
46°C	2.0
49°C	2.6
56°C	16.7
61°C	11.1
66°C	9.8

Table 6.2: Diffusion Coefficients for Probes in LMM1

Firstly, it is noted that all values of D_1 are substantially lower than those observed for the polymeric system. It would therefore appear that diffusion is a more difficult process in a liquid crystalline system that in a non-mesogenic polymer. This is the observation expected, as the interactions with the liquid crystalline system involve diffusion through both a semi-ordered structure (in the S_C mesophase) and a structure comprising many rigid units (in the isotropic phase). Diffusion in PDMS, however, involves interactions with a chain structure which as temperature increases becomes more thermally mobile allowing high diffusion of probes with a similar structure.

The retention of the probes, discussed in (4.3), shows a clear trend with the elution order being $C_6 > C_7 > C_8$. In the smectic C mesophase, this elution order is reflected in

the observed order of D_1. However, at the $S_C \rightarrow I$ phase transition, a marked increase in the value of D_1 is shown for all probes. All the values of D_1 obtained in the smectic C mesophase are of a lower order than those shown in the isotropic phase. The observed order of D_1 also reverses on the phase transition to show $C_8 > C_7 > C_6$ in the isotropic phase, as illustrated in Figure 6.2, followed by a general decrease in D_1 with increasing temperature.

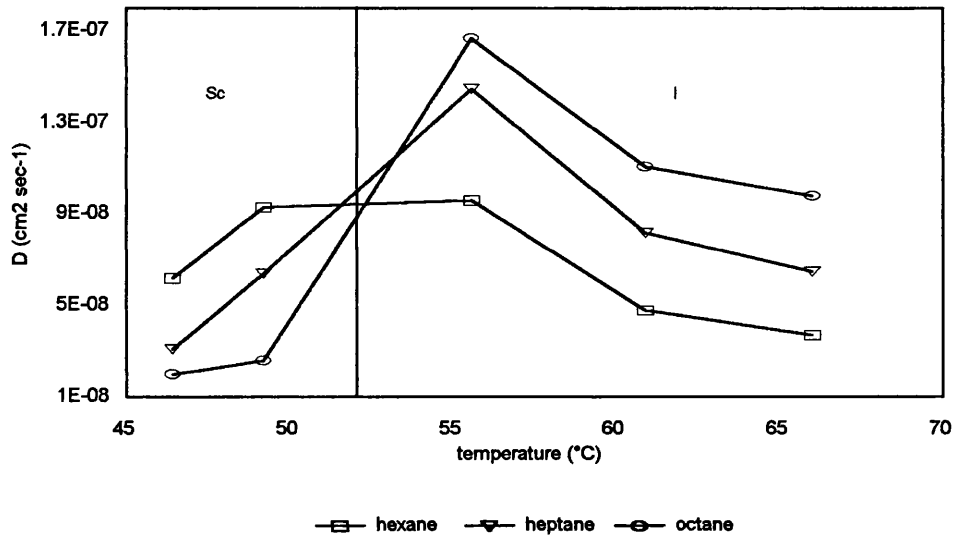

Figure 6.2: Variation of D_1 with Temperature for LMM1

These results therefore show a more marked pattern than those for PDMS. Structurally, the lower values observed in the S_C mesophase a this phase exhibits a higher degree of order, increasing the difficulty by which the probes penetrate the structure, compared with penetration in an isotropic liquid. Considering the individual probes, diffusion occurs most easily with the shorter, less thermally mobile C_6 probe; decreasing as chain length increases, where the probes become less able to penetrate the structure. In the isotropic phase, this reversal in order would not be the expected observation as the thermal energy available to all probes increases. However, this suggests the interaction between the molecular shape and probe molecules is a consideration in the diffusion of the probe, as the shorter and less mobile probes show greater values for D_1.

6.4 DIFFUSION IN LCP1

The Van Deemter plots for hexane, heptane and octane in LCP1 are shown in Appendix 4; Figure 4.10 to Figure 4.12 (for the S_C mesophase) and Appendix 4; Figure

4.13 to Figure 4.15 (for the isotropic phase). From these plots, the C constant is calculated, leading to elucidation of D_1 as shown in Table 6.3.

As an initial comparison is noted that, as with LMM1, the values of D_1 exhibited are of much lower magnitude than those shown by PDMS. Again, this may be considered as a consequence of the interactions between thermally mobile chains of the probe and the rigid structure of the mesogens. A general comparison with LMM1 shows the order in the value of D_1 being identical (i.e. $C_6 > C_7 > C_8$), with hexane showing greater diffusion in the S_C phase of LMM1 whilst the other two probes show similar values in both systems. This suggests the diffusion through the mesophase structure occurs *via* a similar mechanism in both the low molecular mass and polymeric liquid crystalline systems. However, after the $S_C \rightarrow I$ transition an increase in D_1 occurs to a much greater magnitude in LCP1 than that observed by LMM1, as illustrated in Figure 6.3.

Probe	D_1 ($cm^2 s^{-1}$) x 10^8
Hexane	
45°C	8.8
52°C	18.0
56°C	18.0
66°C	22.0
71°C	25.0
76°C	24.0
Heptane	
45°C	2.7
52°C	6.5
56°C	4.7
66°C	16.0
71°C	25.0
76°C	2.0
Octane	
45°C	1.3
52°C	3.2
56°C	3.0
66°C	31.0
71°C	39.0
76°C	14.0

Table 6.3: Diffusion Coefficients for Probes in LCP1

The order of D_1 is also altered to $C_8 > C_6 > C_7$, with reversal not being shown. It can also be observed that on the transition the change in D_1 was most prominent for $C_8 >$

$C_7 > C_6$. Overall, these observations suggest that in the isotropic phase of LCP1, the siloxane backbone acts to dominate the mechanism of diffusion; allowing more efficient diffusion to occur due to interactions with both the mesogens and backbone rather than the mesogens alone, and magnifying the effect of these interactions in the isotropic phase, compared with the mesogenic phase. These findings also underline the role played by the mesogenic portion of the stationary phase in interaction with aliphatic probe molecules.

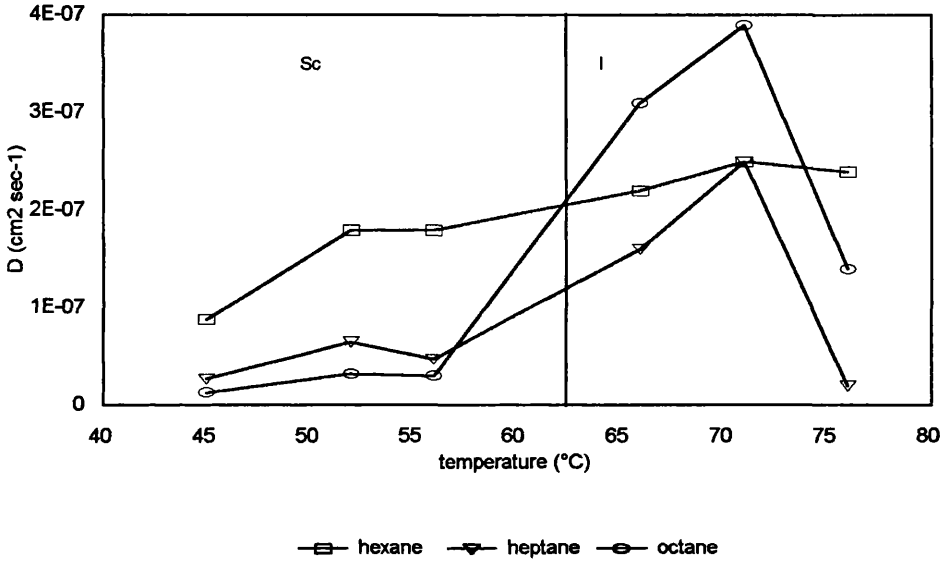

Figure 6.3: Variation of D_1 with Temperature for LCP1

Such observations may be underlined by comparing approximate D_1 values at a "snapshot" temperature in each mesophase. For C_7, such results are given in Table 6.4.

Temperature / °C	PDMS D_1 ($cm^2\ s^{-1}$) x 10^8	LMM1 D_1 ($cm^2\ s^{-1}$) x 10^8	LCP1 D_1 ($cm^2\ s^{-1}$) x 10^8
50°C (S_C mesophase)	170 (no mesophase)	6.4	6.5
70°C (isotropic phase)	57	6.5	25

Table 6.4: Comparison of D_1 for Heptane in Various Phases

These results clarify the trends noted in the mesophase for one particular probe; no trend is shown for PDMS, the effect of a mesophase transition shows little effect for heptane with LMM1, and the similar diffusivity in the mesophase of LCP1 becomes more PDMS-like in the isotropic phase of this material.

6.5 GENERAL CONCLUSIONS

With reference to (1.5.1), the investigation of diffusion in liquid crystalline materials has been carried out. This work allowed observation of marked trends, despite the experimental uncertainties associated with the method, and leads to the following conclusions:

- Diffusion occurs more readily in a non-mesogenic polymers than in a mesogenic stationary phases.

- Penetration occurs more easily by smaller aliphatic molecules in a mesophase, and by larger aliphatic molecules in an isotropic phase.

- Diffusion is affected by the mesogenic phase structure.

- The polymeric backbone exerts minimal effect on diffusion in a mesophase.

- The polymeric backbone contributes to diffusion in the isotropic phase.

The measurements made in determining the diffusion coefficients in liquid crystal polymers were very difficult to obtain accurately, and these results are the first known to this author so allow only preliminary conclusions to be drawn. However, the application of IGC to the study of diffusion in liquid crystalline systems has much potential for future work, as further discussed in (7.3.1e).

Chapter Seven:

GENERAL DISCUSSION, CONCLUSIONS

& FUTURE POSSIBILITIES

The discussion of results presented in Chapters 4, 5 and 6 were undertaken in the text of those chapters, allowing elucidation of the trends and mechanisms of solute-solvent interactions with the various probes. This chapter acts as a general discussion, using the observed solute-solvent interactions and analytical performances to suggest possible structures for liquid crystalline materials which would show enhanced separations. The conclusions drawn throughout this thesis are then summarised, followed by suggestions as to how this work may be extended in future research.

7.1 PREDICTION OF SYSTEMS TO IMPROVE SEPARATION

The studies undertaken throughout this thesis have determined the physiochemical properties of interaction which give rise to analytical separations. These parameters may also be described in terms of the chemical (and therefore physical) structure of the liquid crystalline material with which they are observed. In order to improve enantiomeric separation using these mesophases, an in-depth study of structure-property relationships of the mesogenic systems would be required (as described in 7.3.1), but the results obtained here allow a general description of the "desirable" qualities required of a mesogenic material, and thus the proposal of systems which may be effective in concluding the aims of this project.

It was demonstrated in Chapters 4 and 5 that certain structural properties of the mesophase are desirable for shape-selective separation of analytes. These included:

a. The mesogenic material must be chirally pure.
b. The mesophase structures must be highly ordered.
c. Mesophase transition temperatures and ranges must be large.
d. Polymeric materials are desirable.
e. Correct spacing of mesogens on the polymer backbone is essential.
f. Capillary column chromatography is necessary to achieve efficient separation.

To obtain a chirally pure mesogenic material (**a.**), the synthesis may be as simple as selecting the desired chiral alcohol and linking this to the mesogenic core *via* the esterification reaction, as described in (2.2.1) This reaction does not affect the chirality of the substituents, allowing a chirally pure material to be synthesised. The materials synthesised in this study used 2-methylbutanol, but it is feasible to use many other chiral alcohols under similar reaction conditions. Research by Goodby[284] has investigated the effects of such chiral end-groups, and noted that the number of carbon atoms between the mesogenic core and chiral atom give rise to an "odd-even" effect, switching the configuration of the helical twist exhibited by the mesophase. The

chirality of these materials is also affected by the end-group structure; with small increases in the size of the chiral substituents increasing the pitch of the material, but larger substituents also acting to damp chirality and mesophase structure formation. It is also necessary for the material to contain a short terminal alkyl chain length, as increases again damp the effects attributable to the chiral material. The use of polar groups in the chiral end-group would also prove undesirable, as the increased polarisation they impart to the material would increase the polarisation of the mesogens reflecting a disruption in their ordered structure. Considering these effects, the use of 2-ethylbutanol would appear most desirable, as this would slightly increase the chirality of the mesogen over the systems studied, yet not introduce any detrimental effects.

Once the chiral purity of the mesogen in ensured, the factors which allow a high degree of ordering and high transition temperatures and mesophase ranges must be considered to meet criteria (**b.**) and (**c.**). There are two structural methods of controlling this order: selection of the flexible end group and the mesogenic core. Starting with the flexible end-group, it is a well studied phenomenon[285] that whilst the flexibility of this group is essential for mesophase formation (as proven here in studies of BDH849 and BDH1029), the longer the alkyl chain becomes, the lower mesophase transition temperatures and clearing points are noted[286]. There is also the prevalence of an "odd-even" effect, with an odd number of carbons in the chain leading to higher mesophase temperatures[287-289]. In order to produce a desirable low molecular mass system, a flexible chain length of 5-7 carbons is therefore desirable. For polymeric systems this linkage will act as a flexible spacer for the mesogen, which has shown most desirable properties when C=6[290]. The mesogenic core also imparts great effects on the mesophase structures observed. The structural composition of the core must allow both a high degree of ordering and the retention of mesophase behaviour to high temperatures. It has been shown in this work (Chapter 2) that three aromatic rings in the mesogenic core increase the temperature range greatly over two aromatic rings, and by other workers[291-293] that increased conjugation between these rings increases mesophase transition temperatures and ranges. Thus, a mesogenic core containing a biphenyl linkage conjugated to another aromatic ring *via* an alkene bond would introduce desirable properties.

Polymeric materials show desirable properties for GC applications. Not only do they impart a high degree of processability and durability, but their appended mesogens are able to retain their mesophase properties to higher temperatures. This allows use for high temperature analyses and reduced column bleed, meeting criteria (**d.**) for desirable properties. It has also been shown in this study (**e.**) that the number of backbone units between the appended mesophases must be sufficient to allow free expression of mesogenic structure, as with LCP3 (see 4.4.3) Thus a polysiloxane

backbone with mesogenic appendages interspersed with methyl groups would make the ideal polymeric material. The use of other polymeric backbones also gives rise to mesogenic materials[294,295], but the widespread use of siloxanes as stationary phases and the inherent flexibility in their structure give more confidence in their application as stationary phases.

Considering the points raised so far, two mesogenic materials with the potential to show the correct balance of physical and chemical factors to allow isomer and enantiomer separation are proposed in Figure 7.1.

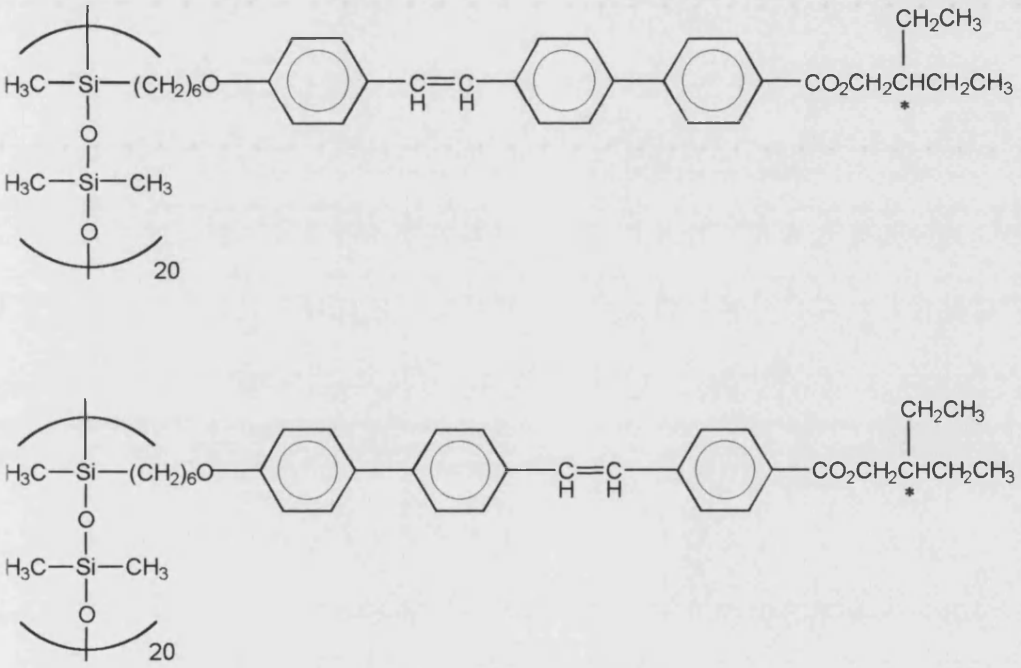

Figure 7.1: Mesogenic Materials with Potential for use as GC Stationary Phases

This is just one example of the type of material which would give rise to the desired mesophase properties. There are many other possible structures, including the inclusion of more than one mesogenic unit on the siloxane backbone to give a co-polymer which exhibits enhanced mesophase properties. This possibility is considered further in (7.3.1d).

Finally, from the findings presented in this thesis the materials described above may not show the necessary separation efficiency as packed column stationary phases. It is therefore essential that they be fabricated into capillary GC columns, to meet criteria (**f.**). Once this has been successfully achieved, the use of such materials as stationary

phases should fulfil the aims of this research, and separate isomeric and enantiomeric analytes.

7.2 THESIS CONCLUSIONS

The aims and objectives of this thesis were described in (1.5.1). Each of the objectives have been met, and a summary of the findings presented here:

- The IGC method may be applied to low molecular mass and polymeric liquid crystalline materials to give accurate and precise physiochemical parameters, when operated under conditions of infinite-dilution.

- The solution properties of solute-solvent interactions are affected significantly by the presence of a chiral mesophase structure. Such a material should be chirally pure, and offer a high degree of order in the mesophase structure. Side-chain liquid crystal polymers also display such properties, their solution behaviour being governed by the alignment of the appended mesogens.

- The differences in solution properties with these materials allow chromatographic separation of some isomers and enantiomers *via* a shape-selective mechanism. The properties of polymeric materials are more favourable considering practical GC application, though currently the efficiency of all separations with these mesophases is low.

- Compared with PDMS, diffusion decreases in a liquid crystalline mesophase structure. Diffusion in liquid crystal polymers is also governed by the mesogenic structure, which gives way to diffusion with the siloxane backbone in the isotropic phase. This is the first example of diffusion studies on liquid crystalline polymers to the knowledge of the author, and therefore opens this area to future exploration.

- The trends observed throughout this research have led to the suggestion of liquid crystalline materials which would have the optimal properties to allow isomer and enantiomer separation when used as a GC stationary phase. Methods to extend this research, based on the findings presented in this thesis, have also been proposed.

Previous work in this field was directed towards either the study of mesophase structure or the determination of analytical performance. This work has drawn correlations between these two areas, and used the observed structure-property relationships to

suggest methods by which the development of liquid crystalline stationary phases for gas chromatography may proceed.

The discussion as to the findings of this thesis is now therefore concluded. Section 7.3 describes possibilities for the direction of future studies in this area which build upon the work described herein.

7.3 FUTURE POSSIBILITIES

Whilst undertaking the work carried out as outlined in this thesis, ways by which the work could be extended became evident. Future work in this area may be concentrated in two main areas; the in-depth study by IGC of liquid crystalline structures and their interactions, and the improvement of analytical separations using these stationary phases. Some methods by which these studies may be carried out are described in this section.

7.3.1 INVERSE GAS CHROMATOGRAPHY

In this thesis, IGC has been used to describe the solution properties of a range of probes in the liquid crystalline stationary phases of interest. By consideration of the methodology, various ways by which the IGC characterisation of liquid crystalline materials could be further extended became apparent. Starting points for further work in these areas are described in this section.

7.3.1a Further Study of the Liquid Crystalline Structure

The results described in Chapter 4 allowed conclusions to be drawn as to the structure of the liquid crystalline mesophases exhibited by the various materials used, and showed how these structures affected the solution properties and analytical performance of the materials. An alternative approach would be to model and study a range of liquid crystalline materials in order to elucidate which materials show the necessary characteristics (as discussed in Chapter 7.1) to act as good solvents for a range of probes. Used in conjunction with IGC, this is a powerful tool for the determination of more detailed structure/property relationships. Such work may be approached from two directions - a purely theoretical study of liquid crystals in order to extend the theoretical knowledge of their structure and interactions, and extend the repertoire of IGC; or an applied study, using materials screened in modelling for further development. This approach is analogous to the way new chemical entities are

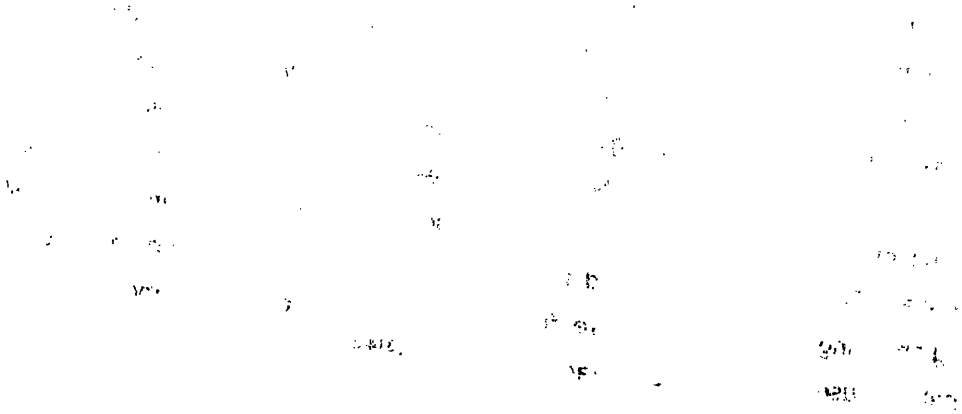

modelled, screened, synthesised and developed in the pharmaceutical industry in order to obtain new products of desired physiochemical characteristics.

Modelling methods for liquid crystalline materials are becoming more powerful with the increased availability of powerful computers, with the Monte-Carlo method being used most frequently[296] to model structure-property relationships such as the order parameter, tilt angle, pitch and polarisation of theoretical systems. Such models are often in good agreement with experimental data obtained after synthesis, and can thus be used to suggest systems with suitable characteristics before time consuming and expensive syntheses are carried out. Such modelling has been proven for low molecular mass liquid crystalline materials, but the appending of these mesogens to a polymeric backbone presents theoretical problems in the calculation of mesophase properties, which indicates the necessity for theoretical advances to develop apace with technological advances.

Physically, once synthesis of the modelled materials has been carried out their physical properties may be determined by a variety of methods; differential scanning calorimetry (enthalpies and transition temperatures), hot stage microscopy (mesophase character, transition temperatures, cholesteric pitch length), X-ray analysis (measurement of layer spacing), electrical methods (polarisability and tilt angle) and polarimetry (optical rotation). These properties may then be referenced to previous structure-property work, and consideration given as to the effects of the mesogenic core, lateral substituents, flexible end-groups, chirality of end-group and polymeric backbone.

Of particular interest to extend this work would be the correlation of physiochemical and analytical properties with factors which affect the structure of the mesophase, such as chirality of the mesogen and pitch, rotation and polarisation of the mesophase. Knowledge of these relationships would allow further detail as to the factors which lead to liquid crystalline materials acting as shape-selective solvents for various isomers.

7.3.1b Extended Description of Solution Behaviour

Chapter 1 described many of the properties which may be studied by application of IGC methodology. This study used IGC in the determination of enthalpies and entropies of solution to describe the mechanism by with solute-solvent interactions formed between probes and liquid crystalline materials. The results obtained gave useful information and allowed a correlation of solution properties with analytical performance, but there are many other parameters which may also be determined by IGC and used to further the theoretical understanding and practical application of liquid crystalline materials.

Interaction parameters have been calculated according to Matheson-Flory theory by Blonski *et al*[297], and much modelling of the mesophase structure has been carried out by Luckhurst and co-workers[298-302]. However, to the knowledge of this author little work has been carried out on the IGC characterisation of polymer liquid crystals. Their theoretical treatment has been investigated by Chow and Martire[303,304], with Moegel *et al*[305] considering the temperature dependence of solution behaviour within a nematic mesophase by IGC. More recently, IGC investigations on liquid crystalline materials have been carried out by Romansky and Guillett[306] and Tovar *et al*[307] with reference to main-chain LCPs and interactions of LCPs in blends respectively. However, there is still much scope for study of the mesophase structure by determination of the Flory-Huggins parameter, χ, solubility parameter, δ, and other factors such as crystallinity and surface energies. These parameters may then be used to further describe the nature of the mesophase and its interaction with solutes of varying properties, and aid in the application of liquid crystalline materials to areas such as analytical chromatography and the improvement of miscibility, processability and mechanical properties of polymers.

An overall approach applicable to such studies has been developed by Abraham *et al*[308-311], who have developed a linear free-energy relationship model to describe solvent behaviour in terms of "structural descriptors" such as dispersion forces, cavities, and polarisability. Building on studies of cyclodextrin stationary phases[312], it may be possible to describe mesogenic systems to both further analyse structure/property relationships, and to predict properties of mesogenic stationary phases.

7.3.1c IGC Study of the Supercooled Region

Another area which has received little attention by workers in IGC is the supercooled mesophase region. One of the reasons so little work has been carried out in this area is the ability of the supercooled region to return to the crystalline state after a period of time, reducing its application by comparison to rapidly-switchable mesophases. IGC studies of the supercooled region by Shillcock[313] indicated a "re-entrant" mesophase which was less ordered than the nematic mesophase from which it was cooled, this reduction in order allowing the re-organisation of the mesogens into the crystalline phase. This work also studied the kinetics of crystallisation from the supercooled region using IGC; a departure from the more traditional calorimetric and optical methods used previously by a variety of workers[314-320].

Such studies are of importance in relation to this thesis as previous work[321-323] has indicated the analytical properties of the supercooled mesophase are highly desirable for the separation of closely-related isomers. These studies made no correlation between the analytical performance and solution behaviour, and made no detailed study of the kinetics of crystallisation which is essential in determining the stability of a supercooled mesophase for analytical applications. There is therefore much work to be carried out in theoretical and applied studies of this peculiar liquid crystalline structure.

7.3.1d Study of Blended Systems

It is well established[324] that the use of liquid crystalline materials as blends with other polymers act to improve the analytical properties of the stationary phase, and in order to understand the method by which the analytical properties are enhanced, it is necessary to obtain data on solution properties. Much work has been carried out on the characterisation of polymer blends by IGC[325,326], although few studies involving liquid crystalline systems have been published.

More recent work[327] involved the blending of base polymers with liquid crystalline materials with β-cyclodextrins which both act to enhance separation of analytes. Such work is described in terms of the analytical performance of the new mesophase, and to the knowledge of the author no determination of the solution properties of such systems has been considered.

Thus, IGC studies of liquid crystal/polymer and liquid crystal/cyclodextrin/polymer blends have scope for future work. The particular importance of such studies would be realised in the fabrication of commercial stationary phases. Whereas a liquid crystalline stationary phase would be expensive to produce, a blended phase which offers a similar level of analytical performance at a competitive cost would find wide-spread use among chromatographers.

7.3.1e Diffusion in Liquid Crystalline Systems

The diffusion trends within liquid crystalline stationary phases presented in Chapter 6 were the result of a small-scale study on three systems, using a limited range of probes. As mentioned in Chapter 6, very little work has been carried out previously on the investigation of diffusion in mesogenic materials, and as this factor has wide effects on retention behaviour it seems logical to undertake further studies in this area. Such studies, as well as covering a greater variety of mesophase structures, would be of most importance to this research if the range of probes were extended to cover polar

and/or aromatic probes. This would allow comparison with the aliphatic probes considered in Chapter 6, and give further information on the interaction between probe and mesophase - painting a clearer picture of the differences in interaction between probes and the mesophase and isotropic structures.

7.3.1f Automation of Instrumentation

The generation of accurate and precise data for IGC studies is a time consuming and often tedious task, with many hours being spent injecting probes into the GC system and taking measurements of the parameters used in calculations, followed by manipulation of these parameters. The productivity of the worker in IGC could be greatly increased by the development of an automated system which (in addition to temperature and injection programming common to analytical laboratories) would also measure flow-rate, ambient temperature, atmospheric pressure and pressure difference across the column. Attachment of the GC system to a suitable data-capture device would greatly increase the sample throughput. In turn, more systems could be studied in a particular time period, and the workers' efforts could be primarily directed to the interpretation of the results. Such a system has been considered by Guillet *et al*[328] who demonstrated that the data obtained by an automated system not only increased productivity, but resulted in the generation of more reliable data by reduction of operator error. It would be highly desirable for research groups involved in IGC work (or even commercial companies) to develop such a system, supported by software allowing calculation of a wide range of analytical and physiochemical parameters from this methodology.

7.3.2 ANALYTICAL APPLICATIONS

In addition to characterising the liquid crystalline materials by IGC, this work also considered their application as stationary phases for analytical gas chromatography. In Chapter 5 differences in analytical behaviour within the various phases was noted, and in (7.1) liquid crystalline materials which may offer enhanced analytical properties were suggested. This section considers ways by which application of such materials may be studied in order to enhance analytical separations, and thus come closer to the goal of commercially available liquid crystalline stationary phases for general enantiomeric separations by GC. All of the suggestions made to further work on analytical separations using these materials are amenable to studies by IGC, and in linking such work with this study it should be assumed IGC data is also required when analytical performance is being measured.

7.3.2a Analysis Using Capillary Column Gas Chromatography

It is clearly shown from the results presented throughout Chapter 5 that liquid crystalline stationary phases used in conjunction with packed column GC do not have sufficient efficiency to effect separations of closely related molecules. This appears to be an inherent feature of the method, rather than of the stationary phases themselves - which in Chapters 4 and 5 are shown to exhibit physiochemical selectivity between these analytes. Repeated attempts to fabricate an efficient capillary GC column were described in (5.5) utilising a variety of methods from literature sources[329-331], but no success was forthcoming. Future efforts to improve the selectivity of these stationary phases must therefore overcome the problems encountered in capillary column coating.

A variety of methods may be attempted to succeed here, from blending the liquid crystalline material with a polymer known to coat capillary columns, to treating the internal structure of the capillary in order to improve its "wettability". It would also be useful for researchers working in this area to spend time in the laboratories of workers who have successfully mastered capillary column coating in order to learn their "secret". Following on from successful coating of such columns, improved analytical results are to be expected (and are indeed reported in the literature[332-334]). The technique of IGC has also been applied to capillary column GC[335] allowing physiochemical measurements and analytical measurements to be generated within the same experiment. IGC using capillary columns gives rise to inherent problems mainly concerned with the mass of stationary phase present in the column, but after this has been accurately determined meaningful results may be elucidated.

7.3.2b Extension of Probe Range

The probe range used in these studies was selected on the basis of availability of both probe, physiochemical parameters, and previous use allowing comparison with literature sources. In order to determine the analytical performance of the column, it is necessary to be a little more adventurous in the selection of probes to present "real" systems of importance in analytical determinations. For example, much work has been carried out on the separation of PAHs[336-339], therefore to allow comparison with these systems, the use of PAH analytes would be desirable. Such extensions in probe choice, however, causes a deviation in the path from IGC studies as physiochemical data is not readily available for such compounds, precluding the calculation of physiochemical parameters by IGC. To overcome this, it is possible to use probes of

well-know properties to examine the mesophase structure and interactions whilst observing the effect these structural changes have on unrelated systems. The data generated by such a method becomes somewhat empirical, and does not allow a rigorous scientific description of the processes taking place. However, at some stage in the development of commercial stationary phases the demands of analytical analyses must take precedence over studies of the mesophase.

A useful and feasible first step in the extension of probes used with these systems would be the use of a wider range of probes (particularly isomeric and enantiomeric probes) and more extensive use of polar probes. Results obtained for such probes (both analytical and physiochemical) would allow a description of stationary phase behaviour with a wider range of samples, and a more in-depth discussion of solute-solvent interactions to be made.

7.3.2c Use of the "Ideal" Stationary Phase

In (7.1) the structural features (both chemical and mesophase) required to achieve optimal separation based on the results obtained in this study were suggested. What better place to start looking for improved analytical performance than with such a structure? The synthesis of such a material would be relatively simple using the procedures outlined in Chapter 2, and its study by packed and capillary column GC could then be carried out in order to generate results comparative with those presented so far. This would not only confirm the validity of these results, but would offer further suggestions as to the next stage in the development of a successful stationary phase.

7.3.2d Utilisation of the Physical Properties of Liquid Crystals

This study has made full use of the ability of the liquid crystalline mesophase to form ordered structures under certain conditions (in this case, temperature). Such unique physical properties of liquid crystalline materials have lead to their use as, for example, display devices and pressure sensors. Each of these applications utilise different features of the liquid crystalline properties, and there is a strong case for taking these properties and applying them to the use of liquid crystals as stationary phases. For example, with the correct instrumentation it would be possible to set up an electric field around a liquid crystal containing GC column which, when activated, would cause alignment of the mesogens to form an ordered structure. This would feasibly overcome temperature barriers and extend the mesophase range far below and above that displayed naturally by the material. At low temperatures this would result in improved separation due to a combination of kinetic and entropic factors, and at high temperatures the shape-selectivity of the mesophase would be retained further. There

are many potential problems associated with the fabrication of such an instrument, arising from the generation of an electric field within a GC oven and the effect the support material would have on an aligned mesophase structure. Indeed, to the author's knowledge only one paper has been published investigating this possibility[340].

7.3.2e Novel Liquid Crystalline Structures

So far, the suggestions for expanding the work in this area have covered "traditional" thermotropic liquid crystalline materials. However, as methods of liquid crystalline synthesis advance, so do the possibilities of utilising these new materials in other areas. Two such possibilities are considered herein.

Firstly, it is possible to synthesise "fixed" liquid crystalline structures, in which the mesophase structure is locked in place. Such syntheses are carried out by the *in-situ* polymerisation of acrylate and diacrylate based liquid crystalline monomers[341]. The materials may be coated from solution before curing by either UV light or thermally-initiated radical polymerisation, which would give rise to cross-linking thereby fixing the mesophase structure. The resultant material would have a very high molecular weight, and thus prevent bleeding from the column during use, even at high temperatures. These materials have a double advantage; the fixed structure allows expression of the mesophase order over a wide range of temperatures, and the mesophase structure is far more ordered than in comparable dynamic systems, which should impart shape-selectivity with all interactions.

Secondly, work by Hjerten *et al*[342-344] has demonstrated effective (non-enantiomeric) separations may be made by the utilisation of a short, "continuous bed" of stationary phase compacted to give a high surface area of contact. Such a technique could be applied to mesogenic stationary phases, particularly if the material had a highly ordered structure. Such columns could be prepared by the polymerisation of diacrylate monomers in a cholesteric liquid crystalline host, and following curing the low molecular mass host could be washed out to leave a porous polymeric network exhibiting the helical structure of the mesogen. Such a material could then be incorporated in such a column, with additional columns linked in series to improve efficiency as necessary.

These suggestions would not be a priority following on from this study, but offer interesting possibilities and insights as to new developments in liquid crystal synthesis and separation science.

7.3.3 CONCLUSION

A range of ways in which the work covered in this thesis may be extended have been suggested, with the ultimate aim of fabricating liquid crystalline stationary phases capable of the separation of a variety of isomers and enantiomers.

Whatever direction future research in this area takes, it is certain that the technique of IGC will reveal further information on the structure and interactions of liquid crystals and liquid crystal polymers, and that their analytical application will effect the separation of analytes on a shape-selective basis - albeit for a limited range of analytes with a particular stationary phase. The range of techniques and disciplines covered by such a development create an interesting and stimulating area of work, and it is hoped that the successful conclusion of such a project will solve one problem, but give rise to many more questions.

REFERENCES

1 Reinitzer F., Monatsh.Chem., **9**, 421, (1888)

2 Goodby J.W., J.Mater.Chem., **1**, 3, 307, (1991)

3 Collings P.J., in Liquid Crystals, Adam Hilger, Bristol, Ch.2, (1990)

4 Kronberg B., Gilson D.F.R. and Patterson D., *Journal Unknown*, 1673, (1976)

5 Gray G.W. and Goodby J.W., Ann.Phys., **3**, 123, (1978)

6 see Ref. 2, Plate 3

7 http://abalone.cwru.edu

8 Brown G.H., J.Chem.Ed., **60** (10), 900, (1983)

9 Nishiyama I. and Goodby J.W., J.Mater.Chem., **3** (2), 149, (1993)

10 Gray G.W., Harrison K.J. and Nash J.A., Electron.Lett., **9**, 130, (1973)

11 Sykes P., in A Guidebook to Mechanism in Organic Chemistry (6^{th} Ed.), Longman, 241, (1986)

12 Loubser C., Wessels P.L., Styring P. and Goodby J.W., J.Mater.Chem., **4** (1), 71, (1994)

13 Yoshizawa A., Yokoyama A., Kikuzaki H. and Hirai T., Liq.Cryst., **14** (2), 513, (1993)

14 Voets G. and Van Dael W., Liq.Cryst., **14** (3), 617, (1993)

15 Lewthwaite R., Goodby J.W. and Toyne K.W., J.Mater.Chem., **3** (3), 241, (1993)

16 Komiya Z., Pugh C. and Schrock R.R., Macromolecules, **25** (14), 3609, (1992)

17 Booth W., Goodby J.W., Hardy J.P., Lettington O.C. and Toyne K.W., J.Mater.Chem., **3** (9), 935, (1993)

18 Krishnamurthy S., Chen S.H. and Blanton T.N., Macromolecules, **25** (20), 5119, (1992)

19 Sato M., Muraki K. and Mukaida K., Macromolecules, **27** (16), 4577, (1994)

20 Neilsen L.E., Polymer Rheology, Dekker, New York, (1977)

21 Murton-Jones D.H., Polymer Processing, Chapman & Hall, New York, (1989)

22 Marichin V.A., Mjasnikova L.P., Zenke D., Hirte R. and Weigel P., Polym.Bul., **12**, 287, (1984)

23 Stevens M.P., in Polymer Chemistry, OUP, (1990)

24 Kampour R.P.. and Robertson R.E., in Polymer Science (Ed. Jenkins A.D.), Ch.11, OUP, (1990)

25 Cassidy P.E., Thermally Stable Polymers, Dekker, New York, (1980)

26 Finkelmann H., Ringsdorf H. and Wendorf J.H., Makromol.Chem., **179**, 273, (1978)

27 Gemmell P.A., Gray G.W. and Lacey D., Mol.Cryst.Liq.Cryst., **122**, 205, (1985)

28 Gray G.W., in Side Chain Liquid Crystal Polymers (Ed. McArdle C.B.), Blackie, 106, (1989)

29 see Ref. 27

30 Ringsdorf H. and Schneller A., Makromol.Chem.Rap.Comm., **3**, 557, (1982)

31 Janini G.M., Laub R.J. and Purnell J.M., in Side Chain Liquid Crystal Polymers (Ed. McArdle C.B.), Blackie, 395, (1989)

32 see Ref. 30

33 Gray G.W., Lacey D., Nestor G. and White M.S., Makromol.Chem.Rap.Comm., **7**, 71, (1986)

34 Craig A.A. and Imrie C.T., Macromolecules, **28** (10), 3617, (1995)

35 Mohlmann G.R. and van der Vorst C.P.J.M., in Side Chain Liquid Crystal Polymers (Ed. McArdle C.B.), Blackie, Ch.12, (1989)

36 Griffin A., Hall C., Hoyle C., Venataram K. and McArdle C.B., Makromol.Chem.Rap. Comm., **9**, 463, (1988)

37 Coles H.J. and Simon R., Polymer, **26**, 1801, (1985)

38 Ulrich D., Polymer, **28**, 533, (1987)

39 Loth H. and Euschen A., Makromol.Chem.Rap.Comm., **9**, 35, (1988)

40 see Ref. 31

41 see Ref. 3, 178

42 Braechel M.J., Canale B. and Notorgiacomo V., Adv.Mat.&Proc., **4**, 39, (1998)

43 James A.T. and Martin A.J.P., Biochem.J., **50**, 679, (1952)

44 Martin A.J.P. and Synge R.L.M., Biochem.J., **35**, 1358, (1941)

45 Eiceman G.A., Hill Jr., H.H. and Davani B., Anal.Chem., **66** (12), 621R, (1994)

46 Smolkova E., Kralova H., Krysl S. and Feltl L., J.Chrom., **241**, 3, (1982)

47 Fischer P., Aichholz R., Bolz U., Juza M. and Krimmer S., Angew.Chem.Int.Ed.Engl., **29** (4), 427, (1990)

48 Armstrong D., Li W., Chang C.D. and Pitha J., Anal.Chem., **62**, 914, (1990)

49 Li W.H., Jin H.L. and Armstrong D.W., J.Chrom., **509**, 303, (1990)

50 Jung M., Schmalzing D. and Schurig V., J.Chrom., **552**, 43, (1991)

51 Naikwadi K.P., Rokushika S., Hatano H. and Ohshima M., J.Chrom., **331**, 69, (1975)

52 Szulc J. and Witkiewicz Z., J.Chrom., **262**, 141, (1983)

53 Betts T.J., J.Chrom., **606**, 281, (1992)

54 Grob R.L., J.Chrom., **125**, 771, (1976)

55 Markides K.E., Nishioha M., Tarbet B., Bradshaw J.S. and Lee M.L., Anal.Chem., **57**, 1296, (1985)

56 Rouse C.A., Finlinson A.C., Tarbet B.J., Pixton J.C., Djordjevic N.M., Markides K.E., Bradshaw J.S. and Lee M.L., Anal.Chem., **60**, 901, (1988)

57 Janssen F. and Kalidin T., J.Chrom., **235**, 323, (1982)

58 Ettre L.S., in Open Tubular Columns for GC, Plenum, New York, 80, (1965)

59 see Ref. 58, 86

60 Berezkin V.G. and Korolev A.A., J.Chrom., **440**, 323, (1988)

61 Lichtenthaler R.N., Liu D.D. and Prausnitz J.M., Macromolecules, **78**, 5, (1974)

62 Grob K., in Making and Manipulating Capillary Columns for GC, Dr.Verlag, Heidelberg, Ch.1, (1986)

63 Skoog D.A., in Principles Of Instrumental Analysis, (3rd ed), Sanders, 741, (1985)

64 see Ref. 58, Ch.2

65 see Ref. 58, Ch.2

66 Lester R., J.Chrom., **156**, 55, (1978)

67 Morrison R.T. and Boyd R.N., in Organic Chemistry, (5th ed.), Allyn and Bacon, 136, (1987)

68 Oliveros L, Minguillon C., Desmazieres B. and Desbene P.L., J.Chrom., **543**, 277, (1991)

69 Dalgleish C.E., J.Chem.Soc., 3940 (1952)

70 Gil-Av E., in Gas Chromatography (Ed. Littlewood A.B.), Inst. Pet., 227, (1966).

71 Ellerichmann T., Bergman A., Franke S., Huhnerfuss H., Jakobsson E., Konig W.A. and Larsson C., Fresenius Envir.Bull., **7**, 244, (1998)

72 Armstrong D., Wang X., Lee J.T. and Liu Y., Chirality, **11**, 82, (1999)

73 Zhang H.B., Zhang J., Fu R.N., Zuo X.B. and Liu H.F., Chromatographia, **48** (3/4), 305, (1998)

74 Armstrong D., Tang Y., Ward T. and Nichols M., Anal.Chem., **65**, 1114, (1993)

75 Berthod A., Li W. and Armstrong D., Anal.Chem., **64**, 873, (1992)

76 Stoev G., J.Chrom., **589**, 257, (1992)

77 Kohler J.E.H., Hohla M., Richters M. and Konig W.A., Angew.Chem.Int.Ed.Engl., **31** (3), 319, (1992)

78 Liu D. and Prausnitz J.M., Ind.Eng.Chem., Fundam., **15** (4), 330, (1976)

79 Fu R., Huang C., Huang Z. and Xu W., J.Chrom., **653**, 173, (1993)

80 Fu R., Jing P., Gu J., Huang Z. and Chen Y., Anal.Chem., **65**, 2141, (1993)

81 Aichholz R., Boltz U. and Fischer P., J.Hi.Res.Chrom., **13**, 234, (1990)

82 Konig W.A., Trends In Anal.Chem., **12** (4), 130, (1993)

83 Anon., J.Hi.Res.Chrom., **16**, 312, (1993)

84 Anon., Supelco Catalogue, **13** (5), 8, (1992)

85 Lee W.S. and ChangChien G.P., Anal.Chem., **70** (19), 4094, (1998)

86 Kelker H., J.Chrom., **112**, 165, (1975)

87 Haky J.E. and Muschik G.M., J.Chrom., **214**, 161, (1981)

88 Haky J.E. and Muschik G.M., J.Chrom., **238**, 367, (1982)

89 Janini G.M., Laub R.J., Purnell J.H. and Tyagi O.S., in Side Chain Liquid Crystal Polymers (Ed. McArdle C.B.), Blackie, Glasgow, 395, (1989)

90 Chiavari G., Chromatographia, **7**, 30, (1974)

91 Martire D.E. and Riedl P., J.Phys.Chem., **72** (10), 3478, (1968)

92 Grushka E. and Solsky J.F., J.Chrom., **99**, 135, (1974)

93 Taylor P., Sep.Sci., **6**, 841, (1971)

94 Warner M., in Side Chain Liquid Crystal Polymers (Ed. McArdle C.B.), Blackie, Ch.2, (1989)

95 Haken J.K., J.Chrom., **300**, 1, (1984)

96 Evans M.B., Chromatographia, **15**, 355, (1982)

97 Frank H., Nicholson G.J. and Bayer E., Angew.Chem., Int.Ed.Engl., **17**, 363, (1978)

98 Trash C.R., J.Chrom.Sci., **11**, 196, (1973)

99 Witkiewicz Z., Pietrzyk M. and Dabrowski R., J.Chrom., **177**, 189, (1979)

100 Witkiewicz Z., J.Chrom., **251**, 311, (1982)

101 Witkiewicz Z., J.Chrom., **466**, 37, (1989)

102 Witkiewicz Z. and Mazur J., LC-GC, **8** (3), 224, (1989)

103 Aspler J.S., in Pyrolysis and GC in Polymer Analysis (eds. Liebman S.A. and Levy E.J.), Dekker, New York, Ch.9, (1985)

104 Braun J.M. and Guillet J.E., Adv.Polym.Sci., 21, 107, (1976)

105 Conder J.R. and Young C.L., Physiochemical Measurement by GC, Wiley, Ch.12, (1977)

106 Gilbert S.G., in Inverse Gas Chromatography (Eds. Lloyd D.R., Ward T.C. and Schreiber H.P.), ACS Symposium Series, Ch.22, (1988)

107 Fowkes F.M., J.Adhesion.Sci.Tech., **1**, 7, (1987)

108 Gutmann V., The Donor-Acceptor Approach to Molecular Interactions, Plenum, New York, (1983)

109 Nardin M., Balard H. and Papirer E., Carbon, **28**, 43, (1990)

110 Coca J., Medina I. and Langer S.H., Chromatographia, **25** (9), 825, (1988)

111 Janini G.M., Johnston K. and Zielinski Jr. W.L., Anal.Chem., **47**, 4, 670, (1975)

112 Kiselev A.V., in Advances in Chromatography (Eds. Giddings J.C. and Keller R.A.), Dekker, New York, (1967)

113 Smidsrod O. and Guillet J.E., Macromolecules, **2**, 272, (1969)

114 Littlewood A.B., Phillips C.S.G. and Price D.T., J.Chem.Soc., 1480, (1958)

115 Ashworth A.J. and Everett D.H., Trans.Farad.Soc., **56**, 1609, (1960)

116 McGlashen M.L. & Williamson A.G., Trans.Farad.Soc., **57**, 588, (1961)

117 Ashworth A.J., Chien C.F., Furio D.L., Hooker D.M., Kopecni M.M., Laub R.J. and Price G.J., Macromolecules, **17**, 1090, (1984)

118 Summers W.R., Tewari Y.B. and Schreiber H.P., Macromolecules, **5** (1), 12, (1972)

119 Hammers W.E. & DeLigny C.L., J.Poly.Sci., Phys.Edn., **12**, 2665, (1974)

120 Lichtenthaler R.N., Liu D.D. and Prausnitz J.H., Berichte der Bunsen-Gesellshaft, **78** (5), 470, (1974)

121 Braun J.M. and Guillet J.E., Poly.Eng.Sci., **17** (7), 434, (1977)

122 see Ref. 115

123 see Ref. 117

124 Stern O., Ann.Physik., **49** (4), 823, (1916)

125 Murrell J.N. and Jenkins.A.D., Properties of Liquids and Solutions (2^{nd} Ed.), Wiley, 116, (1994)

126 see Ref. 125

127 Physical Chemistry Lecture Notes, Sheffield Hallam University, 1992

128 Van Deemter J.J., Zuiderweg F.J., Klinkenberg A., Chem.Eng.Sci., **5**, 271, (1956)

129 Flory P.J., J.Chem.Phys., **9**, 660, (1941)

130 Huggins M., J.Chem.Phys., **9**, 440, (1941)

131 see Ref. 23, 131

132 Prigogine I., Bellmans A. and Naar-Colin C., J.Chem.Phys., **26** (4), 751, (1957)

133 Patterson D., Macromolecules, **2**, 672, (1969)

134 Dee G.T. and Walsh D.J., Macromolecules, **21**, 811, (1988)

135 Hattam P., Du Q. and Munk P., in Inverse Gas Chromatography (Eds. Lloyd D.R., Ward T.C. and Schreiber H.P.), ACS Symposium Series, Ch.4, (1988)

136 Braun J.M. and Guillet J.E., Macromolecules, **8**, 882, (1975)

137 Braun J.M. and Guillet J.E., Macromolecules, **9**, 340, (1976)

138 Stein A.N., Gray D.G. and Guillet J.E., Br.Polym.J., **3**, 175, (1971)

139 see Ref. 105, Ch.2

140 Martin R.L., Anal.Chem., **33**, 347, (1961)

141 Martire D.E., Blasco P.A., Carone P.F., Chow L.C. and Vinci H., J.Phys.Chem., **72** (10), 3488, (1968)

142 see Ref. 140

143 Marciniak W. and Witkiewicz Z., J.Chrom., **207**, 333, (1981)

144 DiPaola-Baranyi G., Braun J.M. and Guillet J.E., Macromolecules, **11**, 1, 224, (1978)

145 Guillet J.E., Romansky M., Price G.J. and van der Mark R., in Inverse Gas Chromatography (Eds. Lloyd D.R., Ward T.C. and Schreber H.P.), ACS Symposium Series, Ch.3, (1988)

146 Shillcock I.M., MPhil Transfer Report, Bath University, (1993)

147 Everett D.H., Trans.Farad.Soc., 1637, (1965)

148 Wicarova O., Novak J. and Janak J., J.Chrom., **51**, 3, (1970)

149 Tseng H.S. and Lloyd D.R., Polymer, **25**, 670, (1984)

150 Patterson D., Tewari Y.B., Schreiber H.P., and Guillet J.E., Macromolecules, **4**, 356, (1971)

151 Gray D.G., Prog.Polym.Sci., **5** (1), 1, (1977)

152 Lavie A. and Guillet J.E., Macromolecules, **2**, 443, (1969)

153 Guillet J.E. and Stein, Macromolecules, **3**, 102, (1979)

154 see Ref. 105, Ch.12

155 see Ref. 154, Ch.10

156 Deshpande D.D., Patterson D., Schreiber H.P. and Su C.S., Macromolecules, **7** (1), 530, (1974)

157 Lichenthaler R.N., Macromolecules, **7**, 565, (1974)

158 see Ref. 120

159 De Vries M.J. and Smit J.H., J.S. African Chem.Inst., **20**, 11, (1967)

160 Sa M. and Sereno A.M., J.Chrom, **600**, 341, (1992)

161 Kontominas M.G., Gavara R. and Giacin J.R., Eur.Polym.J., **30** (2), 265, (1994)

162 Mukhopadhyay P. and Schreiber H.P., Macromolecules, **26**, 6391, (1993)

163 Fafard M., El-Kindi M., Schreiber H.P., DiPaola-Baranyi G. and Hor A.M., J.Adhesion.Sci.Technol., **8** (12), 1383, (1994)

164 Panzer U. and Schreiber H.P., Macromolecules, **25**, 3633, (1992)

165 Mukhopadhyay P. and Schreiber H.P., J.Poly.Sci.:Polym.Phys., *Details Unknown*, (1993)

166 Bosse F., Eisenberg A., El-Kindi M., Deng Z. and Schreiber H.P., J.Adhesion Sci.Tech., **6**, 455, (1992)

167 Tovar G., Carreau P. and Schreiber H.P., J.Adhesion, **63**, 215, (1997)

168 Hegedus C.R. and Kamel I.L., J.Coat.Tech., **65** (820), 31, (1993)

169 Jacob P.N. and Berg J.C., *Journal Unknown*, 458.

170 Lipson J.E.G. and Guillet J.E., J.Coat.Tech., **54** (648), 89, (1982)

171 DiPaola-Baranyi G., Hwang C.J., Hsiao C.K. and Listigovers N., *Journal Unknown*, 414

172 DiPaola-Baranyi G., Guillet J.E., Klein J. and Jeberien H.E., J.Chrom., **166**, 349, (1978)

173 Lipson J.E.G. and Guillet J.E., in Developments in Polymer Characterisation (Ed. Dawkins J.V.), Applied Science Publishers, Barking, 33, (1982)

174 Price G.J., in Inverse Gas Chromatography (Eds. Lloyd D.R., Ward T.C. and Schreber H.P.), ACS Symposium Series, Ch.5, (1988)

175 Voelkel A. and Janas J., J.Chrom.A, **669**, 89, (1994)

176 Gray D.G. and Guillet J.E., Macromolecules, **6**, 223, (1973)

177 Braun J.M., Poos S. and Guillet J.E., Poly.Let.Ed., **14**, 257, (1976)

178 Bonifaci L. and Ravanetti G.P., J.Chrom., **607**, 145, (1992)

179 Jackson P.L. and Huglin M.B., Eur.Polm.J., **31** (1), 63, (1995)

180 Hattam P. and Munk P., Macromolecules, **21**, 2083, (1988)

181 Surana R.K., Danner R.P., Tihminlioglu F. and Duda J.L., J.Poly.Sci,Polym.Phys., *details unknown*, (1996)

182 Farooque A.M. and Deshpande D.D., Polymer, **33** (23), 5005, (1992)

183 Krishnamoorti R., Graessley W.W., Balsara N.P. and Lohse D.J., Macromolecules, **27**, 3073, (1994)

184 Price G.J., in Advances in Chromatography Vol. 28 (Eds. Giddings J.C., Grushka E. and Brown P.R.), Marcel Dekker, New York, 113, (1989)

185 Laub R.J. and Purnell J.H., Anal.Chem., **48** (6), 799, (1976)

186 Adamski P., Dylik-Gromiec A., Klimczyk S. and Wojciechowski M., Mol.Cryst.Liq.Cryst., **35**, 171, (1976)

187 Matsuura M., Saito H., Nakata S., Imai Y. and Inoue T., Polymer, **33** (15), 3210, (1992)

188 Campoy I., Marco C., Gomez M.A. and Fatou J.G., Macromolecules, **25**, 4392, (1992)

189 Cheng S.A.D., Janimak J.J., Lipinski T.M., Sridhar K., Huang X.Y. and Harris F.W, Polymer, **31**, 1122, (1990)

190 Stein A.N., Gray D.G. and Guillet J.E., British Poly.J., **3**, 175, (1971)

191 Avrami M., J.Chem.Phys., **7**, 1103, (1939)

192 Jonsson H., Wallgren E., Hult A. and Gedde U.W., Macromolecules, **23**, 1041, (1990)

193 Liu X., Hu S., Shi L., Xu M., Zhou Q. and Duan X., Polymer, **30**, 273, (1989)

194 Shillcock I.M., Ph.D. Thesis, University of Bath, (1995)

195 see Ref. 100

196 see Ref. 89

197 Finkelmann H., Laub R.J., Roberts W.L. and Smith C.A., in Polynuclear Aromatic Hydrocarbons: Physical and Biological Chemistry (Eds. Cooke M.W., Dennis A.J. and Fisher G.L.), Battelle Press, Columbus, 275, (1981)

198 Apfel M.A., Finkelmann H., Janini G.M., Laub R.J., Luhmann B.H., Price A., Roberts W.L. and Shaw T.J., Anal.Chem., **57**, 651, (1985)

199 Janini G.M., Laub R.G. and Shaw T.J., Macromol.Chem., Rapid Comm., **6**, 57, (1985)

200 Janini G.M., Muschik G.M., Issaq H.J. and Laub R.J., Anal.Chem., **60**, 1119, (1988)

201 Nestor G., White M.S., Gray G.W., Lacey D. and Toyne K.J., Makromol.Chem., **188**, 2759, (1987)

202 Price G.J. and Shillcock I.M., Polymer, **34** (1), 85, (1993)

203 Price G.J. and Shillcock I.M., Can.J.Chem., **73** (11), 1883, (1995)

204 Medina I., Liq.Cryst., **12** (6), 989, (1992)

205 Medina I., Chromatographia, **35** (9-12), 539, (1993)

206 see Ref. 176

207 see Ref. 201

208 see Ref. 58, 85

209 Lecture given by SGE Ltd., University of Bath, (1994)

210 Gray D.G. and Guillet J.E., Poly.Lett.Ed., **12**, 231, (1974)

211 Dewar and Schroeder, J.ACS., **86**, 5235, (1964)

212 Chow L.C. and Martire D.E., J.Phys.Chem., **73**, 1127, (1969)

213 see Ref. 144

214 Parcher J.F. and Westlake T.N., J.Phys.Chem., **81** (4), 307, (1977)

215 Barrales-Rienda J.M. and Gancedo J.V., Macromolecules, **21**, 220, (1988)

216 see Ref. 176

217 Karim K.A. and Bonner D.C., J.App.Polym.Sci., **22**, 1277, (1978)

218 Leung Y.K. and Eichinger B.E., J.Phys.Chem., **78** (1), 60, (1974)

219 DiPaola-Baranyi G., Guillet J.E., Jeberien H.E. and Klein J., Makromol.Chem., **181**, 215, (1980)

220 see Ref. 56

221 see Ref. 99

222 see Ref. 3, Ch.6

223 Rayss J., Witkiewicz Z., Waksmundzki A. and Dabrowski R., J. Chrom, **188**, 107, (1980)

224 see Ref. 143

225 Gray D.G. and Guillet J.E., Macromolecules, **5**, 316, (1972)

226 Gozdz A.S. and Weigmann H.D., J.App.Poly.Sci., **29**, 3965, (1984)

227 Anhang J. and Gray D.G., J.App.Poly.Sci., **27**, 71, (1982)

228 Card T.W., Al-Saigh Z. and Munk P., Macromolecules, **18** (5), 1034, (1985)

229 see Ref. 194

230 see Ref. 88

231 see Ref. 88

232 Romansky M., Smith P.F., Guillet J.E. and Griffin A.C, Macromolecules, **27**, 6297, (1994)

233 see Ref. 203

234 Llorente M.A., Menduina C., and Horta A., J.Poly.Sci., Poly.Phys.Edn., **17**, 189, (1979)

235 Atkins P.W., in Physical Chemistry, (3rd ed.), OUP, 200, (1987)

236 see Ref. 151

237 see Ref. 234

238 Oweimreen G.A., J.Sol.Chem., **11** (2), 105, (1982)

239 Laub R.J. and Purnell J.H., J.Chrom., **155**, 233, (1978)

240 Laub R.J., Purnell J.H., Williams P.S., Harbison M.W.P. and Martire D.E., J.Chrom., **155**, 233, (1978)

241 Roth M. and Novak, J., Macromolecules, **19**, 364, (1986)

242 see Ref. 156
243 Galin M., Molecules, 10 (6), 1239, (1977)
244 Chien C.F., Kopecni M.M., Laub R.J. and Smith C.A., J.Phys.Chem., **85**, 1864, (1981)
245 Chien C.F., Kopecni M.M., and Laub R.J., J.Hi.Res.Chrom., Chrom.Comm., **6**, 577, (1983)
246 see Ref. 61
247 see Ref. 241
248 see Ref. 141
249 Oweimreen G.A., J.Chem.Eng.Data, **31**, 160, (1986)
250 Ghodbane S., Oweimreen G.A. and Martie D.E., J.Chrom., **556**, 315, (1991)
251 Janini G.M., Adv.Chrom., **17**, 231, (1979)
252 Chao Y. and Martire D.E., Anal.Chem., **64**, 1246, (1992)
253 Chao Y. and Martire D.E., J.Phys.Chem, **96** (8), 2489, (1992)
254 Wasik S. and Chester S., J.Chrom., **122**, 451, (1976)
255 Janini G.M., Sato R.I. and Muschik, Anal.Chem., **42**, 2417, (1980)
256 Schroeder J.P., in Liquid Crystals and Plastic Crystals - Vol. 1 (Eds. Gray G.W. and Winsor P.A.), Ellis Horwood, Chichester, 356, (1974)
257 Ziolek A., Witkiewicz Z. and Dabrowski R., J.Chrom., **294**, 139, (1984)
258 Grushka E. and Solsky J.F., J.Chrom., **112**, 145, (1975)
259 see Ref. 87
260 see Ref. 88
261 Lochmuller C.H. and Souter R.W., J.Chrom., **88**, 41, (1974)
262 Lochmuller C.H. and Hinshaw Jr. J.V., J.Chrom., **178**, 411, (1979)
263 Pirkle W.H. and Mahler G.S., in Synthesis and Separations using Functional Polymers (Eds. Sherrington D.C. and Hodge P.), Wiley & Sons, 305, (1988)
264 see Ref. 68
265 see Ref. 63
266 see Ref. 101
267 see Ref. 58
268 see Ref. 55
269 see Ref. 56
270 see Ref. 62, 161
271 Chein C.F., Kopenci M.M. and Laub R.J., Anal.Chem., **52**, 1402, (1980)
272 see Ref. 176
273 see Ref. 177
274 see Ref. 180
275 see Ref. 178
276 see Ref. 181
277 see Ref. 179
278 see Ref. 204
279 see Ref. 205
280 see Ref. 128

281 Giddings J.C., Dynamics of Chromatography - Part One, Dekker, New York, (1965)
282 see Ref. 176
283 see Ref. 177
284 see Ref. 2
285 De Jeu W.H. and Van Der Veen J., Mol.Cryst.Liq.Cryst., **40**, 1, (1977)
286 see Ref. 30
287 see Ref. 3, Ch.7
288 Imrie C.T., Karasz F.E. and Attard G.S., Macromolecules, **26** (3), 539, (1993)
289 see Ref. 27
290 see Ref. 285
291 Kyotani M., Yoshida K., Ogawara K. and Kanetsuna H., J.Polymer Sci.,Polm.Phys., **25**, 501, (1987)
292 Kato T., Kihara H., Uryr T., Fujishima A. and Frechet J.M.J., Macromolecules, **25** (25), 6836, (1992)
293 see Ref. 284
294 Shibaev V.P., Kozlovsky M.V., Beresnew L.A., Blinov L.M. and Plate N.A., Polym.Bull., **12**, 299, (1984)
295 Kosaka Y. and Uryu T., Macromolecules, **27** (4), 6286, (1994)
296 Zhu J.X., Ding J.D., Lua J.M. and Yang Y.L., Polymer, **39** (25), 6455, (1998)
297 Blonski S., Brostow W., Jonah D.A. and Hess M., Macromolecules, **26**, 84, (1993)
298 Ferrarini A., Moro G.J., Nordio P.L., Luckhurst G.R., Mol.Phys., **77** (1), 1, (1992)
299 Luckhurst G.R. and Romano S., J.Chem.Phys., **107** (7), 2557, (1997)
300 Stelzer J., Bates M.A., Longa L. and Luckhurst G.R., J.Chem.Phys., **107** (18), 7483, (1997)
301 Bates M.A. and Luckhurst G.R., Liq.Cryst., **24** (2), 229, (1998)
302 Bates M.A. and Luckhurst G.R., Chem.Phys.Lett., **281** (1-3), 193, (1997)
303 see Ref. 248
304 Chow L.C. and Martire D.E., J.Phys.Chem., **73**, 1127, (1969)
305 Moegel H.J, Kraus G. and Novak, M., J.Chrom., **324**, 29, (1985)
306 Romansky M. and Guillet J.E., Polymer, **35** (3), 584, (1994)
307 see Ref. 167
308 Abraham M.H., Whiting G.S., Doherty R.M., Shuely W.J. and Sakellariou P., Polymer, **33** (10), 2162, (1992)
309 Abraham M.H., Du C.M., Osei-Owusu J.P., Sakellariou P. and Shuely W.J., Eur.Polym.J., **30** (5), 635, (1994)
310 Selves J.L., Abraham M.H. and Burg P., Fluid Phase Equilibria, **148** (1-2), 69, (1998)
311 Oumada F.Z., Roses M.,Bosch E. and Abraham M.H., Anal.Chim.Acta, **382** (3), 301, (1999)
312 Abraham M.H., Anal.Chem., **69** (4), 613, (1997)
313 see Ref. 194
314 Evans U.R., *Journal Unknown,* 365, (1945)
315 Lin J., Wu H. and Li S., Polymer Int., **34**, 141, (1994)

316 see Ref. 186
317 see Ref. 187
318 see Ref. 188
319 see Ref. 189
320 see Ref. 190
321 Vigalok R.V. and Vigdergauz M.S., Izv.Akad.Nauk SSSR, Ser.Khim., 715, (1972)
322 Grushka E. and Solsky J.F., Anal.Chem., **45**, 1836, (1973)
323 Sojak L., Kraus G., Ostrovsky I., Kralovicova E. and Krupcik J., J.Chrom., **206**, 463, (1981)
324 see Ref. 184
325 Price G.J. and Agravat A, Polymer Communications, **30**, 89, (1989)
326 Etxeberria A., Uriarte C., Fernandez-Berridi M.J. and Iruin J.J., Macromolecules, **27**, 1245, (1994)
327 Jing P., Fu R.N., Dai R.J., Ge J.L., Gu J.L., Huang Z. and Chen Y., Chromatographia, **43**, (9/10), *Page Unknown*, (1996)
328 see Ref. 145
329 see Ref. 57
330 see Ref. 58
331 see Ref. 60
332 Mazur J., Witkiewicz Z. and Dabrowski R., J.Chrom., **600**, 123, (1992)
333 Janini G.M., Muschik G.M., Issaq H.J. and Laub R.J., Anal.Chem., **60**, 1119, (1988)
334 Sander L.C., Schneider M. and Wise S.A., J.Microcol.Sep., **6**, 115, (1994
335 see Ref. 210
336 Menster M.K., Bombick D.D., Flora D.B., Bunning T.J., Klei H.E. and Crane R.L., *Journal Unknown*, 1150
337 Nishioka M., Jones B.A., Tarbet B.J., Bradshaw J.S. and Lee M.L., J.Chrom., **357**, 79, (1986)
338 Janini G.M., Muschik G.M and Fox S.D., Chromatographia, **27**, (9/10), 436, (1989)
339 Budzinski H., Garrigues P. and Bellocq J., J.Chrom., **590**, 297, (1992)
340 see Ref. 93
341 Attard G.S., Glyde J.C. and Goltner C.G., Nature, **378** (6555), 366, (1995)
342 Hjerten S., Liao J.L., Srichaiyo T., Chen N., Ericson C., Mohammed Y.M., Palm A., Zeng C.M. and Zhang R., Abs.ACS, **211-ANYL** (1), 90, (1996)
343 Hjerten S., Ind.Eng.Chem.Res., **38** (4), 1205, (1999)
344 Maruska A., Ericson C., Vegvari A. and Hjerten S., J.Chrom.A, **837** (1-2), 25, (1999)

Appendix One:

SYNTHETIC METHODOLOGY

This Appendix contains details as to how the liquid crystalline structures summarised in (2.1) were synthesised. The general synthetic routes described in (2.2) are expanded to give details of reagent quantities, reaction times, characterisation, etc. All transition temperatures were determined by DSC, with mesophase assignments being made by HSM. GPC data was obtained using PDMS as the reference material.

A1.1 SYNTHESIS OF MESOGENS CONTAINING TWO RINGS

A1.1a A LOW MOLECULAR MASS VARIANT ON LCP1 (LMM1)

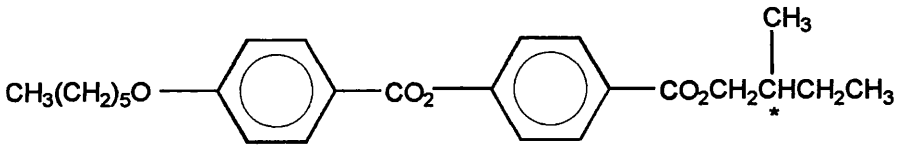

Figure A1.1: Molecular Structure of LMM1

The practical procedure and mechanism for this reaction are as the esterification described in (2.2.1) to give LMM1. The following quantities of reagents were used:

Hexoxybenzoic acid (222 g mol^{-1})	5.33 g (0.024 mol)
Trifluoroaceticanhydride (210 g mol^{-1})	5.88 g (0.028 mol)
Methylbutylhydroxyphenylcarboxylate (208 g mol^{-1})	5.00 g (0.024 mol)
Dichloromethane (Solvent)	250 cm^3

Yield; 7.03 g (71%) Purity; 99.8% (HPLC)

Transitions: K → 39°C → S_C → 52°C → I

NMR: δ_H 0.05 (3H, t), 0.51 (2H, s), 0.90 (6H, m), 1.21 (H, m), 1.36 (6H, m), 1.75 (3H, m), 3.83 (2H, s), 4.11 (H, m), 6.82 (2H, d), 7.12 (2H, d), 8.00 (4H, d).

MS: 413 [M^+], 343, 206, 205, 121.

A1.1b A POLYACRYLATE VARIANT ON LCP1 (LCP2)

The production of a vinyl monomer containing the mesogenic side-group was the first step in the synthesis of a mesogenic acrylate polymer. The monomer required has the structure shown in Figure A1.2.

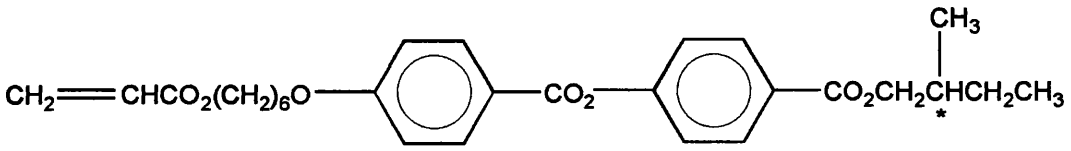

Figure A1.2: Molecular Structure of 2-Ringed Vinyl Mesogen

This was synthesised in the two-stage reaction outlined in Figure A1.3.

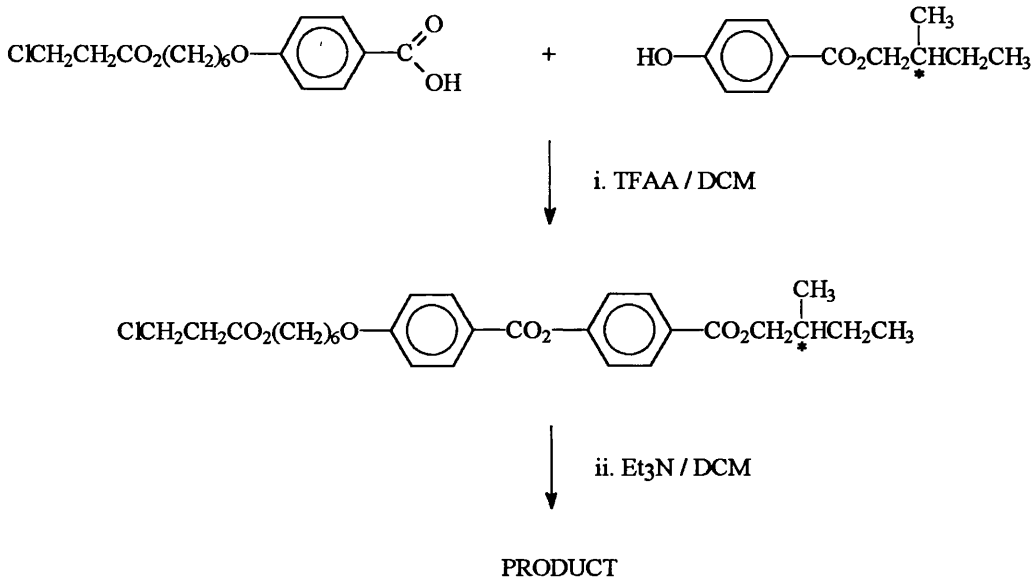

Figure A1.3: Synthesis of 2-Ringed Vinyl Mesogen

Stage one of this synthesis was the *esterification* reaction, the practical procedure and mechanism for this reaction being as described in (2.2.1). The following quantities of reagents were used:

(2-chloropropylhexanoate)oxybenzoic acid (328 g mol^{-1})	9.84 g (0.030 mol)
Trifluoroaceticanhydride (210 g mol^{-1})	6.93 g (0.033 mol)
Methylbutylhydroxyphenylcarboxylate (208 g mol^{-1})	6.24 g (0.030 mol)
Dichloromethane (Solvent)	360 cm^3

Yield; 7.9 g (51%) Purity; 97% (HPLC)

For stage two, the *elimination* step, the product from stage one was taken up in 100 cm^3 DCM, and 50 cm^3 of triethylamine (Et_3N) was added. The reaction mixture stirred overnight, and after reaction was analysed using HPLC. After completion of reaction, the reaction mixture was washed with 4 x 50 cm^3 portions of water, and the organic phase dried and removed. Remaining impurities were removed using a silica column, and the product left to dry overnight in a vacuum oven at 40°C.

Yield; 3.39 g (23.4%) Purity; 99.7%

MS: 481 [M^+], 411, 395, 313, 275, 121.

The acrylate variant on LCP1 then underwent *radical polymerisation* to give the polyacrylate LCP2, the structure of which is given in Figure A1.4.

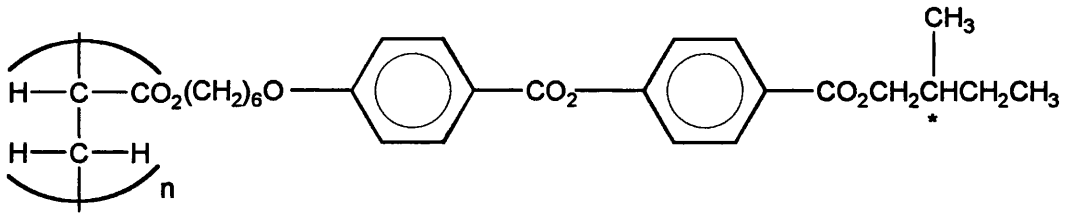

Figure A1.4: Molecular Structure of Polyacrylate Variant on LCP1

The practical procedure and mechanism for this reaction are as the radical polymerisation described in (2.2.2). The following quantities of reagents were used:

Acrylate variant on LCP1 (482 g mol^{-1})	3.39 g (0.007 mol)
AIBN initiator	0.034 g (1% w/w)
Tetrahydrofuran (Solvent)	25 cm^3

Unfortunately, this desired product was not be synthesised due to the impurities in the final reaction mixture. Further attempts at synthesis were made, but these also resulted in an impure final product which could not be purified by recrystallisation or silica-column techniques in the time available.

A1.2 SYNTHESIS OF MESOGENS CONTAINING THREE RINGS

Intermediates were not readily available for the synthesis of the mesogens containing 3 aromatic rings. It was therefore first necessary to synthesis the desired intermediates, before carrying these through to the mesogen syntheses.

A1.2a 4,4'-HYDROXYBIPHENYLCARBOXYLIC ACID

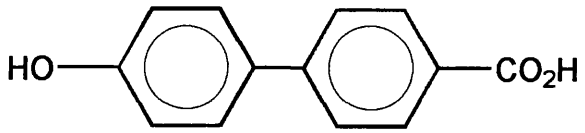

Figure A1.5: Molecular Structure of Hydroxybiphenyl Intermediate

This reaction involved the conversion of hydroxycyanobiphenyl to the hydroxybiphenylcarboxylic acid. The following procedure and quantities of reagents were used:

Hydroxycyanobiphenyl (195 g mol^{-1})	99.45 g (0.51 mol)
Acetic acid (glacial)	1630 cm^3
Sulphuric acid (concentrated)	440 cm^3
Distilled water	2000 cm^3

The cyanobiphenyl, acetic acid and water were carefully combined in a 5000 cm^3 3-necked flask fitted with a condenser, overhead stirrer, and dropping funnel. Sulphuric acid was added slowly with continuous stirring, and the reaction mixture allowed to reflux overnight.

The reaction mixture was analysed by HPLC and when most of the starting material had been converted to product, 2000 cm^3 water was added, and stirred for 20 minutes. This caused precipitation of the product, which was washed with 3 x 200 cm^3 portions of water before being recrystallised from IMS / THF (10:3 ratio).

A yield of 109 g was obtained (100%), and the melting point of the solid found to be 294°C, which compares well to the quoted value (Aldrich, 295°C).

MS: 214 [M^+], 94.

The hydroxybiphenylcarboxylicacid was then used in the synthesis of methylbutylhydroxybiphenylcarboxylate (A1.2b).

A1.2b 4, 4'-METHYLBUTYLHYDROXYBIPHENYLCARBOXYLATE

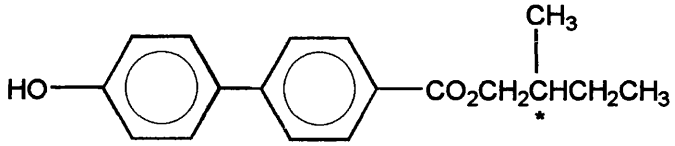

Figure A1.6: Molecular Structure of Chiral Mesogen Intermediate

The next stage in liquid crystal synthesis was the preparation of a chiral intermediate, the structure of which is shown in Figure A1.6. This was carried out by reacting the hydroxybiphenylcarboxylic acid with a chiral alcohol to give the above product, which due to the mechanism of reaction remains chirally pure. The following procedure and quantities of reagents were used:

Hydroxybiphenylcarboxylic acid (214 g mol^{-1})	95.0 g (0.44 mol)
S(-)-2-methylbutanol (88 g mol^{-1})	77.4 g (0.88 mol)
Toluene sulphonic acid (p-TSA) (catalyst)	0.6 g
Toluene (solvent)	200 cm^3

The above reagents were stirred together in a round-bottomed flask, heated to boiling, and left to reflux overnight using a Dean-Stark trap to remove water. If the reaction had not proceeded to completion, more p-TSA was added, and the mixture again left to reflux overnight.

The reaction mixture was cooled, filtered, and the volume of toluene reduced to allow washing with 2 x 200 cm^3 portions of water. A solid precipitated, and was filtered for analysis by HPLC. The product given was found to contain a 7% impurity, and attempts at recrystallisation and silica column purification did not significantly improve the purity in the time available. A small amount of pure product was recovered.

A1.2c A 3-RINGED LOW MOLECULAR MASS VARIANT ON LCP1

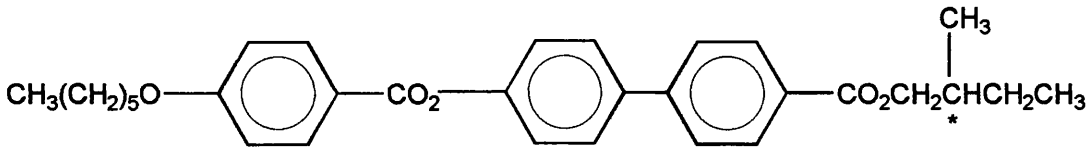

Figure A1.7: Molecular Structure of LMM2

The mechanism of the reaction resulting in the structure shown in Figure A1.7 is as the esterification described in (2.2.1). Unfortunately, this desired product could not be synthesised due to the impurity of the intermediate. An attempt at synthesis was made using the impure intermediate, but this resulted in an impure final product which could not be purified by recrystallisation or silica-column techniques in the time available.

A1.4d 3-RINGED SILOXANE VARIANTS ON LCP1

In the synthesis of side-chain siloxane polymers, the first step is the synthesis of a reactive intermediate which is then grafted onto the polymer backbone. The required 3-ringed low molecular mass vinyl substituent has the structure:

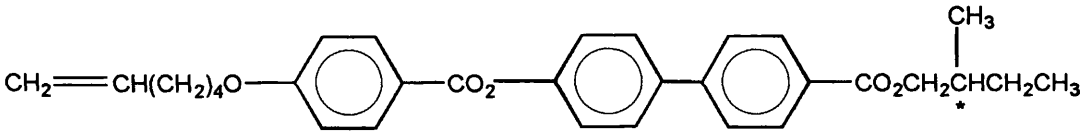

Figure A1.8: Molecular Structure of 3-Ringed Vinyl Intermediate

The procedure and mechanism for the reaction used to obtain the 3-ringed vinyl intermediate shown in Figure A1.8 are as the esterification described in (2.2.1). The following quantities of reagents were used:

Hexenoxybenzoic acid (220 g mol^{-1})	7.13 g (0.032 mol)
Trifluoroacetic anhydride (210 g mol^{-1})	7.35 g (0.035 mol)
Methylbutylhydroxybiphenylcarboxylate (284 g mol^{-1})	9.08 g (0.032 mol)
Dichloromethane (Solvent)	360 cm^3

Yield; 15.6 g (87%) Purity; 99.9% (HPLC)

Transitions: K → 83°C → S_C → 103°C → S_A → 155°C → N → 168°C → I

NMR: δ_H 1.00 (5H, m), 1.31 (H, m), 1.58 (3H, m), 1.71 (H, s), 1.85 (3H, m), 2.14 (2H, m), 4.05 (2H, t), 4.20 (2H, m), 5.05 (2H, m), 5.85 (H, m), 6.95 (2H, d), 7.30 (2H, d), 7.67 (4H, d), 8.15 (4H, m).

MS: 487 [M^+], 417, 399, 203, 121.

Firstly, the synthesis of a 3-ringed variant on LCP1 (LCP2) was carried out, the resultant structure being shown in Figure A1.9.

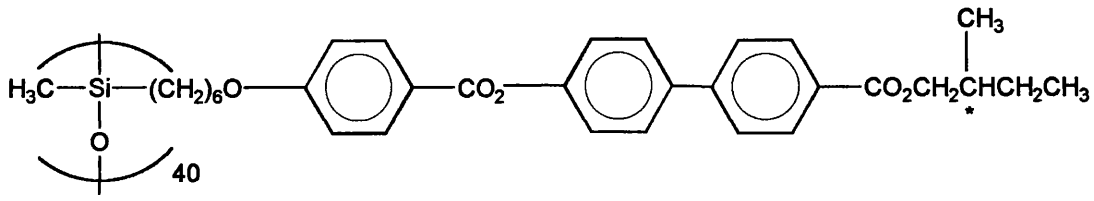

Figure A1.9: Molecular Structure of LCP2

The procedure and mechanism for this reaction are as the hydrosilyation reaction described (2.2.3). The reaction was allowed to proceed until the Si-H peak, as indicated by ir spectroscopy, was no longer visible. The following quantities of reagents were used:

Vinyl substituent - section 3.5.4 (486 g mol^{-1})	4.86 g (0.010 mol)
Polymethylhydrosiloxane (64 g mol^{-1} per unit)	0.58 g (0.009 mol)
Chloroplatinic acid	4 drops
Toluene (sieve dried)	150 cm^3

Yield; 3.07 g (61%) Purity; 99.7%. No starting material remaining. (GPC)

M_w; 33200 M_n; 14100 M_w/M_n; 2.34

Transitions: Tg; 22°C S_C → 226°C → S_A → 238°C → I

NMR: δ_H 0.13 (4H, s), 0.60 (2H, s), 0.95 (6H, m), 1.25 (H, m), 1.43 (6H, s), 1.62 (H, s), 1.85 (4H, m), 3.75 (4H, m), 3.95 (4H, m), 4.18 (4H, m).

A 3-ringed variant copolymer of LCP1 (LCP3), containing 50% mesogenic groups was next to be synthesised, the resultant structure being shown in Figure A1.10.

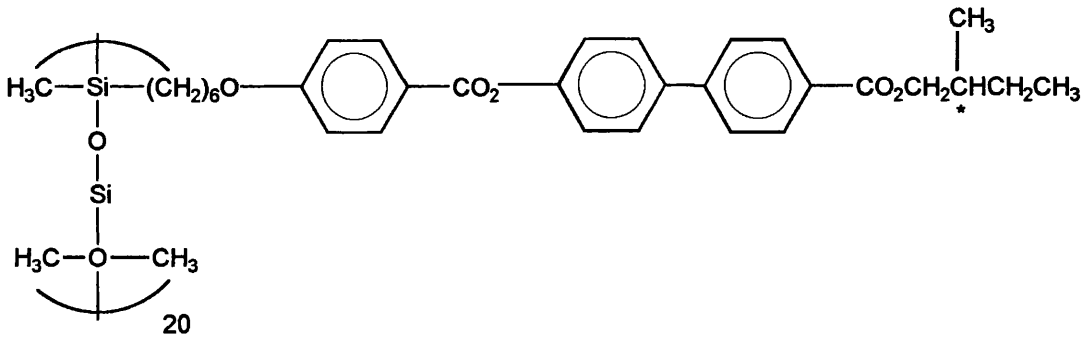

Figure A1.10: Molecular Structure of LCP3

The procedure and mechanism for this reaction are as the hydrosilyation reaction described (2.2.3). The reaction was allowed to proceed until the Si-H peak, as indicated by ir spectroscopy, was no longer visible. The following quantities of reagents were used:

Vinyl substituent - section 3.5.4 (486 g mol^{-1})	4.86 g (0.010 mol)
Polymethylhydrosiloxane (142 $gmol^{-1}$ per unit)	1.29 g (0.009 mol)
Chloroplatinic acid	4 drops
Toluene (sieve dried)	150 cm^3

Yield; 4.3 g (75%) Purity; 99.5% (GPC)

M_w; 23300 M_n; 12500 M_w/M_n; 1.85

Transitions: Tg; 4°C $S_C \rightarrow$ 191°C $\rightarrow$ I

NMR: δ_H 0.10 (4H, s), 0.65 (2H, s), 1.00 (6H, m), 1.25 (H, m), 1.43 (6H, s), 1.62 (H, s), 1.85 (4H, m), 3.75 (4H, m), 3.95 (4H, m), 4.20 (4H, m).

Appendix Two:

RETENTION DIAGRAMS &

PHYSIOCHEMICAL RESULT TABLES

Appendix two contains the retention diagrams and tables of physiochemical results obtained from the IGC studies considered in Chapter 4. The standard deviation for the results obtained by linear regression are given in parentheses.

A2.1 BDH770: ln Vg°, ln γ^{∞}, ln Ω^{∞}, ΔH^s, ΔH^e, ΔS^s, ΔS^e

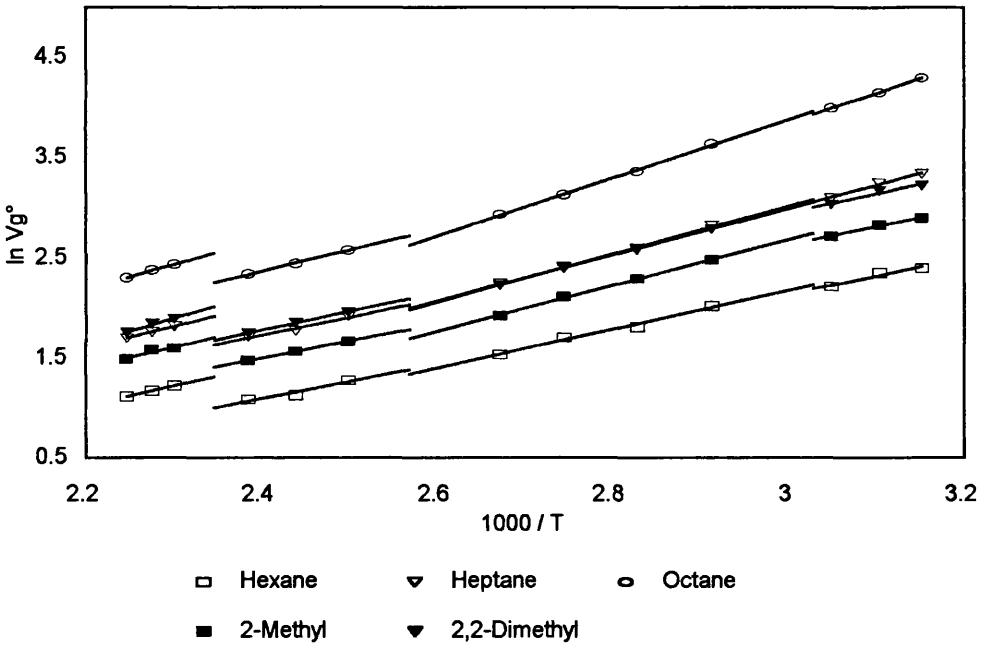

Figure A2.1: ln Vg° vs 1/T for Aliphatic Probes in BDH770

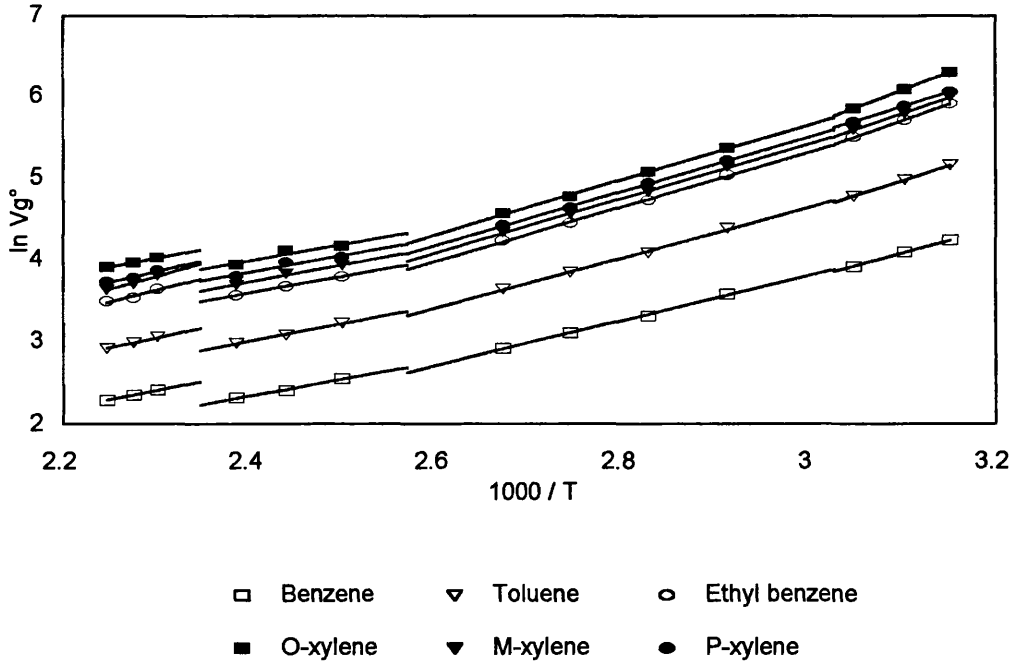

Figure A2.2: ln Vg° vs 1/T for Aromatic Probes in BDH770

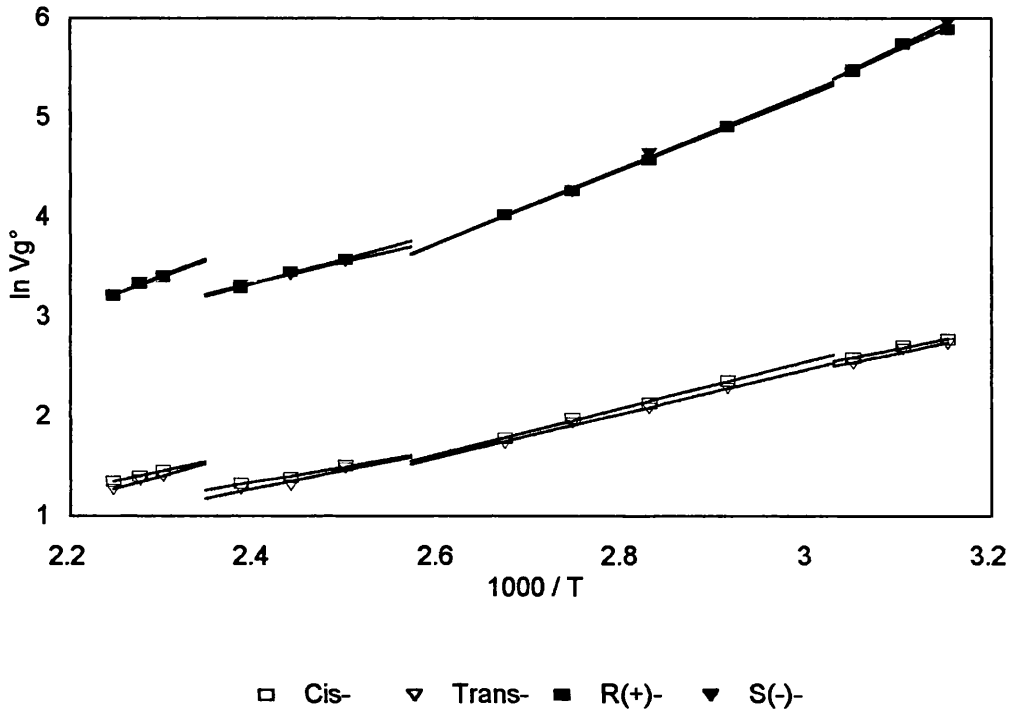

Figure A2.3: ln Vg° vs 1/T for Isomeric Probes in BDH770

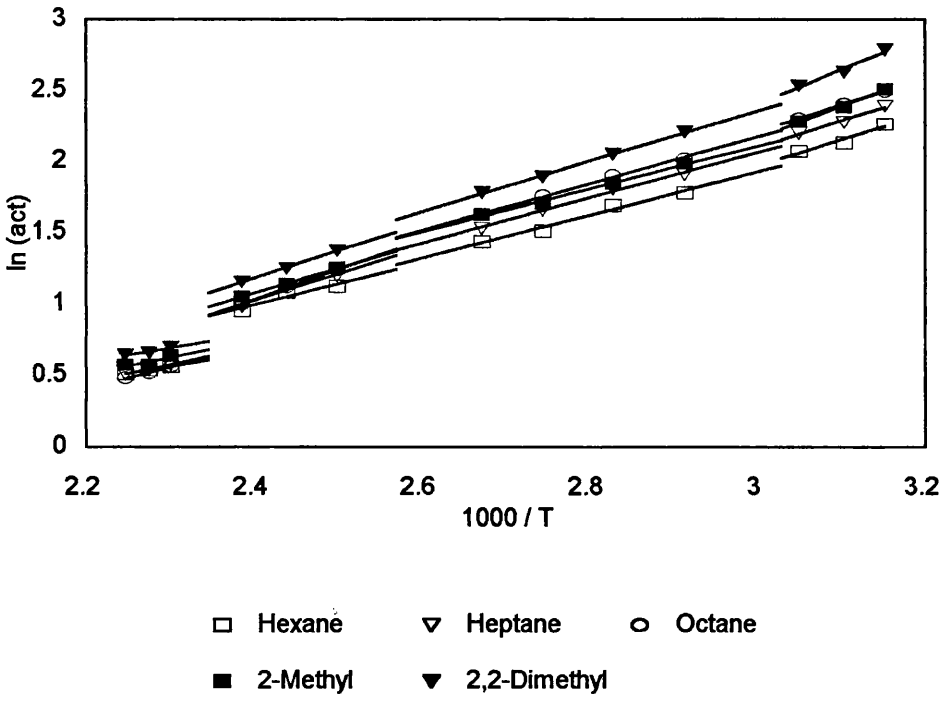

Figure A2.4: ln γ^{∞} vs 1/T for Aliphatic Probes in BDH770

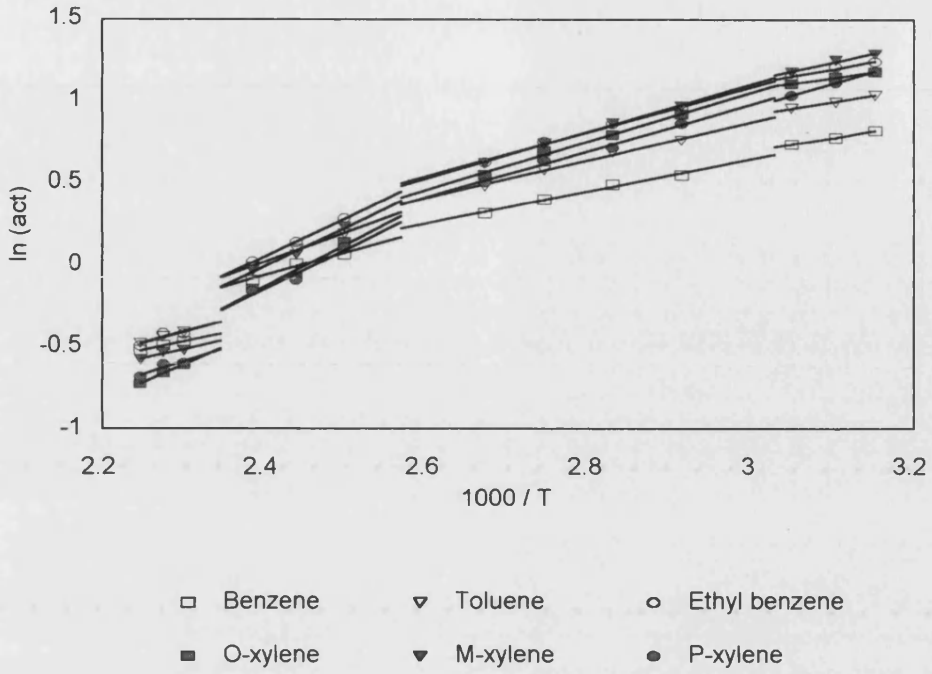

Figure A2.5: ln γ^{∞} vs 1/T for Aromatic Probes in BDH770

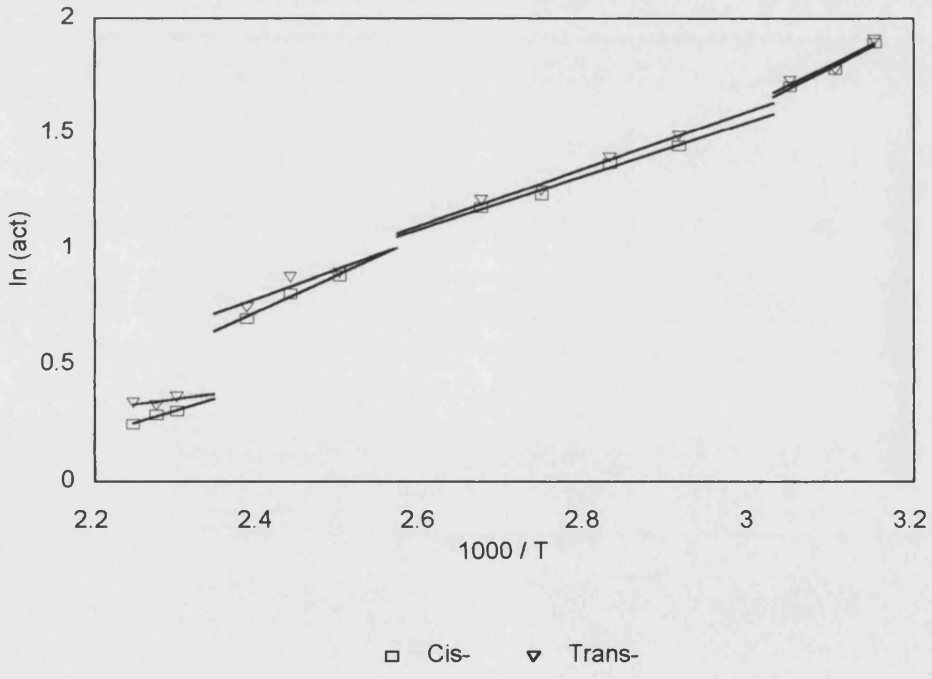

Figure A2.6: ln γ^{∞} vs 1/T for Isomeric Probes in BDH770

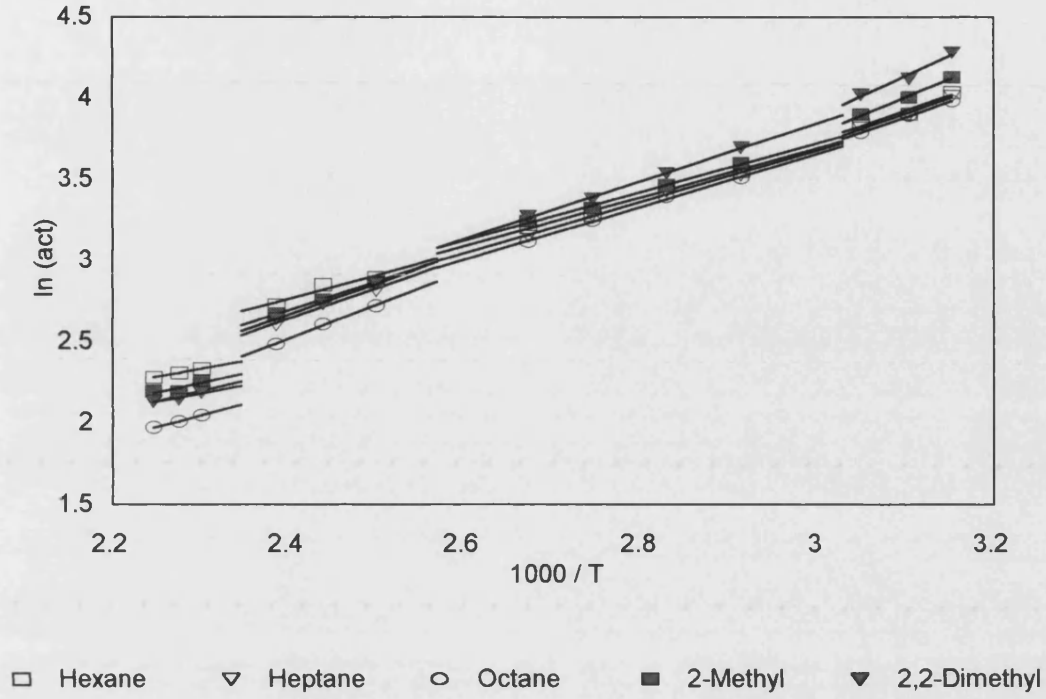

Figure A2.7: ln Ω^{∞} vs 1/T for Aliphatic Probes in BDH770

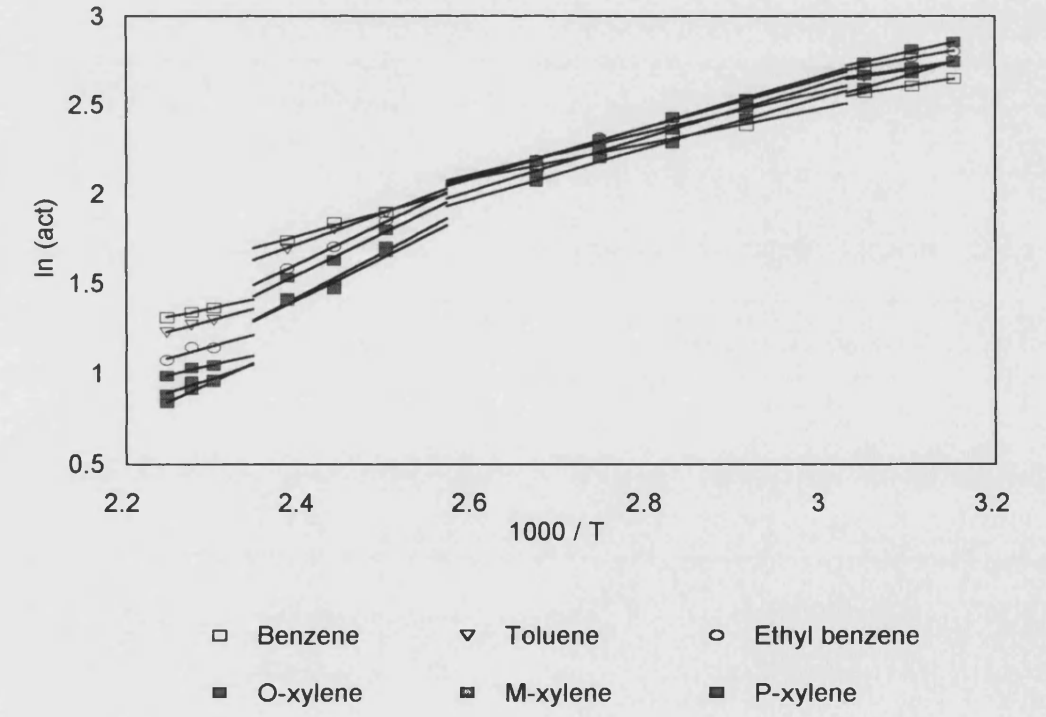

Figure A2.8: ln Ω^{∞} vs 1/T for Aromatic Probes in BDH770

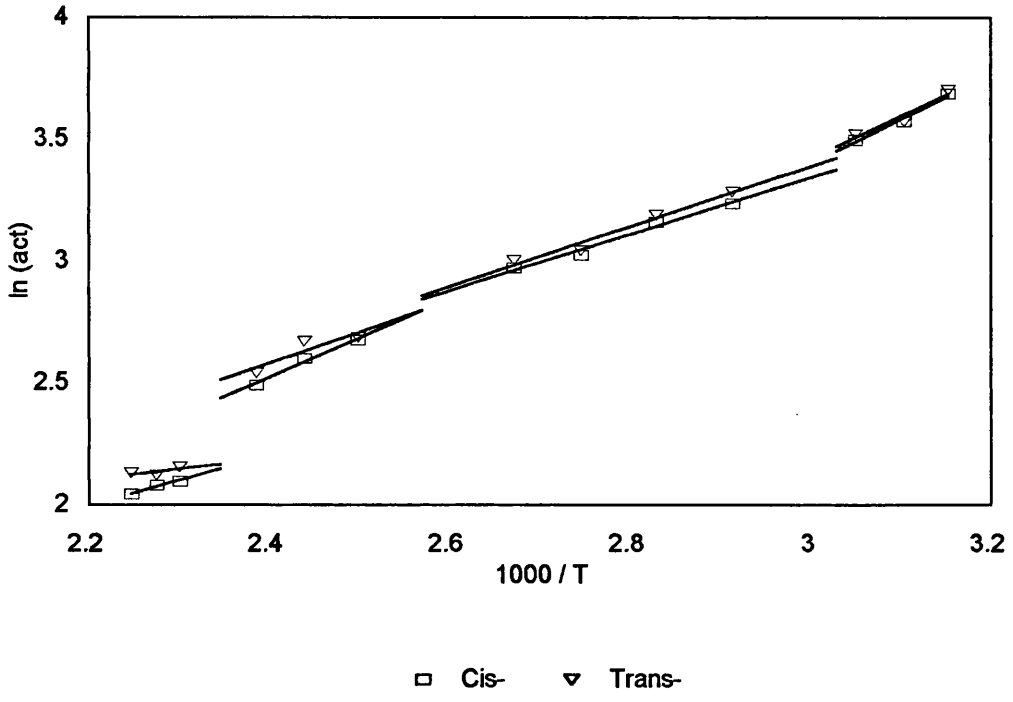

Figure A2.9: ln Ω° vs 1/T for Isomeric Probes in BDH770

Probe	Enthalpic kJ mol^{-1}			Entropic J mol^{-1} K^{-1}		
	ΔH^s	ΔH^e	ΔH^{vap}	ΔS^s	ΔS^e	ΔS^{vap}
Hexane	-15.06 (0.46)	15.37 (0.47)	-30.43 (0.93)	-13.21 (0.03)	29.75 (0.03)	-42.96 (0.06)
Heptane	-19.54 (0.26)	15.67 (0.27)	-35.21 (0.53)	-19.55 (0.02)	29.59 (0.02)	-49.14 (0.04)
Octane	-24.53 (0.02)	15.50 (0.01)	-40.02 (0.03)	-27.40 (0.01)	28.13 (0.01)	-55.53 (0.02)
2-Me	-15.09 (0.20)	18.43 (0.21)	-33.52 (0.41)	-9.21 (0.01)	37.29 (0.02)	-46.50 (0.03)
2,2-DiMe	-15.32 (0.43)	20.53 (0.44)	-35.85 (0.87)	-7.18 (0.03)	41.63 (0.03)	-48.82 (0.06)
Benzene	-25.96 (0.06)	6.68 (0.07)	-32.64 (0.13)	-32.37 (0.01)	14.24 (0.01)	-46.61 (0.02)
Toluene	-30.45 (0.03)	6.42 (0.04)	-36.87 (0.07)	-38.96 (0.01)	11.63 (0.01)	-50.58 (0.02)
Ethylbenzene	-33.76 (0.15)	7.22 (0.14)	-40.98 (0.29)	-43.09 (0.01)	12.43 (0.01)	-55.52 (0.02)
O-Xylene	-36.37 (0.06)	5.90 (0.05)	-42.26 (0.11)	-48.06 (0.01)	8.77 (0.01)	-56.83 (0.02)
M-Xylene	-32.43 (0.16)	9.02 (0.15)	-41.45 (0.31)	-38.27 (0.01)	17.69 (0.01)	-55.96 (0.02)
P-Xylene	-29.25 (0.03)	11.90 (0.02)	-41.15 (0.05)	-27.71 (0.01)	27.66 (0.01)	-55.37 (0.02)
Cis-	-15.37 (0.29)	15.18 (0.30)	-30.55 (0.59)	-11.12 (0.02)	32.18 (0.02)	-43.31 (0.04)
Trans-	-16.02 (0.48)	14.44 (0.49)	-30.46 (0.97)	-13.48 (0.04)	29.80 (0.04)	-43.28 (0.08)
R(+)	-34.54 (0.59)	n/a	n/a	-45.61 (0.04)	n/a	n/a
S(-)	-37.76 (0.17)	n/a	n/a	-55.35 (0.01)	n/a	n/a

Table A2.1: Physiochemical Results for BDH770 in the Crystalline Phase

Probe	Enthalpic kJ mol^{-1}			Entropic J mol^{-1} K^{-1}		
	ΔH^s	ΔH^e	ΔH^{vap}	ΔS^s	ΔS^e	ΔS^{vap}
Hexane	-16.09 (0.17)	12.57 (0.16)	-28.67 (0.33)	-16.03 (0.03)	21.74 (0.03)	-37.77 (0.06)
Heptane	-20.00 (0.12)	13.23 (0.10)	-33.22 (0.22)	-20.71 (0.02)	22.56 (0.02)	-43.28 (0.04)
Octane	-24.10 (0.10)	13.63 (0.08)	-37.73 (0.18)	-25.91 (0.02)	22.84 (0.01)	-48.75 (0.03)
2-Me	-19.12 (0.07)	12.50 (0.09)	-31.62 (0.16)	-20.87 (0.01)	20.03 (0.02)	-40.90 (0.03)
2,2-DiMe	-19.27 (0.04)	14.79 (0.06)	-34.06 (0.10)	-18.75 (0.01)	24.80 (0.01)	-43.55 (0.01)
Benzene	-22.78 (0.10)	8.16 (0.09)	-30.94 (0.19)	-22.50 (0.02)	19.08 (0.02)	-41.59 (0.02)
Toluene	-25.43 (0.10)	9.67 (0.08)	-35.10 (0.18)	-23.58 (0.02)	21.76 (0.01)	-45.34 (0.03)
Ethylbenzene	-27.59 (0.11)	11.33 (0.09)	-38.92 (0.20)	-24.45 (0.02)	24.96 (0.02)	-49.41 (0.04)
O-Xylene	-27.82 (0.11)	12.40 (0.10)	-40.22 (0.22)	-22.35 (0.02)	28.43 (0.02)	-50.78 (0.04)
M-Xylene	-27.43 (0.09)	12.02 (0.07)	-39.45 (0.18)	-23.17 (0.02)	26.89 (0.01)	-50.05 (0.03)
P-Xylene	-27.35 (0.11)	11.81 (0.11)	-39.16 (0.22)	-22.20 (0.02)	27.31 (0.02)	-49.51 (0.04)
Cis-	-19.33 (0.12)	9.66 (0.12)	-28.99 (0.24)	-22.59 (0.02)	16.10 (0.02)	-38.69 (0.04)
Trans-	-18.43 (0.14)	10.25 (0.15)	-28.69 (0.29)	-20.54 (0.03)	17.50 (0.03)	-38.04 (0.03)
R(+)	-30.60 (0.10)	n/a	n/a	-34.22 (0.02)	n/a	n/a
S(-)	-31.32 (0.20)	n/a	n/a	-36.13 (0.04)	n/a	n/a

Table A2.2: Physiochemical Results for BDH770 in the Smectic C Mesophase

Probe	Enthalpic kJ mol^{-1}			Entropic J mol^{-1} K^{-1}		
	ΔH^s	ΔH^e	ΔH^{vap}	ΔS^s	ΔS^e	ΔS^{vap}
Hexane	-14.09 (0.49)	12.03 (0.47)	-26.12 (0.96)	-10.52 (0.04)	20.62 (0.04)	-31.14 (0.08)
Heptane	-14.92 (0.35)	15.54 (0.33)	-30.46 (0.68)	-7.27 (0.03)	28.81 (0.03)	-36.09 (0.06)
Octane	-17.40 (0.12)	17.27 (0.10)	-34.67 (0.22)	-7.91 (0.01)	32.89 (0.01)	-40.80 (0.02)
2-Me	-14.23 (0.04)	14.66 (0.06)	-28.88 (0.10)	-7.51 (0.01)	26.26 (0.01)	-33.77 (0.02)
2,2-DiMe	-15.40 (0.08)	16.00 (0.10)	-31.39 (0.18)	-8.00 (0.01)	28.61 (0.01)	-36.60 (0.02)
Benzene	-17.17 (0.27)	11.42 (0.25)	-28.58 (0.52)	-7.54 (0.02)	27.92 (0.02)	-35.46 (0.04)
Toluene	-17.87 (0.15)	14.85 (0.14)	-32.72 (0.29)	-3.67 (0.01)	35.47 (0.01)	-39.14 (0.02)
Ethylbenzene	-16.86 (0.04)	19.39 (0.05)	-36.25 (0.09)	3.63 (0.01)	46.09 (0.01)	-42.46 (0.02)
O-Xylene	-16.45 (0.63)	21.23 (0.64)	-37.68 (1.27)	7.89 (0.05)	52.06 (0.05)	-44.18 (0.10)
M-Xylene	-17.42 (0.28)	19.57 (0.30)	-36.99 (0.58)	3.39 (0.02)	47.03 (0.03)	-43.63 (0.05)
P-Xylene	-16.79 (0.62)	19.93 (0.63)	-36.72 (1.25)	5.91 (0.05)	49.05 (0.05)	-43.14 (0.10)
Cis-	-13.05 (0.24)	13.47 (0.22)	-26.52 (0.26)	-6.01 (0.02)	26.27 (0.02)	-32.28 (0.04)
Trans-	-15.47 (0.63)	10.61 (0.62)	-26.08 (1.25)	-12.34 (0.05)	18.92 (0.05)	-31.27 (0.10)
R(+)	-20.88 (0.24)	n/a	n/a	-8.18 (0.02)	n/a	n/a
S(-)	-17.95 (0.01)	n/a	n/a	-1.12 (0.01)	n/a	n/a

Table A2.3: Physiochemical Results for BDH770 in the Nematic Mesophase

Probe	Enthalpic kJ mol^{-1}			Entropic J mol^{-1} K^{-1}		
	ΔH^s	ΔH^e	ΔH^{vap}	ΔS^s	ΔS^e	ΔS^{vap}
Hexane	-16.63 (0.02)	7.99 (0.03)	-24.62 (0.05)	-13.89 (0.01)	13.72 (0.01)	-27.61 (0.02)
Heptane	-18.35 (0.02)	10.48 (0.03)	-28.83 (0.05)	-12.92 (0.01)	19.33 (0.01)	-32.25 (0.02)
Octane	-21.03 (0.11)	11.84 (0.12)	-32.87 (0.23)	-13.95 (0.01)	22.62 (0.01)	-36.57 (0.02)
2-Me	-17.36 (0.75)	9.86 (0.76)	-27.22 (1.51)	-12.37 (0.03)	17.50 (0.03)	-29.86 (0.06)
2,2-DiMe	-21.33 (0.30)	8.36 (0.31)	-29.69 (0.61)	-19.11 (0.01)	13.49 (0.01)	-32.60 (0.02)
Benzene	-18.92 (0.06)	8.29 (0.50)	-27.21 (0.56)	-9.28 (0.01)	22.94 (0.01)	-32.23 (0.02)
Toluene	-20.58 (0.11)	10.75 (0.10)	-31.33 (0.21)	-7.79 (0.01)	28.08 (0.01)	-35.87 (0.02)
Ethylbenzene	-23.73 (0.79)	10.97 (0.78)	-34.70 (1.57)	-10.19 (0.03)	28.64 (0.03)	-38.82 (0.06)
O-Xylene	-18.07 (0.21)	18.22 (0.20)	-36.30 (0.41)	6.04 (0.01)	46.96 (0.01)	-40.92 (0.01)
M-Xylene	-26.37 (0.30)	9.31 (0.30)	-35.68 (0.60)	-14.88 (0.01)	25.67 (0.01)	-40.56 (0.01)
P-Xylene	-22.17 (0.64)	13.26 (0.63)	-35.43 (1.27)	-4.72 (0.02)	35.37 (0.02)	-40.09 (0.04)
Cis-	-16.42 (0.19)	8.53 (0.18)	-24.95 (0.37)	-11.50 (0.01)	17.07 (0.01)	-28.57 (0.02)
Trans-	-21.03 (0.48)	3.48 (0.49)	-24.51 (0.97)	-22.52 (0.02)	5.06 (0.01)	-27.58 (0.03)
R(+)	-28.71 (0.54)	n/a	n/a	-23.55 (0.02)	n/a	n/a
S(-)	-30.27 (0.47)	n/a	n/a	-27.04 (0.02)	n/a	n/a

Table A2.4: Physiochemical Results for BDH770 in the Isotropic Phase

A2.2 BDH849: ln Vg°, ln γ^{∞}, ln Ω^{∞}, ΔH^s, ΔH^e, ΔS^s, ΔS^e

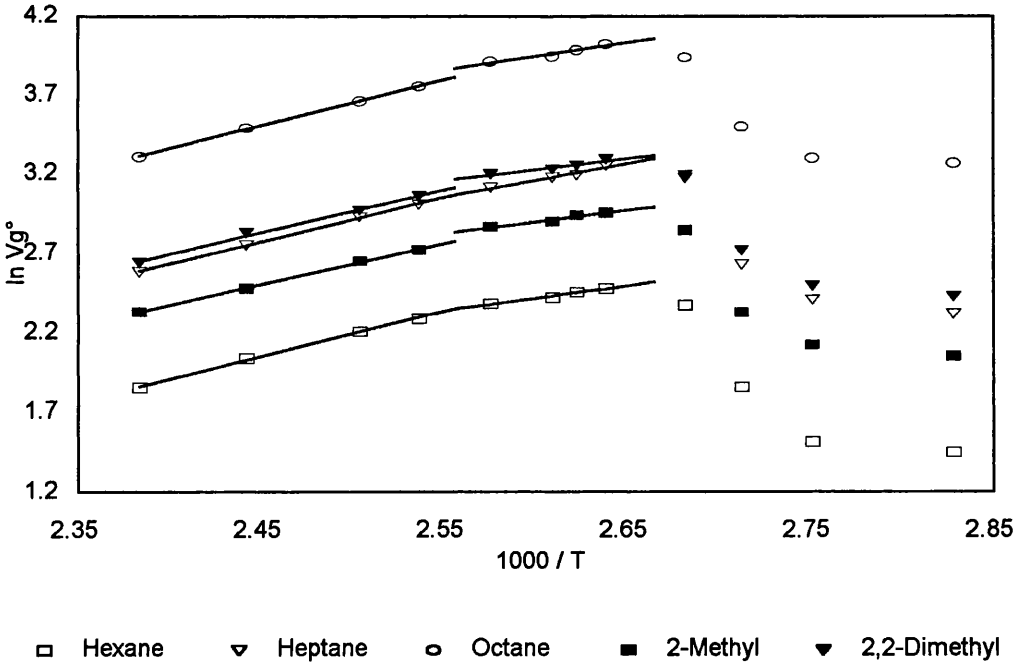

Figure A2.10: ln Vg° vs 1/T for Aliphatic Probes in BDH849

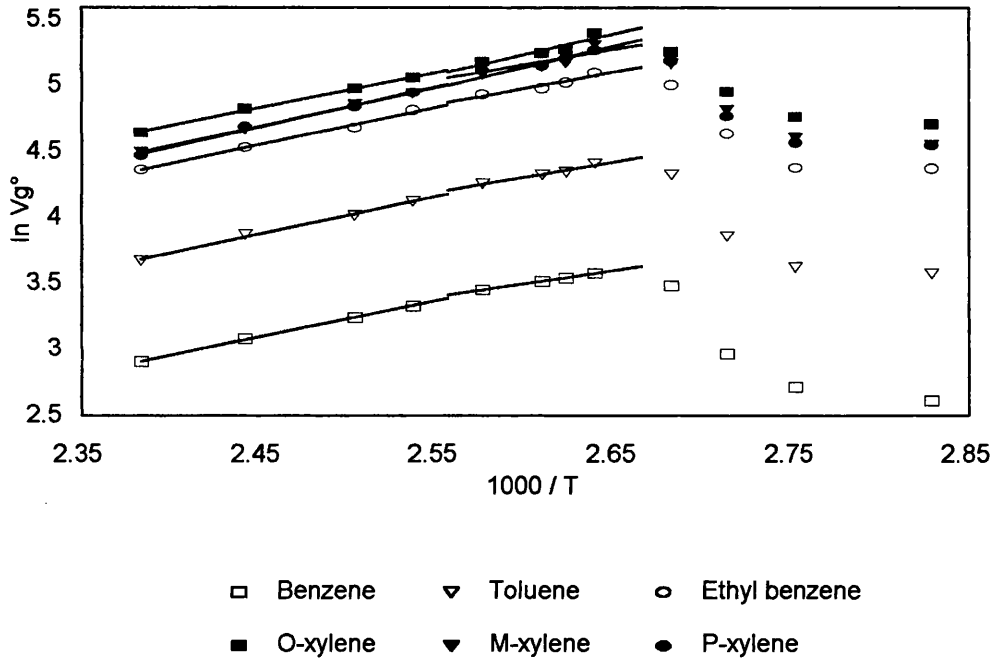

Figure A2.11: ln Vg° vs 1/T for Aromatic Probes in BDH849

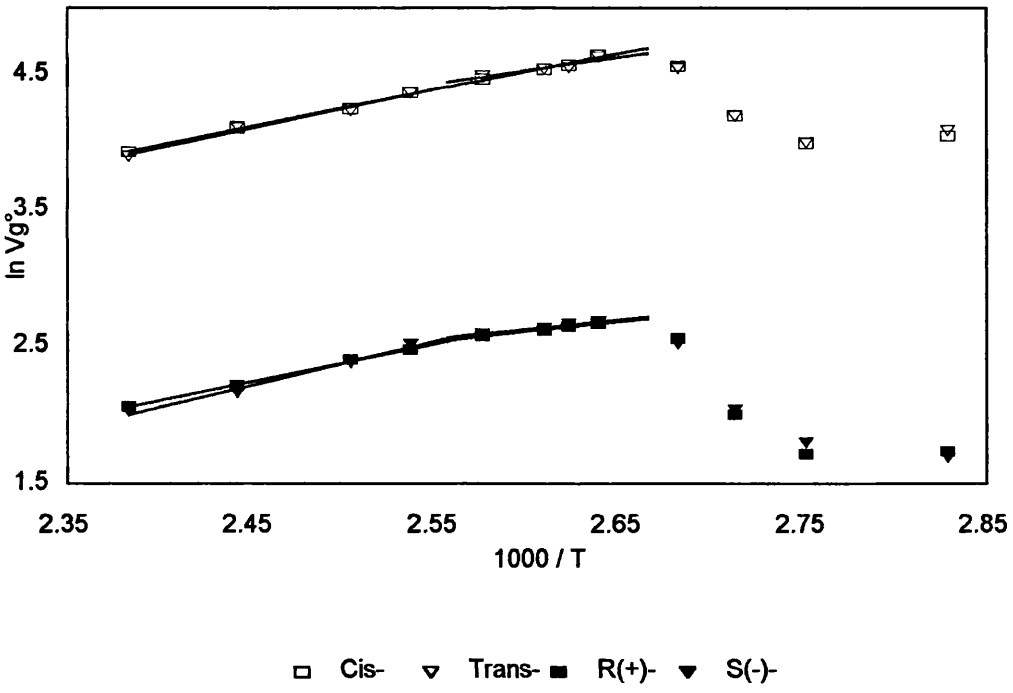

Figure A2.12: ln Vg° vs 1/T for Isomeric Probes in BDH849

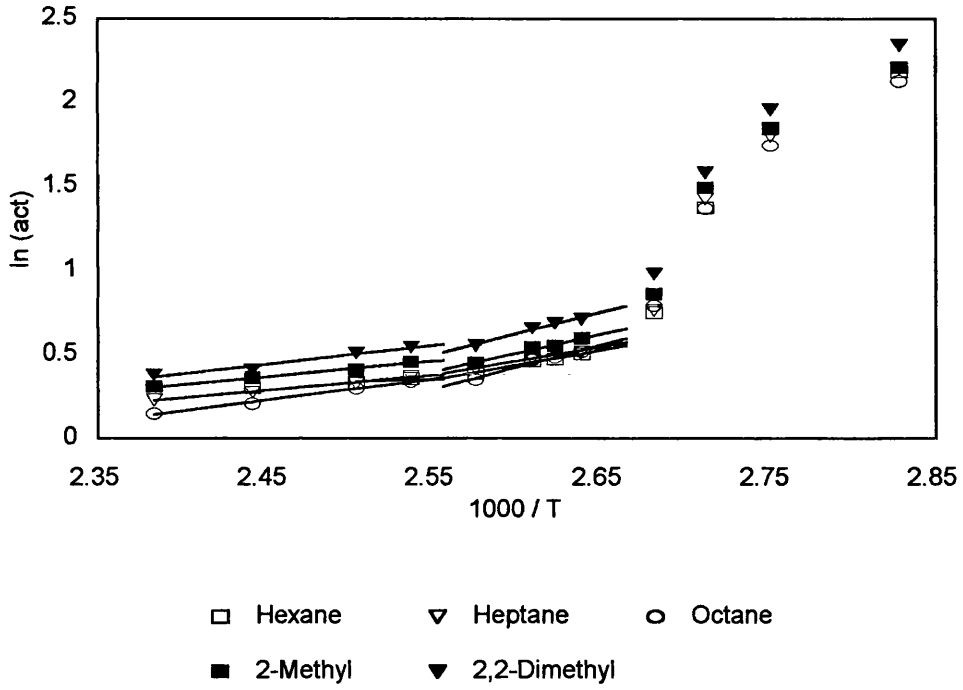

Figure A2.13: ln γ^{∞} vs 1/T for Aliphatic Probes in BDH849

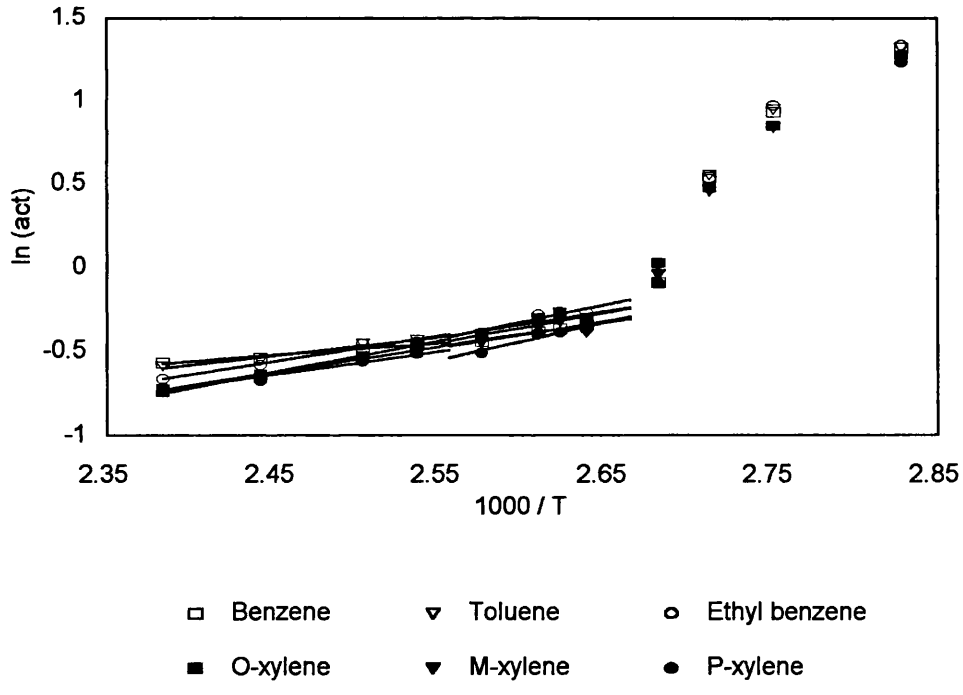

Figure A2.14: ln γ^{∞} vs 1/T for Aromatic Probes in BDH849

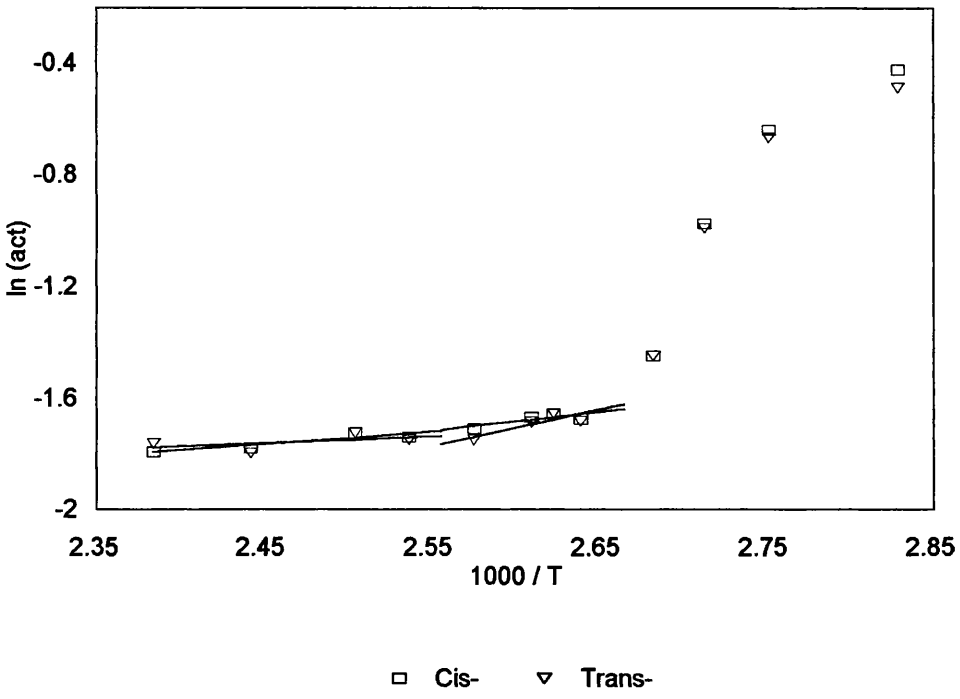

Figure A2.15: ln γ^{∞} vs 1/T for Isomeric Probes in BDH849

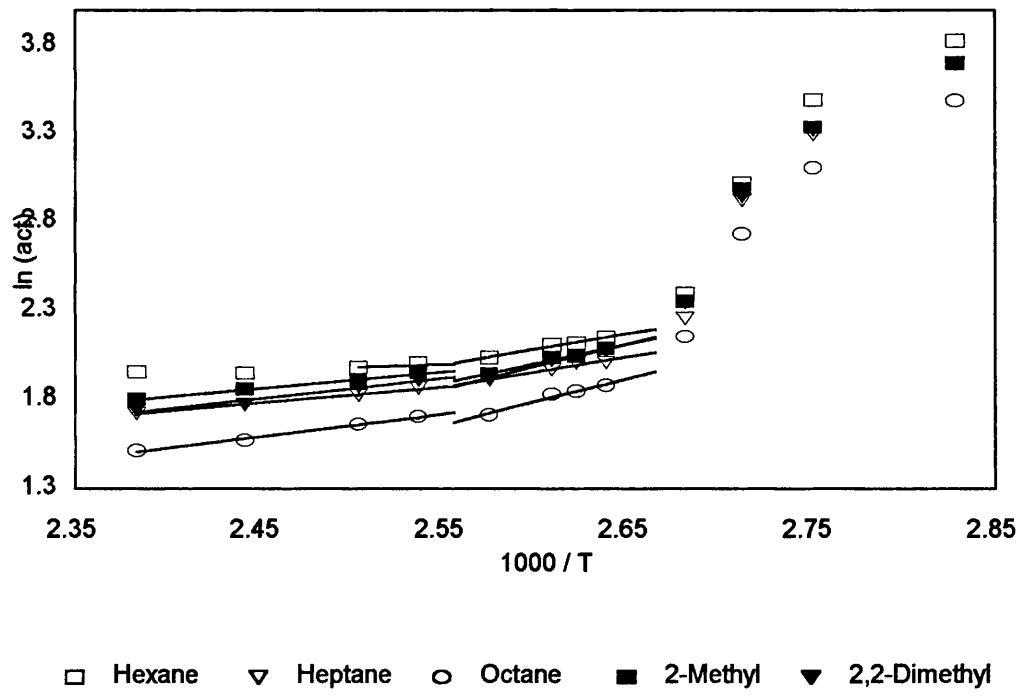

Figure A2.16: ln Ω^{∞} vs 1/T for Aliphatic Probes in BDH849

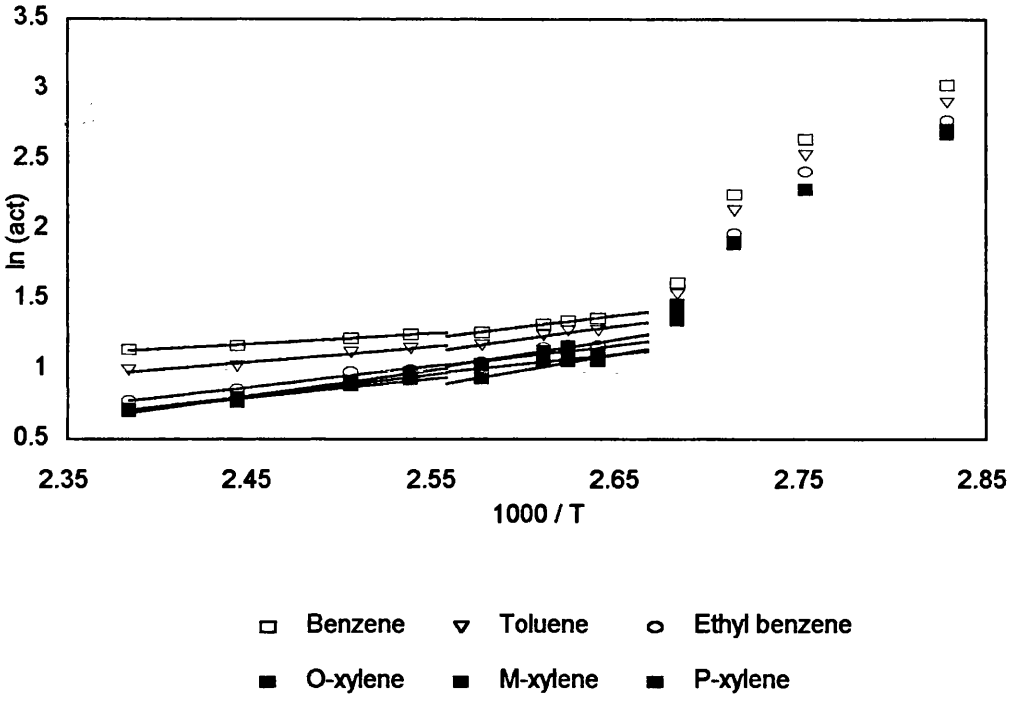

Figure A2.17: ln Ω° vs 1/T for Aromatic Probes in BDH849

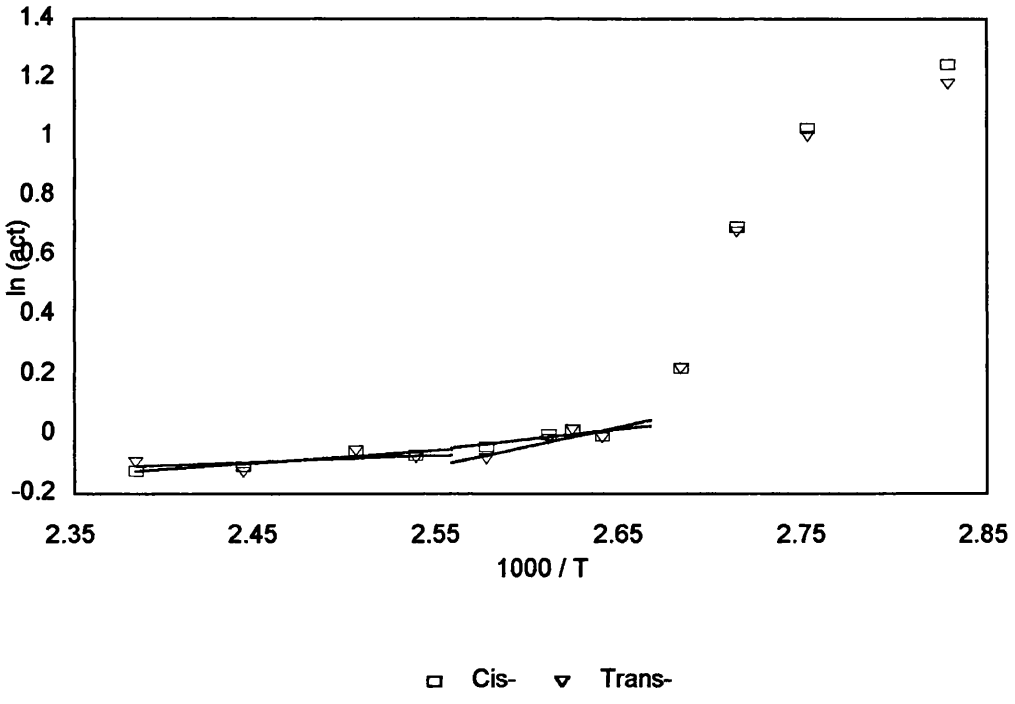

Figure A2.18: ln Ω° vs 1/T for Isomeric Probes in BDH849

Probe	Enthalpic kJ mol^{-1}			Entropic J mol^{-1} K^{-1}		
	ΔH^s	ΔH^e	ΔH^{vap}	ΔS^s	ΔS^e	ΔS^{vap}
Hexane	-12.80 (0.17)	14.60 (0.12)	-27.40 (0.29)	0.99 (0.01)	34.31 (0.01)	-33.32 (0.02)
Heptane	-17.53 (0.30)	14.31 (0.06)	-31.84 (0.36)	-5.15 (0.01)	33.37 (0.01)	-38.53 (0.02)
Octane	-14.37 (0.34)	21.82 (0.08)	-36.19 (0.42)	9.63 (0.02)	53.21 (0.01)	-43.58 (0.03)
2-Me	-11.84 (0.23)	18.43 (0.06)	-30.27 (0.29)	7.48 (0.01)	43.70 (0.01)	-36.22 (0.02)
2,2-DiMe	-11.40 (0.27)	21.36 (0.16)	-32.76 (0.43)	11.36 (0.01)	50.37 (0.02)	-39.01 (0.03)
Benzene	-16.56 (0.07)	13.20 (0.06)	-29.76 (0.13)	0.26 (0.01)	37.64 (0.01)	-37.38 (0.02)
Toluene	-19.18 (0.34)	14.72 (0.16)	-33.90 (0.40)	0.17 (0.02)	41.25 (0.02)	-41.08 (0.04)
Ethylbenzene	-20.47 (0.60)	17.09 (0.17)	-37.56 (0.77)	2.40 (0.03)	47.13 (0.02)	-44.73 (0.05)
O-Xylene	-25.98 (0.91)	12.92 (0.13)	-38.91 (1.04)	-9.80 (0.04)	36.42 (0.01)	-46.22 (0.05)
M-Xylene	-26.40 (1.05)	11.77 (0.06)	-38.17 (1.11)	-11.68 (0.05)	33.89 (0.01)	-45.58 (0.06)
P-Xylene	-19.23 (0.55)	18.67 (0.19)	-37.90 (0.74)	7.13 (0.03)	52.20 (0.02)	-45.06 (0.05)
Cis-	-22.22 (0.38)	5.57 (0.14)	-27.80 (0.42)	-5.95 (0.02)	28.50 (0.02)	-34.45 (0.04)
Trans-	-16.57 (0.56)	10.82 (0.27)	-27.40 (0.83)	8.78 (0.03)	42.33 (0.03)	-33.54 (0.06)
R(+)	-12.22 (0.12)	n/a	n/a	4.13 (0.01)	n/a	n/a
S(-)	-11.90 (0.12)	n/a	n/a	5.10 (0.01)	n/a	n/a

Table A2.5: Physiochemical Results for BDH849 in the Cholesteric Mesophase

Probe	Enthalpic kJ mol^{-1}			Entropic J mol^{-1} K^{-1}		
	ΔH^s	ΔH^e	ΔH^{vap}	ΔS^s	ΔS^e	ΔS^{vap}
Hexane	-23.52 (0.10)	2.74 (0.12)	-26.26 (0.22)	-26.38 (0.01)	4.04 (0.14)	-30.41 (0.15)
Heptane	-23.08 (0.04)	7.53 (0.06)	-30.61 (0.10)	-19.32 (0.01)	16.08 (0.01)	-35.39 (0.02)
Octane	-24.23 (0.06)	10.61 (0.08)	-34.84 (0.14)	-16.04 (0.01)	24.11 (0.01)	-40.14 (0.02)
2-Me	-21.23 (0.06)	7.80 (0.06)	-29.03 (0.12)	-17.03 (0.01)	16.05 (0.01)	-33.08 (0.02)
2,2-DiMe	-22.21 (0.14)	9.33 (0.16)	-31.54 (0.30)	-16.72 (0.02)	19.20 (0.02)	-35.92 (0.04)
Benzene	-22.78 (0.05)	5.93 (0.06)	-28.71 (0.11)	-15.86 (0.01)	18.85 (0.01)	-34.71 (0.02)
Toluene	-23.77 (0.15)	9.07 (0.16)	-32.84 (0.31)	-11.82 (0.02)	26.58 (0.02)	-38.40 (0.04)
Ethylbenzene	-23.77 (0.17)	12.62 (0.17)	-36.39 (0.34)	-6.18 (0.02)	35.57 (0.02)	-41.75 (0.04)
O-Xylene	-22.32 (0.11)	15.49 (0.12)	-37.81 (0.23)	-0.30 (0.01)	43.14 (0.01)	-43.44 (0.02)
M-Xylene	-24.36 (0.05)	12.75 (0.05)	-37.11 (0.10)	-6.45 (0.01)	36.43 (0.01)	-42.88 (0.02)
P-Xylene	-25.35 (0.18)	11.49 (0.19)	-36.85 (0.37)	-8.94 (0.02)	33.46 (0.02)	-42.39 (0.04)
Cis-	-23.09 (0.14)	3.57 (0.14)	-26.66 (0.28)	-8.15 (0.02)	23.41 (0.02)	-31.57 (0.04)
Trans-	-24.25 (0.27)	1.98 (0.27)	-26.22 (0.54)	-11.07 (0.03)	19.49 (0.03)	-30.56 (0.06)
R(+)	-22.92 (0.10)	n/a	n/a	-23.31 (0.01)	n/a	n/a
S(-)	-26.56 (0.27)	n/a	n/a	-32.43 (0.03)	n/a	n/a

Table A2.6: Physiochemical Results for BDH849 in the Isotropic Phase

A2.3 BDH1029: ln Vg°, ln γ^{∞}, ln Ω^{∞}, ΔH^{s}, ΔH^{e}, ΔS^{s}, ΔS^{e}

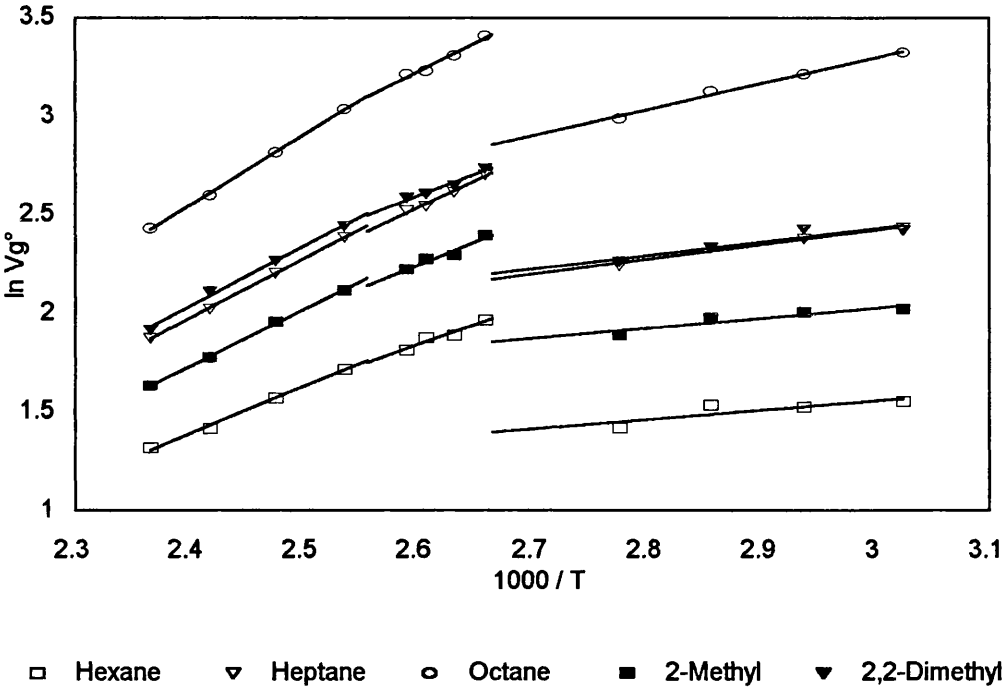

Figure A2.19: ln Vg° vs 1/T for Aliphatic Probes in BDH1029

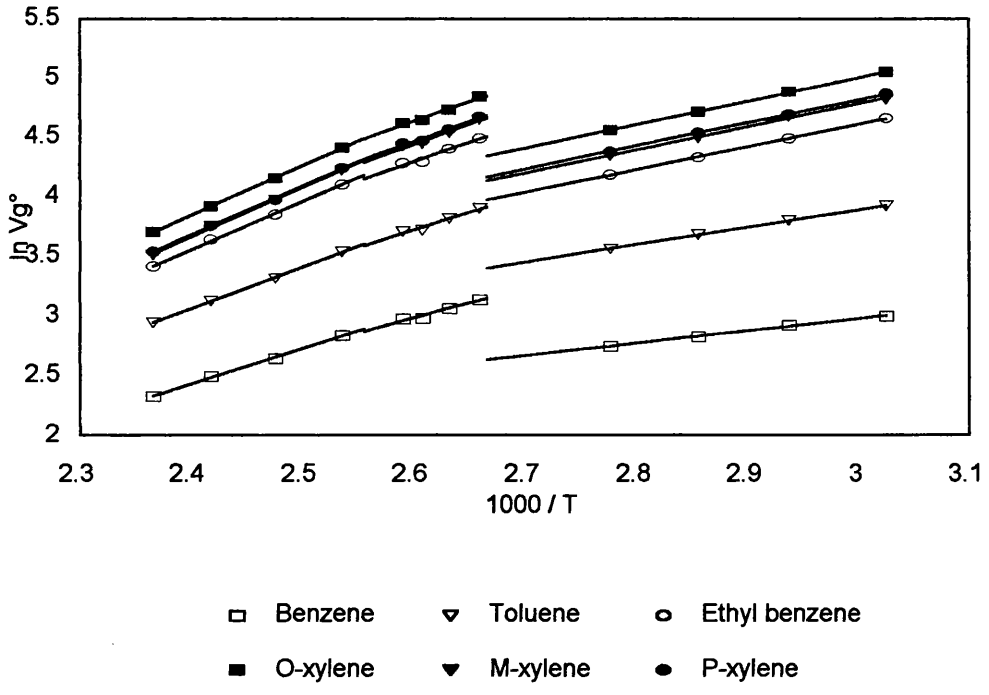

Figure A2.20: ln Vg° vs 1/T for Aromatic Probes in BDH1029

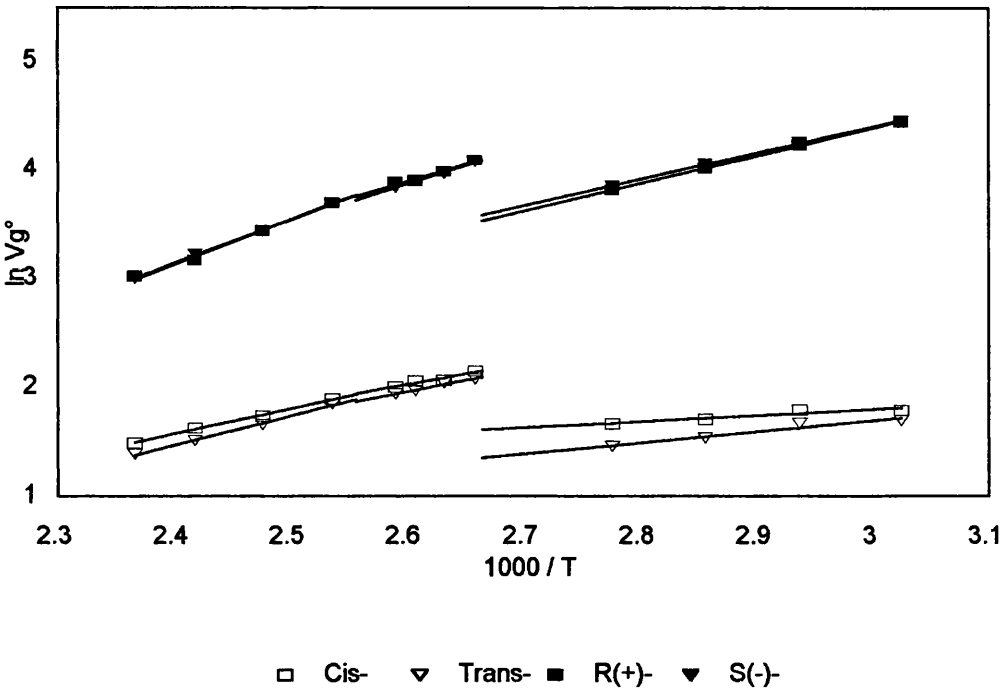

Figure A2.21: ln Vg° vs 1/T for Isomeric Probes in BDH1029

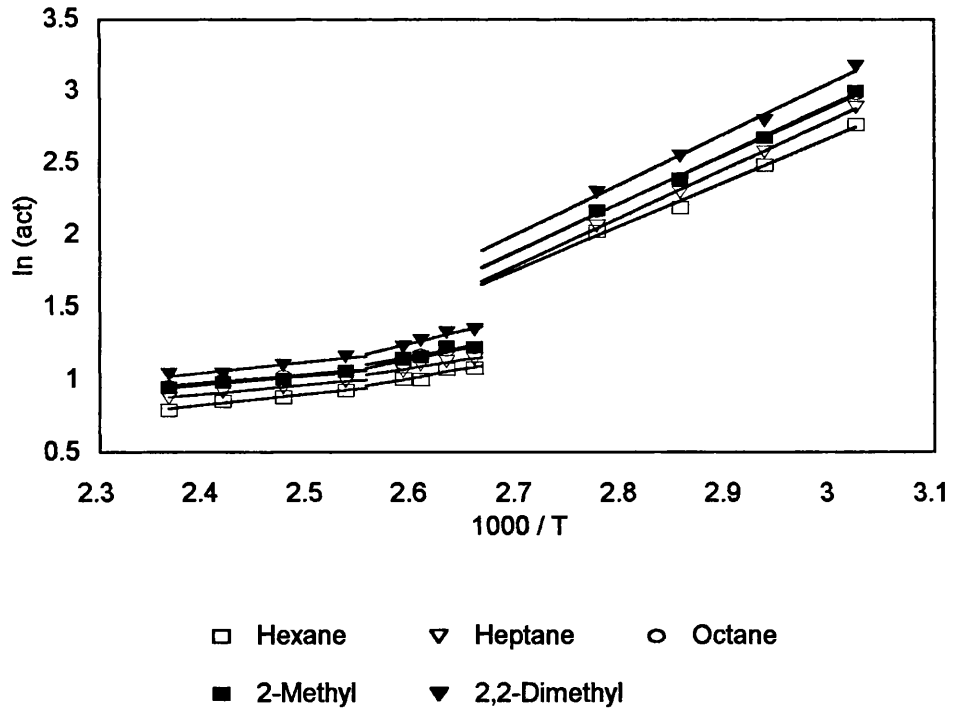

Figure A2.22: ln γ^{∞} vs 1/T for Aliphatic Probes in BDH1029

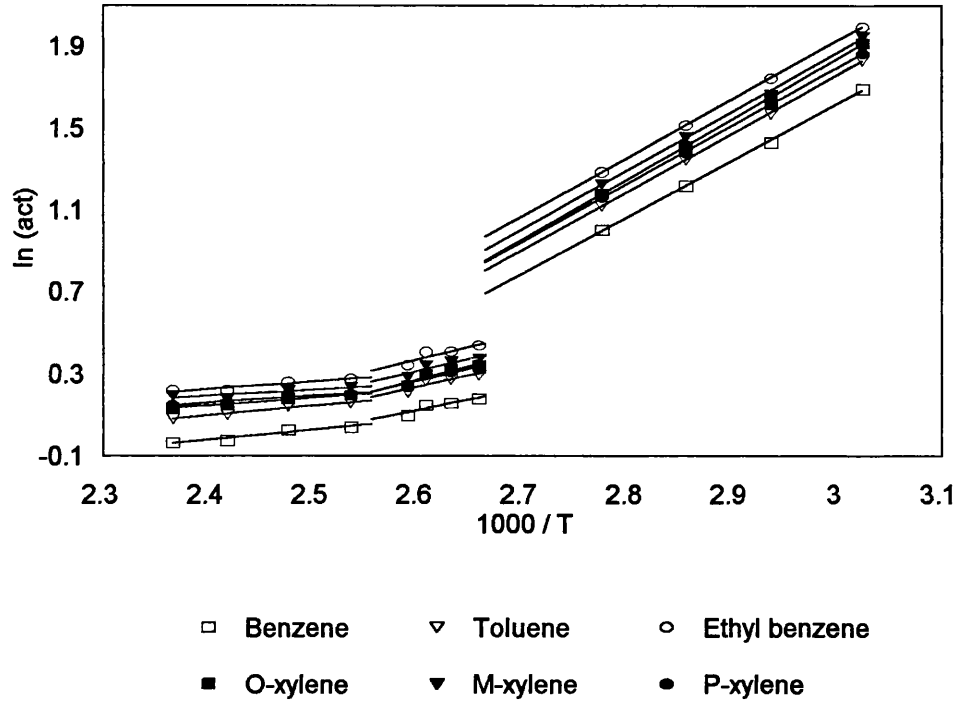

Figure A2.23: ln γ^{∞} vs 1/T for Aromatic Probes in BDH1029

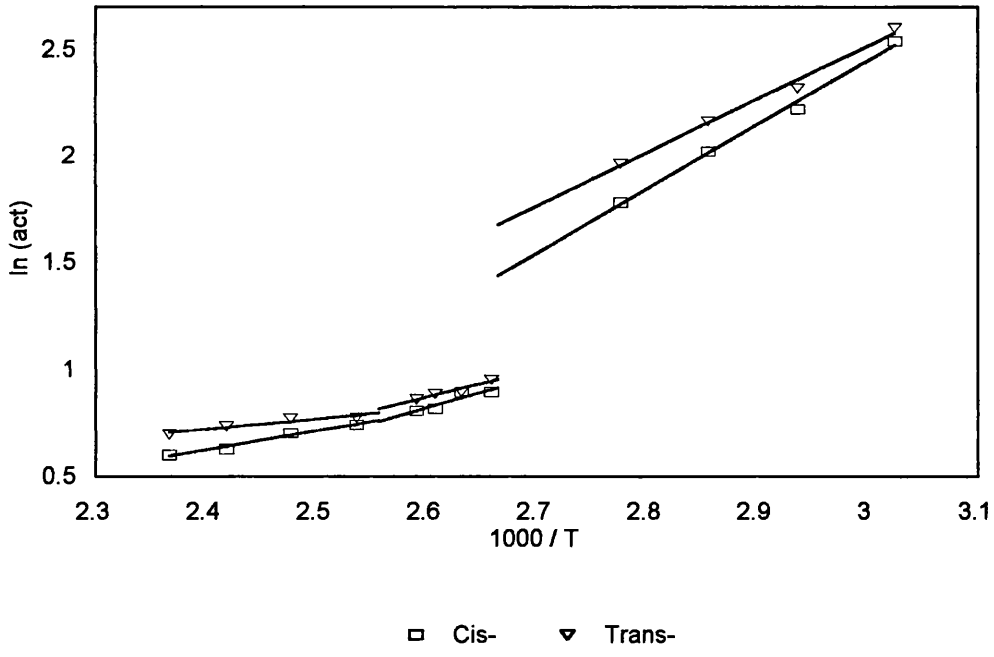

Figure A2.24: ln γ^{∞} vs 1/T for Isomeric Probes in BDH1029

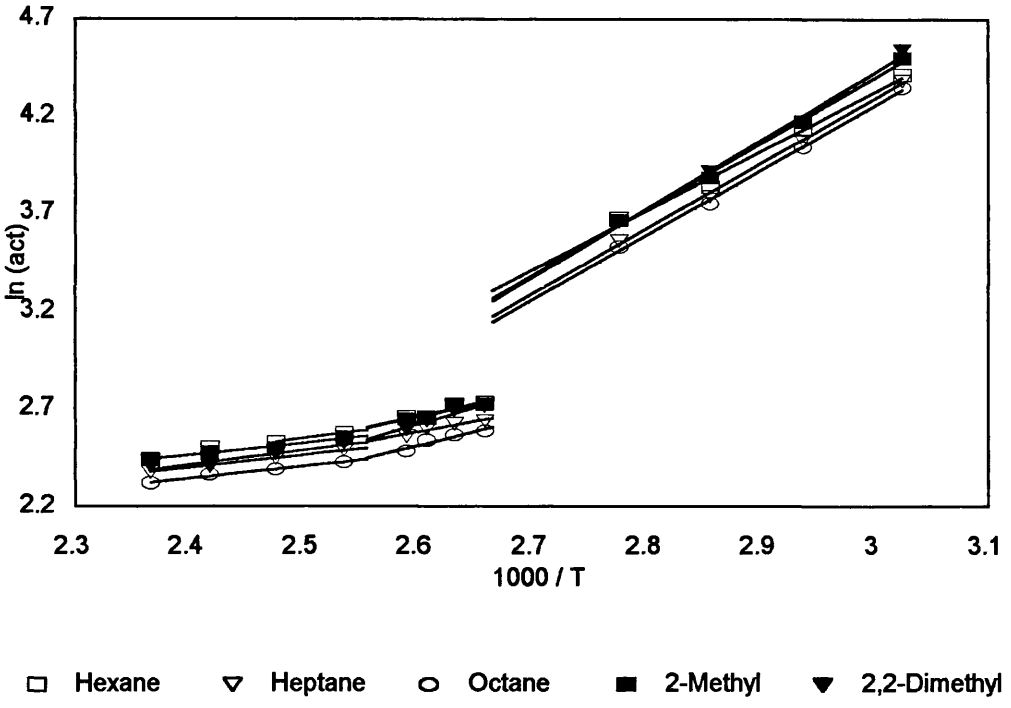

Figure A2.25: ln Ω° vs 1/T for Aliphatic Probes in BDH1029

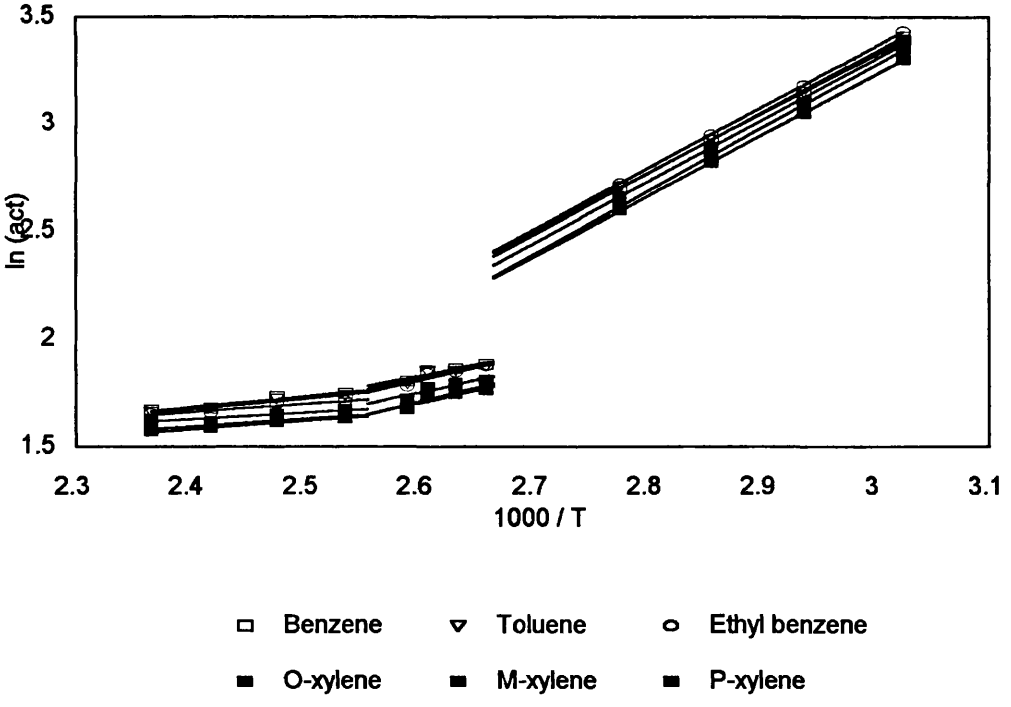

Figure A2.26: ln Ω° vs 1/T for Aromatic Probes in BDH1029

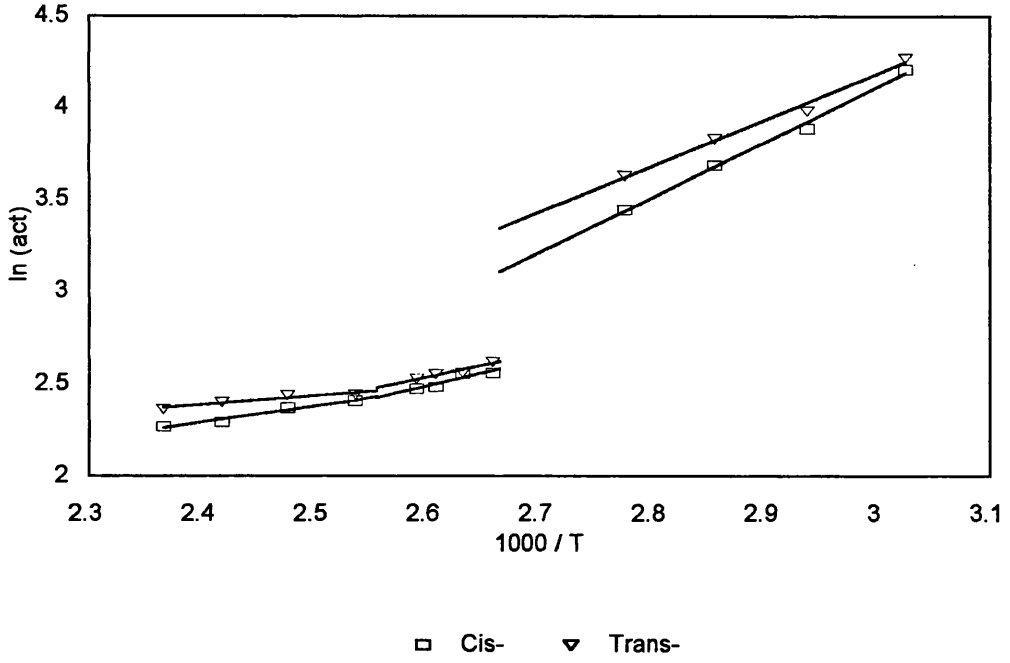

Figure A2.27: ln Ω^{∞} vs 1/T for Isomeric Probes in BDH1029

Probe	Enthalpic kJ mol^{-1}			Entropic J mol^{-1} K^{-1}		
	ΔH^s	ΔH^e	ΔH^{vap}	ΔS^s	ΔS^e	ΔS^{vap}
Hexane	-4.03 (0.22)	25.29 (0.23)	-29.32 (0.45)	15.05 (0.04)	53.63 (0.04)	-38.58 (0.08)
Heptane	-6.23 (0.09)	27.72 (0.11)	-33.95 (0.20)	15.64 (0.02)	59.94 (0.02)	-44.29 (0.04)
Octane	-10.98 (0.10)	27.57 (0.12)	-38.55 (0.22)	8.66 (0.02)	58.71 (0.02)	-50.05 (0.04)
2-Me	-4.27 (0.15)	28.06 (0.17)	-32.32 (0.32)	18.22 (0.03)	60.06 (0.03)	-41.84 (0.06)
2,2-DiMe	-5.69 (0.19)	29.04 (0.21)	-34.73 (0.40)	17.32 (0.04)	61.70 (0.04)	-44.38 (0.08)
Benzene	-8.62 (0.04)	22.94 (0.06)	-31.56 (0.10)	13.07 (0.01)	55.38 (0.01)	-42.31 (0.02)
Toluene	-12.06 (0.02)	23.68 (0.04)	-35.74 (0.06)	10.32 (0.01)	56.43 (0.01)	-46.12 (0.02)
Ethylbenzene	-15.85 (0.02)	23.80 (0.01)	-39.65 (0.03)	4.94 (0.01)	55.40 (0.01)	-50.46 (0.02)
O-Xylene	-16.46 (0.02)	24.48 (0.03)	-40.94 (0.05)	6.38 (0.01)	58.17 (0.01)	-51.79 (0.02)
M-Xylene	-16.27 (0.08)	23.89 (0.09)	-40.16 (0.17)	5.13 (0.01)	56.16 (0.02)	-51.02 (0.03)
P-Xylene	-16.28 (0.01)	23.59 (0.03)	-39.87 (0.04)	5.39 (0.01)	55.85 (0.01)	-50.46 (0.02)
Cis-	-4.52 (0.16)	25.06 (0.17)	-29.58 (0.33)	15.52 (0.03)	54.85 (0.03)	-39.33 (0.06)
Trans-	-8.44 (0.18)	20.91 (0.19)	-29.34 (0.37)	2.92 (0.03)	41.80 (0.04)	-38.87 (0.07)
R(+)	-21.11 (0.03)	n/a	n/a	-12.76 (0.01)	n/a	n/a
S(-)	-20.14 (0.06)	n/a	n/a	-9.69 (0.01)	n/a	n/a

Table A2.7: Physiochemical Results for BDH1029 in the Crystalline Phase

Probe	Enthalpic kJ mol^{-1}			Entropic J mol^{-1} K^{-1}		
	ΔH^s	ΔH^e	ΔH^{vap}	ΔS^s	ΔS^e	ΔS^{vap}
Hexane	-16.84 (0.39)	10.70 (0.39)	-27.54 (0.78)	-14.30 (0.02)	19.40 (0.02)	-33.69 (0.04)
Heptane	-22.74 (0.27)	9.26 (0.27)	-32.00 (0.54)	-23.88 (0.01)	15.05 (0.01)	-38.93 (0.02)
Octane	-24.24 (0.38)	12.11 (0.37)	-36.36 (0.75)	-22.05 (0.02)	21.97 (0.02)	-44.02 (0.04)
2-Me	-19.74 (0.43)	10.68 (0.42)	-30.42 (0.85)	-18.51 (0.02)	18.10 (0.02)	-36.61 (0.04)
2,2-DiMe	-18.33 (0.31)	14.58 (0.30)	-32.91 (0.62)	-11.92 (0.02)	27.48 (0.02)	-39.40 (0.04)
Benzene	-21.07 (0.34)	8.81 (0.34)	-29.89 (0.64)	-15.83 (0.02)	21.89 (0.02)	-37.72 (0.04)
Toluene	-24.84 (0.39)	9.19 (0.30)	-34.03 (0.69)	-19.50 (0.02)	21.92 (0.02)	-41.42 (0.04)
Ethylbenzene	-27.46 (0.43)	10.25 (0.43)	-37.71 (0.86)	-21.56 (0.02)	23.56 (0.02)	-45.12 (0.04)
O-Xylene	-27.98 (0.37)	11.07 (0.36)	-39.05 (0.73)	-20.08 (0.02)	26.51 (0.02)	-46.59 (0.04)
M-Xylene	-28.48 (0.41)	9.83 (0.41)	-38.31 (0.82)	-22.98 (0.02)	22.95 (0.02)	-45.93 (0.04)
P-Xylene	-28.18 (0.40)	9.85 (0.39)	-38.03 (0.79)	-22.01 (0.02)	23.40 (0.02)	-45.42 (0.04)
Cis-	-15.91 (0.42)	12.03 (0.42)	-27.93 (0.84)	-10.35 (0.02)	24.46 (0.02)	-34.80 (0.04)
Trans-	-17.07 (0.27)	10.47 (0.27)	-27.54 (0.54)	-13.92 (0.01)	20.00 (0.01)	-33.92 (0.02)
R(+)	-26.19 (0.47)	n/a	n/a	-21.59 (0.02)	n/a	n/a
S(-)	-28.54 (0.22)	n/a	n/a	-27.91 (0.01)	n/a	n/a

Table A2.8: Physiochemical Results for BDH1029 in the Cholesteric Mesophase

Probe	Enthalpic kJ mol^{-1}			Entropic J mol^{-1} K^{-1}		
	ΔH^s	ΔH^e	ΔH^{vap}	ΔS^s	ΔS^e	ΔS^{vap}
Hexane	-19.88 (0.11)	6.31 (0.10)	-26.19 (0.21)	-22.00 (0.14)	8.25 (0.01)	-30.25 (0.15)
Heptane	-25.13 (0.03)	5.41 (0.03)	-30.54 (0.06)	-29.74 (0.01)	5.48 (0.01)	-35.22 (0.02)
Octane	-29.77 (0.07)	4.99 (0.05)	-34.76 (0.12)	-36.12 (0.01)	3.83 (0.01)	-39.95 (0.02)
2-Me	-23.79 (0.07)	5.17 (0.08)	-28.96 (0.15)	-28.53 (0.01)	4.37 (0.01)	-32.90 (0.02)
2,2-DiMe	-25.22 (0.15)	6.25 (0.17)	-31.47 (0.32)	-29.46 (0.02)	6.27 (0.02)	-35.73 (0.04)
Benzene	-24.48 (0.09)	4.16 (0.09)	-28.65 (0.18)	-24.40 (0.01)	10.17 (0.01)	-34.56 (0.02)
Toluene	-28.83 (0.07)	3.96 (0.06)	-32.78 (0.13)	-29.57 (0.01)	8.67 (0.01)	-38.24 (0.02)
Ethylbenzene	-33.27 (0.08)	3.05 (0.09)	-36.32 (0.17)	-36.14 (0.01)	5.44 (0.01)	-41.58 (0.02)
O-Xylene	-34.57 (0.04)	3.17 (0.03)	-37.74 (0.07)	-36.89 (0.01)	6.40 (0.01)	-43.28 (0.02)
M-Xylene	-34.54 (0.10)	2.51 (0.11)	-37.05 (0.21)	-36.33 (0.01)	4.41 (0.01)	-42.74 (0.02)
P-Xylene	-33.96 (0.09)	2.83 (0.09)	-36.79 (0.18)	-36.79 (0.01)	5.45 (0.01)	-42.24 (0.02)
Cis-	-19.30 (0.11)	7.30 (0.11)	-26.59 (0.22)	-19.08 (0.01)	12.32 (0.01)	-31.40 (0.02)
Trans-	-22.16 (0.14)	3.99 (0.12)	-26.15 (0.26)	-26.79 (0.02)	3.60 (0.01)	-30.39 (0.03)
R(+)	-33.68 (0.26)	n/a	n/a	-40.63 (0.03)	n/a	n/a
S(-)	-33.52 (0.08)	n/a	n/a	-40.18 (0.10)	n/a	n/a

Table A2.9: Physiochemical Results for BDH1029 in the Isotropic Phase

A2.4 LMM1: ln Vg°, ln γ^{∞}, ln Ω^{∞}, ΔH^s, ΔH^e, ΔS^s, ΔS^e

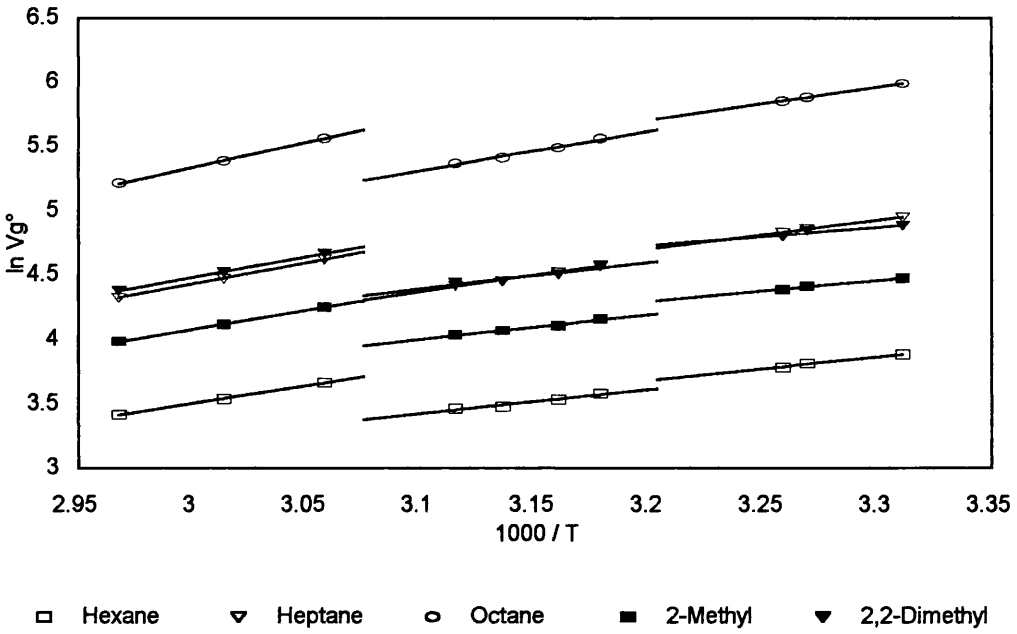

Figure A2.28: ln Vg° vs 1/T for Aliphatic Probes in LMM1

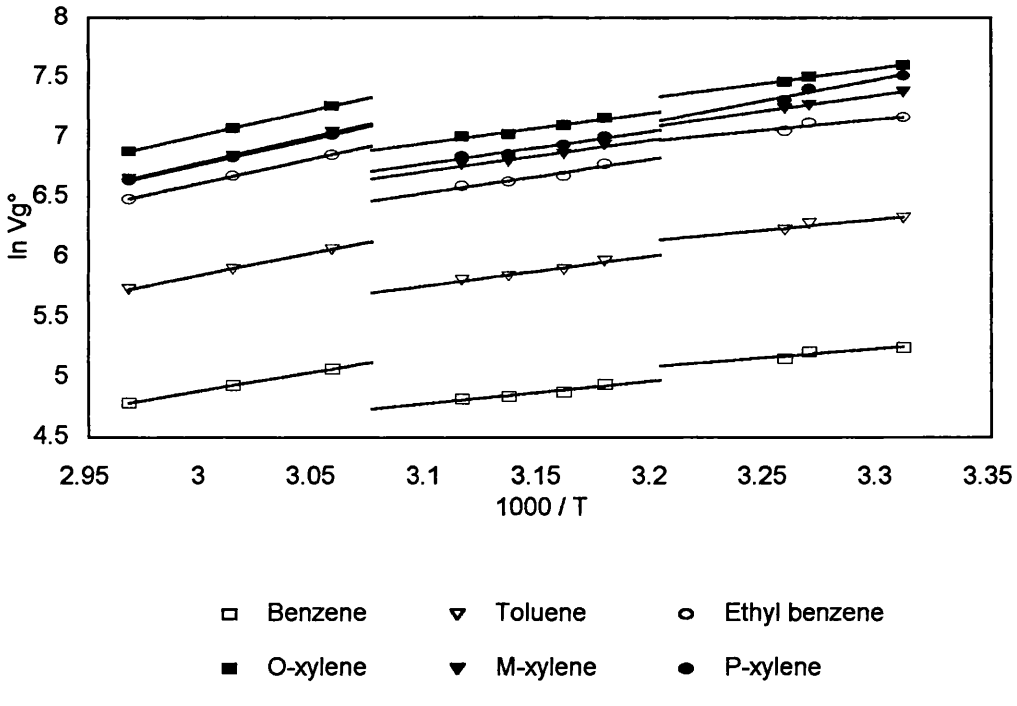

Figure A2.29: ln Vg° vs 1/T for Aromatic Probes in LMM1

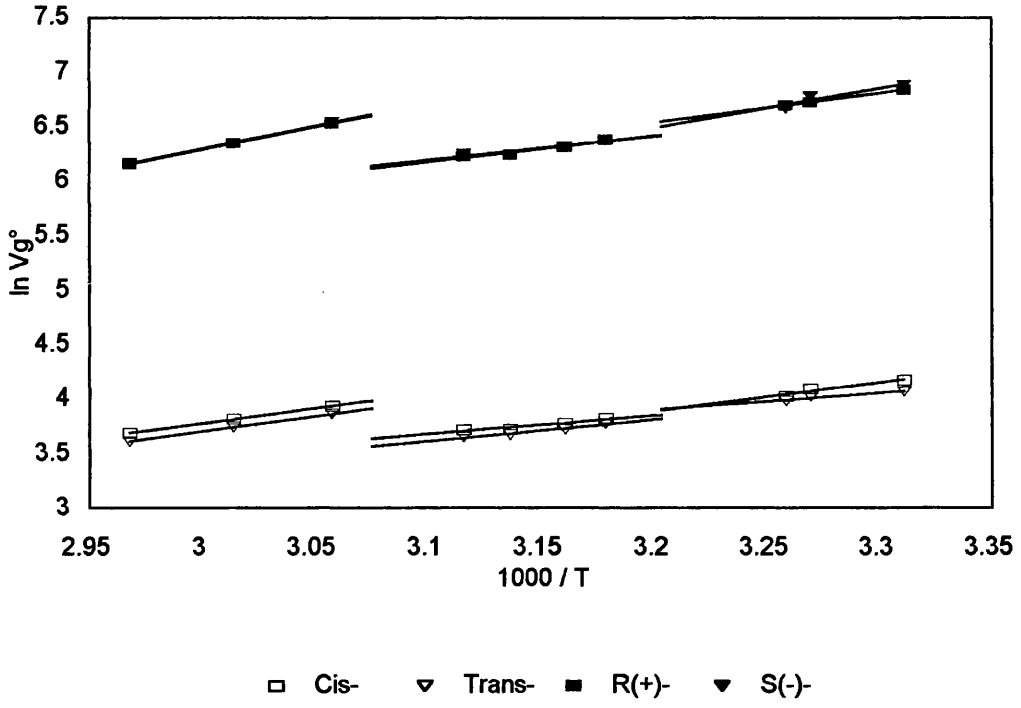

Figure A2.30: ln Vg° vs 1/T for Isomeric Probes in LMM1

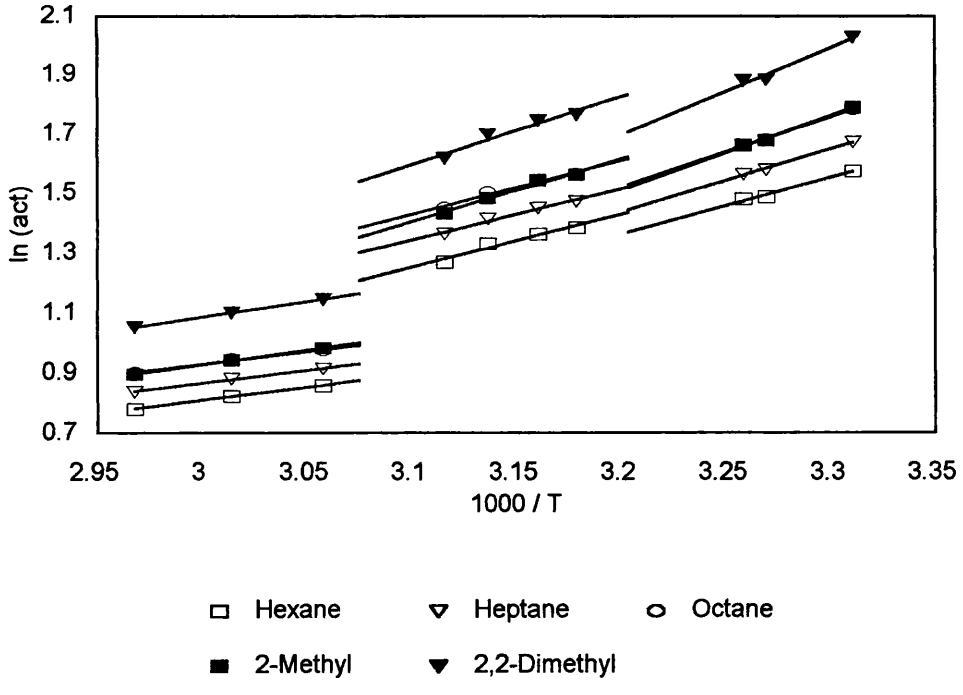

Figure A2.31: ln γ^{∞} vs 1/T for Aliphatic Probes in LMM1

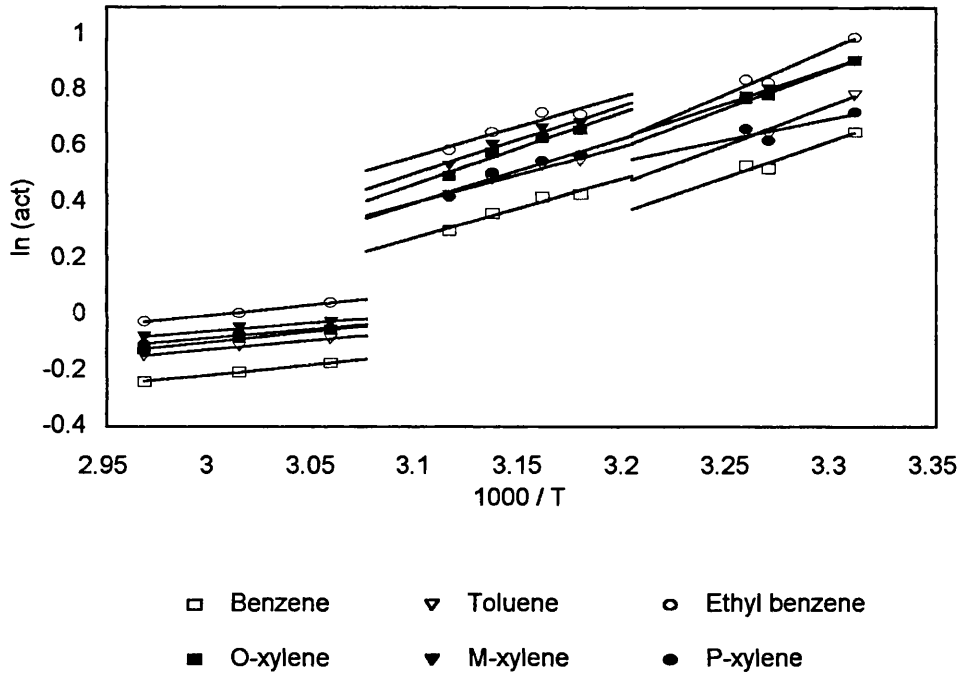

Figure A2.32: ln γ^{∞} vs 1/T for Aromatic Probes in LMM1

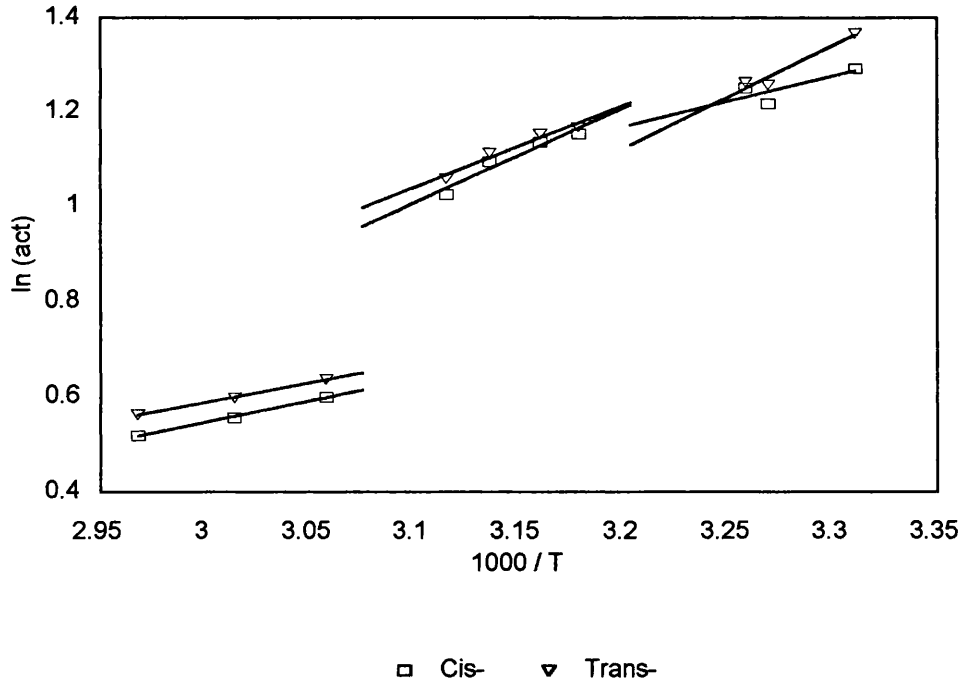

Figure A2.33: ln γ^{∞} vs 1/T for Isomeric Probes in LMM1

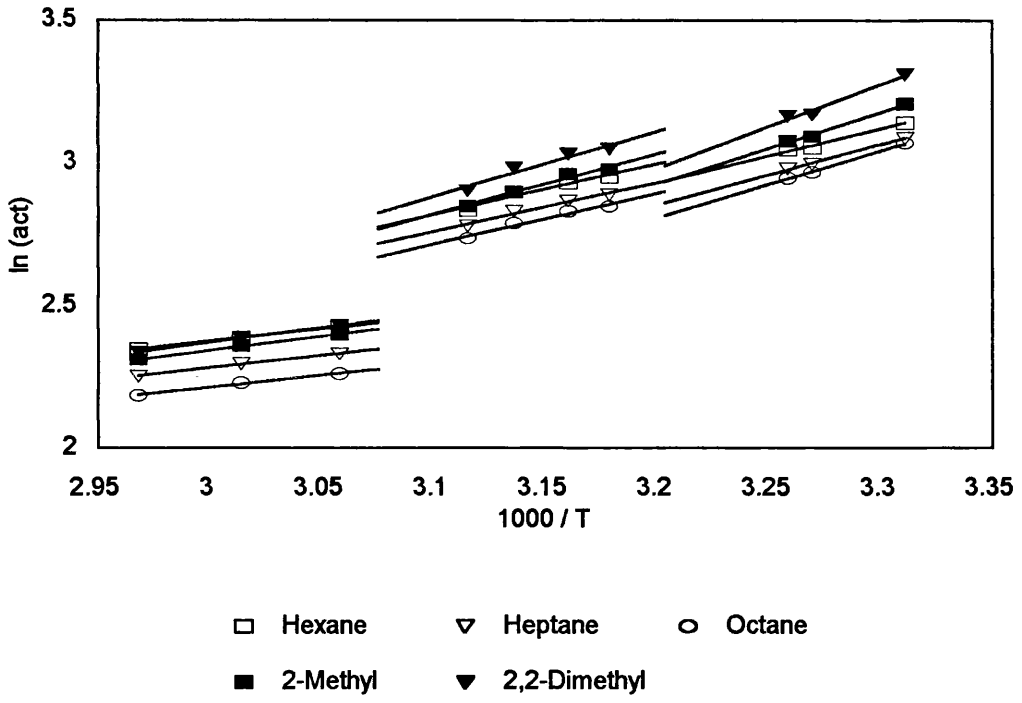

Figure A2.34: ln Ω° vs 1/T for Aliphatic Probes in LMM1

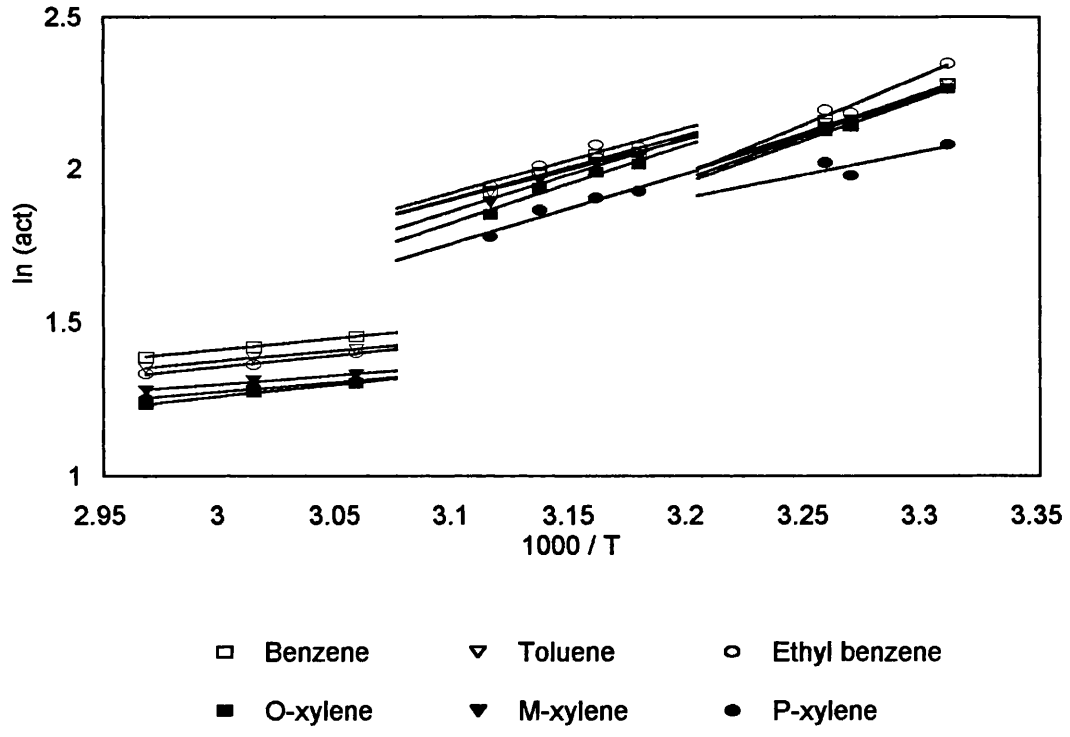

Figure A2.35: ln Ω° vs 1/T for Aromatic Probes in LMM1

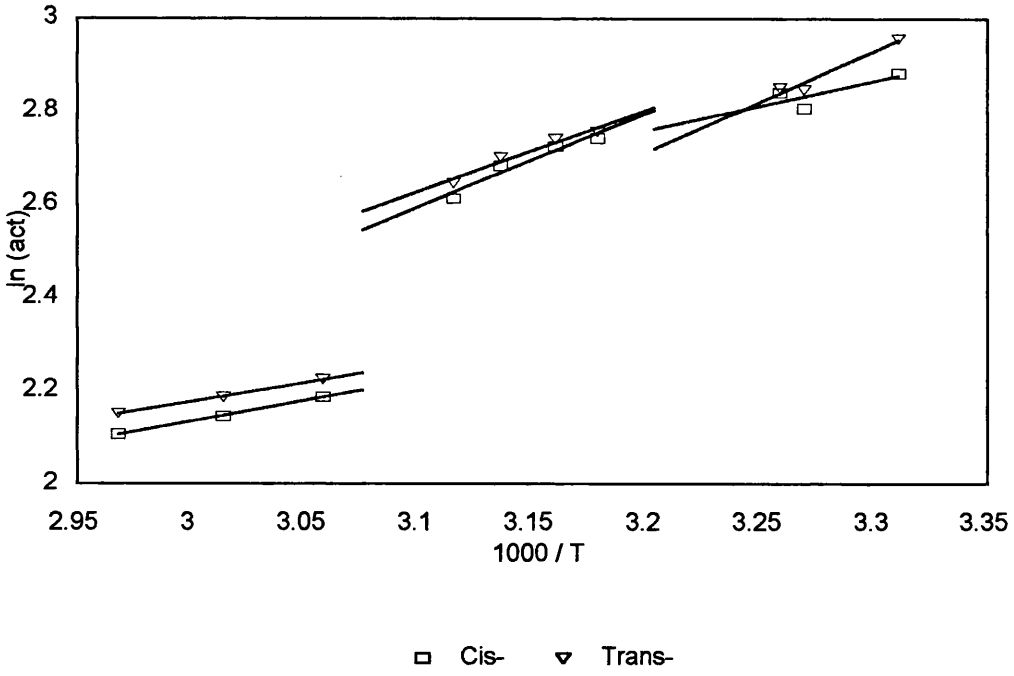

Figure A2.36: ln Ω^{∞} vs 1/T for Isomeric Probes in LMM1

Probe	Enthalpic kJ mol^{-1}			Entropic J mol^{-1} K^{-1}		
	ΔH^s	ΔH^e	ΔH^{vap}	ΔS^s	ΔS^e	ΔS^{vap}
Hexane	-15.46 (0.23)	15.89 (0.24)	-31.35 (0.47)	-4.68 (0.01)	39.52 (0.01)	-44.20 (0.02)
Heptane	-18.76 (0.13)	17.55 (0.13)	-36.31 (0.26)	-6.74 (0.01)	44.20 (0.01)	-50.94 (0.02)
Octane	-21.75 (0.10)	19.61 (0.11)	-41.36 (0.21)	-7.99 (0.01)	50.08 (0.01)	-58.07 (0.02)
2-Me	-13.56 (0.18)	20.98 (0.18)	-34.54 (0.36)	6.54 (0.01)	54.58 (0.01)	-48.04 (0.02)
2,2-DiMe	-12.17 (0.51)	24.63 (0.52)	-36.80 (1.03)	14.58 (0.02)	64.72 (0.02)	-50.14 (0.04)
Benzene	-12.56 (0.70)	21.01 (0.70)	-33.58 (1.40)	16.29 (0.03)	64.17 (0.03)	-47.89 (0.06)
Toluene	-14.74 (0.69)	23.14 (0.70)	-37.89 (1.39)	18.04 (0.03)	70.13 (0.03)	-52.10 (0.06)
Ethylbenzene	-15.49 (0.83)	26.71 (0.84)	-42.21 (1.67)	22.52 (0.03)	80.23 (0.03)	-57.71 (0.06)
O-Xylene	-20.63 (0.29)	22.86 (0.29)	-43.49 (0.58)	9.12 (0.01)	68.16 (0.01)	-59.03 (0.02)
M-Xylene	-22.17 (0.03)	20.47 (0.03)	-42.64 (0.06)	2.18 (0.01)	60.23 (0.01)	-58.05 (0.02)
P-Xylene	-29.71 (1.08)	12.62 (1.08)	-42.33 (2.16)	-21.61 (0.04)	35.81 (0.04)	-57.42 (0.08)
Cis-	-22.40 (0.83)	8.93 (0.83)	-31.33 (1.66)	-25.20 (0.03)	18.87 (0.03)	-44.07 (0.06)
Trans-	-13.22 (0.52)	18.17 (0.52)	-31.39 (1.04)	4.28 (0.02)	48.80 (0.02)	-44.52 (0.04)
R(+)	-22.08 (0.17)	n/a	n/a	-2.13 (0.01)	n/a	n/a
S(-)	-30.19 (1.16)	n/a	n/a	-28.50 (0.04)	n/a	n/a

Table A2.10: Physiochemical Results for LMM1 in the Crystalline Phase

Probe	Enthalpic kJ mol^{-1}			Entropic J mol^{-1} K^{-1}		
	ΔH^s	ΔH^e	ΔH^{vap}	ΔS^s	ΔS^e	ΔS^{vap}
Hexane	-15.82 (0.30)	14.84 (0.30)	-30.67 (0.60)	-6.40 (0.01)	35.59 (0.01)	-42.00 (0.02)
Heptane	-21.21 (0.20)	14.29 (0.20)	-35.49 (0.40)	-15.20 (0.01)	33.10 (0.01)	-48.31 (0.02)
Octane	-25.45 (0.24)	14.91 (0.24)	-40.36 (0.48)	-20.54 (0.01)	34.33 (0.01)	-54.87 (0.02)
2-Me	-16.24 (0.23)	17.55 (0.23)	-33.78 (0.46)	-2.90 (0.01)	42.71 (0.01)	-45.61 (0.02)
2,2-DiMe	-16.94 (0.42)	19.15 (0.42)	-36.09 (0.84)	-1.78 (0.02)	46.08 (0.02)	-47.87 (0.04)
Benzene	-15.50 (0.36)	17.38 (0.36)	-32.88 (0.72)	5.90 (0.02)	51.54 (0.02)	-45.64 (0.04)
Toluene	-20.66 (0.28)	16.47 (0.27)	-37.13 (0.55)	-1.98 (0.01)	47.69 (0.01)	-49.67 (0.02)
Ethylbenzene	-23.45 (0.54)	17.84 (0.53)	-41.29 (1.07)	-4.17 (0.03)	50.59 (0.03)	-54.77 (0.06)
O-Xylene	-21.22 (0.40)	21.35 (0.39)	-42.57 (0.79)	6.21 (0.02)	62.29 (0.02)	-56.08 (0.04)
M-Xylene	-21.78 (0.39)	19.97 (0.38)	-41.75 (0.78)	2.50 (0.02)	57.69 (0.02)	-55.18 (0.04)
P-Xylene	-22.37 (0.46)	19.07 (0.46)	-41.44 (0.92)	1.20 (0.02)	55.78 (0.02)	-54.58 (0.04)
Cis-	-14.02 (0.37)	16.74 (0.36)	-30.76 (0.74)	1.29 (0.02)	43.52 (0.02)	-42.23 (0.04)
Trans-	-16.23 (0.28)	14.47 (0.27)	-30.70 (0.55)	-6.11 (0.01)	36.21 (0.01)	-42.32 (0.02)
R(+)	-20.12 (0.41)	n/a	n/a	3.13 (0.02)	n/a	n/a
S(-)	-18.14 (0.59)	n/a	n/a	9.42 (0.03)	n/a	n/a

Table A2.11: Physiochemical Results for LMM1 in the Smectic C Mesophase

Probe	Enthalpic kJ mol^{-1}			Entropic J mol^{-1} K^{-1}		
	ΔH^s	ΔH^e	ΔH^{vap}	ΔS^s	ΔS^e	ΔS^{vap}
Hexane	-22.82 (0.04)	7.14 (0.03)	-29.96 ()	-25.13 (0.02)	14.69 (0.01)	-39.82 (0.02)
Heptane	-27.44 (0.06)	7.24 (0.05)	-34.67 ()	-31.28 (0.01)	14.50 (0.01)	-45.78 (0.02)
Octane	-32.47 (0.08)	6.92 (0.07)	-39.84 ()	-38.85 (0.01)	13.02 (0.01)	-51.87 (0.02)
2-Me	-24.79 (0.03)	8.23 (0.03)	-33.01 ()	-26.27 (0.01)	15.29 (0.01)	-41.56 (0.02)
2,2-DiMe	-26.75 (0.02)	8.62 (0.01)	-35.37 ()	-28.83 (0.01)	16.82 (0.01)	-45.65 (0.02)
Benzene	-25.99 (0.01)	6.18 (0..01)	-32.18 ()	-23.15 (0.01)	20.33 (0.01)	-43.48 (0.02)
Toluene	-30.75 (0.03)	5.63 (0.03)	-36.38 ()	-29.45 (0.01)	17.93 (0.01)	-47.37 (0.02)
Ethylbenzene	-34.16 (0.05)	6.24 (0.06)	-40.40 ()	-33.30 (0.01)	18.73 (0.01)	-52.03 (0.02)
O-Xylene	-35.26 (0.05)	6.42 (0.04)	-41.68 ()	-33.28 (0.01)	20.06 (0.01)	-53.34 (0.02)
M-Xylene	-36.03 (0.09)	4.86 (0.08)	-40.89 ()	-37.48 (0.01)	15.04 (0.01)	-52.52 (0.02)
P-Xylene	-35.33 (0.10)	5.26 (0.09)	-40.59 ()	-35.48 (0.01)	16.46 (0.01)	-51.94 (0.02)
Cis-	-22.74 (0.03)	7.41 (0.04)	-30.15 ()	-22.67 (0.01)	17.69 (0.01)	-40.36 (0.02)
Trans-	-23.16 (0.03)	6.83 (0.04)	-29.99 ()	-24.53 (0.01)	15.60 (0.01)	-40.13 (0.02)
R(+)	-34.41 (0.02)	n/a	n/a	-36.76 (0.01)	n/a	n/a
S(-)	-34.72 (0.15)	n/a	n/a	-37.65 (0.01)	n/a	n/a

Table A2.12: Physiochemical Results for LMM1 in the Isotropic Phase

A2.5 LCP1: ln Vg°, ln Ω^{∞}, ΔH^{s}, ΔH^{e}, ΔS^{s}, ΔS^{e}

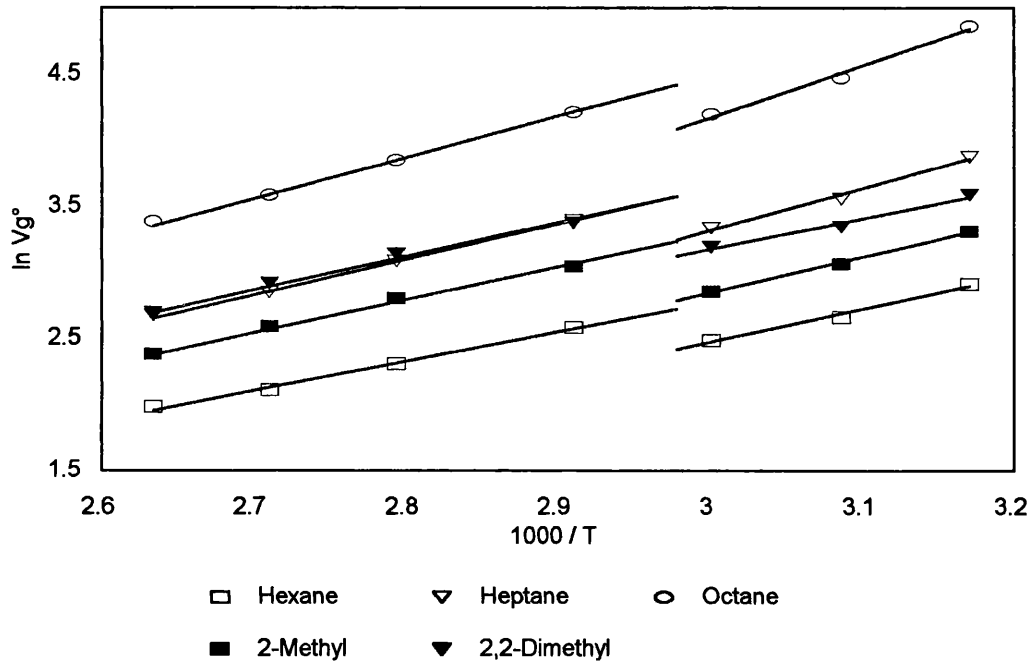

Figure A2.37: ln Vg° vs 1/T for Aliphatic Probes in LCP1

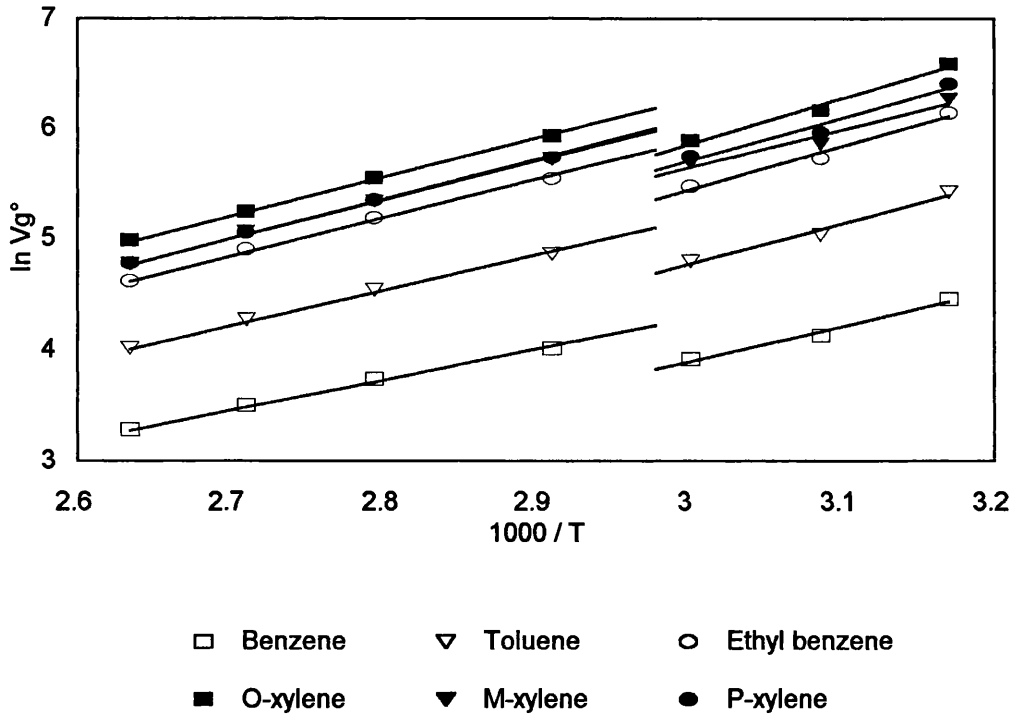

Figure A2.38: ln Vg° vs 1/T for Aromatic Probes in LCP1

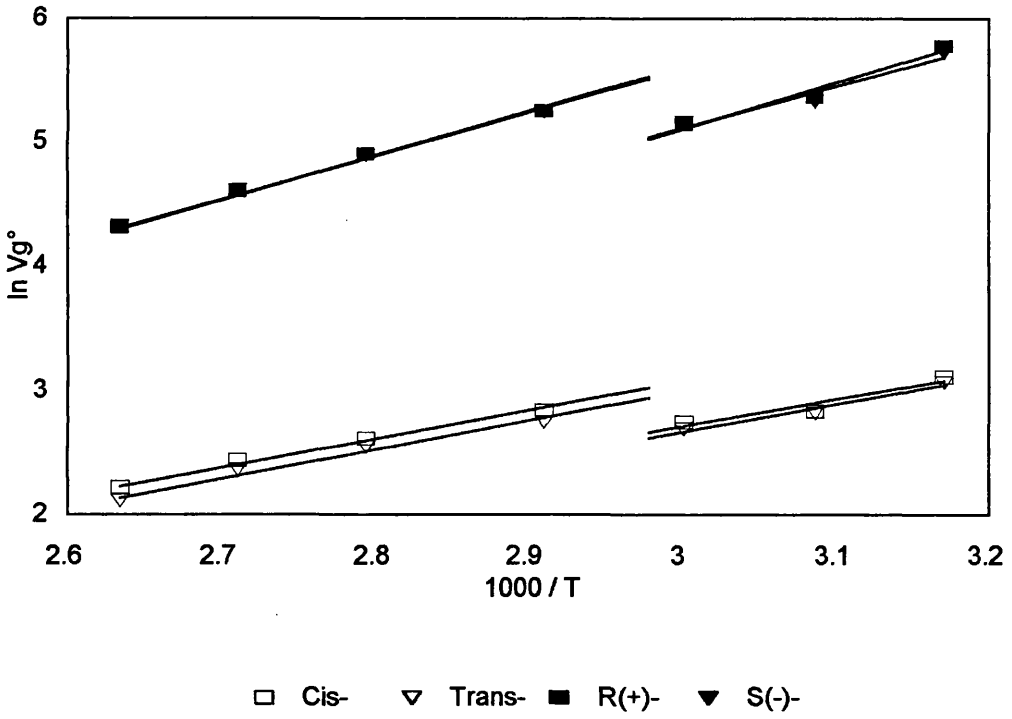

Figure A2.39: ln Vg° vs 1/T for Isomeric Probes in LCP1

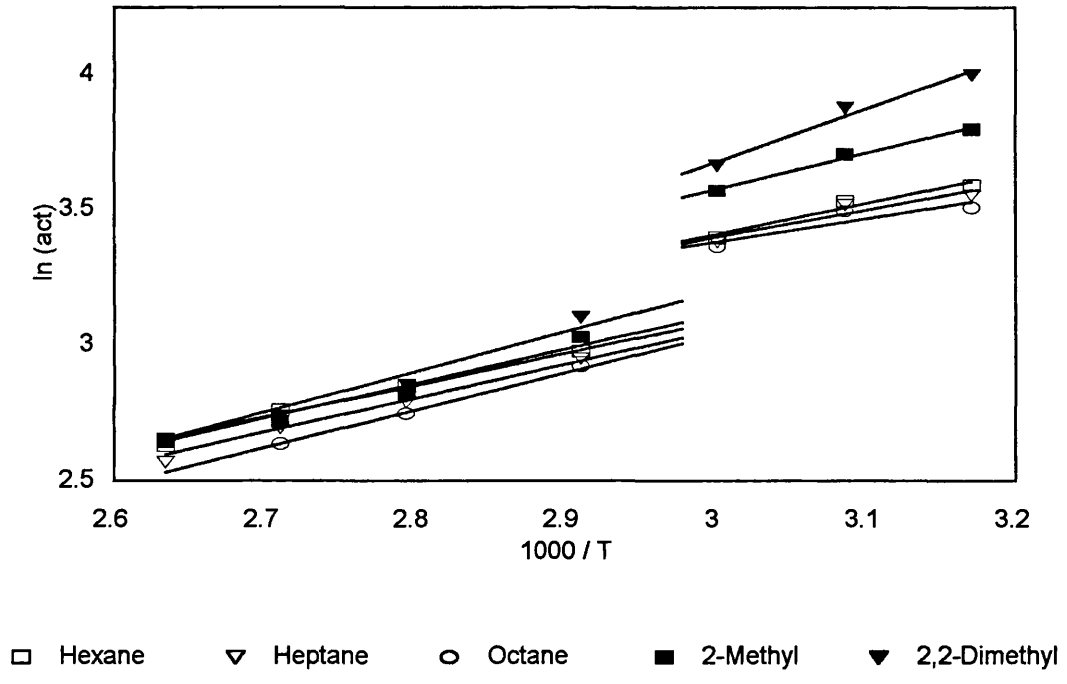

Figure A2.40: ln Ω° vs 1/T for Aliphatic Probes in LCP1

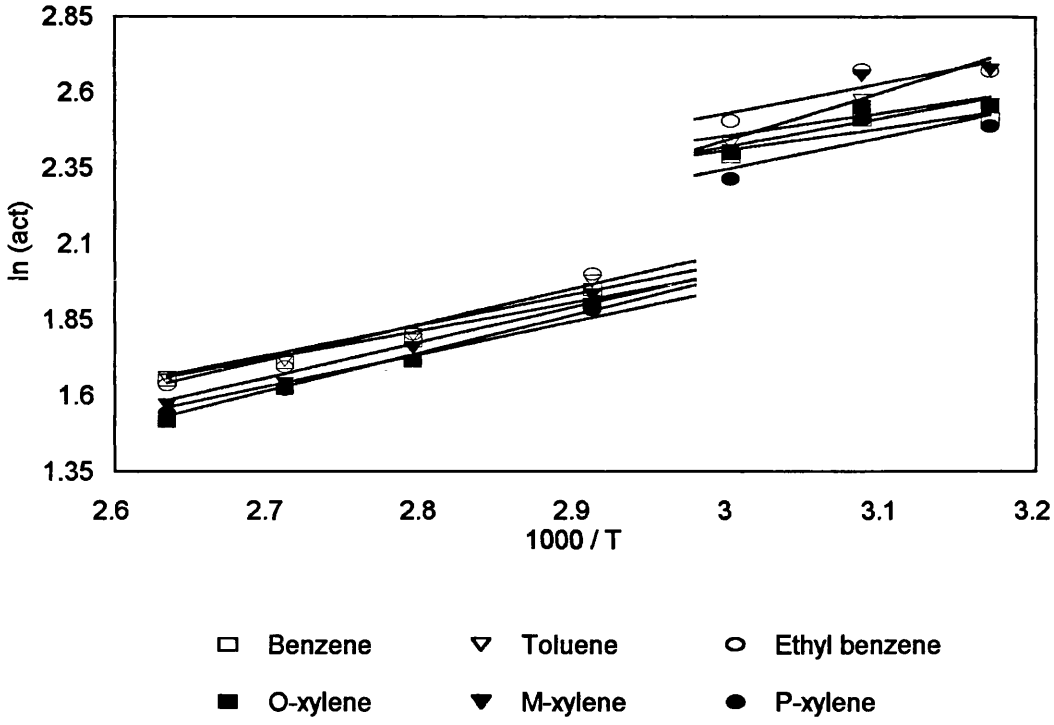

Figure A2.41: ln Ω° vs 1/T for Aromatic Probes in LCP1

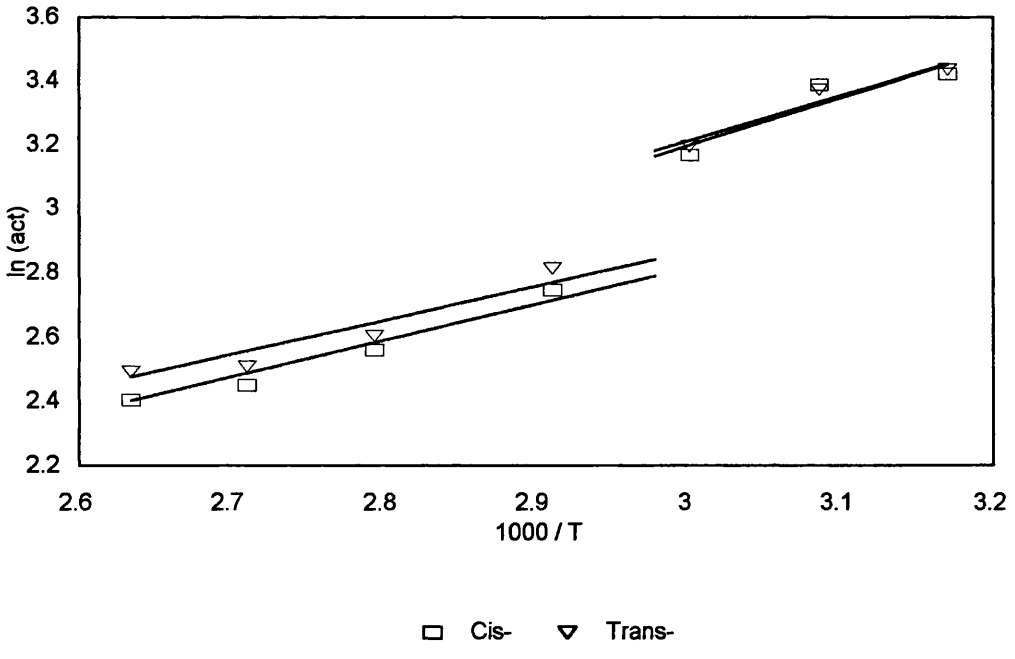

Figure A2.42: ln Ω° vs 1/T for Isomeric Probes in LCP1

Probe	Enthalpic kJ mol^{-1}			Entropic J mol^{-1} K^{-1}		
	ΔH^s	ΔH^e	ΔH^{vap}	ΔS^s	ΔS^e	ΔS^{vap}
Hexane	-20.83 (0.28)	9.52 (0.26)	-30.35 (0.53)	-27.77 (0.03)	47.86 (0.03)	-75.63 (0.06)
Heptane	-26.68 (0.34)	8.44 (0.33)	-35.12 (0.67)	-38.31 (0.04)	43.46 (0.04)	-81.77 (0.08)
Octane	-32.71 (0.42)	7.20 (0.40)	-39.92 (0.82)	-49.31 (0.05)	38.80 (0.05)	-88.11 (0.10)
2-Me	-22.28 (0.16)	11.15 (0.14)	-33.43 (0.30)	-29.02 (0.02)	50.13 (0.02)	-79.15 (0.04)
2,2-DiMe	-19.24 (0.31)	16.53 (0.30)	-35.77 (0.61)	-17.16 (0.04)	64.32 (0.04)	-81.48 (0.08)
Benzene	-26.52 (0.42)	6.04 (0.41)	-32.56 (0.83)	-33.03 (0.05)	46.25 (0.05)	-79.28 (0.10)
Toluene	-30.60 (0.53)	6.19 (0.51)	-36.79 (1.04)	-38.01 (0.06)	45.23 (0.06)	-83.24 (0.11)
Ethylbenzene	-32.81 (0.60)	8.08 (0.58)	-40.89 (1.18)	-39.02 (0.07)	49.11 (0.07)	-88.13 (0.14)
O-Xylene	-34.46 (0.55)	7.71 (0.53)	-42.17 (1.08)	-40.55 (0.07)	48.90 (0.06)	-89.44 (0.13)
M-Xylene	-28.41 (0.80)	12.95 (0.78)	-41.36 (1.58)	-24.13 (0.10)	64.45 (0.09)	-88.58 (0.19)
P-Xylene	-32.44 (0.76)	8.62 (0.74)	-41.05 (1.50)	-35.74 (0.10)	52.24 (0.09)	-87.99 (0.19)
Cis-	-18.04 (0.65)	12.45 (0.64)	-30.48 (1.29)	-17.41 (0.08)	58.60 (0.08)	-76.00 (0.16)
Trans-	-18.52 (0.39)	11.86 (0.38)	-30.38 (0.77)	-19.23 (0.05)	56.72 (0.05)	-75.94 (0.10)
R(+)	-30.93 (0.69)	n/a	n/a		n/a	n/a
S(-)	-27.64 (0.76)	n/a	n/a		n/a	n/a

Table A2.13: Physiochemical Results for LCP1 in the Smectic C Mesophase

Probe	Enthalpic kJ mol^{-1}			Entropic J mol^{-1} K^{-1}		
	ΔH^s	ΔH^e	ΔH^{vap}	ΔS^s	ΔS^e	ΔS^{vap}
Hexane	-18.60 (0.08)	9.70 (0.07)	-28.31 (0.15)	-18.57 (0.02)	51.10 (0.02)	-69.67 (0.04)
Heptane	-22.49 (0.07)	10.34 (0.08)	-32.83 (0.15)	-23.06 (0.02)	52.03 (0.02)	-75.09 (0.04)
Octane	-25.86 (0.08)	11.43 (0.10)	-37.29 (0.18)	-26.09 (0.02)	54.34 (0.03)	-80.43 (0.05)
2-Me	-20.69 (0.10)	10.55 (0.13)	-31.24 (0.23)	-20.57 (0.03)	52.16 (0.03)	-72.73 (0.06)
2,2-DiMe	-21.36 (0.12)	12.33 (0.15)	-33.70 (0.27)	-19.71 (0.03)	55.72 (0.04)	-75.42 (0.07)
Benzene	-22.92 (0.10)	7.68 (0.12)	-30.60 (0.22)	-19.00 (0.03)	54.55 (0.03)	-73.56 (0.06)
Toluene	-26.46 (0.11)	8.30 (0.13)	-34.76 (0.14)	-22.22 (0.03)	55.08 (0.03)	-77.30 (0.06)
Ethylbenzene	-28.86 (0.12)	9.67 (0.15)	-38.53 (0.27)	-23.53 (0.03)	57.71 (0.04)	-81.24 (0.07)
O-Xylene	-29.45 (0.07)	10.39 (0.10)	-39.84 (0.17)	-22.12 (0.02)	60.52 (0.03)	-82.64 (0.05)
M-Xylene	-29.41 (0.10)	9.67 (0.12)	-39.09 (0.22)	-23.71 (0.03)	58.23 (0.03)	-81.94 (0.06)
P-Xylene	-29.95 (0.10)	8.85 (0.12)	-38.80 (0.22)	-25.16 (0.03)	56.24 (0.03)	-81.40 (0.06)
Cis-	-19.26 (0.11)	9.39 (0.14)	-28.65 (0.25)	-18.06 (0.03)	52.60 (0.04)	-70.66 (0.07)
Trans-	-19.51 (0.16)	8.81 (0.18)	-28.32 (0.34)	-19.46 (0.04)	50.47 (0.05)	-69.93 (0.09)
R(+)	-29.79 (0.16)	n/a	n/a	-28.58 (0.04)	n/a	n/a
S(-)	-29.18 (0.14)	n/a	n/a	-26.89 (0.04)	n/a	n/a

Table A2.14: Physiochemical Results for LCP1 in the Isotropic Phase

A2.6 LCP2: ln Vg°, ln Ω^{∞}, ΔH^{s}, ΔH^{e}, ΔS^{s}, ΔS^{e}

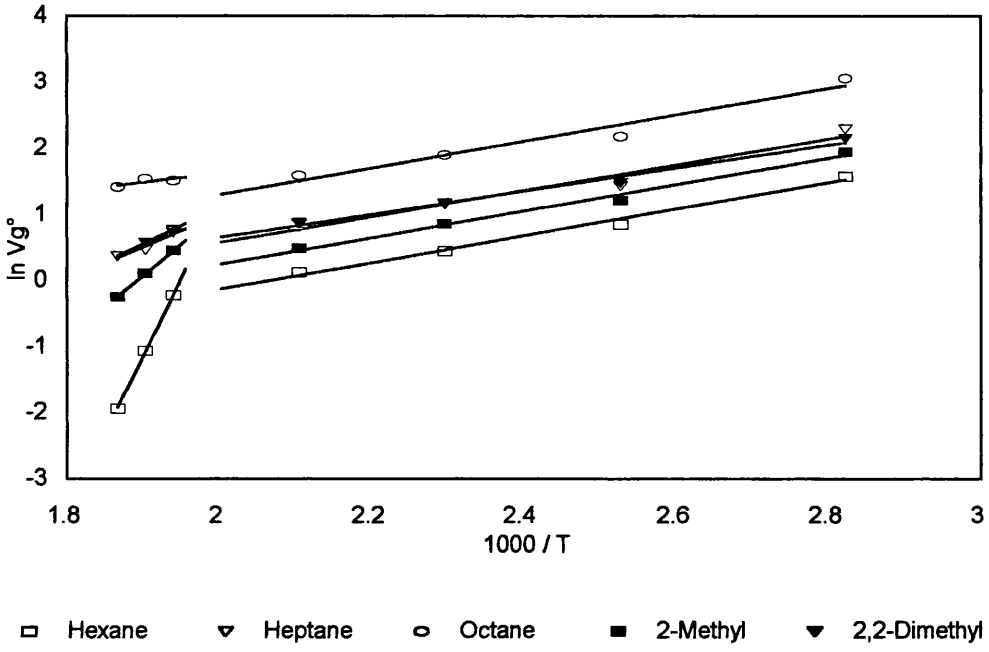

Figure A2.43: ln Vg° vs 1/T for Aliphatic Probes in LCP2

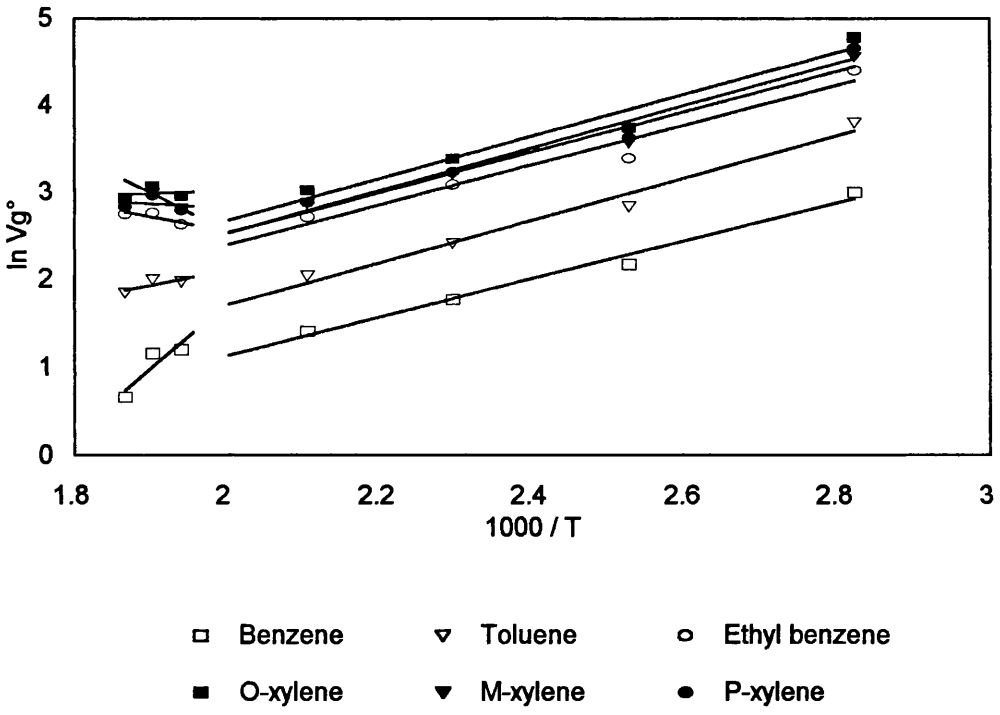

Figure A2.44: ln Vg° vs 1/T for Aromatic Probes in LCP2

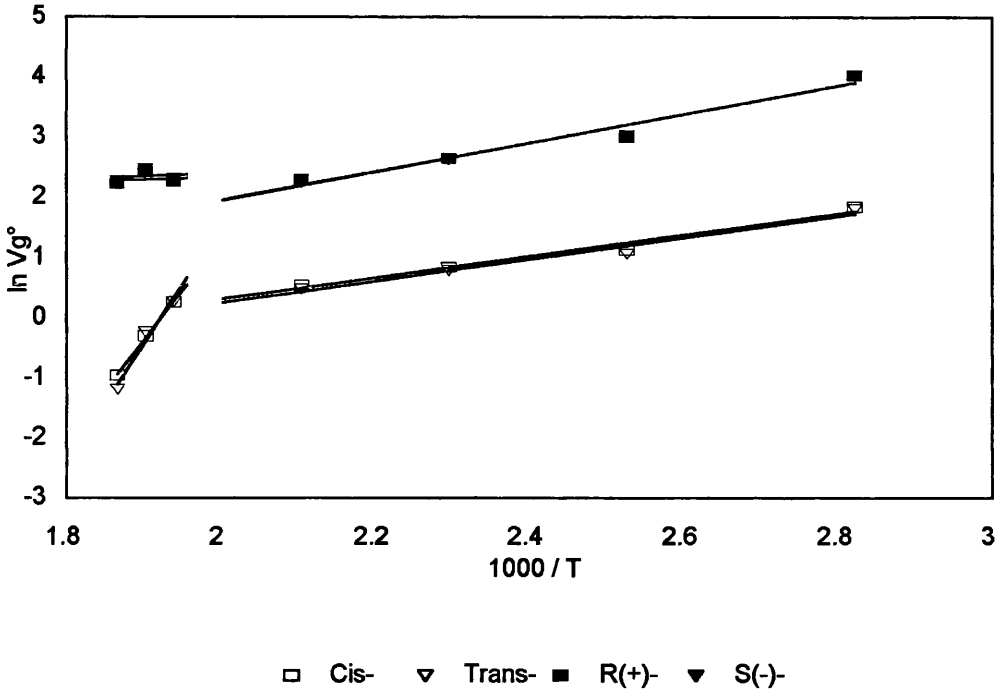

Figure A2.45: ln Vg° vs 1/T for Isomeric Probes in LCP2

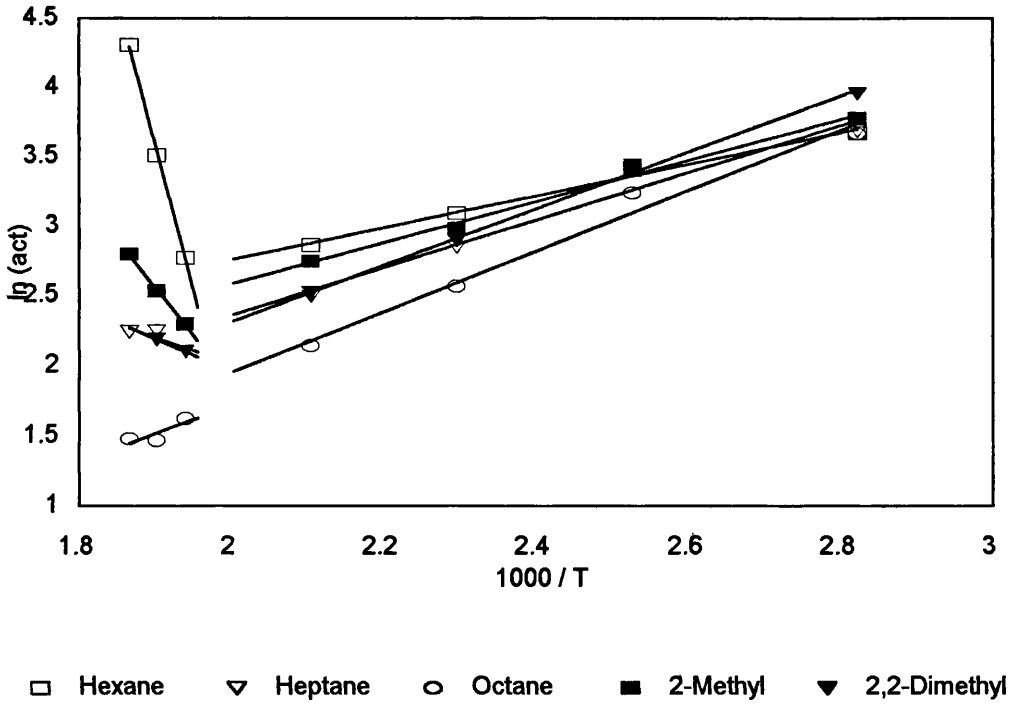

Figure A2.46: ln Ω° vs 1/T for Aliphatic Probes in LCP2

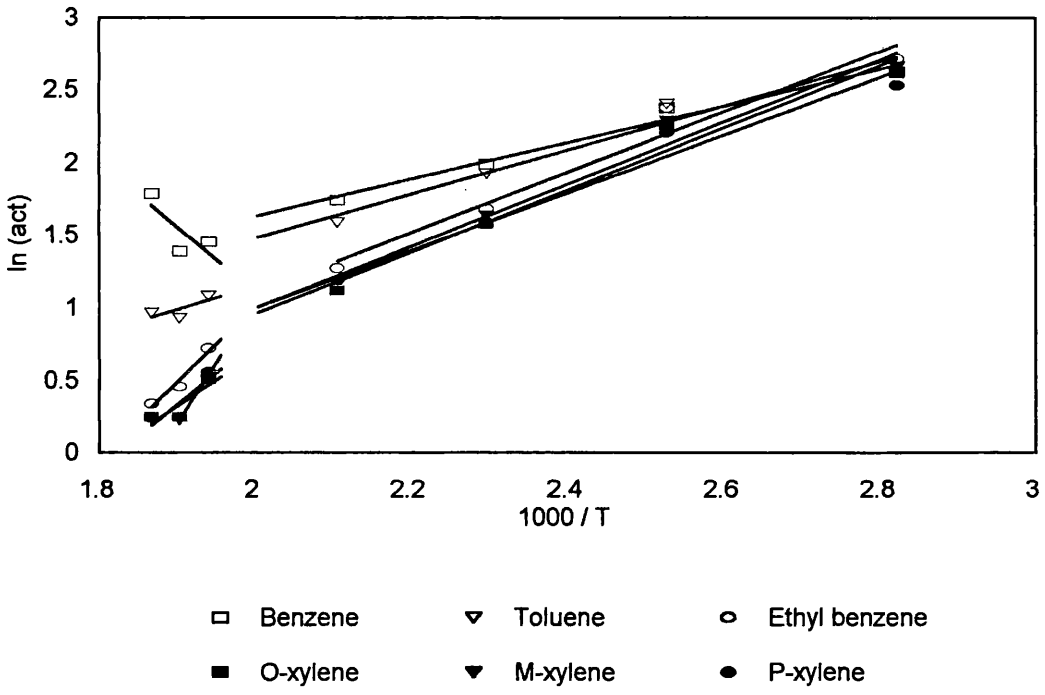

Figure A2.47: ln Ω^{∞} vs 1/T for Aromatic Probes in LCP2

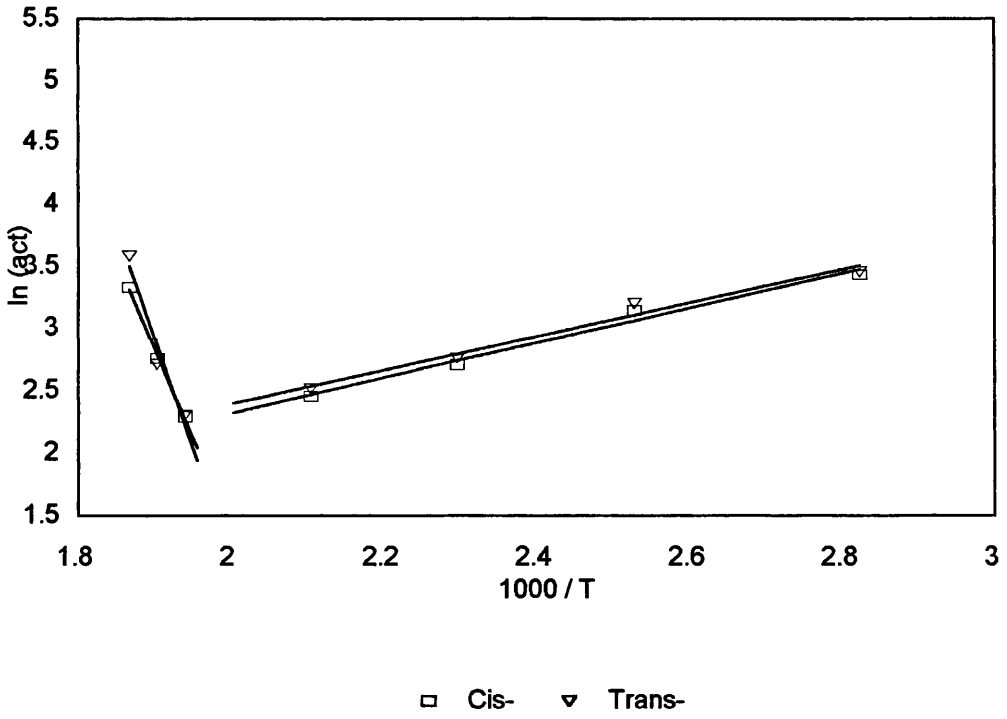

Figure A2.48: ln Ω^{∞} vs 1/T for Isomeric Probes in LCP2

Probe	Enthalpic kJ mol^{-1}			Entropic J mol^{-1} K^{-1}		
	ΔH^s	ΔH^e	ΔH^{vap}	ΔS^s	ΔS^e	ΔS^{vap}
Hexane	-16.72 (0.14)	9.50 (0.07)	-26.22 (0.21)	-20.31 (0.07)	45.55 (0.38)	-65.87 (0.45)
Heptane	-16.37 (0.29)	14.19 (0.22)	-30.56 (0.51)	-13.79 (0.16)	57.01 (0.12)	-70.79 (0.28)
Octane	-16.71 (0.29)	18.07 (0.22)	-34.78 (0.51)	-8.43 (0.16)	67.06 (0.12)	-75.49 (0.28)
2-Me	-16.69 (0.15)	12.28 (0.10)	-28.97 (0.25)	-17.12 (0.08)	51.32 (0.05)	-68.43 (0.13)
2,2-DiMe	-14.54 (0.15)	16.90 (0.09)	-31.44 (0.24)	-9.44 (0.08)	61.73 (0.05)	-71.17 (0.13)
Benzene	-18.20 (0.19)	10.48 (0.13)	-28.68 (0.32)	-12.81 (0.10)	57.39 (0.07)	-70.19 (0.17)
Toluene	-20.19 (0.26)	12.62 (0.20)	-32.81 (0.46)	-12.00 (0.14)	61.87 (0.01)	-73.87 (0.15)
Ethylbenzene	-19.08 (0.34)	17.26 (0.28)	-36.35 (0.62)	-4.06 (0.18)	73.12 (0.15)	-77.18 (0.33)
O-Xylene	-20.08 (0.33)	17.73 (0.27)	-37.81 (0.60)	-3.73 (0.18)	75.26 (0.15)	-78.99 (0.33)
M-Xylene	-19.38 (0.32)	17.75 (0.26)	-37.13 (0.58)	-3.53 (0.17)	74.97 (0.14)	-78.49 (0.31)
P-Xylene	-20.39 (0.33)	16.48 (0.26)	-36.86 (0.59)	-5.59 (0.17)	72.42 (0.14)	-78.00 (0.31)
Cis-	-14.90 (0.19)	11.67 (0.13)	-26.57 (0.32)	-13.12 (0.10)	53.75 (0.07)	-66.88 (0.17)
Trans-	-14.98 (0.21)	11.19 (0.15)	-26.17 (0.36)	-13.77 (0.11)	52.18 (0.08)	-65.95 (0.19)
R(+)	-19.79 (0.34)	n/a	n/a	-9.27 (0.18)	n/a	n/a
S(-)	-19.72 (0.31)	n/a	n/a	-9.06 (0.17)	n/a	n/a

Table A2.15: Physiochemical Results for LCP2 in the Smectic C Mesophase

Probe	Enthalpic kJ mol^{-1}			Entropic J mol^{-1} K^{-1}		
	ΔH^s	ΔH^e	ΔH^{vap}	ΔS^s	ΔS^e	ΔS^{vap}
Hexane	-195.28 (0.66)	-174.43 (0.07)	-20.85 (0.73)	-366.37 (0.03)	-311.85 (0.04)	-54.52 (0.07)
Heptane	-40.30 (1.18)	-15.80 (1.16)	-24.50 (2.34)	-58.12 (0.06)	-0.12 (0.06)	-58.00 (0.12)
Octane	-11.09 (1.27)	16.73 (1.29)	-27.82 (2.56)	5.50 (0.07)	66.32 (0.07)	-60.83 (0.14)
2-Me	-79.54 (0.25)	-56.90 (0.26)	-22.63 (0.51)	-136.30 (0.01)	-81.21 (0.01)	-55.09 (0.02)
2,2-DiMe	-44.58 (n/a)	-19.72 (n/a)	-24.87 (n/a)	-65.87 (n/a)	-8.57 (n/a)	-57.31 (n/a)
Benzene	-61.18 (3.64)	-37.55 (3.66)	-23.82 (7.30)	-93.86 (0.19)	-34.34 (0.18)	-59.53 (0.37)
Toluene	-14.10 (1.42)	13.44 (1.43)	-27.54 (2.85)	3.50 (0.07)	66.26 (0.07)	-62.77 (0.14)
Ethylbenzene	13.40 (1.08)	43.70 (1.10)	-30.30 (2.18)	62.28 (0.06)	126.73 (0.06)	-64.45 (0.12)
O-Xylene	-2.98 (2.03)	29.76 (2.05)	-32.74 (4.08)	33.33 (0.10)	101.62 (0.11)	-68.29 (0.21)
M-Xylene	37.20 (n/a)	69.94 (n/a)	-32.75 (n/a)	109.80 (n/a)	178.98 (n/a)	-69.18 (n/a)
P-Xylene	4.00 (2.33)	36.36 (2.34)	-32.36 (4.67)	45.61 (0.12)	114.08 (0.12)	-68.46 (0.24)
Cis-	-138.12 (0.87)	-117.67 (0.89)	-20.45 (1.76)	-251.47 (0.45)	-197.40 (0.05)	-54.00 (0.50)
Trans-	-164.96 (3.79)	-144.60 (3.81)	-20.36 (7.60)	-303.04 (0.20)	-249.33 (0.20)	-53.70 (0.40)
R(+)	-2.03 (2.94)	n/a	n/a	29.44 (0.15)	n/a	n/a
S(-)	-4.73 (2.81)	n/a	n/a	24.73 (0.15)	n/a	n/a

Table A2.16: Physiochemical Results for LCP2 in the Isotropic Phase

A2.7 LCP3: ln Vg°, ln Ω^{∞}, ΔH^{s}, ΔH^{e}, ΔS^{s}, ΔS^{e}

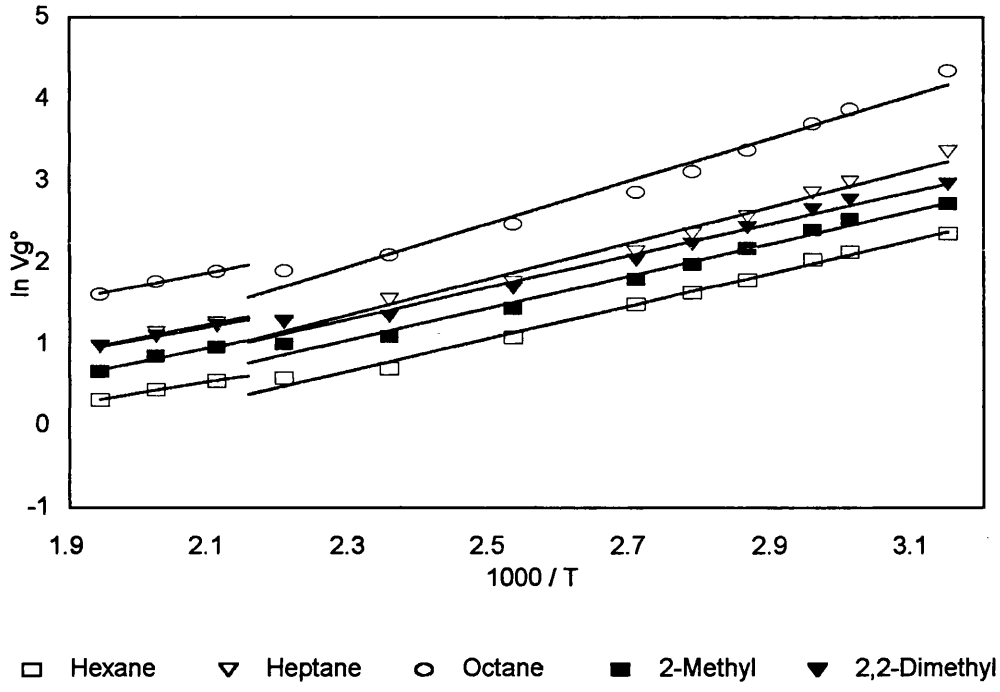

Figure A2.49: ln Vg° vs 1/T for Aliphatic Probes in LCP3

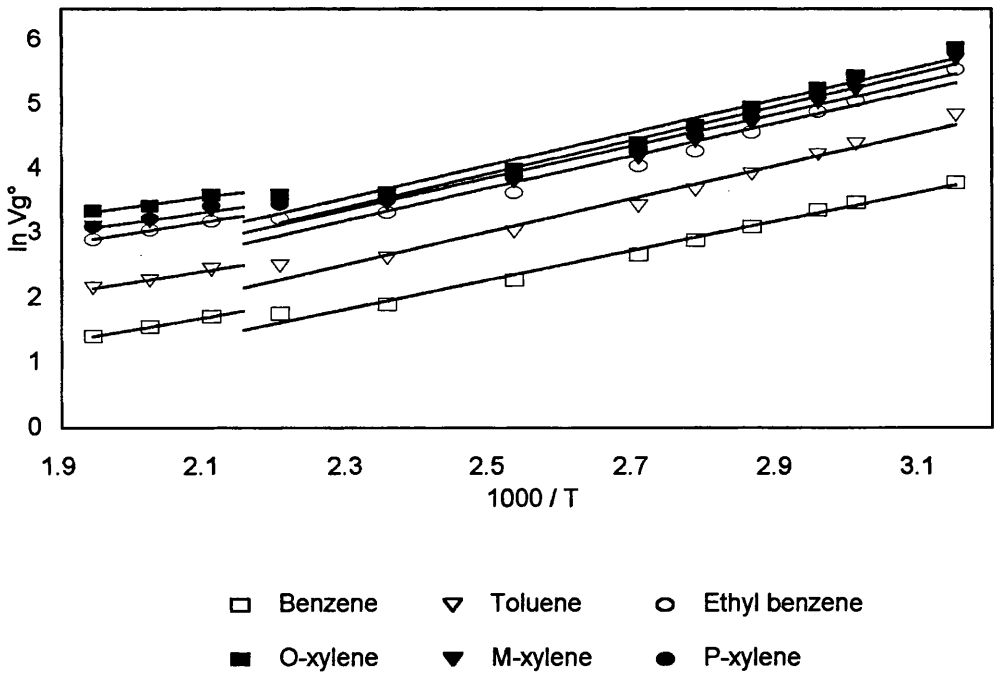

Figure A2.50: ln Vg° vs 1/T for Aromatic Probes in LCP3

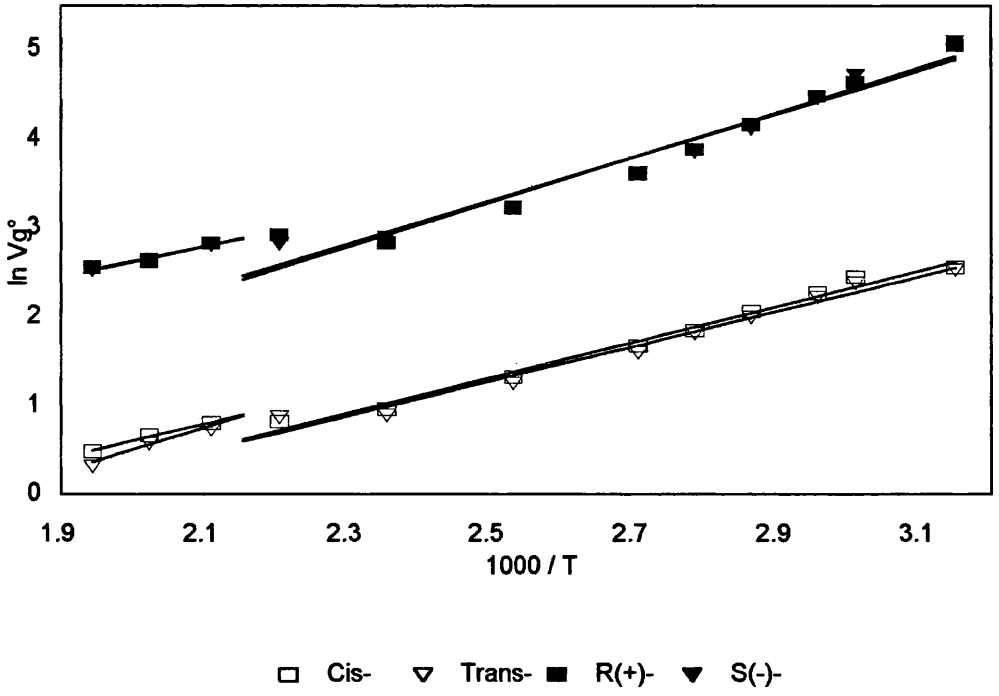

Figure A2.51: ln Vg° vs 1/T for Isomeric Probes in LCP3

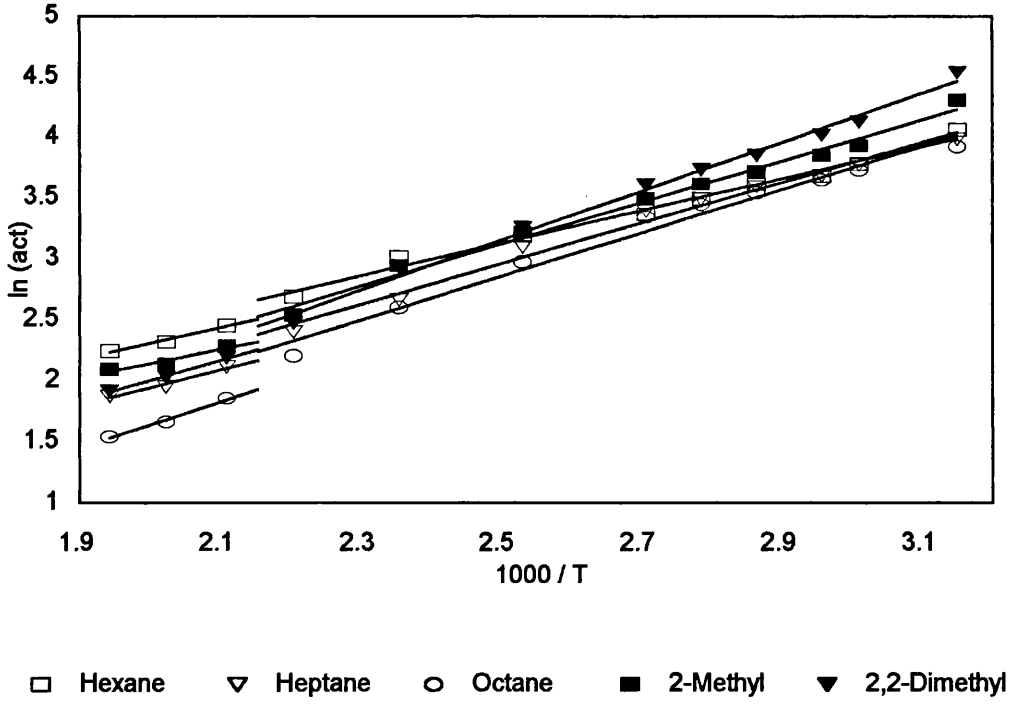

Figure A2.52: ln Ω^{∞} vs 1/T for Aliphatic Probes in LCP3

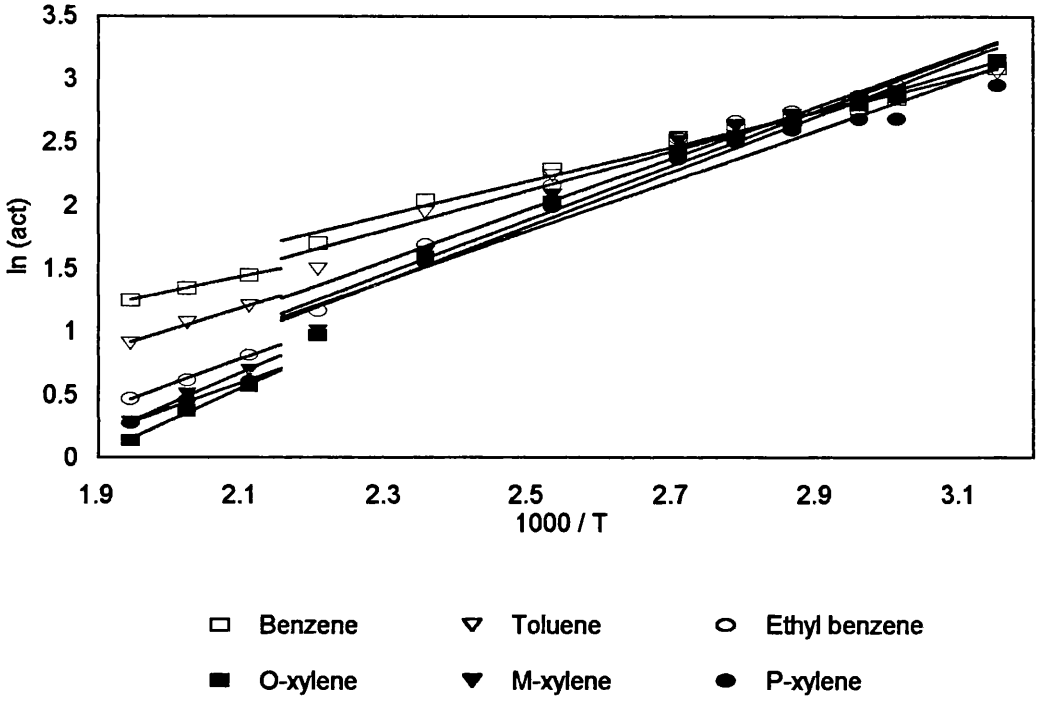

Figure A2.53: ln Ω^{∞} vs 1/T for Aromatic Probes in LCP3

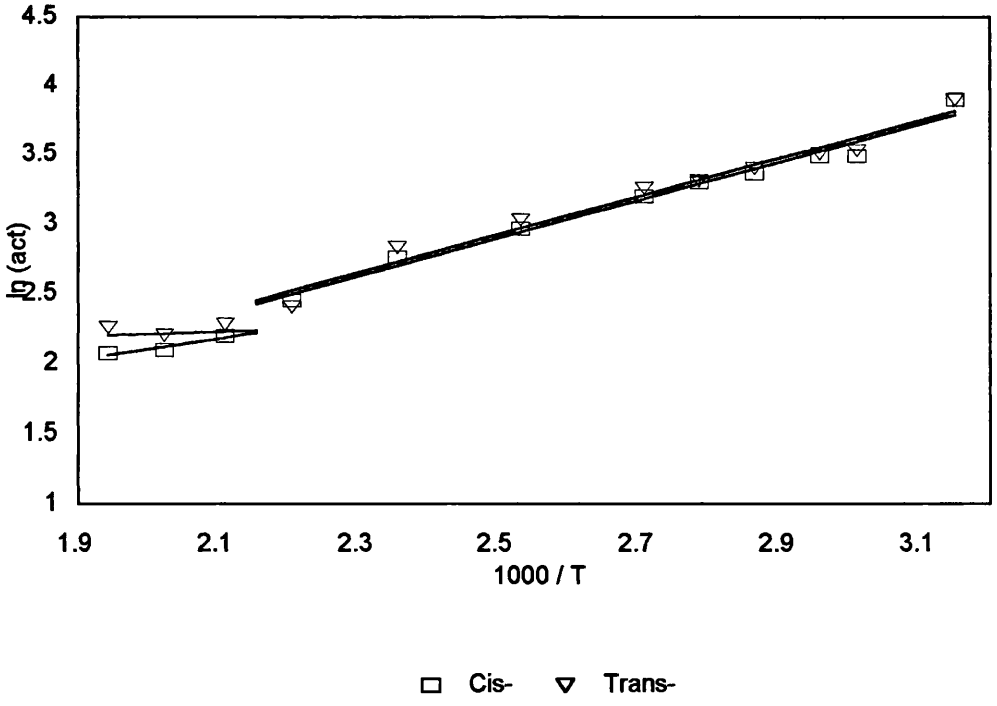

Figure A2.54: ln Ω^{∞} vs 1/T for Isomeric Probes in LCP3

Probe	Enthalpic kJ mol^{-1}			Entropic J mol^{-1} K^{-1}		
	ΔH^s	ΔH^e	ΔH^{vap}	ΔS^s	ΔS^e	ΔS^{vap}
Hexane	-16.64 (0.07)	11.07 (0.06)	-27.71 (0.13)	-18.42 (0.06)	48.27 (0.05)	-66.69 (0.11)
Heptane	-18.34 (0.12)	13.85 (0.08)	-32.19 (0.20)	-16.60 (0.10)	55.37 (0.07)	-71.97 (0.17)
Octane	-21.73 (0.15)	14.86 (0.10)	-36.59 (0.25)	-19.45 (0.13)	57.68 (0.09)	-77.13 (0.22)
2-Me	-16.35 (0.09)	14.24 (0.07)	-30.59 (0.16)	-14.58 (0.08)	55.01 (0.06)	-69.59 (0.14)
2,2-DiMe	-16.20 (0.09)	16.84 (0.07)	-33.04 (0.16)	-12.11 (0.08)	60.17 (0.06)	-72.29 (0.14)
Benzene	-18.74 (0.09)	11.32 (0.06)	-30.06 (0.15)	-13.62 (0.08)	57.12 (0.05)	-70.75 (0.13)
Toluene	-21.17 (0.14)	13.04 (0.10)	-34.21 (0.24)	-13.49 (0.13)	60.99 (0.09)	-74.48 (0.22)
Ethylbenzene	-20.96 (0.19)	16.98 (0.14)	-37.93 (0.33)	-7.34 (0.17)	70.90 (0.13)	-78.25 (0.30)
O-Xylene	-21.23 (0.19)	18.07 (0.15)	-39.30 (0.34)	-5.08 (0.16)	74.73 (0.13)	-79.80 (0.29)
M-Xylene	-20.65 (0.21)	17.91 (0.17)	-38.56 (0.38)	-5.27 (0.19)	73.89 (0.15)	-79.16 (0.34)
P-Xylene	-21.74 (0.21)	16.54 (0.17)	-38.28 (0.38)	-7.43 (0.19)	71.22 (0.15)	-78.64 (0.34)
Cis-	-16.69 (0.09)	11.35 (0.08)	-28.04 (0.17)	-16.64 (0.08)	51.02 (0.07)	-67.65 (0.15)
Trans-	-16.31 (0.11)	11.39 (0.09)	-27.70 (0.20)	-15.99 (0.10)	50.90 (0.08)	-66.89 (0.18)
R(+)	-20.24 (0.21)	n/a	n/a	-8.98 (0.19)	n/a	n/a
S(-)	-20.89 (0.19)	n/a	n/a	-10.73 (0.17)	n/a	n/a

Table A2.17: Physiochemical Results for LCP3 in the Smectic C Mesophase

Probe	Enthalpic kJ mol^{-1}			Entropic J mol^{-1} K^{-1}		
	ΔH^s	ΔH^e	ΔH^{vap}	ΔS^s	ΔS^e	ΔS^{vap}
Hexane	-11.50 (0.13)	10.65 (0.16)	-22.15 (0.29)	-5.40 (0.02)	48.71 (0.02)	-54.11 (0.04)
Heptane	-13.92 (0.20)	12.12 (0.23)	-26.04 (0.43)	-4.64 (0.02)	53.42 (0.03)	-58.07 (0.05)
Octane	-13.90 (0.15)	15.77 (0.19)	-29.68 (0.34)	0.67 (0.02)	62.19 (0.02)	-61.51 (0.04)
2-Me	-14.69 (0.29)	9.61 (0.33)	-24.30 (0.62)	-8.75 (0.03)	46.74 (0.04)	-55.39 (0.07)
2,2-DiMe	-12.89 (0.05)	13.61 (0.09)	-26.50 (0.14)	-2.73 (0.01)	54.83 (0.01)	-57.56 (0.02)
Benzene	-15.17 (0.23)	9.72 (0.01)	-24.89 (0.24)	-3.53 (0.01)	55.53 (0.01)	-59.06 (0.02)
Toluene	-14.47 (0.18)	14.45 (0.15)	-28.91 (0.33)	3.96 (0.02)	66.45 (0.02)	-62.50 (0.04)
Ethylbenzene	-14.57 (0.11)	17.37 (0.15)	-31.94 (0.26)	10.03 (0.01)	74.74 (0.02)	-64.71 (0.03)
O-Xylene	-12.29 (0.28)	21.72 (0.25)	-34.01 (0.53)	18.01 (0.03)	85.82 (0.03)	-67.81 (0.03)
M-Xylene	-13.02 (0.23)	20.62 (0.21)	-33.64 (0.43)	14.51 (0.03)	82.50 (0.02)	-67.99 (0.05)
P-Xylene	-16.70 (0.19)	16.70 (0.16)	-33.40 (0.35)	7.40 (0.02)	74.95 (0.02)	-67.55 (0.04)
Cis-	-15.89 (0.21)	6.21 (0.25)	-22.10 (0.46)	-12.60 (0.02)	41.66 (0.03)	-54.26 (0.05)
Trans-	-20.48 (1.09)	1.35 (1.12)	-21.84 (2.21)	-22.60 (0.13)	31.04 (0.13)	-53.64 (0.26)
R(+)	-13.66 (0.44)	n/a	n/a	8.67	n/a	n/a
S(-)	-14.37 (0.10)	n/a	n/a	7.18	n/a	n/a

Table A2.18: Physiochemical Results for LCP3 in the Isotropic Phase

Appendix Three:

ANALYTICAL RESULTS

This Appendix contains tables of analytical results obtained according to the calculations shown in (1.3.2) and discussed in Chapter 5. These results cover all liquid crystalline materials, the solution behaviour of which was described in Chapter 4. Values in parentheses indicate experimental uncertainties as calculated in (3.3.2)

A3.1 ANALYTICAL RESULTS FOR BDH509

Temperature (°C)	α	R_S	N for R_S=1.5 (m)
44	2.508 (0.025)	0.908 (0.018)	188
54	2.388 (0.024)	1.015 (0.020)	252
55	2.324 (0.023)	1.975 (0.040)	271
76	2.169 (0.022)	1.258 (0.025)	445
85	2.186 (0.022)	1.091 (0.022)	554
96	2.083 (0.021)	1.043 (0.021)	767
106	2.067 (0.020)	0.966 (0.019)	889
115	2.000 (0.020)	0.844 (0.017)	1095
132	2.000 (0.020)	0.622 (0.012)	1310
146	1.926 (0.019)	0.817 (0.016)	1530
148	1.941 (0.019)	1.076 (0.022)	1480
154	2.00 (0.020)	0.966 (0.019)	1625
166	1.844 (0.018)	0.836 (0.017)	2140
176	1.793 (0.018)	0.902 (0.018)	2720

Table A2.1: Analytical Results for Hexane and Heptane

Temperature (°C)	α	R_S	N for R_S=1.5 (m)
44	1.139 (0.011)	1.125 (0.023)	2610
54	1.025 (0.010)	0.142 (0.003)	71000
55	1.046 (0.010)	0.349 (0.007)	20940
76	1.060 (0.011)	0.205 (0.004)	14100
85	1.098 (0.011)	0.167 (0.003)	5990
96	1.078 (0.011)	0.145 (0.003)	9790
106	1.049 (0.010)	0.064 (0.001)	24800
115	1.076 (0.011)	0.181 (0.004)	11200
132	1.044 (0.010)	0.100 (0.002)	33600
146	0.991 (0.010)	-0.022 (0.001)	743000
148	0.968 (0.010)	-0.076 (0.002)	56800
154	1.014 (0.010)	0.032 (0.001)	334000
166	1.011 (0.010)	0.022 (0.001)	630000
176	1.000 (0.010)	0.000 (0.001)	n/a

Table A2.2: Analytical Results for m-xylene and p-xylene

Temperature (°C)	α	R_S	N for R_S=1.5 (m)
44	1.030 (0.010)	0.025 (0.001)	160000
54	1.050 (0.011)	0.067 (0.001)	70000
55	1.024 (0.010)	0.059 (0.001)	293000
76	1.049 (0.010)	0.074 (0.001)	118000
85	1.043 (0.010)	0.052 (0.001)	229000
96	1.053 (0.011)	0.062 (0.001)	204000
106	1.059 (0.011)	0.065 (0.001)	173000
115	1.056 (0.011)	0.071 (0.001)	232000
132	1.031 (0.010)	0.035 (0.001)	805000
146	1.067 (0.011)	0.084 (0.002)	204000
148	1.077 (0.011)	0.118 (0.002)	147000
154	1.051 (0.011)	0.076 (0.002)	359000
166	1.114 (0.011)	0.162 (0.003)	94600
176	1.030 (0.010)	0.047 (0.001)	1250000

Table A2.3: Analytical Results for cis- and trans-2-hexene

Temperature (°C)	α	R_S	N for R_S=1.5 (m)
44	1.037 (0.010)	0.181 (0.004)	31900
54	0.957 (0.010)	-0.102 (0.002)	22000
55	1.003 (0.010)	0.014 (0.001)	4310000
76	0.930 (0.009)	-0.151 (0.003)	9180
85	0.994 (0.010)	-0.009 (0.001)	1940000
96	1.022 (0.010)	0.034 (0.001)	148000
106	0.987 (0.010)	-0.018 (0.001)	409000
115	0.975 (0.010)	-0.043 (0.001)	121000
132	0.980 (0.010)	-0.039 (0.001)	208000
146	1.011 (0.010)	0.021 (0.001)	758000
148	0.974 (0.010)	-0.056 (0.001)	133000
154	1.004 (0.010)	0.009 (0.001)	5300000
166	0.980 (0.010)	-0.038 (0.001)	265000
176	0.951 (0.010)	-0.087 (0.002)	44600

Table A2.4: Analytical Results for R(+) and S(-)-2-methylchloropropionate

A3.2 ANALYTICAL RESULTS FOR BDH770

Temperature (°C)	α	R_S	N for R_S=1.5 (m)
44	2.565 (0.026)	1.177 (0.024)	256
49	2.455 (0.025)	0.991 (0.020)	285
55	2.425 (0.024)	0.883 (0.018)	316
70	2.24 (0.022)	0.715 (0.014)	470
80	2.167 (0.022)	0.687 (0.014)	606
91	2.000 (0.020)	0.545 (0.011)	844
101	2.031 (0.020)	0.498 (0.10)	978
127	1.889 (0.019)	0.401 (0.008)	1580
137	1.903 (0.019)	0.374 (0.007)	1870
146	1.867 (0.019)	0.356 (0.007)	2046
162	1.810 (0.018)	0.417 (0.008)	1790
166	1.800 (0.018)	0.384 (0.008)	1960
172	1.789 (0.018)	0.368 (0.007)	2150

Table A2.5: Analytical Results for Hexane and Heptane

Temperature (°C)	α	R_S	N for R_S=1.5 (m)
44	1.065 (0.011)	0.163 (0.003)	10600
49	1.097 (0.011)	0.218 (0.004)	5040
55	1.108 (0.011)	0.212 (0.004)	4230
70	1.077 (0.011)	0.144 (0.003)	8390
80	1.121 (0.011)	0.183 (0.004)	3820
91	1.081 (0.011)	0.086 (0.002)	8580
101	1.093 (0.011)	0.086 (0.002)	6990
127	1.108 (0.011)	0.089 (0.002)	5980
137	1.149 (0.011)	0.114 (0.002)	3434
146	1.116 (0.011)	0.081 (0.002)	5710
162	1.067 (0.011)	0.079 (0.002)	15100
166	1.063 (0.011)	0.073 (0.001)	17300
172	1.095 (0.011)	0.100 (0.002)	8240

Table A2.6: Analytical Results for m-xylene and p-xylene

Temperature (°C)	α	R_S	N for R_S=1.5 (m)
44	1.047 (0.010)	0.071 (0.001)	83500
49	1.033 (0.010)	0.047 (0.001)	170000
55	1.055 (0.011)	0.071 (0.001)	71700
70	1.077 (0.011)	0.095 (0.002)	52300
80	1.055 (0.011)	0.061 (0.001)	121000
91	1.042 (0.010)	0.045 (0.001)	238000
101	1.051 (0.011)	0.049 (0.001)	212000
127	1.023 (0.010)	0.020 (0.001)	1330000
137	1.081 (0.011)	0.063 (0.001)	151000
146	1.056 (0.011)	0.047 (0.001)	311000
162	1.060 (0.011)	0.057 (0.001)	206000
166	1.042 (0.010)	0.037 (0.001)	439000
172	1.091 (0.011)	0.071 (0.001)	116000

Table A2.7: Analytical Results for cis- and trans-2-hexene

Temperature (°C)	α	R_S	N for R_S=1.5 (m)
44	0.940 (0.009)	-0.184 (0.004)	9460
49	0.994 (0.010)	-0.014 (0.001)	1200000
55	0.979 (0.010)	-0.041 (0.001)	89600
70	1.004 (0.010)	0.008 (0.001)	2320000
80	0.934 (0.009)	-0.099 (0.002)	9660
91	1.010 (0.010)	0.012 (0.001)	527000
101	1.023 (0.010)	0.003 (0.001)	880000
127	1.023 (0.010)	0.020 (0.001)	144000
137	1.026 (0.010)	0.021 (0.001)	120000
146	0.982 (0.010)	-0.014 (0.001)	241000
162	0.987 (0.010)	-0.011 (0.001)	406000
166	0.994 (0.010)	-0.005 (0.001)	2340000
172	0.997 (0.010)	-0.002 (0.001)	8040000

Table A2.8: Analytical Results for R(+) and S(-)-2-methylchloropropionate

A3.3 ANALYTICAL RESULTS FOR BDH849

Temperature (°C)	α	R_S	N for R_S=1.5 (m)
80	2.389 (0.024)	0.588 (0.012)	1660
90	2.444 (0.024)	0.712 (0.014)	1350
95	2.160 (0.022)	0.632 (0.013)	1220
100	2.222 (0.022)	0.938 (0.019)	565
106	2.167 (0.022)	0.891 (0.018)	550
108	2.085 (0.021)	0.883 (0.018)	593
110	2.130 (0.021)	0.900 (0.018)	592
115	2.071 (0.021)	0.913 (0.018)	648
121	2.051 (0.021)	0.818 (0.016)	756
126	2.056 (0.021)	0.894 (0.018)	798
136	2.032 (0.020)	0.753 (0.015)	992
146	2.077 (0.021)	0.634 (0.013)	1160

Table A2.9: Analytical Results for Hexane and Heptane

Temperature (°C)	α	R_S	N for R_S=1.5 (m)
80	0.995 (0.010)	-0.007 (0.001)	2520000
90	0.962 (0.010)	-0.054 (0.001)	39700
95	0.957 (0.010)	-0.060 (0.001)	27200
100	1.020 (0.010)	0.030 (0.001)	122000
106	0.960 (0.010)	-0.062 (0.001)	26700
108	1.036 (0.010)	0.059 (0.001)	38500
110	1.009 (0.010)	0.018 (0.001)	677000
115	1.032 (0.010)	0.069 (0.001)	51200
121	1.005 (0.010)	0.012 (0.001)	1780000
126	0.986 (0.010)	-0.029 (0.001)	273000
136	1.021 (0.010)	0.038 (0.001)	132000
146	0.973 (0.010)	-0.040 (0.001)	76800

Table A2.10: Analytical Results for m-xylene and p-xylene

Temperature (°C)	α	R_S	N for R_S=1.5 (m)
80	1.043 (0.010)	0.024 (0.001)	882000
90	0.917 (0.090)	-0.056 (0.001)	146000
95	0.967 (0.010)	-0.025 (0.001)	707000
100	1.038 (0.010)	0.048 (0.001)	280000
106	0.983 (0.010)	-0.025 (0.001)	1050000
108	0.983 (0.010)	-0.026 (0.001)	970000
110	0.982 (0.010)	-0.028 (0.001)	1000000
115	0.981 (0.010)	-0.033 (0.001)	843000
121	0.959 (0.010)	-0.065 (0.001)	204000
126	1.023 (0.010)	0.039 (0.001)	826000
136	1.057 (0.011)	0.081 (0.002)	197000
146	1.032 (0.010)	0.034 (0.001)	710000

Table A2.11: Analytical Results for cis- and trans-2-hexene

Temperature (°C)	α	R_S	N for R_S=1.5 (m)
80	0.960 (0.010)	-0.048 (0.001)	48000
90	0.995 (0.010)	-0.005 (0.001)	3910000
95	1.004 (0.010)	0.005 (0.001)	5070000
100	1.018 (0.010)	0.027 (0.001)	201000
106	1.012 (0.010)	0.018 (0.001)	414000
108	1.018 (0.010)	0.029 (0.001)	185000
110	1.000 (0.010)	0.000 (0.001)	n/a
115	0.974 (0.010)	-0.036 (0.001)	86200
121	1.003 (0.010)	0.004 (0.001)	6390000
126	1.011 (0.010)	0.015 (0.001)	590000
136	0.988 (0.010)	-0.016 (0.001)	484000
146	1.035 (0.010)	0.040 (0.001)	73700

Table A2.12: Analytical Results for R(+) and S(-)-2-methylchloropropionate

A3.4 ANALYTICAL RESULTS FOR BDH1029

Temperature (°C)	α	R_S	N for R_S=1.5 (m)
57	2.407 (0.024)	0.745 (0.015)	1030
67	2.346 (0.023)	0.710 (0.014)	1180
77	2.222 (0.022)	0.670 (0.013)	1300
87	2.280 (0.023)	0.661 (0.013)	1350
103	2.089 (0.021)	0.779 (0.016)	800
107	2.071 (0.021)	0.746 (0.015)	900
110	1.951 (0.020)	0.765 (0.015)	1080
113	2.026 (0.020)	0.805 (0.016)	1070
121	1.946 (0.019)	0.654 (0.013)	1320
131	1.882 (0.019)	0.619 (0.012)	1710
140	1.833 (0.018)	0.566 (0.011)	2280
149	1.741 (0.017)	0.490 (0.010)	3210

Table A2.13: Analytical Results for Hexane and Heptane

Temperature (°C)	α	R_S	N for R_S=1.5 (m)
57	1.045 (0.010)	0.059 (0.001)	27000
67	1.018 (0.010)	0.026 (0.001)	170000
77	1.044 (0.010)	0.066 (0.001)	31700
87	1.037 (0.010)	0.053 (0.001)	48000
103	1.020 (0.010)	0.033 (0.001)	139000
107	1.025 (0.010)	0.037 (0.001)	89500
110	1.022 (0.010)	0.032 (0.001)	116000
113	1.023 (0.010)	0.033 (0.001)	110000
121	1.015 (0.010)	0.022 (0.001)	264000
131	1.000 (0.010)	0.000 (0.001)	n/a
140	1.003 (0.010)	0.003 (0.001)	7420000
149	1.029 (0.010)	0.025 (0.001)	112000

Table A2.14: Analytical Results for m-xylene and p-xylene

Temperature (°C)	α	R_S	N for R_S=1.5 (m)
57	1.097 (0.011)	0.050 (0.001)	137000
67	1.133 (0.011)	0.071 (0.001)	82500
77	1.185 (0.012)	0.101 (0.002)	55100
87	1.231 (0.012)	0.126 (0.003)	41200
103	1.080 (0.010)	0.071 (0.001)	91800
107	1.020 (0.010)	0.023 (0.001)	1310000
110	1.089 (0.011)	0.096 (0.002)	85500
113	1.070 (0.010)	0.077 (0.002)	147000
121	1.048 (0.010)	0.052 (0.001)	327000
131	1.081 (0.010)	0.078 (0.002)	151000
140	1.121 (0.011)	0.121 (0.002)	88600
149	1.103 (0.011)	0.095 (0.002)	142000

Table A2.15: Analytical Results for cis- and trans-2-hexene

Temperature (°C)	α	R_S	N for R_S=1.5 (m)
57	0.990 (0.010)	-0.016 (0.001)	551000
67	0.977 (0.010)	-0.032 (0.001)	122000
77	0.958 (0.010)	-0.064 (0.001)	37900
87	0.965 (0.010)	-0.053 (0.001)	59700
103	1.011 (0.010)	0.014 (0.001)	593000
107	1.018 (0.010)	0.023 (0.001)	232000
110	0.994 (0.010)	-0.008 (0.001)	1750000
113	1.045 (0.010)	0.057 (0.001)	41600
121	1.004 (0.010)	0.005 (0.001)	5980000
131	1.005 (0.010)	0.006 (0.001)	4760000
140	0.951 (0.010)	-0.055 (0.001)	42700
149	1.021 (0.010)	0.021 (0.001)	343000

Table A2.16: Analytical Results for R(+) and S(-)-2-methylchloropropionate

A3.5 ANALYTICAL RESULTS FOR LMM1

Temperature (°C)	α	R_S	N for R_S=1.5 (m)
29	2.872 (0.029)	1.286 (0.026)	110
33	2.850 (0.029)	1.339 (0.027)	115
34	2.853 (0.029)	1.353 (0.027)	115
41	2.713 (0.027)	1.342 (0.027)	130
43	2.684 (0.027)	1.290 (0.026)	135
46	2.661 (0.027)	1.329 (0.027)	140
48	2.598 (0.026)	1.343 (0.027)	145
54	2.609 (0.026)	1.508 (0.030)	135
59	2.54 (0.025)	1.544 (0.031)	145
64	2.481 (0.025)	1.414 (0.028)	160

Table A2.17: Analytical Results for Hexane and Heptane

Temperature (°C)	α	R_S	N for R_S=1.5 (m)
29	1.143 (0.012)	1.203 (0.024)	2300
33	1.145 (0.012)	1.083 (0.022)	2300
34	1.071 (0.011)	0.710 (0.014)	8500
41	1.071 (0.011)	0.591 (0.012)	8500
43	1.077 (0.011)	0.344 (0.007)	7300
46	1.059 (0.011)	0.188 (0.004)	12000
48	1.072 (0.011)	0.243 (0.005)	8200
54	0.983 (0.010)	-0.107 (0.002)	119500
59	0.985 (0.010)	-0.102 (0.002)	166500
64	0.990 (0.010)	-0.052 (0.001)	381000

Table A2.18: Analytical Results for m-xylene and p-xylene

Temperature (°C)	α	R_S	N for R_S=1.5 (m)
29	1.112 (0.011)	0.123 (0.003)	6500
33	1.074 (0.011)	0.084 (0.002)	14000
34	1.044 (0.010)	0.050 (0.001)	39000
41	1.047 (0.010)	0.059 (0.001)	37500
43	1.050 (0.011)	0.062 (0.001)	35500
46	1.051 (0.011)	0.067 (0.001)	34000
48	1.067 (0.011)	0.091 (0.002)	20800
54	1.071 (0.011)	0.106 (0.002)	16000
59	1.074 (0.011)	0.114 (0.002)	16000
64	1.076 (0.011)	0.116 (0.002)	16500

Table A2.19: Analytical Results for cis- and trans-2-hexene

Temperature (°C)	α	R_S	N for R_S=1.5 (m)
29	0.951 (0.010)	-0.289 (0.006)	14000
33	0.950 (0.010)	-0.180 (0.003)	13600
34	1.044 (0.010)	0.050 (0.001)	39000
41	1.047 (0.010)	0.059 (0.001)	37500
43	0.997 (0.010)	-0.008 (0.001)	3778000
46	1.001 (0.010)	0.002 (0.001)	120000000
48	0.979 (0.010)	-0.062 (0.001)	84000
54	0.989 (0.010)	-0.038 (0.001)	328000
59	1.001 (0.010)	0.003 (0.001)	39000000
64	0.993 (0.010)	-0.025 (0.001)	753000

Table A2.20: Analytical Results for R(+) and S(-)-2-methylchloropropionate

A3.6 ANALYTICAL RESULTS FOR LCP1

Temperature (°C)	α	R_S	N for R_S=1.5 (m)
40	2.630 (0.026)	0.929 (0.019)	200
50	2.454 (0.025)	1.029 (0.021)	300
60	2.335 (0.023)	1.022 (0.020)	400
70	2.249 (0.022)	1.273 (0.025)	400
85	2.172 (0.022)	0.897 (0.018)	500
95	2.094 (0.021)	0.922 (0.018)	700
105	1.998 (0.020)	0.754 (0.015)	900
115	1.916 (0.019)	0.584 (0.012)	1300

Table A2.21: Analytical Results for Hexane and Heptane

Temperature (°C)	α	R_S	N for R_S=1.5 (m)
40	1.150 (0.011)	1.070 (0.021)	2300
50	1.111 (0.011)	0.516 (0.010)	4100
60	1.059 (0.011)	0.295 (0.006)	13500
70	1.013 (0.010)	0.038 (0.001)	241500
85	1.013 (0.010)	0.044 (0.001)	261000
95	0.993 (0.010)	-0.021 (0.001)	895500
105	1.001 (0.010)	-0.003 (0.001)	30000000
115	1.096 (0.010)	0.092 (0.001)	77500

Table A2.22: Analytical Results for m-xylene and p-xylene

Temperature (°C)	α	R_S	N for R_S=1.5 (m)
40	1.049 (0.010)	0.051 (0.001)	78700
50	1.015 (0.010)	0.018 (0.001)	1093000
60	1.059 (0.011)	0.070 (0.001)	80900
70	1.100 (0.011)	0.149 (0.003)	28400
85	1.071 (0.011)	0.104 (0.002)	65000
95	1.083 (0.011)	0.111 (0.002)	59700
105	1.112 (0.011)	0.133 (0.003)	47600
115	1.096 (0.011)	0.092 (0.002)	77400

Table A2.23: Analytical Results for cis- and trans-2-hexene

Temperature (°C)	α	R_S	N for R_S=1.5 (m)
40	1.056 (0.011)	0.167 (0.003)	15100
50	1.031 (0.010)	0.081 (0.002)	48900
60	0.987 (0.010)	-0.031 (0.001)	290300
70	1.002 (0.010)	0.007 (0.001)	9801600
85	1.014 (0.010)	0.039 (0.001)	252000
95	0.997 (0.010)	-0.007 (0.001)	656700
105	0.990 (0.010)	-0.021 (0.001)	556200
115	0.990 (0.010)	-0.023 (0.001)	614500

Table A2.24: Analytical Results for R(+) and S(-)-2-methylchloropropionate

A3.7 ANALYTICAL RESULTS FOR LCP2

Temperature (°C)	α	R_S	N for R_S=1.5 (m)
81	2.056 (0.021)	0.644 (0.013)	1500
123	1.784 (0.018)	0.360 (0.007)	7000
162	2.013 (0.020)	0.334 (0.007)	7800
202	2.070 (0.021)	0.293 (0.006)	10100
229	4.313 (0.043)	0.278 (0.006)	8500
234	2.008 (0.020)	0.263 (0.005)	8200
237	3.644 (0.036)	0.277 (0.006)	8000
242	2.582 (0.026)	0.278 (0.006)	8200
252	4.611 (0.046)	0.250 (0.005)	8700

Table A2.25: Analytical Results for Hexane and Heptane

Temperature (°C)	α	R_S	N for R_S=1.5 (m)
81	1.102 (0.011)	0.162 (0.003)	6300
123	1.059 (0.011)	0.055 (0.001)	29000
162	1.032 (0.010)	0.024 (0.001)	121000
201	1.009 (0.010)	0.006 (0.001)	1666000
229	1.021 (0.010)	0.014 (0.001)	365500
234	1.021 (0.010)	0.014 (0.001)	273000
237	0.962 (0.010)	-0.027 (0.001)	105000
242	0.980 (0.010)	-0.015 (0.001)	350000
252	0.977 (0.010)	-0.029 (0.001)	253000

Table A2.26: Analytical Results for m-xylene and p-xylene

Temperature (°C)	α	R_S	N for R_S=1.5 (m)
81	1.047 (0.010)	0.038 (0.001)	48500
123	1.067 (0.011)	0.032 (0.001)	141500
162	1.054 (0.011)	0.027 (0.001)	1413000
201	1.058 (0.011)	0.025 (0.001)	690500
229	1.154 (0.012)	0.028 (0.001)	174500
234	1.037 (0.010)	0.015 (0.001)	3368000
237	1.429 (0.014)	0.011 (0.001)	14000000
242	1.000 (0.010)	0.000 (0.001)	n/a
252	0.938 (0.009)	-0.011 (0.001)	4778500

Table A2.27: Analytical Results for cis- and trans-2-hexene

Temperature (°C)	α	R_S	N for R_S=1.5 (m)
81	1.008 (0.010)	0.011 (0.001)	1244000
123	0.972 (0.010)	-0.037 (0.001)	188500
162	1.014 (0.010)	0.016 (0.001)	1196500
201	0.989 (0.010)	-0.007 (0.001)	2136000
229	0.967 (0.010)	-0.022 (0.001)	255000
234	0.918 (0.009)	-0.056 (0.001)	25000
237	0.970 (0.010)	-0.017 (0.001)	361000
242	0.935 (0.009)	-0.046 (0.001)	55000
252	0.954 (0.010)	-0.037 (0.001)	99000

Table A2.28: Analytical Results for R(+) and S(-)-2-methylchloropropionate

A3.8 ANALYTICAL RESULTS FOR LCP3

Temperature (°C)	α	R_S	N for R_S=1.5 (m)
44	2.718 (0.027)	0.640 (0.013)	380
59	2.335 (0.023)	0.645 (0.013)	630
65	2.245 (0.022)	0.646 (0.013)	780
76	2.169 (0.022)	0.640 (0.013)	1150
86	2.049 (0.020)	0.633 (0.013)	1640
96	1.903 (0.019)	0.575 (0.012)	2540
122	1.954 (0.020)	0.390 (0.008)	4040
151	2.315 (0.023)	0.537 (0.011)	3800
180	2.006 (0.020)	0.288 (0.006)	6930
201	2.019 (0.020)	0.278 (0.006)	6770
221	1.986 (0.020)	0.271 (0.005)	8030
241	1.923 (0.019)	0.233 (0.005)	10800

Table A2.29: Analytical Results for Hexane and Heptane

Temperature (°C)	α	R_S	N for R_S=1.5 (m)
44	1.136 (0.011)	0.638 (0.013)	2970
59	1.204 (0.012)	0.697 (0.014)	1590
65	1.136 (0.011)	0.306 (0.006)	3360
76	1.096 (0.011)	0.184 (0.004)	6950
86	1.090 (0.011)	0.142 (0.003)	8600
96	1.118 (0.011)	0.124 (0.002)	5860
122	1.070 (0.011)	0.063 (0.001)	19000
151	1.063 (0.011)	0.075 (0.002)	28800
180	1.021 (0.010)	0.015 (0.001)	245600
201	1.078 (0.011)	0.040 (0.001)	19400
221	1.044 (0.010)	0.022 (0.001)	64700
241	1.001 (0.010)	0.001 (0.001)	61000000

Table A2.30: Analytical Results for m-xylene and p-xylene

Temperature (°C)	α	R_S	N for R_S=1.5 (m)
44	1.029 (0.010)	0.015 (0.001)	554000
59	1.073 (0.011)	0.046 (0.001)	99000
65	1.049 (0.010)	0.032 (0.001)	263000
76	1.067 (0.011)	0.046 (0.001)	194000
86	1.039 (0.010)	0.027 (0.001)	704000
96	1.080 (0.011)	0.053 (0.001)	248000
122	1.076 (0.011)	0.043 (0.001)	462000
151	1.074 (0.011)	0.006 (0.001)	815500
180	0.953 (0.010)	-0.021 (0.001)	1511500
201	1.080 (0.011)	0.032 (0.001)	813000
221	1.098 (0.011)	0.035 (0.001)	694000
241	1.1875 (0.012)	0.046 (0.001)	338000

Table A2.31: Analytical Results for cis- and trans-2-hexene

Temperature (°C)	α	R_S	N for R_S=1.5 (m)
44	0.950 (0.010)	-0.160 (0.003)	18600
59	0.928 (0.009)	-0.117 (0.002)	9400
65	1.018 (0.010)	0.020 (0.004)	198000
76	1.039 (0.010)	0.045 (0.001)	51400
86	1.023 (0.010)	0.026 (0.001)	176000
96	0.983 (0.010)	-0.021 (0.001)	330000
122	0.990 (0.010)	-0.012 (0.001)	1244000
151	0.947 (0.009)	-0.035 (0.001)	60000
180	1.105 (0.011)	0.065 (0.001)	21000
201	1.016 (0.010)	0.006 (0.001)	750000
221	0.975 (0.010)	-0.009 (0.001)	334000
241	1.032 (0.010)	0.011 (0.001)	251500

Table A2.32: Analytical Results for R(+) and S(-)-2-methylchloropropionate

Appendix Four:

VAN DEEMTER PLOTS

This Appendix contains the Van Deemter plots used to obtain diffusion coefficients described in Chapter 6. These plots cover PDMS, LMM1 and LCP1 in their various phases.

A4.1 VAN DEEMTER PLOTS FOR PDMS

The following Van Deemter plots were obtained using the PDMS column described in (2.3.1), and the resultant diffusion coefficients are presented in (6.2).

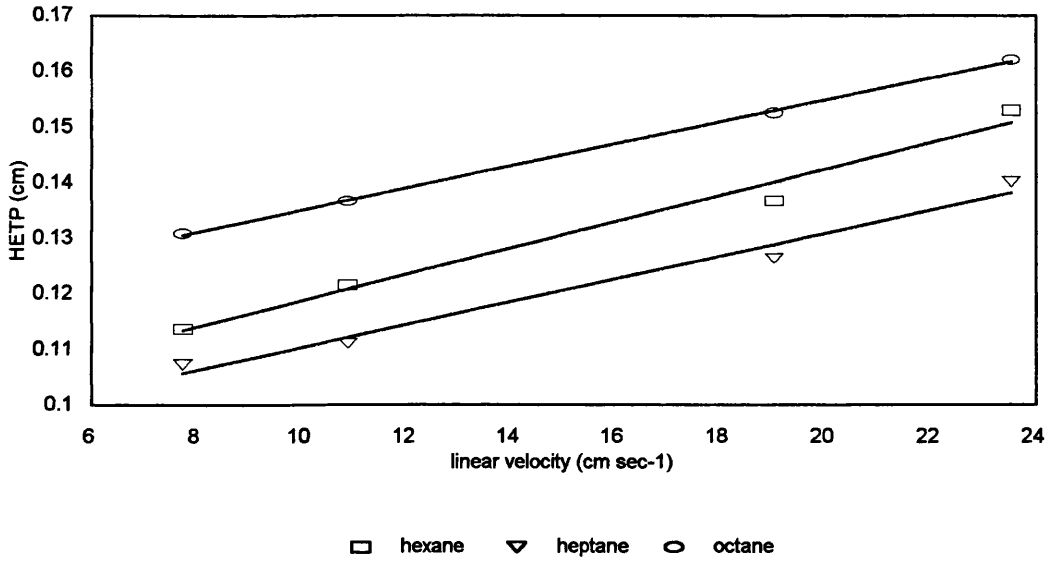

Figure A4.1: Van Deemter Plot for PDMS at 60°C

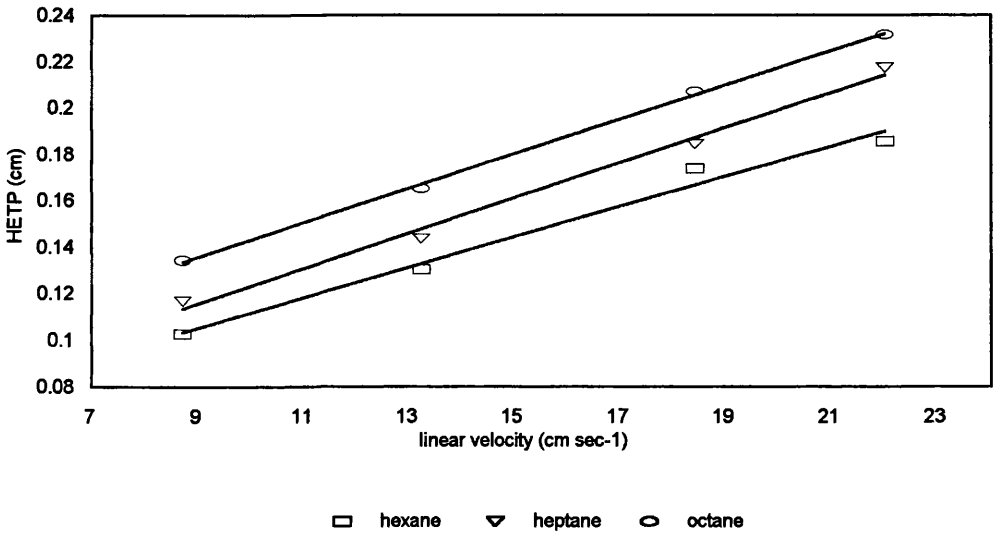

Figure A4.2: Van Deemter Plot for PDMS at 71°C

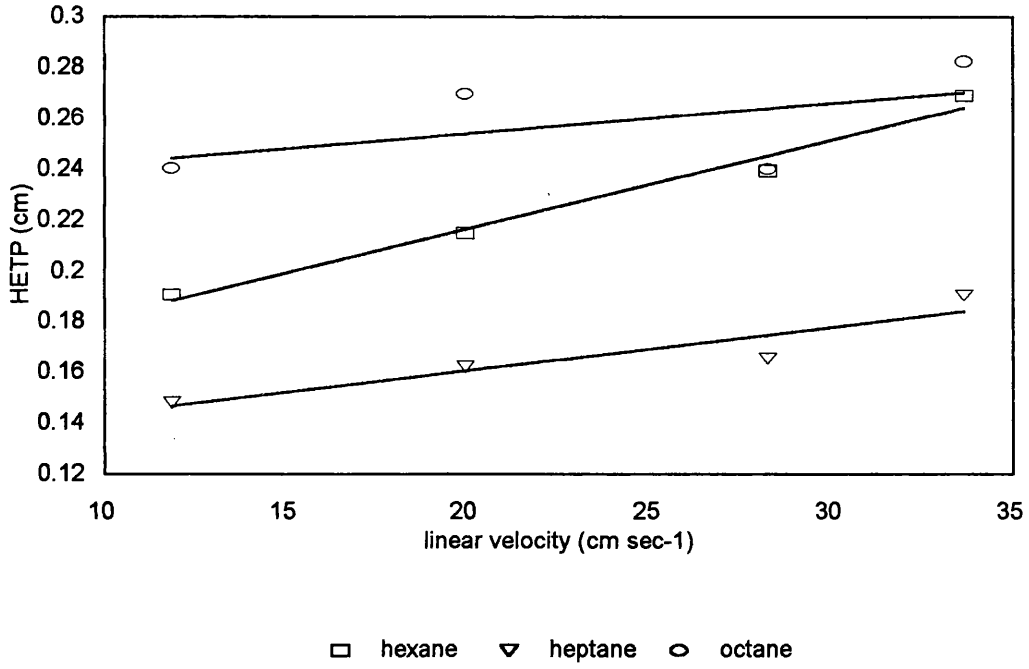

Figure A4.3: Van Deemter Plot for PDMS at 81°C

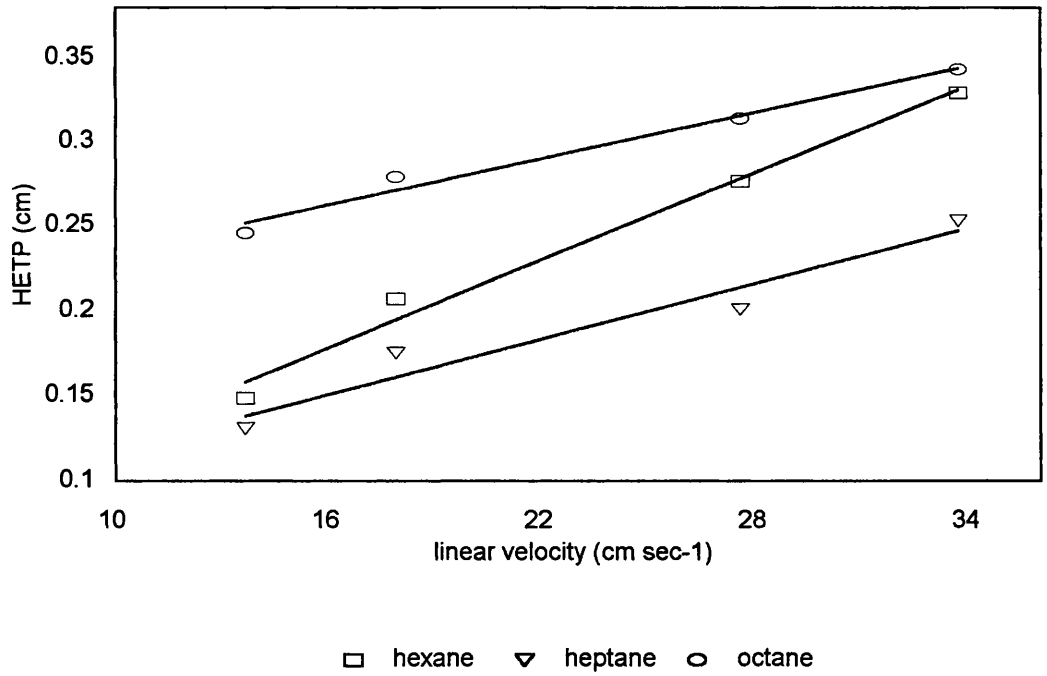

Figure A4.4: Van Deemter Plot for PDMS at 91°C

A4.2 VAN DEEMTER PLOTS FOR LMM1

The Van Deemter plots obtained in the smectic C mesophase and isotropic phase obtained on the LMM1 column (2.3.1) are presented here. The resultant diffusion coefficients are presented in (6.3).

A4.2.1 SMECTIC C MESOPHASE

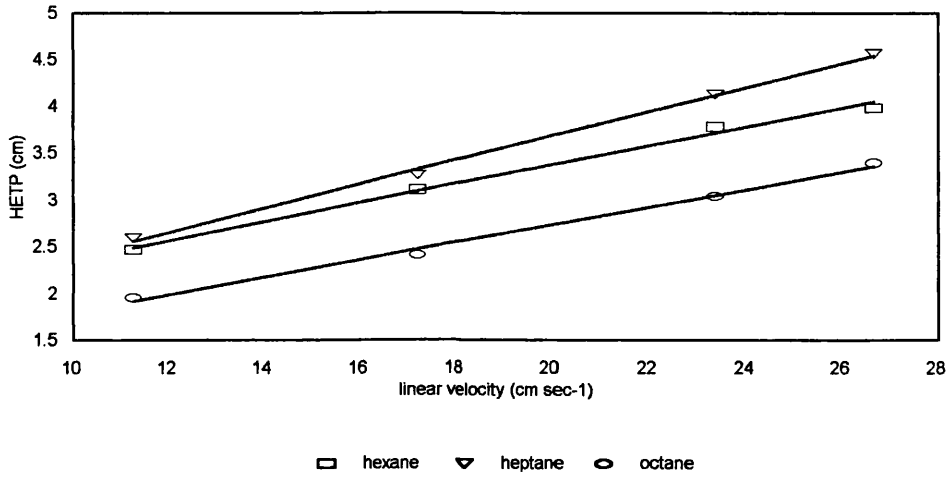

Figure A4.5: Van Deemter Plot for LMM1 at 46°C

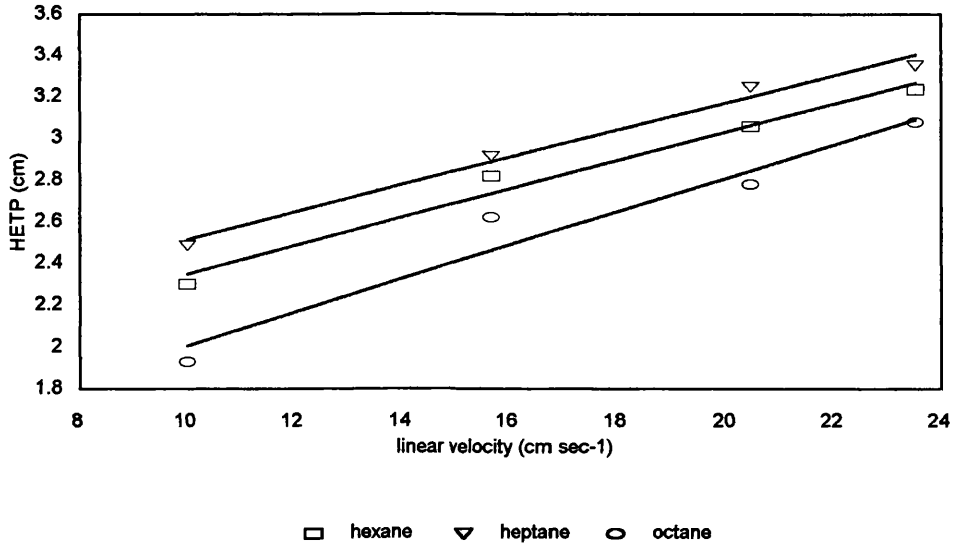

Figure A4.6: Van Deemter Plot for LMM1 at 49°

A4.2.2 ISOTROPIC PHASE

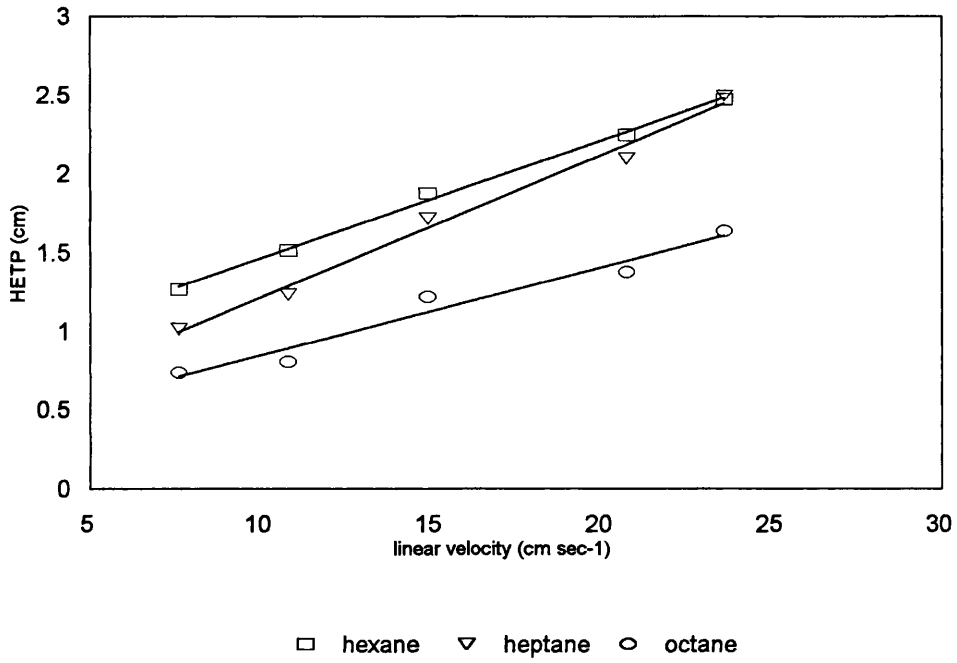

Figure A4.7: Van Deemter Plot for LMM1 at 56°C

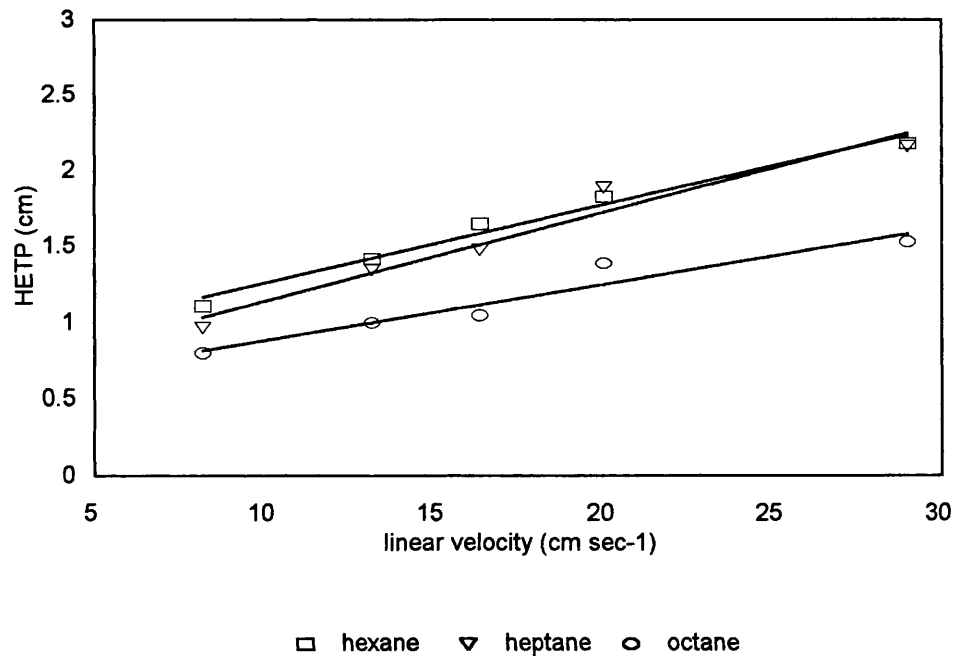

Figure A4.8: Van Deemter Plot for LMM1 at 61°C

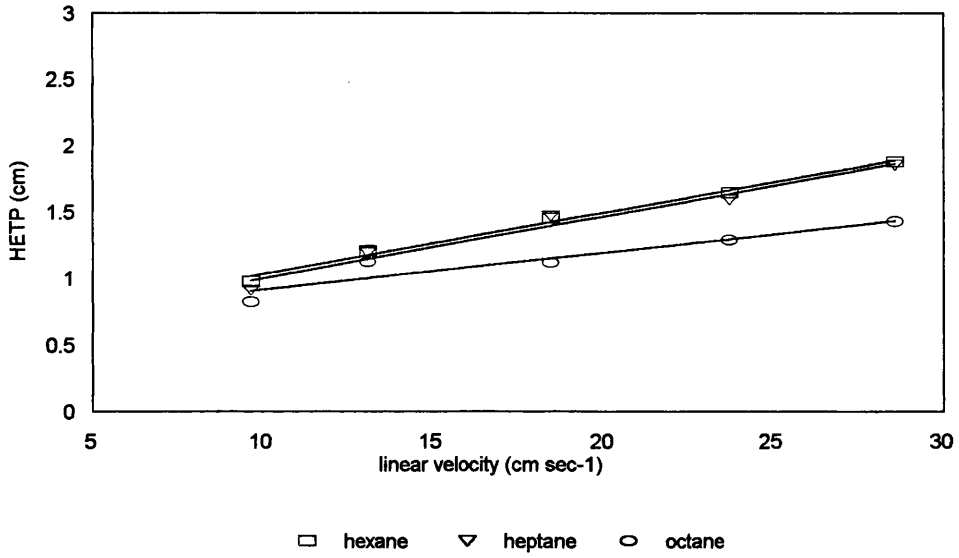

Figure A4.9: Van Deemter Plot for LMM1 at 66°C

A4.3 VAN DEEMTER PLOTS FOR LCP1

The Van Deemter plots obtained in the smectic C mesophase and isotropic phase obtained on the LCP1 column (2.3.1) are presented here. The resultant diffusion coefficients are presented in (6.4).

A4.3.1 SMECTIC C MESOPHASE

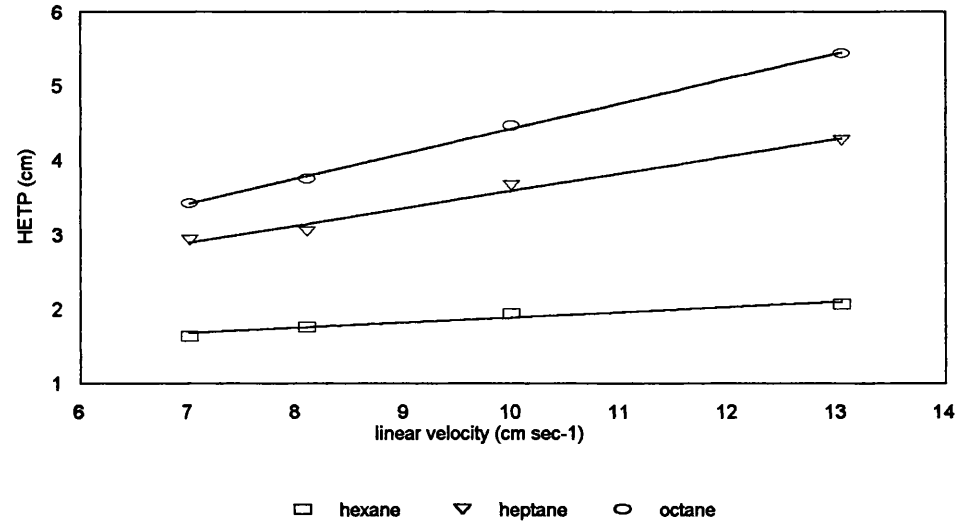

Figure A4.10: Van Deemter Plot for LCP1 at 45°C

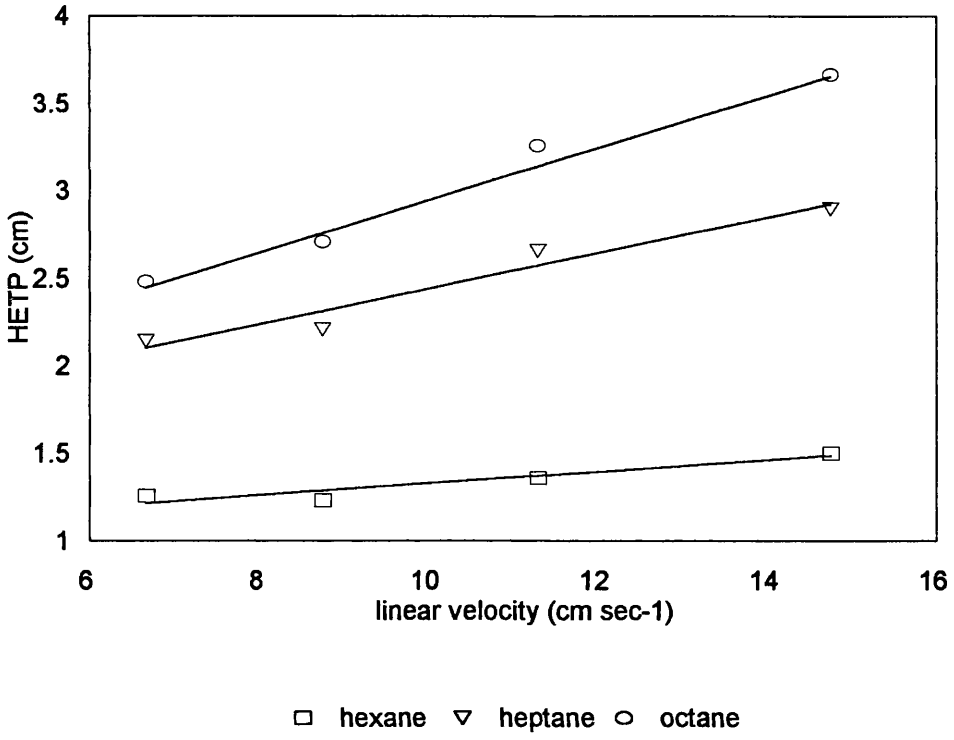

Figure A4.11: Van Deemter Plot for LCP1 at 52°C

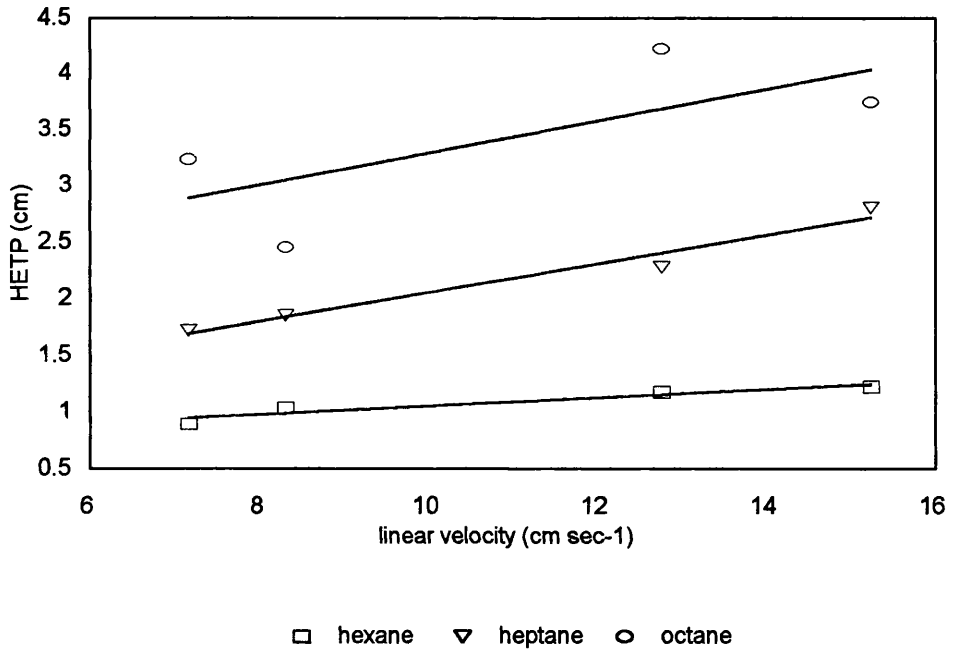

Figure A4.12: Van Deemter Plot for LCP1 at 56°C

A4.3.2 ISOTROPIC MESOPHASE

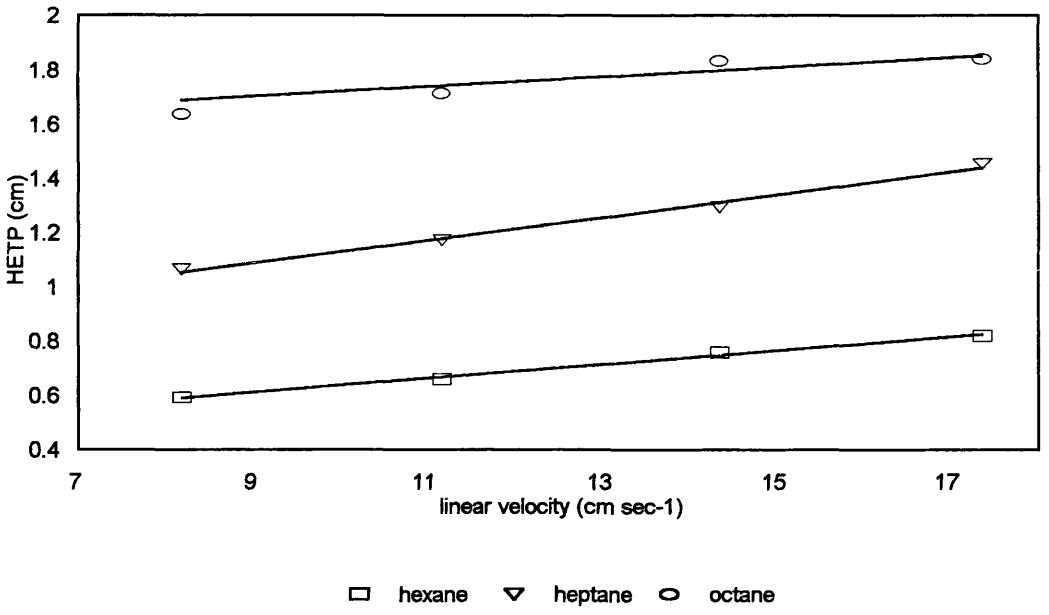

Figure A4.13: Van Deemter Plot for LCP1 at 66°C

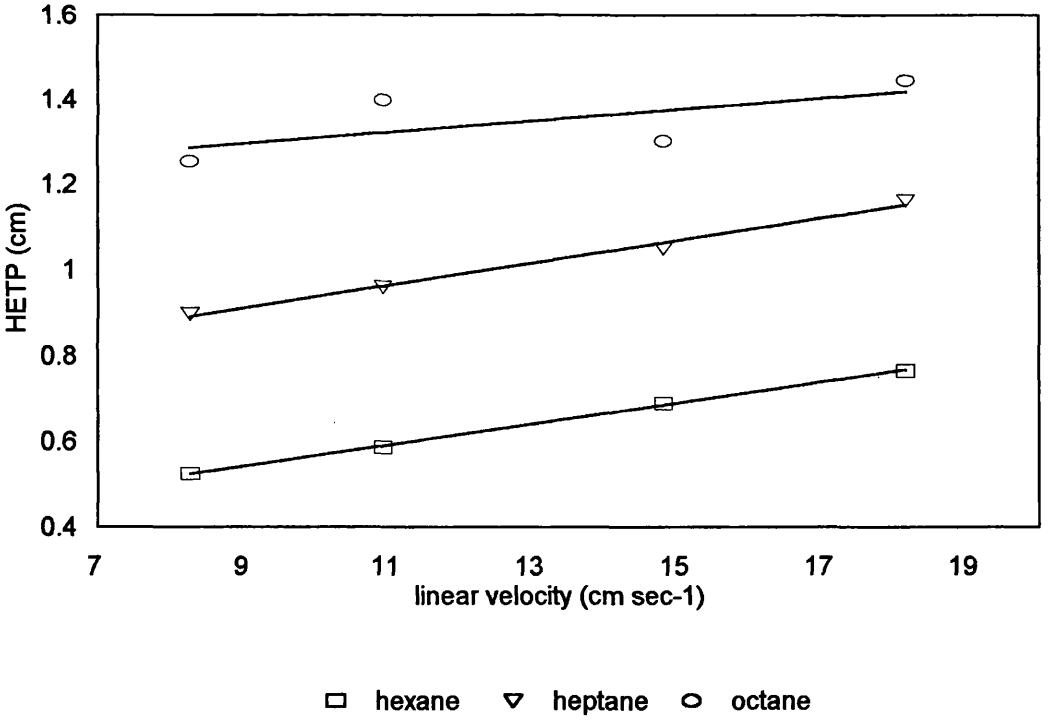

Figure A4.14: Van Deemter Plot for LMM1 at 71°C

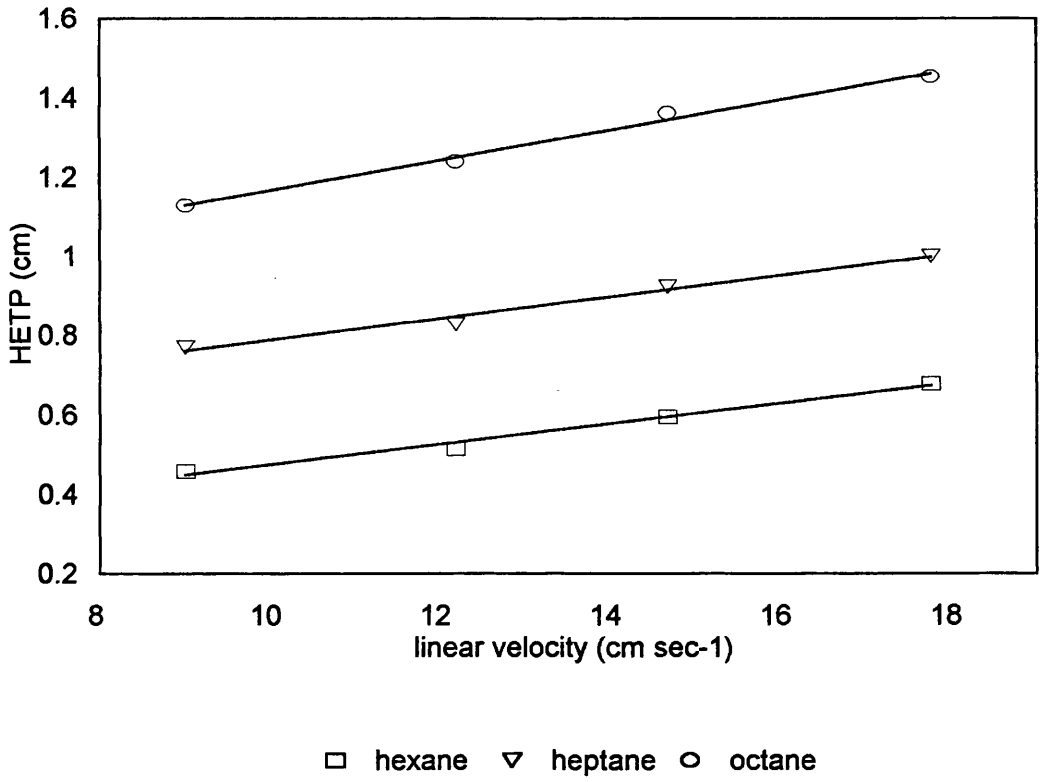

Figure A4.15: Van Deemter Plot for LMM1 at 76°C